DESIGN OF ROAD FOUNDATIONS

by

Nicholas H Thom, M.A. (Cantab)

Thesis submitted to the University of Nottingham for the degree of Doctor of Philosophy

MAY 1988

CONTENTS

		Page
ABSTRACT		
ACKNOWLEDGEMENTS		
LIST OF SYMBOLS, SUBSCRIPTS AND SUPERSCRIPTS		
CHAPTER 1	INTRODUCTION	1
CHAPTER 2	REVIEW OF GRANULAR MATERIAL TESTING AND MODELLING	5
2.1	Testing Devices Available	7
2.2	Mathematical Modelling - Elastic Behaviour	10
2.3	Mathematical Modelling - Plastic Behaviour	15
2.4	Pavement Analysis	17
CHAPTER 3	APPARATUS DESCRIPTION	19
3.1	Triaxial Apparatus	19
3.1.1	150mm Diameter Facility	20
3.1.2	75mm Diameter Facility	24
3.2	Hollow Cylinder Apparatus	24
3.3	Miniature Pavement Tester	31
CHAPTER 4	DRY GRANULAR MATERIAL BEHAVIOUR	36
4.1	A New Elastic Stress-Strain Model	37
4.1.1	Shear Behaviour	39
4.1.2	Volumetric Behaviour (Isotropic)	51
4.1.3	Volumetric Behaviour (with shear)	54
4.2	Elastic Behaviour - Correlation with Laboratory Test Data	59
4.2.1	Triaxial Data	59
4.2.2	Hollow Cylinder Data	64
4.2.3	Complex Stress Path Data	74

		Page
4.3	Plastic Behaviour	80
	4.3.1 Method of Investigation	82
	4.3.2 Monotonic Loading Curves	87
	4.3.3 Development of Shear Model	90
	4.3.4 Development of Volumetric Model	94
	4.3.5 Frequency Effects	96
4.4	Plastic Behaviour - Correlation with Laboratory Test Data	97
4.5	Summary	103
CHAPTER 5	EFFECT OF MATERIAL VARIABLES	104
5.1	Standard Test Routine	105
5.2	Use of Results	107
	5.2.1 Elastic Behaviour	108
	5.2.2 Plastic Behaviour	113
5.3	Effect of Grading Curve Shape and Degree of Compaction	115
	5.3.1 Elastic Behaviour	118
	5.3.2 Plastic Behaviour	122
	5.3.3 Summary	124
5.4	Effect of Particle Size	125
	5.4.1 Tests on Single Sized Material	126
	5.4.2 Tests on Graded Dolomitic Limestone	131
	5.4.3 Comparison with Delft University Tests	137
	5.4.4 Conclusions	140
5.5	Effect of Mineral Type	141
CHAPTER 6	EFFECT OF MOISTURE	152
6.1	To Confirm the Effective Stress Principle	153
6.2	Tests at Different Gradings	156

		Page
6.2.1	Permeability	156
6.2.2	Compaction	159
6.2.3	Suction - Negative Pore Pressure	162
6.2.4	Elastic Testing	165
6.2.5	Plastic Testing	170
6.3	Tests on Site Materials	171
6.4	Discussion	175
CHAPTER 7	PAVEMENT ANALYSIS - THE GRANMAT PROGRAM	177
7.1	The Aims of GRANMAT	178
7.2	Program Description	179
7.2.1	Analysis Type	181
7.2.2	Details of Iterative Process	183
7.2.3	Accounting for Moisture	190
7.2.4	The Unsurfaced Condition	193
7.2.5	Plastic Strain Computation	195
7.2.6	Input/Output Format	198
7.2.7	Program Summary	201
7.3	Assessment of Validity of Output	202
7.3.1	Pavement Test Facility	203
7.3.2	Data from Site Instrumentation	208
7.3.3	Surface Deflections under the Falling Weight Deflectometer	211
7.3.4	Comparison with BISTRO	213
7.3.5	Summary	215
CHAPTER 8	COMPACTION	216
8.1	Aims and Achievements of Compaction	216
8.2	Effect of Subgrade Support	219
8.3	Overcompaction	221

		Page
8.4	Influence of Roller Speed	223
8.5	Stress Distribution after Compaction	224
8.6	Conclusions	226
CHAPTER 9	FIELD MEASUREMENTS	227
9.1	Review of Current Practice	228
9.2	Testing Devices Available	230
9.2.1	Falling Weight Deflectometer	230
9.2.2	Clegg Impact Hammer	233
9.2.3	Dynamic Cone Penetrometer	235
9.2.4	Plate Bearing Test	236
9.2.5	BOMAG Terrameter	237
9.3	Description of Site Trials	238
9.3.1	A610 Kimberley Bypass	238
9.3.2	Wakefield Haul Road	239
9.3.3	A52 Friskney Realignment	240
9.3.4	A52 Bicker Realignment	241
9.3.5	A46 Dunholme Bypass	241
9.4	Analysis of Results	242
9.4.1	Falling Weight Deflectometer	242
9.4.2	Dynamic Cone Penetrometer	246
9.4.3	Plate Bearing Test	246
9.4.4	Clegg Impact Hammer	250
9.4.5	BOMAG Terrameter	255
9.5	Conclusions	258
CHAPTER 10	DESIGN CONSIDERATIONS	260
10.1	Results from GRANMAT	262
10.2	Application to Different Design Conditions	274
10.2.1	Short Term Haul Road	274

Page

10.2.2 Long Term Unsurfaced Road (or Surface Dressed) 275

10.2.3 Thinly Surfaced Road 276

10.2.4 Heavily Trafficked Road 277

10.2.5 Summary 277

10.3 Achievement of Granular Material Requirements 278

10.4 Subgrade Treatment 280

10.5 Treatment of Moisture 281

10.6 Specification 282

CHAPTER 11 CONCLUSIONS AND RECOMMENDATIONS FOR FUTURE WORK 292

11.1 Laboratory Facilities 292

11.1.1 Hollow Cylinder Apparatus 292

11.1.2 Miniature Pavement Tester 293

11.1.3 A Simple Laboratory Test Device 294

11.2 Material Investigation 295

11.2.1 Other Materials 297

11.2.2 Correlation with Stone Properties 297

11.2.3 Permeability 298

11.3 Computer Analysis 298

11.4 Site Work 300

11.4.1 Further Data 301

11.4.2 Apparatus Development 301

11.5 Design 302

REFERENCES 303

APPENDIX A Elastic Stress Strain Data from the Hollow Cylinder Apparatus

APPENDIX B Constants Describing Elastic and Plastic Behaviour

APPENDIX C Computer Program 'GRANMAT' Written in Turbo-Basic

PHOTOGRAPHS

ABSTRACT

Research has been conducted into the fundamental mechanical properties of a granular material. This has involved the use of both a repeated load triaxial apparatus and a new hollow cylinder apparatus, which has required development and modification. Building on the foundation of earlier research at Nottingham, models have been developed which predict the stress-strain behaviour of a dry granular material under any combination of applied stresses. This includes repeatable elastic behaviour and the development of irrecoverable plastic strain. The accuracy of these models has been tested as far as possible using available test equipment.

The effects of varying particle gradation, degree of compaction, maximum particle size and mineral type have been explored using a repeated load triaxial apparatus. The effect of moisture has also been investigated with respect to both full and partial saturation.

A computer program (GRANMAT) has been written, which makes use of the stress-strain equations developed, to analyse a road pavement structure consisting of thin bituminous surfacing, granular base and subgrade. The reliability of the program has been assessed and areas of necessary improvement indicated.

In-situ testing at a number of road sites is described and analysed with respect to both the effect of compaction on a granular road foundation and the use of a number of in-situ test devices.

Finally, the information gained, in the laboratory and on site, is brought together in a series of design suggestions for granular road foundations, with particular reference to results from the GRANMAT computer program.

ACKNOWLEDGEMENTS

The author would like to acknowledge the contribution made by a number of individuals and organisations without whose active assistance and support this thesis would not have been possible.

Firstly, acknowledgement is due to the Science and Engineering Research Council, who sponsored the research project upon which this thesis is based, and to Scott Wilson Kirkpatrick and Partners who allowed the author to be seconded for the duration of the project.

Secondly, the author is grateful to the Civil Engineering Department of Nottingham University under Professor P S Pell for providing the necessary facilities. In particular he would like to mention the following people:-

Professor S F Brown, who guided the research as project supervisor,

A R Dawson, who worked in close co-operation on a parallel project,

J Moody, who ensured the successful operation of laboratory equipment throughout,

F S A Tomlinson, who typed this thesis,

C Brayley, who drew the figures for this thesis.

Many other colleagues and friends have provided advice, assistance and support, too many unfortunately to name individually.

Thirdly, thanks are given to the following organisations who provided both equipment and information in connection with testing on site:-

Lincolnshire County Council,

Nottinghamshire County Council,

Bomag UK Ltd.

Finally, special thanks are due to the author's wife Jackie for her support and patience.

Symbols used in this Thesis:

b	parameter describing intermediate principal stress
E	elastic modulus (axial stress/axial strain)
fn	mathematical function
G	shear modulus (shear stress/shear strain)
K	bulk modulus (mean normal stress/volumetric strain)
KO	initial stress ratio (horizontal stress/vertical stress)
l	stress path length
ln	naperian logarithm
mr	radial displacement
mv	vertical displacement
N	number of load applications
p	mean normal stress
q	axial deviator stress
r	radial distance
s	mean in-plane stress
t	shear stress on a plane
z	vertical distance
γ	shear strain
δ	change in a quantity
ε	strain
θ	sum of three orthogonal normal stresses
σ	stress
τ	shear stress
ϕ	angle of friction

Note: Many letters are also used as constants in equations.

Subscripts used in this Thesis

0	initial conditions
1	first principal direction
2	second principal direction
3	third principal direction
f	failure
h	horizontal
i	a stress state
j	a second stress state
m	mean
max	maximum
p	plastic
r	repeated/radial
s	shear
t	tangential
v	volumetric/vertical
x	a direction
y	a direction orthogonal to x
z	a direction orthogonal to x and y

Superscript used in this Thesis

'	effective (ie subtracting pore pressure effects)

CHAPTER ONE

INTRODUCTION

In times past the design philosophy for the majority of man's constructions was empirical. A building was constructed in a certain way because the experience of many similar successful buildings suggested that it was satisfactory. If, one day, a structure collapsed, then the next time it would be made stronger. This philosophy was applied to roads also.

However, in recent centuries our knowledge of material properties, mechanics, statics and mathematics has generally enabled us to rationalize our approach to design. It has become less empirical and more analytical. This approach has led to the construction of metal ships, slim looking bridges and fragile looking dams, but the business of road building has remained solidly empirical until very recently. It cannot be argued that this is due to the additional complexity of a road structure when our capacity to analyse immensely complex structures such as aircraft is considered; it must rather be that the consequences of a rut in a road are rather less drastic than a ship sinking, a dam bursting or a bridge collapsing. However, it makes sense to apply our twentieth century capabilities to the humble problem of the road, all the more so since highway reconstruction is

becoming a very expensive and disruptive activity.

The recent Transport and Road Research Laboratory publication LR 1132 (Powell et al 1984) has opened the way in this country to an analytical approach which many individuals and organisations have been seeking for a number of years. The structural layers are designed to have appropriate thicknesses to prevent rutting and cracking taking place according to design charts based on laboratory and field data. This parallels design method proposals put forward at Nottingham (Brown et al 1985) which took a similar form and are now contained in a design manual produced by Mobil Oil (1985). However, the approach to foundation design remains empirical, though the dual purpose of carrying construction traffic and supporting the finished road is taken into consideration.

One of the problems which has inhibited the analysis of a road foundation is the lack of understanding which exists in the way soils and unbound aggregates behave under load. The theories of linear elasticity have been so useful and so powerful for so many materials that the urge to try to use them for soils is almost irresistable, whereas numerous studies have clearly indicated the fundamental incorrectness of such an approach. This has led to enormous inaccuracy in the analysis of road foundations and to the consequent shelving of analytical design concepts. More recently, as will be shown in chapter 2, research has been undertaken, both into the fundamental mechanisms of granular material behaviour and also into the way such material behaviour

can be included in the analysis of a road situation. Computer analysis techniques have been developed utilizing the new knowledge of material behaviour and various predictive methods have arisen to model the stresses and strains under a load.

At present, however, much work remains, both in extending our fundamental knowledge of unbound aggregates and also in enabling us to assess the properties of a given material. To date, insufficient work has been done in exploring the importance of such parameters as particle size distribution, maximum particle size, state of compaction and moisture content, let alone in comparing different types of mineral. At present we write specifications for grading, particle crushing, soundness etc, but often do not have sufficient logical grounds for adopting the limits we do. Sometimes, so it appears, the limits are determined more by what the industry is capable of rather than what is theoretically justifiable.

The concern, then, that lies behind this project is that all the many aspects of road foundation behaviour are explored, collated and brought to light in such a way that the important areas can be readily identified and attended to. The task has been a very broad one, which has inevitably meant that many areas have not been covered in any great depth and that some rely solely on the reported work of others. None the less, an attempt has been made to follow every important strand concerning the behaviour of granular materials in general and road foundations in particular,

and to tie the strands together into a set of design suggestions. Some of these suggestions will be firm, resting on adequate data; others will be tentative and require additional research in specific areas. The aim, however, is to paint as complete a picture as possible even though the detail may be blurred in places. Later work will, it is hoped, fill in the fine details once a vision of the whole has been seen, but to attack the details first is to invite a distorted final picture.

It is hoped that the sequence of chapters in this thesis will provide a logical path from understanding of granular materials in general, through the effects of various parameters and the influence of the foundation on the whole structure, to site problems and eventually to a discussion of design. This work is, however, far from the last word on the subject as will be made clear in chapter 11, where numerous recommendations for further research are made.

CHAPTER TWO

REVIEW OF GRANULAR MATERIAL TESTING AND MODELLING

Before proceeding to examine the various ways of testing and mathematically modelling granular material, it is useful to observe the type of stress strain behaviour which commonly emerges, whatever the test apparatus used. Fig 2.1 traces the relationship between shear stress and shear strain over a number of load applications for a gravel tested in a triaxial apparatus. No scales are shown because it is purely the form of relationship which is of interest here. It may be seen that the graph consists of an initial loading curve, followed by a series of unload-reload loops, all of similar shape, but progressing across the figure as strain builds up. This strain accumulation is taking place at an ever decreasing rate as the number of load applications increases. It appears that there are at least three distinct areas of behaviour to be investigated, which may or may not have some interdependency. They are:

(i) The shape of the initial loading curve.

(ii) The characteristic form of the load-unload loop.

(iii) The way in which strain accumulates with increasing number of load applications.

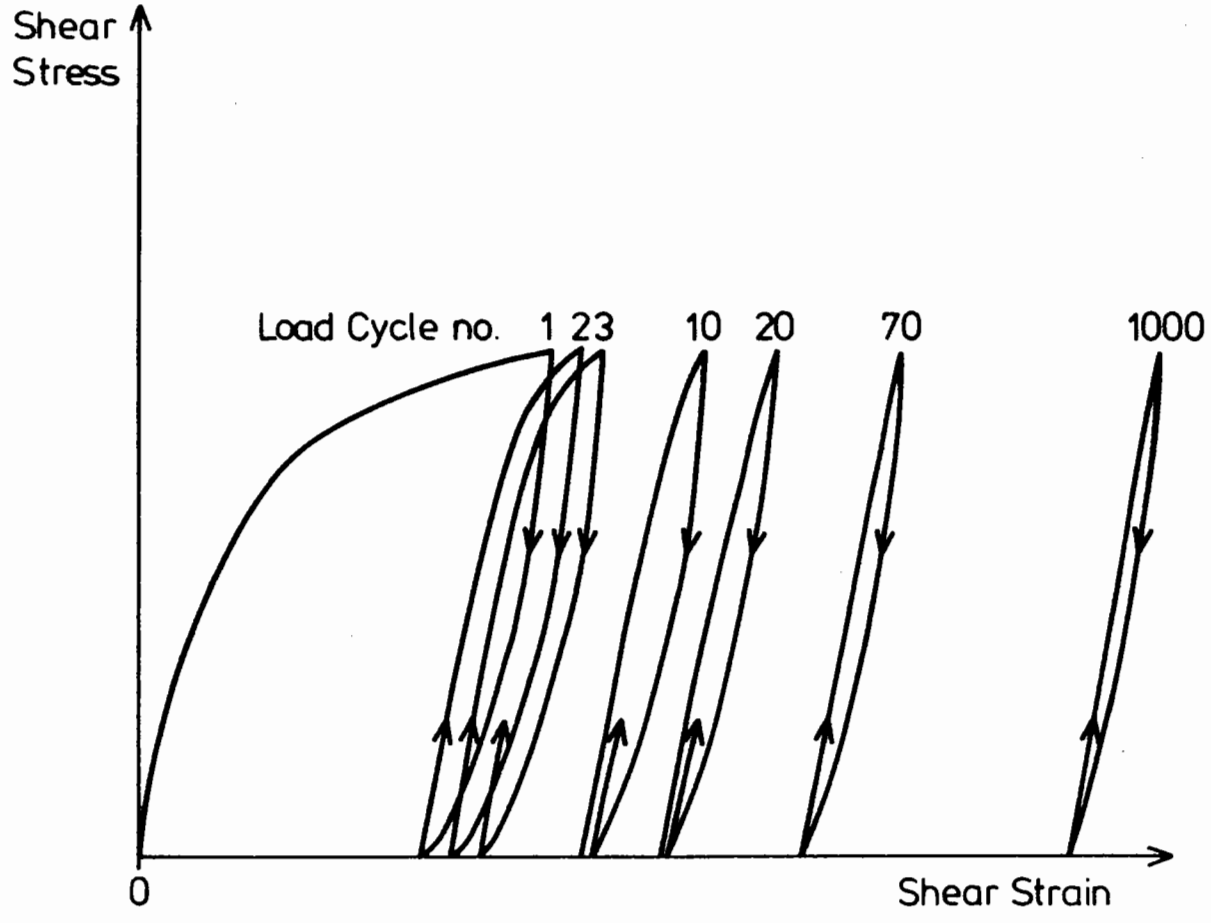

Fig. 2·1 Typical Granular Material Behaviour

The first of these, of course, includes the behaviour which would have been exhibited if the load had been allowed to increase to its peak value (where the material fails) instead of being subjected to repeated loading. This relationship, termed the monotonic loading curve, has been very extensively studied by geotechnical researchers over a number of years. It is the simplest area of study since no repeated load facility is required in the testing apparatus. However, in the case of a road foundation layer, it is clear that repeated loading is important and must therefore be applied in testing in connection with this project. This chapter will therefore examine briefly the different laboratory testing devices currently in use, explaining their capabilities, before proceeding to study the current state of knowledge of granular materials.

2.1 TESTING DEVICES AVAILABLE

From the example of granular material behaviour in fig 2.1 it can be seen that the properties are far from linear and that a sophisticated testing device is therefore desirable. The more independently controlled stress components which can be applied, the more complete will be the possible understanding of behaviour to be gained. However, the problems of strain measurement and general mechanical complexity may then become excessive.

The triaxial apparatus has, for years, been seen as a reasonable compromise. In it, a cylinder of material is subjected to two independently controlled stress components, a pressure acting in

every direction through a surrounding compressed fluid and a vertically acting additional load supplied down a central shaft. By means of these two components, confining stress and deviator stress, many simple loading situations can be effectively simulated. This project has made extensive use of two such triaxial facilities incorporating repeated loading capability and, because of their relative simplicity, they will probably continue to be used as a fairly standard research tool.

The limitations of the triaxial apparatus are evident in that only two stress components are varied independently out of a maximum of six for completely general conditions. Other relatively simple pieces of equipment are the shear box (eg Pike 1973) and simple shear apparatus (Roscoe 1953). Both of these also involve two independent stress components, basically shear and normal stress on a plane, and they can therefore be used in conjunction with the triaxial apparatus to increase the amount of information available on a particular material.

To control three or more components of stress is more complicated. The 'true triaxial apparatus' is one possibility, where two orthogonal horizontal stresses are independently applied, as well as a vertical stress, to a cube of material. However, the advance in terms of real situations satisfactorily simulated is not great. A significant improvement on this is the directional shear cell (Arthur et al 1977), a fairly recent innovation. This takes the form of a cube of material,

independently stressed in three orthogonal directions as for the true triaxial apparatus, but with the additional facility that shear stress can be applied horizontally to the vertical cube faces. This is achieved by sets of horizontal strands, attached to the membranes on the vertical faces. Thus, four independent stresses are applied, leaving out only two directions of shear. However, the specimen itself is then inevitably surrounded by a mass of mechanical equipment and the method used for strain measurement is to x-ray a grid of lead pellets embedded in the specimen at the time of its manufacture. Sensitivity is therefore greatly reduced and the apparatus is not suitable for small strain problems, such as that of a road.

Testing of specimens of a hollow cylindrical shape has been performed for many years on solids such as metals and concrete and also, occasionally, on soils and granular materials. However, interest has been growing and a machine for testing such specimens was constructed a few years ago at Imperial College, London (Hight et al 1983). Two gains are made by a hollow cylinder apparatus over a triaxial device. A confining stress and axial deviator stress can be applied in the same way, but it is also possible both to apply a torque to the cylindrical shape and also to vary the pressure in the centre of the cylinder from the external confining stress. Application of a torque generates shear stresses on horizontal and vertical planes in the wall of the cylinder, whereas variation of internal pressure imposes variation in circumferential stress much greater than variation in radial stress perpendicular to the wall. It is not quite true

to say that four stress components can be completely independently varied since the two horizontal stresses are tied to some extent, but it is nearly true. An advantage of this piece of equipment is that the specimen is still accessible and instrumentation can be directly attached enabling accurate strain measurement. A disadvantage is that some stress non-uniformity is inevitable, particularly when there is a difference between internal and external confining stress. These problems have been thoroughly investigated by Hight et al (1983) in connection with the Imperial College machine and it was found that, so long as the ratios of diameter to wall thickness and height to diameter were sufficiently large, such non-uniformities could be ignored.

Particularly because of the possibility of accurate small strain measurement, the hollow cylinder apparatus is clearly suited to the study of a granular material for pavement analysis. It is therefore fortunate that such a machine has recently been constructed at Nottingham University (O'Reilly 1985), with dimension ratios of an even more satisfactory nature than the Imperial College machine, and with the facility for repeated loading. It is described, as are the triaxial devices used in this project, in chapter 3.

2.2 MATHEMATICAL MODELLING - ELASTIC BEHAVIOUR

That part of the behaviour exemplified in fig 2.1 which has been most thoroughly explored in connection with road foundations is

the repeatable loop formed under cyclic loading. It has been found, in fact, that it is generally possible to return to a particular stress path at any stage in a test and see approximately the same repeatable loop.

Being repeatable, apart from a small accumulated permanent strain in each cycle, this is termed the elastic (or resilient) characteristic for that particular stress path. It is clearly non-linear and shows hysteresis. Nevertheless, it is common, and under certain circumstances quite acceptable, to use linear elastic theory as an approximation where the stress changes involved are relatively small. This may be true in a road foundation under a thick layer of stiff bitumen or cement bound material.

A much used and quite simple modification to linear elastic theory is usually known as the K-theta model (Hicks and Monismith 1971). In it the elastic modulus is related to the stress state according to a power law as follows:

$$E = K_1 \, \theta^{K_2} \qquad 2.1$$

where: E = elastic modulus

θ = the sum of any three orthogonal normal stresses

K_1 , K_2 are constants

This equation is quite successful in modelling the type of stress path in the triaxial apparatus where confining stress is held constant and deviator stress is cycled, but can give considerable error under other circumstances.

One feature of the elastic stress strain characteristic is the hysteresis loop, an indication that energy is being absorbed into the material, and one way of achieving such behaviour mathematically is by use of a damping ratio. This concept can cover more than one fundamental happening; it can relate to viscous fluid flow within a material, friction or even inertia, but by use of it a hysteretic behaviour results. Testing using a resonant column (eg Alarçon et al 1986) generally involves analysis using an elastic modulus and damping ratio, but it can usefully be employed in assessing hollow cylinder data also (Sousa and Monismith 1987). Mamlouk and Davies (1984) have developed a pavement analysis program specifically for assessing dynamic loading where a damping ratio is used for each pavement layer, including granular material.

The approach taken at Nottingham in the past has been to ignore the shape of the hysteresis loop and to consider a secant stiffness; ie the total strain between end points of a stress path, ignoring intermediate states. It has also been considered useful to separate behaviour into shear and volumetric components. Thus, equations have been developed, first by Boyce (1976) then by Pappin (1979), by which shear and volumetric

strain have been expressed in terms of the triaxial stress parameters. The equations relate to triaxial tests carried out on a carboniferous limestone road base material and those developed by Pappin are as follows:

$$\varepsilon_v = A\,\delta\left[p'^{B}\,(1 - C\,(q/p')^2)\right] \qquad 2.2$$

$$\varepsilon_s = D\,\delta\left[q/p'\right] \cdot \left(\sqrt{(p'_r{}^2 + q_r{}^2)}/p'_m\right)^E \qquad 2.3$$

where: ε_v, ε_s are elastic volumetric, shear strain

δ means 'change in'

p' = mean normal effective stress (confining stress + $\frac{1}{3}$ deviator stress)

q = axial deviator stress

subscript 'r' = 'repeated'; ie difference between maximum and minimum values

subscript 'm' = 'mean'

A,B,C,D,E are constants

Equations 2.2 and 2.3 have formed the basis for elastic material modelling at Nottingham since. Indeed they have found favour with other workers worldwide (Uzan 1985, Sweere et al 1987) and they form the starting point from which the present work has sought to develop. The basic components may be stated thus:

(a) Volumetric strain is non-linearly dependent on change in mean normal effective stress.

(b) Shear strain depends on change in a shear stress ratio.

(c) Volumetric strain has a dilatent term depending on shear stress ratio.

(d) Shear strain contains a stress path length dependency.

A simplification has been proposed by Mayhew (1983) to the shear strain equation on the basis of a series of triaxial tests on two materials. It takes the form:

$$\dot{\varepsilon}_s = A\,\delta\left[q.p'^{B}\right]$$

where: A, B are constants

Accuracy of prediction is undoubtedly reduced by this simplification, but the additional ease of computation generated may justify this.

O'Reilly (1985) used Pappin's equations and discovered that it was possible not only to predict the total shear strain for a given cyclic stress path, but also to satisfactorily predict the entire hysteresis loop. This represented a major piece of evidence to support the form of Pappin's model and would not be possible if Mayhew's simplification were accepted. However, it was not possible to do the same for volumetric strain without some amendment to the model. His technique will be referred to in section 4.2.

2.3 MATHEMATICAL MODELLING - PLASTIC BEHAVIOUR

Of the behaviour revealed by fig 2.1 both the monotonic loading curve and the accumulation of strain under cyclic load would come under the description of plastic behaviour. However, from the standpoint of road analysis, it is definitely the latter which is more significant and which is referred to here, although chapter 4 will suggest that the two are in fact linked.

Many researchers have noted the tendency of a granular material to develop plastic strain under repeated load and have observed some general trends. Barksdale (1972) has observed that the strain appears to accumulate according to the logarithm of number of load applications, but Brown (1974) reports that the strain rate can suddenly start to increase again, leading to failure. However, there is a lack of adequate modelling techniques currently in existence. Lentz (1979) also observed the logarithmic dependence of strain on number of cycles and developed an equation relating such plastic strain to the shape of the monotonic loading curve using a regression technique. Another approach is to postulate a movable plastic boundary to an elastic stress strain region (eg McVay and Taesiri 1985), allowing hysteresis and plastic strain development to be modelled.

At Nottingham, Pappin (1979) performed a few tests to investigate accumulated plastic strain and noted that, with one exception, all his shear strain results could be described using the same function of number of cycles. The equation he suggested was:

$$\varepsilon_{sp} = fn\ (N) \times l \times (q/p')^{2.8}_{max} \qquad 2.4$$

where: ε_{sp} = plastic shear strain

l = stress path length in p', q space

N = number of load applications

It may be seen that, besides the function, which was actually a power function, strain is related to the maximum value of a shear stress ratio achieved during the stress path and to the stress path length. Both these dependencies are fairly logical and the data was satisfactorily modelled by such means, except in one case where the strain accumulation rate began to increase to failure after a few thousand load applications. The modelling of the first one hundred cycles of load was also poor and therefore ignored, and no satisfactory way was found of predicting plastic volumetric strain.

Shaw (1980) suggested that the difference in mean normal effective stress p' between the point on the stress path closest to failure and the failure value was of critical importance, but his data was not sufficiently extensive to prove this.

2.4 PAVEMENT ANALYSIS

The most commonly used type of analysis in assessing pavements makes use of multi-layer linear elastic theory. This requires the provision of a constant Elastic Modulus and Poisson's Ratio for each pavement layer including granular base and subgrade, a clear source of inaccuracy. However, in situations where the granular layer is relatively insignificant it has been shown (eg Brown and Pell 1967) that such analysis can give quite good results. An example of this type of program is BISTRO (Peutz et al 1968).

One area of great disagreement between a linear analysis and observed fact can be seen at the base of a granular layer where tensile stresses are predicted horizontally, whereas it is well known that granular material is incapable of sustaining significant tension. Various techniques have been tried from the insertion of 'no tension' criteria (eg Doddihal and Pandey 1984) to layer subdivision, some of which have led to improvements in stress and strain prediction, but it has been understood for a long time that only total departure from linear theory will ever produce consistently realistic results. SENOL (Brown and Pappin 1982) was written with the aim of meeting this need. It is a finite element analysis program using non-linear bulk and shear moduli in the granular material. These moduli are based on equations 2.2 and 2.3 above which Pappin proposed. The results from SENOL are promising and show quite good correlation between measured and computed stresses and strains, although there are

still convergence problems if the unsurfaced condition is analysed.

Another program of the same type as SENOL is DIANA which is currently under development at Delft Technical University in the Netherlands (Sweere et al 1987). A rather different approach is taken by Barksdale et al (1982) whose program GAPPS7 is based on a slightly different set of stress strain equations, but also non-linear and realistic. He includes a capability for computing irrecoverable plastic deformation.

It is clear that the problem of accurate analysis of pavements including granular material is one that is still not completely solved. This is true of a purely elastic analysis, particularly for the unsurfaced condition, but is even more so for the problem of rut prediction.

CHAPTER THREE

APPARATUS DESCRIPTION

Since the majority of the work undertaken during this project was in the laboratory, this chapter is devoted to describing the major pieces of apparatus used. However, since much of the equipment was 'inherited' from previous researchers, reference will be made to earlier full descriptions and the various additions and modifications made during this project will be described in more detail.

3.1 TRIAXIAL APPARATUS

As mentioned in chapter 2, the triaxial apparatus has for years been the most important single device for investigating the stress strain characteristics of soils and granular materials, particularly in connection with repeated loading. A triaxial facility for repeated load testing of 150mm diameter specimens has been in use at Nottingham for over a decade and has been extensively used for this project. It was also decided, in the interests of speed, to use a 75mm diameter facility, making use of apparatus already in existence for the testing of fine grained soils, but amending the instrumentation. These two devices are described below.

3.1.1 150mm Diameter Facility

This machine was constructed in the mid 1970's at Nottingham for the purpose of testing granular materials. A detailed record may be found in Boyce (1976). It is capable of cycling both deviator and confining stresses. Fig 3.1 shows the general arrangement in some detail and Plates 1 and 2 are photographs of it.

Confining stress is applied through the medium of silicone oil and recorded by a pressure cell within the fluid. Cyclic loads are achieved by the use of a piston connected to a servo-hydraulic ram, the pressure being controlled by feedback from the pressure cell. A small correction is necessary at very low confining stresses for the difference in level between the centre of the specimen and the pressure cell, and also for the membrane stretched over the specimen.

Deviator stress is applied axially, again by means of a servo-hydraulic control system, through a loading ram incorporating a strain gauged load cell onto the top platen. Negative deviator stress is obtained by use of a shear pin connection at the top of the loading ram and sealed evacuated cavities between the top platen and the loading ram, and between the bottom platen and the mounting block. The load is maintained by feedback from the load cell. Again, minor corrections have to be applied for self weight of top platen and specimen and, also, for the area of the load ram shaft over which confining stress does not act. For cyclic loading a signal generator is used, allowing sinusoidal,

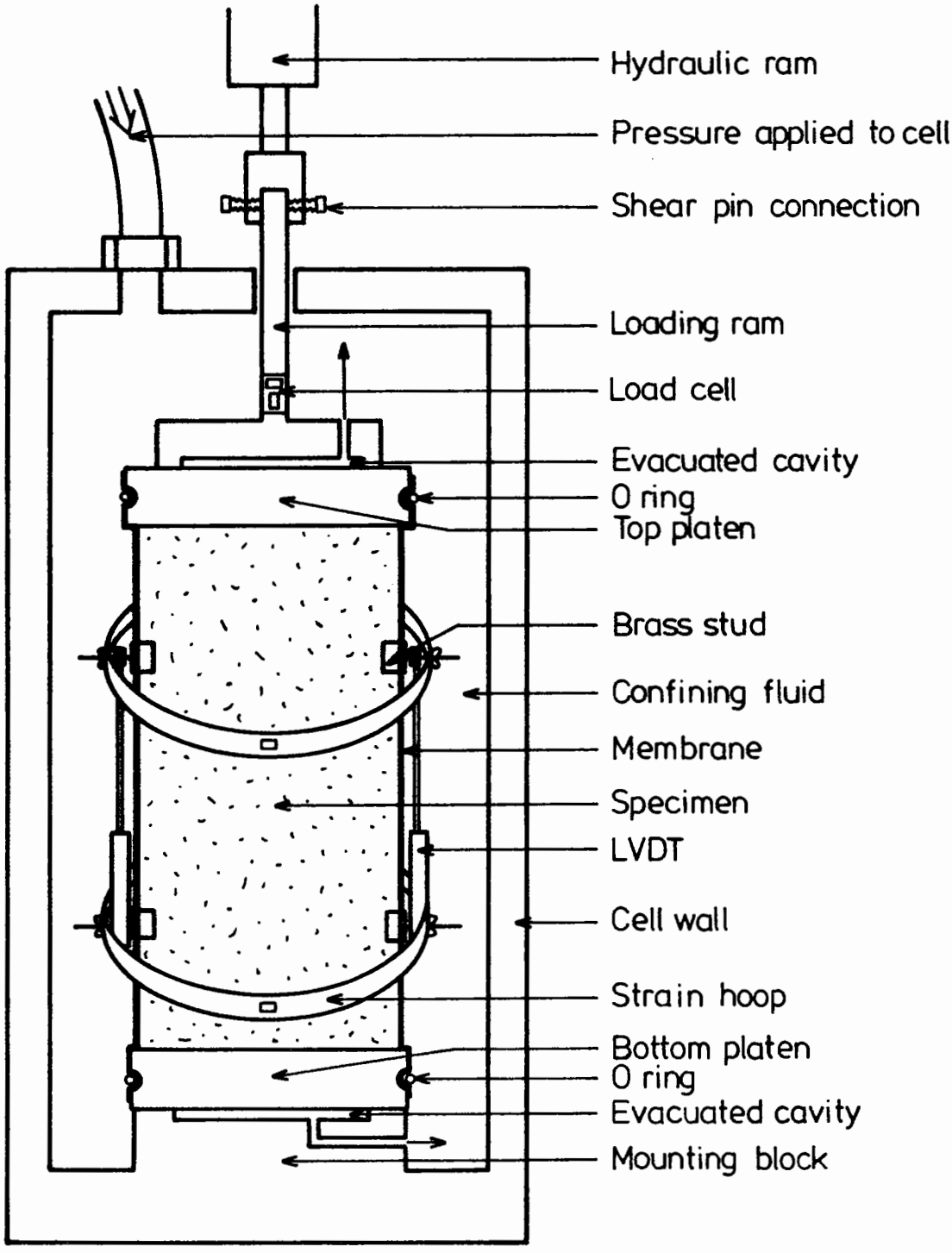

Fig.3.1 150mm Triaxial Facility

square or triangular wave forms of frequencies between .001Hz and 100Hz.

Deformation measurements are made from four brass studs embedded in the sides of the specimen during preparation and into which threaded rods are then screwed. The reason for this is that unquantifiable strains occur at each specimen platen interface and strain determination is therefore confined to the central portion of the specimen. Axial deformations are measured using linear variable differential transformers (LVDTs) mounted between the two pairs of threaded rods 150mm apart, one either side of the specimen to obtain an averaged strain. Radial deformations are given by araldite hoops incorporating strain gauges, also attached via the threaded rods to the brass studs. Two hoops are considered sufficient to give a good averaged strain.

Stress strain relationships are recorded on an x-y plotter through a device for automatically averaging the two axial and radial deformation readings and also combining them to give volumetric and shear strains directly. Sensitivity is of the order of 10 microstrain.

Pore pressure can also be measured by means of a strain gauged pressure cell situated outside the triaxial cell, connected through the base and a short copper tube to the bottom platen and thence to the specimen itself. To introduce water into a specimen, a tube from a reservoir of de-aired water can be

connected, through either the top or bottom platen. The reservoir can also be pressurized if desired to provide back pressure.

Specimen manufacture is achieved by compacting the material into a cylindrical mould of the appropriate size. Firstly a latex rubber membrane is attached by an 'O' ring to the bottom platen, then stretched up the inside of the mould and held at the top by a temporary extension piece. A vacuum applied through the wall of the mould ensures that the membrane lies flat against it. The brass studs described above will already have been attached to the membrane at this stage: they are made up of two pieces which screw together clamping the membrane between them. Once the mould is set up the material is placed and compacted, either using a vibrating table and small surcharge or, more commonly in this work, by hand tamping. Five layers are normally used. The extension piece is then taken off and the top platen attached, again using an 'O' ring to secure the membrane. The specimen can next be placed in the apparatus, a vacuum applied internally through one of the platens and the mould removed. It is commonly found that the process of compaction has punctured the membrane and it is therefore standard practice to add another at this stage to ensure no leakage. Finally the threaded rods and instruments described above are attached and the specimen is ready to be tested.

3.1.2 75mm Diameter Facility

This piece of apparatus (Plate 3) is very similar in principle to the larger one, differing in that there is no facility to cycle confining stress automatically. It makes use of a basic triaxial cell several of which have been used for a number of years in tests on clays (eg Overy 1982). Air is the confining medium and pressure is applied through a valve from a high pressure air line. Deviator stress is again applied by a servo-hydraulic system and monitored by a load cell.

Strain measurements are also similar. LVDT's are used over an 80mm gauge length and a smaller pair of strain gauged araldite hoops has been made to suit the smaller specimen size. The instruments are again connected to studs clamped to the membrane. Specimen manufacture follows the same pattern as above except that no second membrane has been found to be necessary.

3.2 HOLLOW CYLINDER APPARATUS

The Nottingham facility was designed by O'Reilly (1985) and he gives a full description of its design and construction. However, this project was the first to use it and some modifications have been made as a result of early experience with it. Also, the method of strain measurement was introduced under this project. A summary of its current specifications and initial use is given by O'Reilly et al (1987).

Plates 4 and 5 show the apparatus and instrumentation details. Fig 3.2 shows a cross-section through it and gives the dimensions and general loading arrangements. It is believed to be the largest repeated load device of its kind in the world at present. 'Confining stress', as applied to a triaxial specimen, is not possible since there is no external cell. Instead, a manually controllable vacuum is applied to the pores of the granular material through the bottom platen, giving an upper limit of about 80kPa. A port through the top plate enables the pressure in the central void to be varied either above or below atmospheric, thereby varying the circumferential stress far more than the radial stress, although some additional non-uniformity is set up. The axial and torque loading system consists of two servo-hydraulic actuators, one vertical, one horizontal and attached to a lever arm. Some redesign has been done, including the development of a new slip coupling (fig 3.3), allowing axial load and torque to be applied down the same shaft. The stroke of both actuators is 100mm, giving generous capacity for vertical straining but restricting the angle of twist of the top platen to $\pm$ 12^{o} which gives about $\pm$ 6% maximum torsional shear strain in the specimen.

Stress control is given by feedback from a load cell, situated immediately above the top plate. This has also been redesigned and is shown in fig 3.4. Tests have so far shown no interdependency between the axial and torque readings from the cell, although some drift is evident, requiring checking at

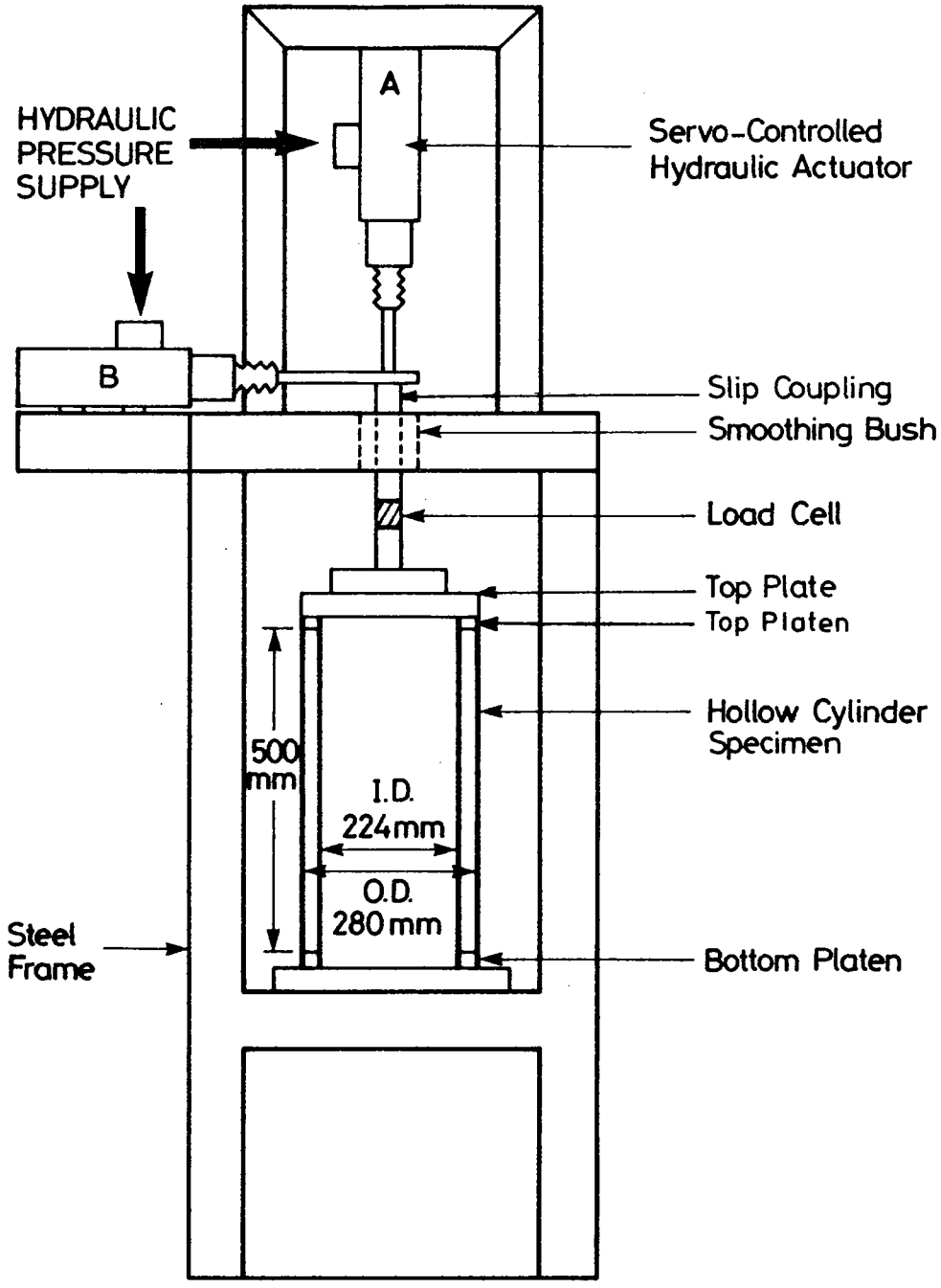

Fig. 3.2 Hollow Cylinder Apparatus -
Basic Arrangement.

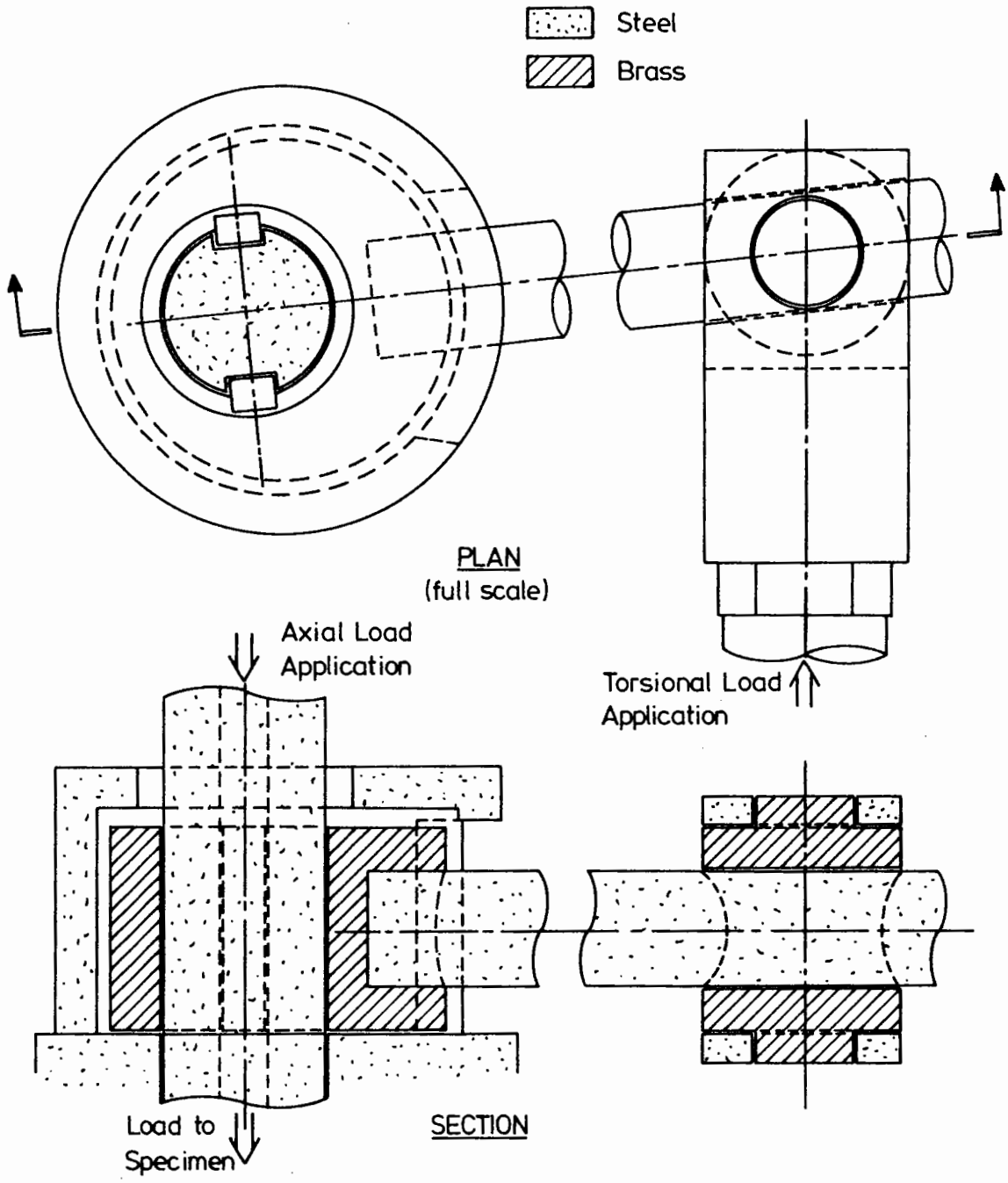

Fig. 3.3 Detail of Axial and Torsional Load Coupling

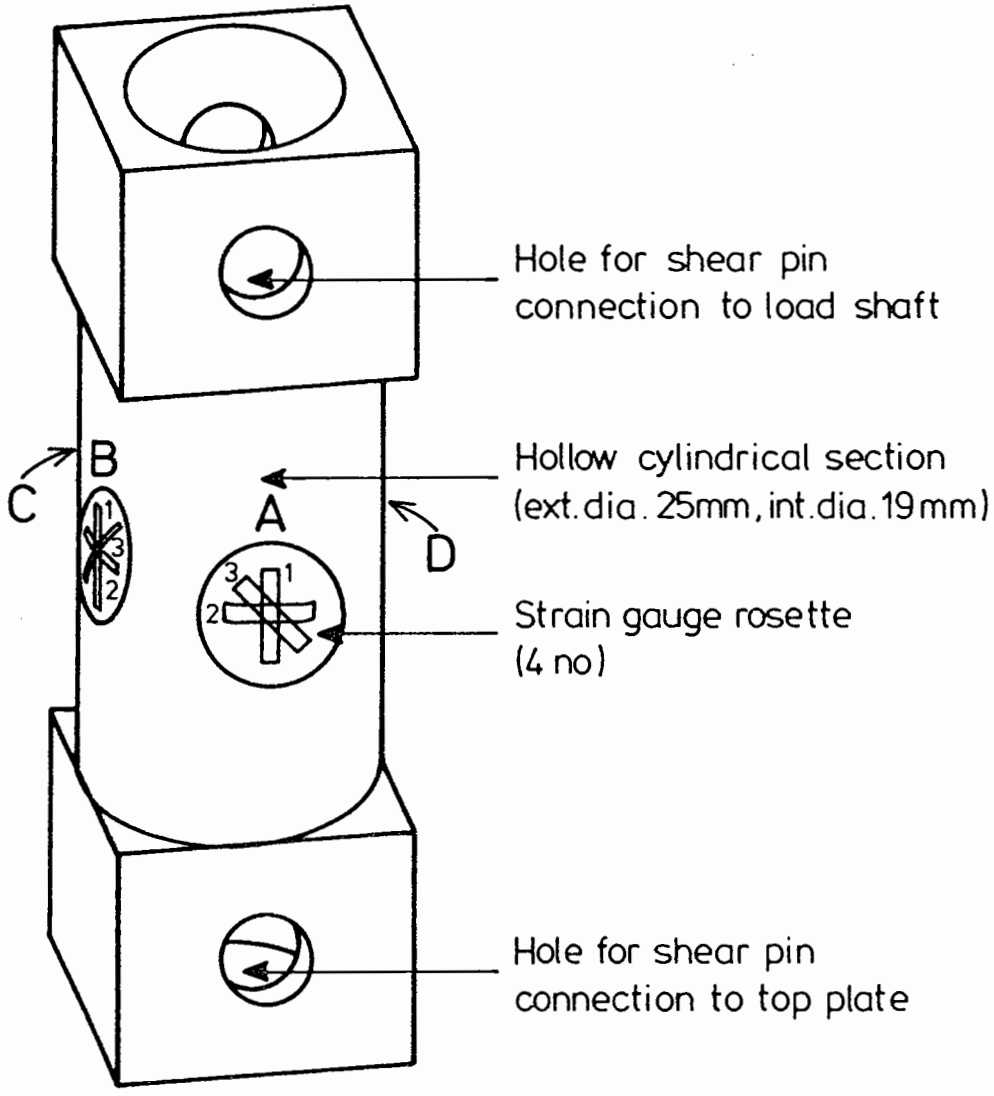

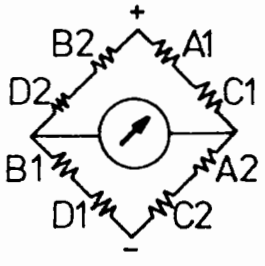

Axial Load Circuit

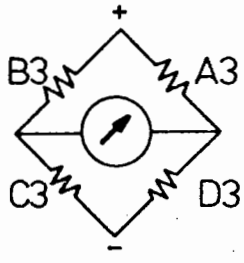

Torque Circuit

Fig. 3.4 Hollow Cylinder Load Cell

intervals during a test. The strain measurement system which has been devised makes use of the equipment already in use in triaxial testing. Again, brass studs are used, clamped to the membrane and embedded in the specimen on both internal and external faces. Circumferential strain, which is equivalent to the strain across a diameter, is measured by a pair of strain gauged araldite hoops mounted internally between studs at diametrically opposite locations. The two hoops are positioned 90^{o} apart so as to enable a reasonable average strain to be determined even if the specimen deforms in a rather irregular manner. Radial strain, ie variation in wall thickness, is measured by pairs of inductive strain coils, such as are also used for in-situ measurement in the ground (Brown and Brodrick 1977). The coils are glued to the inner and outer membranes at points immediately opposite each other and the current induced in one coil as a result of a larger AC current applied to the other depends on their separation. A maximum sensitivity of 25 microstrain is possible. Axial strain is measured by two external vertically mounted LVDT's with 150mm gauge lengths, on opposite sides of the specimen to allow for uneven straining. The remaining strain to be measured is the torsional shear which is given by two LVDTs mounted at 45^{o} to the vertical on the outside of the specimen using a 100mm gauge length. This 45^{o} strain contains components of vertical and circumferential which have to be subtracted to leave the torsional shear strain.

The system at present makes use of the same analogue control unit and signal generator as the 75mm diameter triaxial facility,

giving sinusoidal, square or triangular waveform output with variable phase difference between axial and torque stress. Data was generally recorded using an x-y plotter.

Specimen manufacture follows a similar principle to the triaxial case except that the shape is rather more complex. Outer and inner circular moulds form the shape of the specimen and membranes are attached to the bottom platen by 'O' rings, stretched up to the top of the moulds and held in position by vacuum in the case of the outer membrane. The material is then added and compacted by manual tamping using a large number of thin layers. Once complete, the top platen is placed in position and the two membranes stretched over it and clamped to it. The arrangement for attaching the inner membrane to both top and bottom platens is complicated, involving the tightening together of two conical faces with the membrane between them. Next, a vacuum is applied to the material through the bottom platen and the moulds are removed. The outer mould is in three segments which come apart; the inner mould has been designed to fold in on itself so that it can then be lifted out through the centre of the top platen.

This leaves the specimen in a state where the instruments can be attached, the top plate added and the loading shaft connected up for testing.

3.3 MINIATURE PAVEMENT TESTER

A description is included of this apparatus because it has been designed and built as part of this project although no useful results have yet been obtained. The theory behind it will be explained in chapter 5 (section 5.4.4), but the design brief was to construct a device such that a tenth scale wheel travelling at one hundredth of typical vehicle velocity could apply one tenth of the typical contact stress to a miniature pavement. In fact, the eventual solution (Plate 6) had four parallel wheels which could be individually loaded and an infinitely variable speed control up to a certain maximum value. The full scale quantities simulated and the scaled values used are shown in table 3.1.

The apparatus consists of a traveller, not unlike that of a gantry crane which runs on square box section rails at either side of the miniature test pavement. The general layout and some details are shown in fig 3.5. Drive is transmitted from an electric motor to one wheel on either rail and adequate grip is ensured by clamping against another small wheel along the underside of the rail. Microswitches are activated by the traveller at the end of each pass and the motor is reversed by a relay, allowing continuous operation. By these means a thousand passes can be achieved in just over an hour. A variable resistor allows the speed of travel to be controlled manually with an upper limit imposed by the relay reaction time in combination with an increasing tendency towards derailment at high speeds.

Table 3.1 Details of Miniature Pavement Tester Specification

Quantity	Full Scale	Miniature
Wheel Diameter	600 mm	60 mm
Load	10-60 kN	10-60 N
Contact Pressure	400-1000 kPa	40-100 kPa
Speed of Travel	0-30m/sec (67 mph)	0-0.3m/sec
Wheel Separation	1.5m	150mm
Length of Run	12m	1.2m

Decision:	Dimensions(d)	x	f	
Consequence:	Dead load stress	x	f	
	Other stresses(σ) (+pore pressures)	x	f	
	Areas(A)	x	f^2	
	Forces(F)	x	f^3	($F=\sigma A$)
	Permeability(k)	x	f^2	($k \propto A$)
	Water flow rate(Q)	x	f^4	($Q=kA\sigma/d$)
	Pulse duration(T)	x	$1/f$	($T=d^3/Q$)
	Velocity(v)	x	f^2	($v=d/T$)

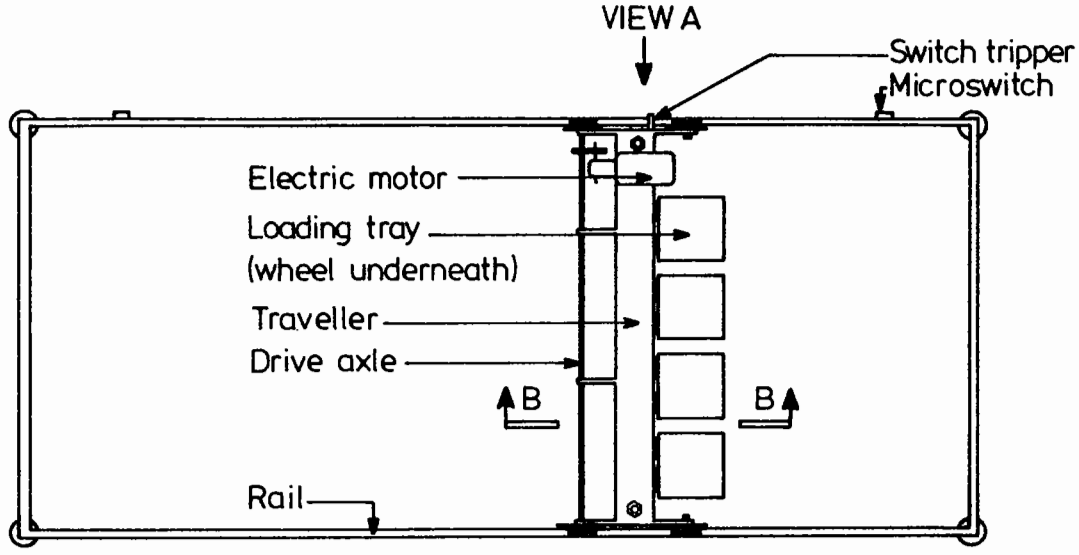

AERIAL VIEW
(12·5 : 1)

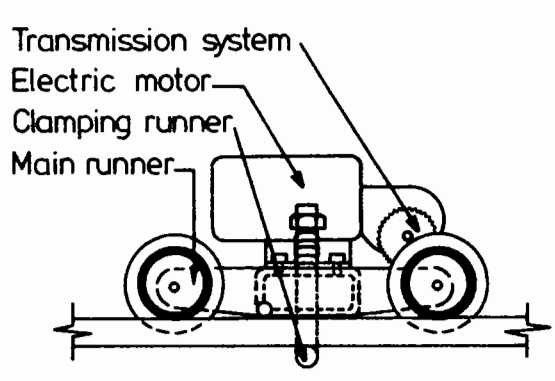

VIEW A
(5 : 1)

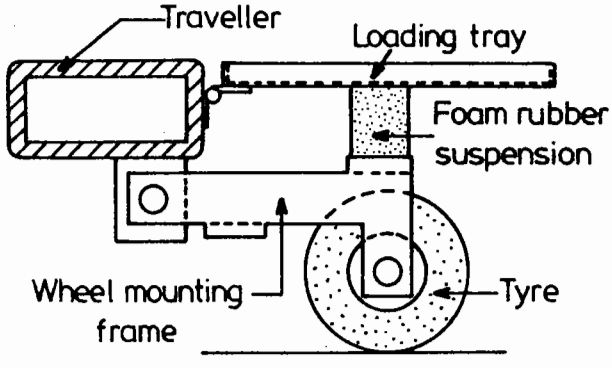

SECTION B-B
(2·5 : 1)

Fig. 3.5 Miniature Pavement Tester

The wheels which actually apply load to the pavement are attached to a mounting frame and connected by a hinge to the traveller, so that complete freedom of vertical movement is allowed. Load is applied in the form of weights placed on trays, also hinged to the traveller, and resting on a foam rubber suspension pad attached to the top of each wheel mounting frame. The suspension pad absorbs much of the potential shocks due to unevenness of the pavement. The wheels themselves consist of miniature rubbery plastic tyres on a machined metal hub with foam rubber compressed into the space between hub and tyre to simulate the effect of air pressurization. Although the pressure distribution may be somewhat different from that under a real tyre, the contact area was of approximately the desired size.

The apparatus has been commissioned; two miniature pavements consisting of various thicknesses and densities of 4 mm down crushed granite overlying clay have been constructed and tested to at least a thousand load applications. A problem was found initially in that, because of friction in the wheel bearings, the wheels acted as ploughs and created deep furrows in the granular material. The solution which has been adopted so far is to apply an emulsion paint to the surface, rather like a surface dressing, which absorbs horizontal friction forces because of its tensile properties, but transmits virtually all the vertical forces because of its flexibility. This has resulted in controlled rut development which has been observed to increase roughly according to the logarithm of the number of passes. This ties in with the

general observations of granular material behaviour made in section 2.3, and lends some confidence to use of the apparatus.

The potential for use is clear in that construction of a pavement is a relatively quick process. Four wheels allow either variation in applied load or pavement variation to be made and the useful pavement length (1.2m) allows at least three different sections to be tested at one time. So far, the only measurement which it has been possible to make is rut depth, but it may be possible to develop instruments of a sufficiently small size to record the accumulation of deformation below the surface also. Chapter 11 will refer to possible future use.

CHAPTER FOUR

DRY GRANULAR MATERIAL BEHAVIOUR

In order to make progress in understanding the behaviour and design of a granular road foundation, it is necessary to establish equations which realistically describe the mechanical properties which it exhibits. Several such equations have been referred to in chapter 2, all of which have their own particular advantages. Most have been derived from the results of triaxial tests. This project has had the benefit of the use of a hollow cylinder apparatus (ref. section 3.2) and it has, therefore, been possible to examine such equations in a new and very searching light.

As was mentioned in chapter 2, there are three areas of the mechanical behaviour of granular materials that require study; namely, elastic response, monotonic behaviour and accumulation of strain under cyclic loading. In this chapter, the latter two will be combined under the general heading of plastic behaviour (section 4.3) and will be discussed after a thorough examination of elastic modelling.

4.1 A NEW ELASTIC STRESS-STRAIN MODEL

When a granular material is straining, there are clearly several sorts of motion taking place, involving inter-particle slippage, rotation and possibly even fracture. However, this needs to be simplified. During elastic straining from one stress state to another, the particles change from being 'locked' in one position, in the first stress state, and rearrange themselves by translating and rotating slightly to become locked in a second position, in the second stress state. No large movements can generally be detected but, by means of this small rearrangement, stresses are transmitted along totally different lines through the material. Some contacts will have opened up slightly, some small gaps will have closed and now form stress transmitting contacts.

If all the particles were completely hard and rigid, then the situation described above would be dependent totally on its geometry. Two geometric properties can be seen as of possible significance; particle shape and surface roughness. The roughness clearly limits the amount of slippage between particles that can take place, while the general shape determines how well they can be packed together. Being purely geometric properties,

any constants governing resultant stress-strain behaviour would be dimensionless, and the relevant stress parameters would also have to be expressed as dimensionless quantities, presumably stress ratios. The equation proposed by Pappin (1979) governing shear strain is a relationship of this form, being expressed in terms of the ratio q/p (eq 2.3), although his equation for volumetric strain is not (eq 2.2). (Note: p will be used in this chapter rather than p' since the conditions considered are dry and the two are therefore identical). It is the belief expressed here that equations of this type, including dimensionless stress ratios, should form the core of any realistic stress-strain model for granular material, ie that the geometric properties of the material are of first importance; mineral stiffness is secondary.

However, it is undoubtedly not true that any aggregate particle can be considered as completely rigid. Therefore, the reasoning developed in the previous paragraph will require some qualification. If total rigidity were assumed and stress ratios were the only parameters permitted, then the strain in passing from stress state A to stress state B would be the same as that from stress state 2A (all stresses doubled) to 2B. The stress change in the latter case, however, is twice that in the former, meaning that the changes in all particle contact forces would also be twice as great. Of course, if rigidity is assumed, this is no problem but, if not, this will clearly result in different behaviour being observed for the two stress paths. It would seem

likely that a path involving greater stress change would allow more strain, since it would demand more particle deformation at the contacts. This, indeed, corresponds to the stress path length term which Pappin proposed in his elastic shear strain equation (eq 2.3), although none was included for volumetric strain.

The following sub-sections detail the development of a new elastic behavioural model for granular material, which is based on the above general ideas, together with evidence from laboratory testing.

4.1.1 Shear Behaviour

In the same way as has been done by several workers at Nottingham University (eg Boyce (1976), Pappin (1979)), it was decided to continue to separate strain into its shear and volumetric components, since it appeared to be both a successful and logical move. However, the problem which required addressing, when considering shear behaviour, was that of expressing it in a way suitable for use under completely general stress conditions. Two

alternative systems immediately presented themselves; that of stress and strain invariants, together with a set of angles to describe the directions of principal stress and strain and, possibly, a 'b value' (Symes et al 1984) to describe the intermediate principal stress; alternatively there was the system of normal and shear stresses and strains on a set of three mutually orthogonal axes. The former system has gained favour with a number of researchers involved in investigating general stress space, particularly principal stress rotation, and has allowed such concepts as the influence of the angle of principal stress rotation and the influence of the 'b value' to be explored (Symes et al 1984, Wong and Arthur 1985). Problems arise, however, in that the directions of principal stress and strain are not normally the same and any relationship taking this into account is likely to be very complex. The system of relating everything to a set of fixed orthogonal axes is simpler in concept but may, by its simplicity, lead to error. However, in the interests of simplicity, particularly in terms of application to computer analysis of a pavement structure, it was decided to pursue the 'fixed axes' system and to check its viability.

Early results from the hollow cylinder apparatus gave encouragement when the following two points were noticed in relation to elastic strain.

(a) Triaxial shear strain, that is vertical strain less horizontal strain, responded to changes in the triaxial stress parameters of confining stress and axial deviator stress as expected. However, any shear stress superimposed on horizontal and vertical planes (due to torsional loading), whether static or varying, had a seemingly negligible effect on the triaxial shear strain, although it did, of course, induce shear in other directions.

(b) Shear strain within the 'plane' of the wall of the specimem appeared completely unaffected by the magnitude of the out-of-plane principal stress.

These results came from early tests on Mid-Ross sand, involving a very limited programme and at a stage when the apparatus was suffering from a number of minor electrical problems, resulting in poor stress control. No numbers are, therefore, included at this stage, simply the two above observations.

If observation (b) is valid then it is necessary to develop in-plane stress parameters, rather than to use p and q, which take account of out-of-plane stresses. Yet, it is clear that the equation proposed by Pappin, using the ratio q/p, has been shown to give quite acceptable results and, indeed, is now used by other researchers. Any new parameter should not, therefore, differ greatly from q/p under triaxial conditions.

Stresses within a plane can be conveniently represented by use of a Mohr Circle plot. Fig 4.1 shows a typical in-plane stress state in this way, where σ_1 and σ_3 are principal stresses. Each point on the circle represents the shear and normal stresses in a particular direction. Now, for the case of triaxial stresses and strains, the direction of maximum shear strain is constrained to coincide with the direction of maximum shear stress represented by point A in fig 4.1. Therefore, the shear stress ratio t/s (see fig 4.1), relating to that direction, might be considered a useful dimensionless parameter, or possibly 2t/s to give a direct comparison with q/p. However, it was noticed that use of this parameter gave significant underestimates of shear strain at high stress ratios, ie near failure.

Considering fig 4.1 again, although point A represents the direction of maximum shear stress, it does not represent the maximum shear stress ratio. Also, although maximum shear strain occurs in the same direction as for stress, there is shear strain occurring in every other direction except on the principal axes. It was, therefore, decided to obtain a parameter by averaging the shear stress ratios around a Mohr Circle. Such a parameter could therefore be written:

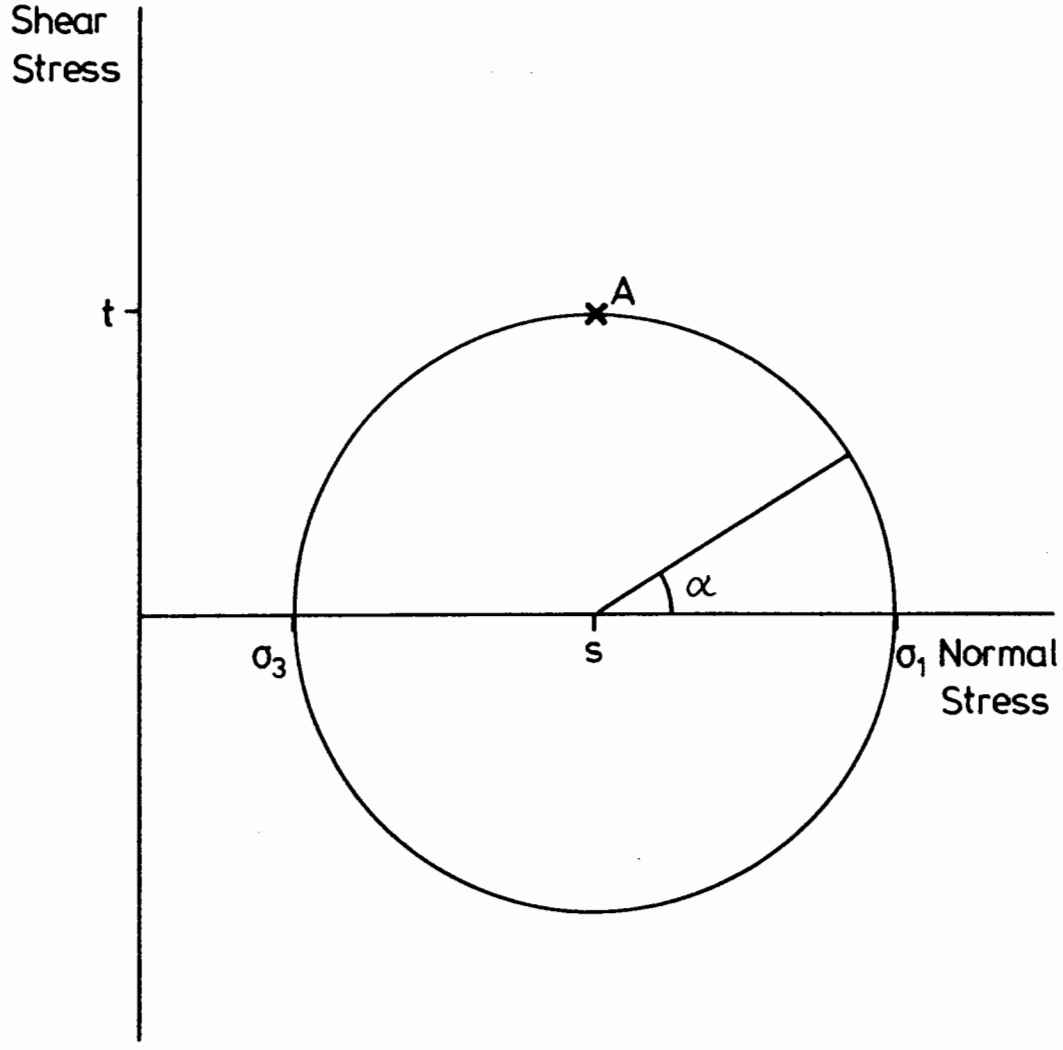

Fig. 4.1 Mohr Circle of Stress

$$\text{Shear parameter} = \int_0^{\pi} \frac{t.\sin\alpha}{s+t.\cos\alpha}\, d\alpha \qquad 4.1$$

$$= \left[- \ln (s + t.\cos\alpha) \right]_0^{\pi}$$

$$= \ln \frac{s + t}{s - t} \qquad 4.2$$

$$= \ln \frac{\sigma_1}{\sigma_3} \qquad 4.3$$

To illustrate the difference between the above parameter and the others considered, ie q/p and 2t/s, fig 4.2 maps out their respective values on a p,q plot, assuming triaxial stress conditions. The following points can be drawn from the figure:

(i) All three parameters give similar values at low stress ratios.

(ii) The $\ln (\sigma_1/\sigma_3)$ parameter generally lies between the other two except at high stress ratios where it begins to exceed q/p. The 2t/s parameter is consistently lowest, particularly so at high stress ratios.

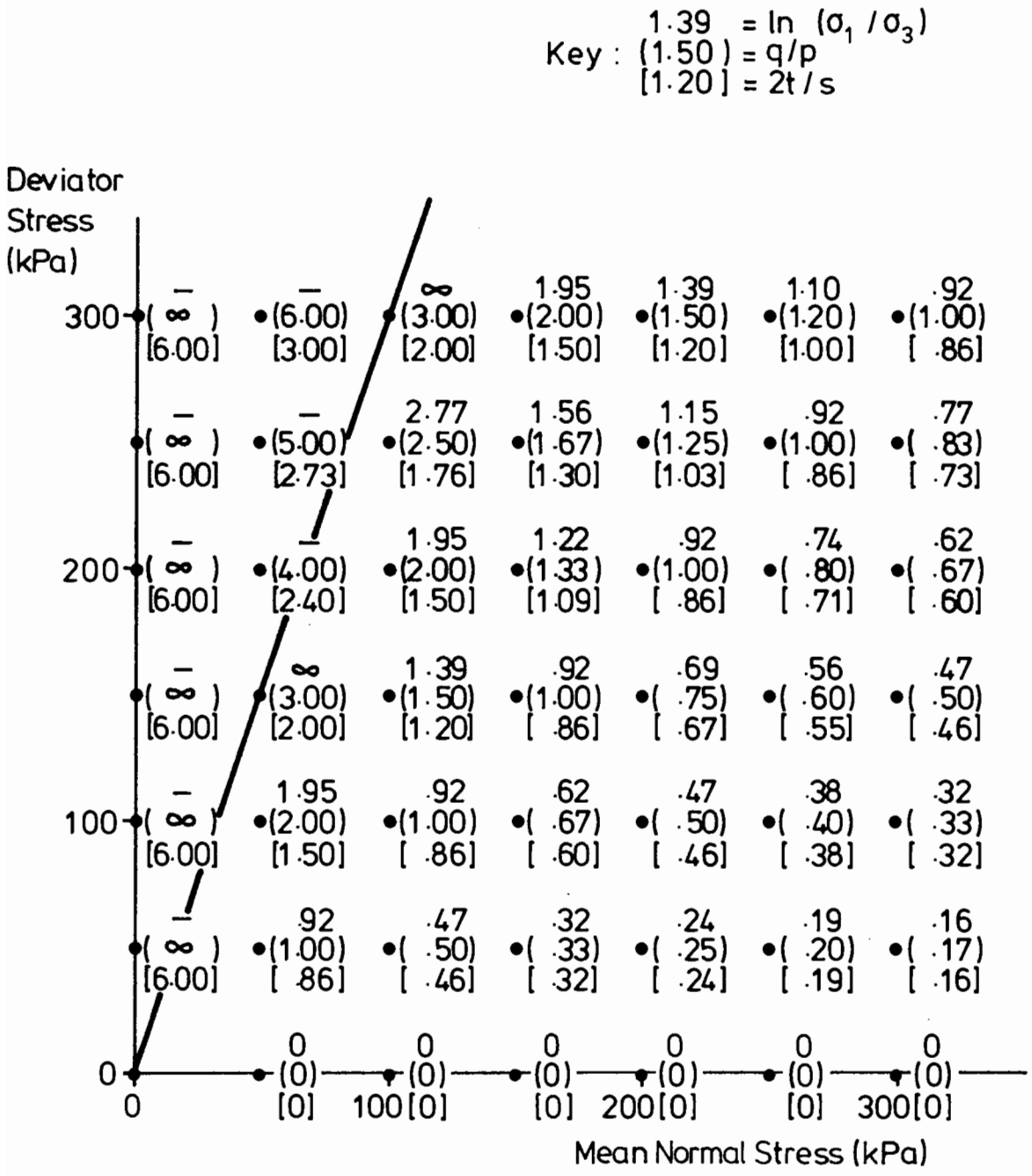

Fig. 4.2 Comparison of Shear Stress Parameters

(iii) The $\ln(\sigma_1/\sigma_3)$ parameter tends to infinity as the 1:3 line is reached; ie the line where σ_3 passes from compressive to tensile. Both the other two give finite values with tensile σ_3.

From the above comparison it may be stated with confidence that use of $\ln(\sigma_1/\sigma_3)$ as a shear stress parameter will not generate very different results from use of q/p under triaxial conditions. It fulfils the requirement of being an in-plane parameter and appears more realistic than 2t/s. It also has the logically desirable property of indicating infinite strain as an impossible tensile stress state is reached. It has, therefore, been chosen for inclusion into the new elastic shear strain model.

So far, discussion has centred on triaxial conditions. However, the Mohr Circle in fig 4.1 could just as easily represent conditions of simple shear, simulated in the hollow cylinder apparatus by application of torsional load with zero axial deviator stress. Point A then represents the situation on a horizontal plane, and eq 4.2 can be used for the appropriate shear stress parameter. Now, according to observation (a), earlier in this section, torsional loading has negligible influence on triaxial shear, even though the vertical and horizontal stresses may no longer be principal. It may,

therefore, be permissible to superpose the effects of triaxial and torsional loading, treating each as if the other did not exist. The only exception would be if triaxial loading altered the value of 's' in eq 4.2 for the torsional shear stress parameter. Thus, two separate equations might be written for shear in a plane relative to fixed axes, say x and y, as follows:

$$\varepsilon_x - \varepsilon_y = \text{fn}\ (\ln(\sigma_x/\sigma_y)) \qquad 4.4$$

$$2\,\gamma_{xy} = \text{fn}\ \left(\ln \frac{s_{xy} + t_{xy}}{s_{xy} - t_{xy}}\right) \qquad 4.5$$

where:

σ_x, σ_y are normal stresses in directions x and y

$s_{xy} = (\sigma_x + \sigma_y)/2$

t_{xy} is the shear stress perpendicular to directions x and y

$\varepsilon_x, \varepsilon_y$ are strains in directions x and y

γ_{xy} is the shear strain relating to the direction of t_{xy}

The function (fn) in equations 4.4 and 4.5 will be the same.

This system for dealing with shear means that, under general stress conditions, there will be six separate senses of shear to consider, two in each of three orthogonal planes. Such a system lends itself to computational procedures where a fixed grid of points or elements is being considered.

The next questions to answer are: firstly, the nature of the function in equations 4.4 and 4.5 and, secondly, the form of any additional elements to take account of stress path length, which Pappin observed to be significant. Fig 4.3 shows the results for shear strain from a triaxial test on a specimen of crushed dolomitic limestone. Several stress paths were applied and all the results shown relate to paths with constant confining stress and cyclic axial deviator stress. As can be seen, each point plotted relates shear strain to change in the shear stress parameter $\ln(\sigma_1/\sigma_3)$ and the scales used are logarithmic. It is evident that, in the main, the points lie neatly on a set of parallel straight lines, distinguished by the magnitude of deviator stress change δq and that, in this case, the lines are at 45°, implying a linear relationship. Closer inspection also reveals that lines relating to deviator stress changes a factor of two different from each other (eg 50 and 100, 150 and 300) are approximately equally spaced, implying that the multiplier in such a linear relationship is proportional to a power of deviator stress change. In fact, an equation of that form describing the results is given in the insert on fig 4.3.

However, fig 4.3 relates to triaxial conditions and to one sort of stress path. In general, this research has found that the relationship between shear strain and the shear stress parameter $\ln(\sigma_1/\sigma_3)$ is not necessarily linear; it may require a power which could be either more or less than one. It has also been

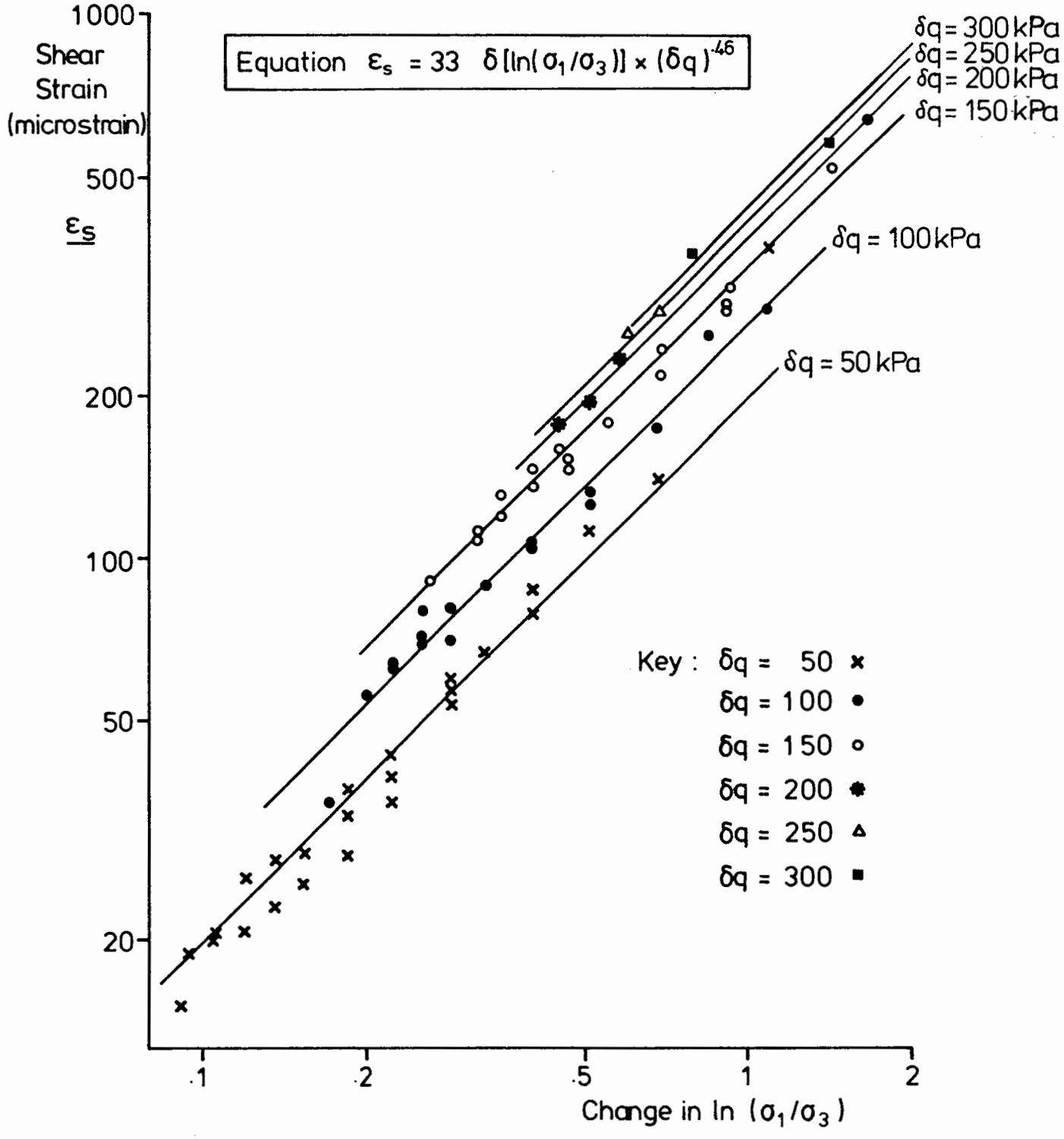

Fig. 4.3 Shear Strain Results - Crushed Dolomitic Limestone

found that the stress path length should not only take account of shear stress change, as by using δq but also normal stress. This, indeed, was recognized by Pappin in the form of his stress path length factor. From an empirical rather than theoretical standpoint, observations have led to the use of $\delta t + \frac{1}{3}\delta s$ as a seemingly appropriate stress path length for shear. Under more general stress conditions this stress path length term will be different for the two shear terms in eqs 4.4 and 4.5. The δs part will be the same, but the δt will be that which is appropriate to each component of shear, as if the other component was not there, in just the same way as was proposed for the two shear stress ratio parameters. Thus the two equations, relative to fixed axes x and y become:

$$\varepsilon_x - \varepsilon_y = A.\left[\delta \ln(\sigma_x/\sigma_y)\right]^B . \left[\tfrac{1}{2}\delta(\sigma_x-\sigma_y) + \tfrac{1}{6}\delta(\sigma_x+\sigma_y)\right]^C \quad 4.6$$

$$2\gamma_{xy} = A.\left[\delta \ln \frac{s_{xy} + t_{xy}}{s_{xy} - t_{xy}}\right]^B . \left[\delta t_{xy} + \tfrac{1}{6}\delta(\sigma_x+\sigma_y)\right]^C \quad 4.7$$

where: σ_x, σ_y, s_{xy}, t_{xy}, ε_x, ε_y and γ_{xy} are as defined for eqs 4.4 and 4.5.

A, B and C are material constants

δ indicates 'change in'

The stress path length components required are actually the absolute values, since a negative stress path length has no meaning.

The above equations appear complex, but, when it is recognized that three constants are sufficient to predict elastic shear movement under the most general stress conditions, then it may be seen that, for solutions to complicated problems, these equations allow very simple computation. However, a knowledge of shear strain is not sufficient on its own and the following sub-sections develop a model for volumetric stain on similar lines.

4.1.2 Volumetric Behaviour (Isotropic)

In this sub-section, it is elastic volumetric straining under purely isotropic stress conditions that is considered; ie no shear is taking place. Under such conditions there is clearly only one stress parameter to vary and that is mean normal stress p. In the equation proposed by Pappin (eq 2.2), it was variation in p taken to a power less than one that was used to describe the behaviour. However, if the desirability of a non-dimensional stress parameter, proposed earlier, is pursued, then it is necessary to develop a rather different equation.

If the stiffness, or ratio of stress change to strain change, is dependent on the level of stress, p, then an equation of very general form may be written as follows:

$$\varepsilon_v = \text{fn}\ (p).\ \delta p$$

where: ε_v = volumetric strain

If a non-dimensional format were to be a requirement, then the function fn (p) would have to become A/p, where A is a constant, and the equation could then be written:

$$\varepsilon_v = A\ \delta p/p$$

integrating between states i and j:

$$\varepsilon_v = A \int_i^j \frac{1}{p}\ dp$$

$$\varepsilon_v = A \ln (p_j/p_i) = A\ \delta \ln p \qquad 4.8$$

The train of reasoning leading to equation 4.8 is based solely on an over-riding requirement for a non-dimensional format to be observed, which may, of course, be an erroneous step. Fig 4.4 is therefore included, showing the results of a series of thirteen isotropic stress paths, performed in a triaxial apparatus on a specimen of crushed dolomitic limestone. The stress parameter $\ln(p_j/p_i)$, or $\delta \ln(p)$, is plotted against volumetric strain on logarithmic scales. The points can be represented by a series of parallel straight lines, distinguished by the absolute magnitude of stress change δp, in much the same way as in fig 4.3 for shear strain. In fact, the lines can be described using an equation of very similar format to that shown on fig 4.3, and the equation is included in the insert to fig 4.4. In general terms, it is of the form:

$$\varepsilon_v = A\ (\delta \ln p)^B .\ (\delta p)^C \qquad 4.9$$

where: A,B and C are constants (not those in eq. 4.6 and 4.7).

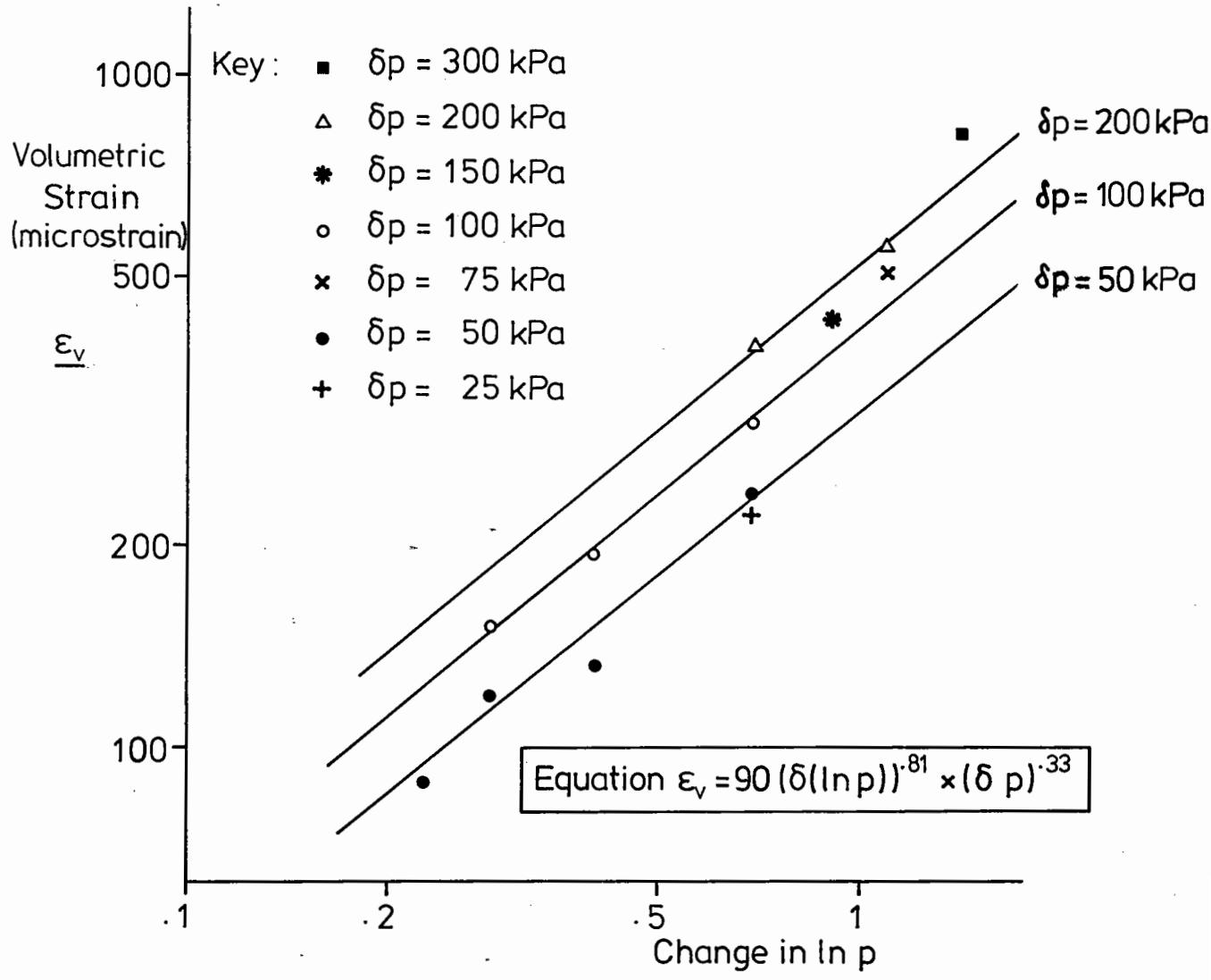

Fig. 4.4 Volumetric Strain Results - Crushed Dolomitic Limestone

Further evidence will be presented in section 4.2 for the validity of this equation but, at this stage, it is sufficient to say that it both fits the desired format of a non-dimensional term with a stress path length factor and also appears to fit the data so far.

4.1.3 Volumetric Behaviour (with shear)

Conditions of stress are not, of course, usually isotropic and it is common knowledge that, as a granular material shears, it generally dilates; that is, it exhibits negative volumetric strain. This fact was recognized by Pappin (eq 2.2), who amended his volumetric stress parameter accordingly, using $(q/p)^2$ as the appropriate shear parameter. The logic behind this squared term can be seen in that it allows positive and negative shear to have the same effect on volumetric change. It has also been shown by Pappin to give reasonably good results under triaxial stress conditions.

In this research it was decided to separate out the volumetric strains due to change in mean normal stress and those due to shearing action, summing two equations to obtain the overall volumetric strain. The approach taken was, therefore, to compute

constants pertaining to the equation for isotropic stress conditions and, then, to use that equation to work out a set of theoretical volumetric strains for stress paths including non-zero shear. The difference between actual measured volumetric strain and the theoretical was then taken to be due to shearing action. This procedure was followed for the results from the specimen of dolomitic limestone referred to earlier. Since Pappin had used $(q/p)^2$ successfully in modifying his equation, it was decided to make use of the square of the shear stress parameter $\ln(\sigma_1/\sigma_3)$ in forming a new equation for volumetric strain due to shearing action. Fig 4.5 shows a plot of dilatent volumetric strain against change in $(\ln(\sigma_1/\sigma_3))^2$ for the dolomitic limestone, again plotted on logarithmic scales.

There is certainly more scatter in these results than was apparent in figs 4.3 and 4.4, probably because the difference between two numbers is being plotted. However, they tend to lie on a line, and there appears, in this case, to be no stress path length dependency. The equation of the line is given in the insert to fig 4.5. Given the combined uncertainties of strain measurement and the isotropic strain model, it is considered that fig 4.5 demonstrates a reasonably firm relationship between the component of volumetric strain due to shear and the suggested parameter $\delta\ (\ln(\sigma_1/\sigma_3))^2$. The absence of any stress path length

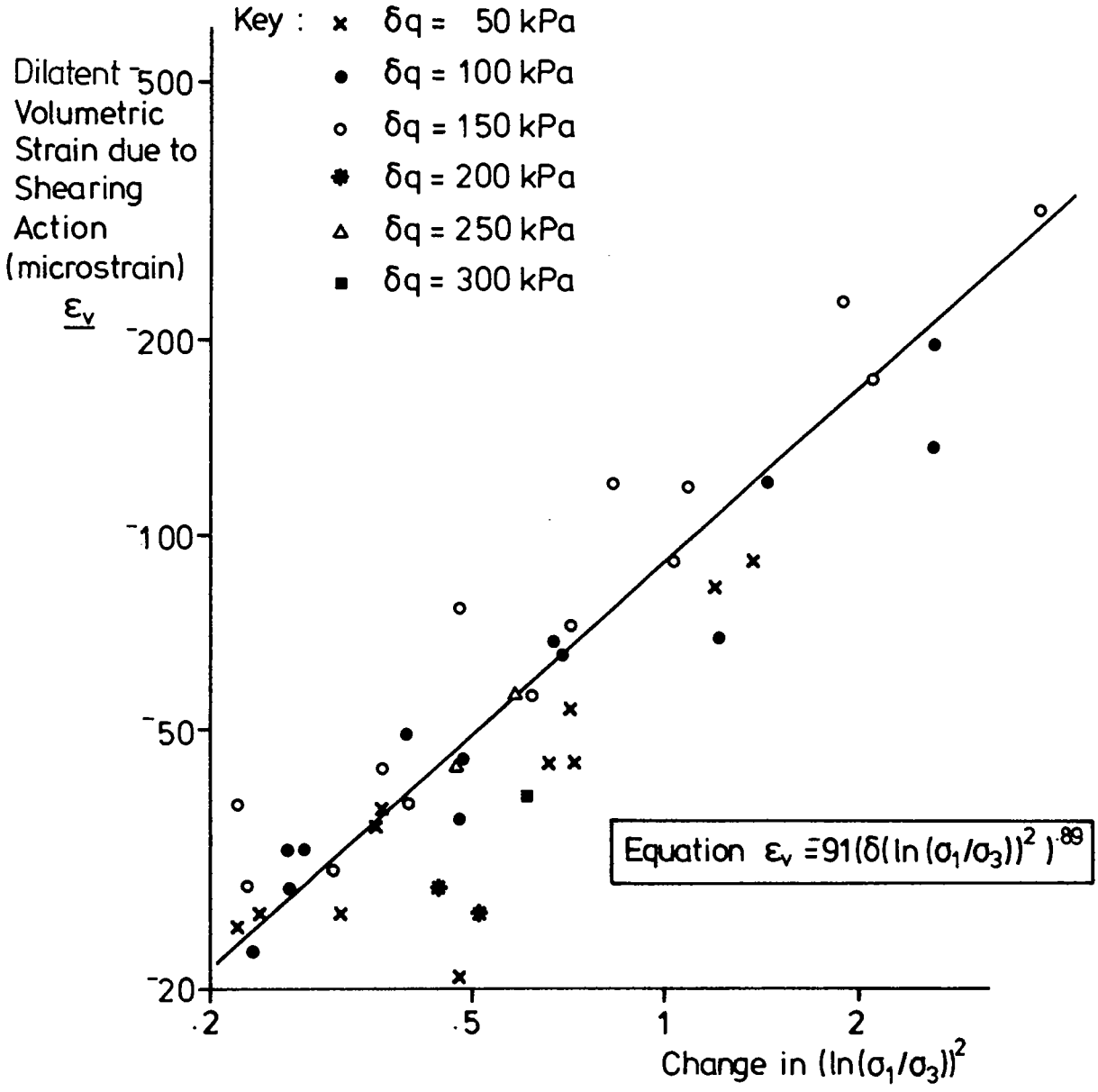

Fig. 4.5 Volumetric Strain due to Shearing Action - Crushed Dolomitic Limestone

dependency appears to be a usual but not invariable feature. The full elastic volumetric strain equation for triaxial conditions thus becomes:

$$\varepsilon_v = A\ (\delta \ln p)^B \cdot (\delta p)^C - D(\delta((\ln(\sigma_1/\sigma_3))^2))^E \qquad 4.10$$

where: A,B,C,D,E are constants

To extend eq 4.10 to more general stress conditions, it was necessary to study results from the hollow cylinder apparatus, where it appeared that the correct course of action was to sum components of volumetric strain due to each 'sense' of shear. There would, therefore, in general stress space be six components, made up of two from each of the three orthogonal planes, in the same way that shear itself was split into six components. Eq 4.10 would be rewritten:

$$\varepsilon_v = A\ (\delta \ln p)^B \cdot (\delta p)^C - D \sum_i^6 (\delta((\ln \frac{s + t}{s - t})^2))^E \qquad 4.11$$

This, then, is the general volumetric strain equation proposed here as part of a new elastic stress-strain model, together with the shear equation developed in sub-section 4.1.1. Only limited

evidence has so far been presented to demonstrate the suitability of the model, but this will be corrected in section 4.2, where it is compared with Pappin's equations and also with the $K\theta$ model (see section 2.2). In potential, it has the advantage that it is designed to cover every possible stress condition, whereas Pappin had to apply corrections to his equations, first to take account of triaxial extension space and then to cater for general conditions. It is also of a form convenient to use in computer analysis. The following section will attempt to demonstrate its predictive capabilities.

4.2 ELASTIC BEHAVIOUR - CORRELATION WITH LABORATORY TEST DATA

Having discussed the theoretical reasoning behind the choice of stress-strain model in the previous section, evidence is now presented to test its accuracy against other models currently in use. The data used here comes from two laboratory testing devices, the triaxial apparatus (described in section 3.1) and the hollow cylinder apparatus (section 3.2), together representing the limit of present capabilities in element testing.

4.2.1 Triaxial Data

In his research, Pappin tested his behavioural model for dry carboniferous limestone against an extensive series of stress paths from the repeated load triaxial apparatus, giving reasonably good agreement between measured and predicted values. As an initial check on the model developed in this thesis, it was, therefore, considered appropriate to compare its performance with Pappin's using the same data. Parameters were, therefore, chosen to fit the data as well as possible, resulting in the following equations:

$$\varepsilon_v = 80\ \delta(\ln p).\ \delta p^{.31} - 84\ \delta((\ln(\sigma_1/\sigma_3))^2)$$

$$\varepsilon_s = 82\ (\delta(\ln(\sigma_1/\sigma_3)))^{1.37}.\ (\delta t + \tfrac{1}{3}\delta s)^{.25}$$

where: ε_v, ε_s, p, σ_1, σ_3, s, t and δ are as already defined.

Fig 4.6 is a diagram in p,q space of the stress paths covered. The same 'net' of paths was applied, with minor variations, at five different levels of 'average' mean normal stress, as shown. Since the paths lie at various angles, extend into both triaxial extension and compression space, and cover a wide range of mean normal stress levels, it is considered that the fullest possible range of straight line paths has been explored.

Fig 4.7 is a plot of predicted against measured volumetric strain; it shows the predictions both from the new model and from Pappin's model. The two are clearly of comparable accuracy and, in fact, the standard deviations of the predictions about the measured values are 25.7 microstrain (new model) and 33.2 microstrain (Pappin), giving a slight advantage to the new model. Similarly, fig 4.8 shows the shear strain results, where shear strain is defined as two thirds the difference between axial and radial strain, according to strain invariant theory, as used by Pappin. Again, very similar levels of accuracy are achieved. The standard deviations are 21.7 microstrain (new model) and 22.8 microstrain (Pappin).

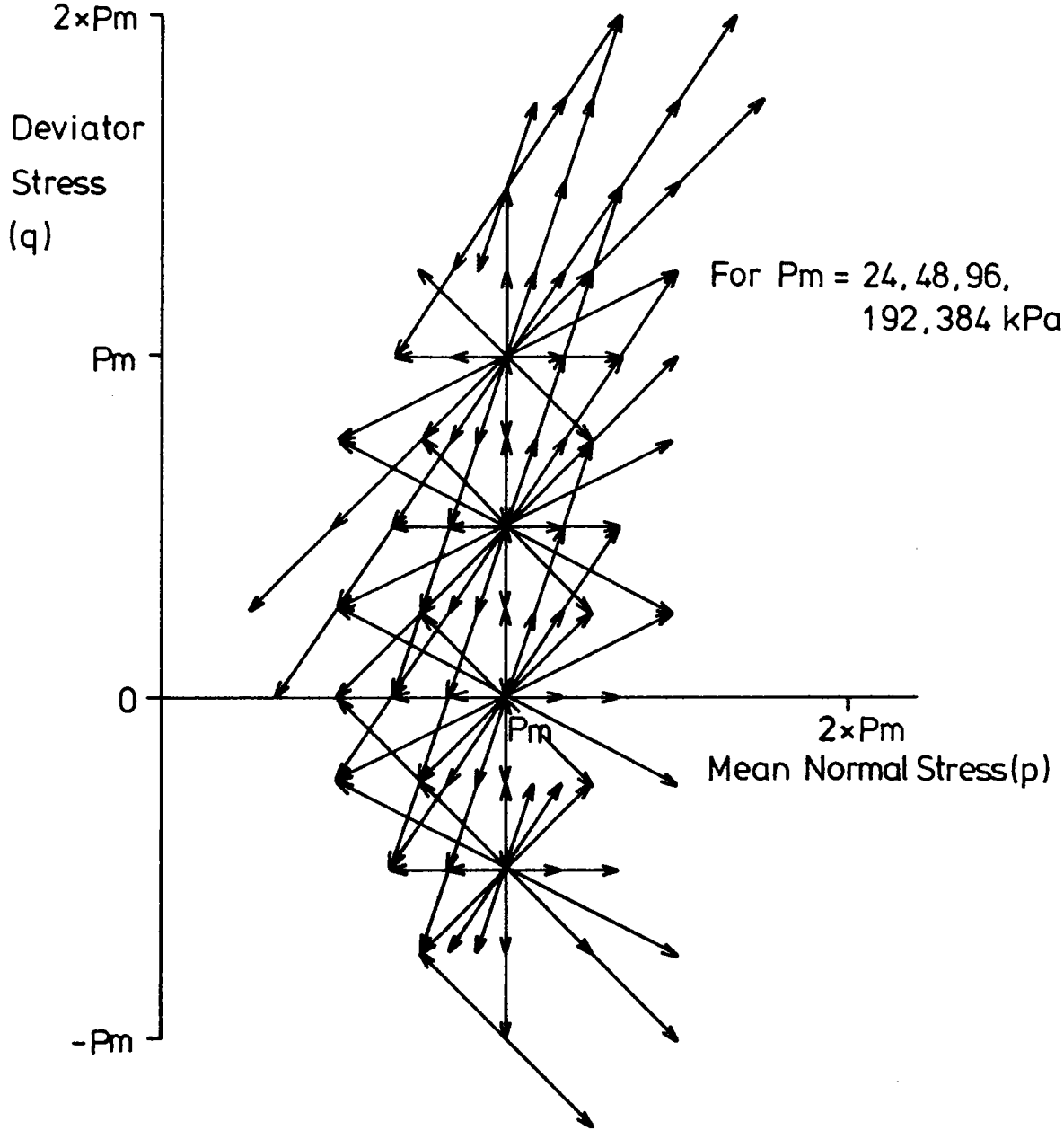

Fig. 4.6 Stress Paths used by Pappin

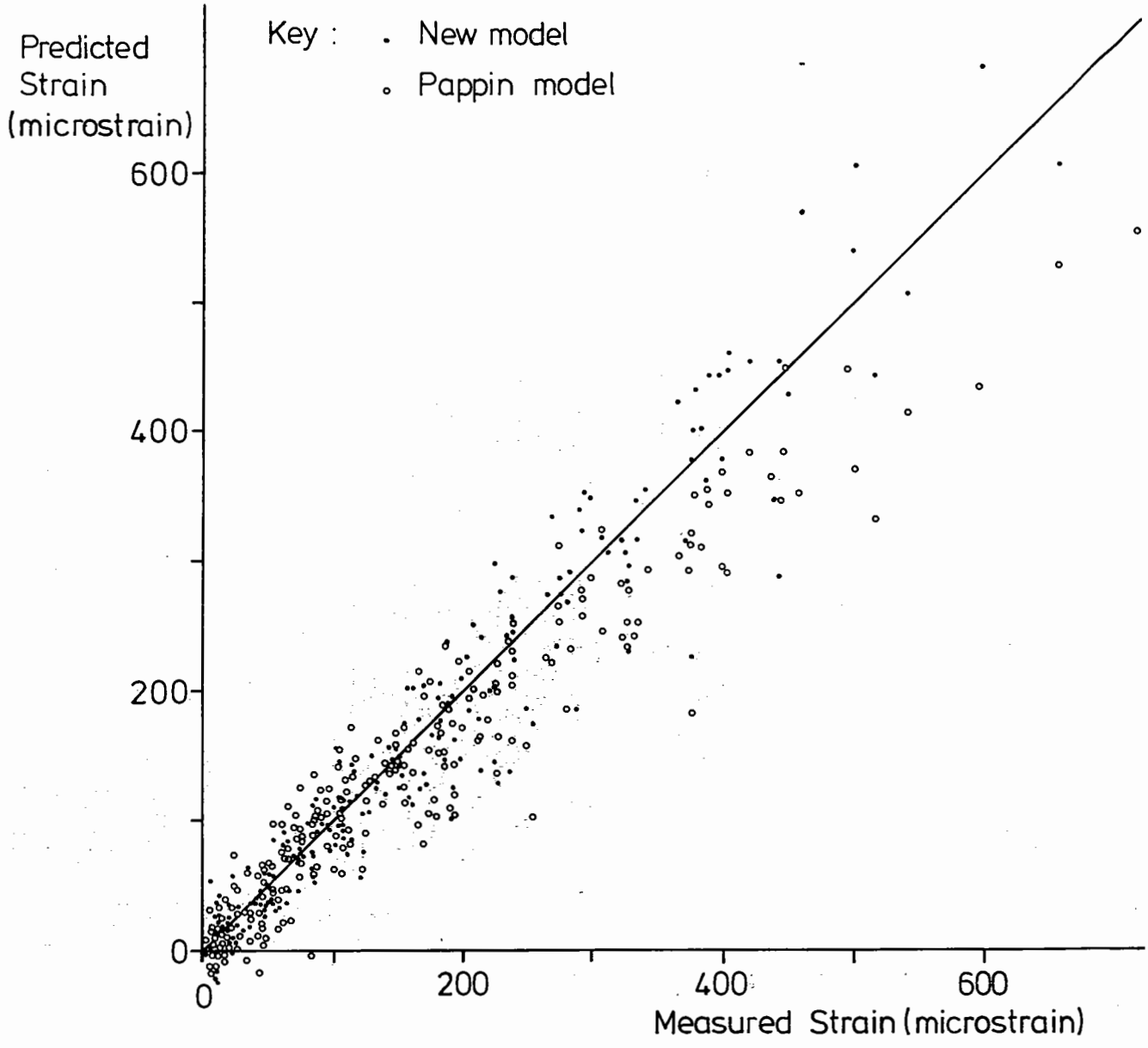

Fig. 4.7 Prediction of Volumetric Strain - Pappin's Results

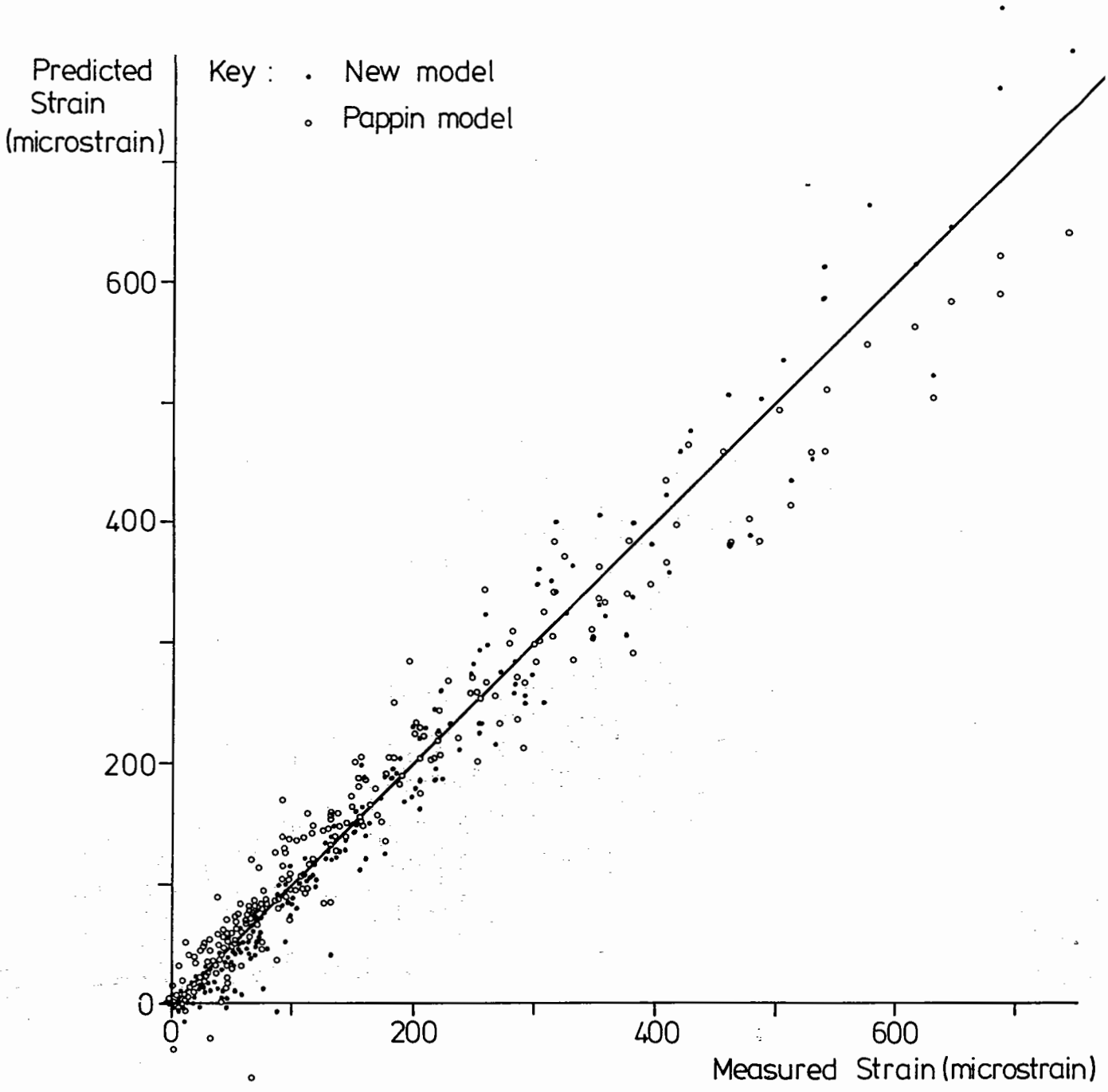

Fig. 4.8 Prediction of Shear Strain - Pappin's Results

From the above, it is clear that the new model performs as well as, or slightly better than, the Pappin model over the comprehensive range of triaxial stress paths covered. In fact, a more detailed analysis reveals that the main area of improvement is in paths extending into triaxial extension, an area where Pappin found it necessary to adjust the levels of stress ratio q/p by appealing to the Mohr Coulomb failure criterion.

4.2.2 Hollow Cylinder Data

A more severe test of model applicability has recently been provided by results from the hollow cylinder apparatus. During the course of this research, only two materials have been tested in the apparatus, Mid-Ross sand from Scotland and a 4 mm down crushed granite from Bardon Hill quarry in Leicestershire. It is the latter which has been much more extensively tested, including a series of 278 stress paths, mostly involving rotation of principal stresses, and it is these which lend themselves to testing the predictions of behavioural models.

Details of the apparatus, specimen preparation, instrumentation and data acquisition have been given in section 3.2. This section will examine the results.

The stress paths covered and resultant strains are given in Appendix A, but have not been plotted out because they are too numerous. Testing was carried out at three levels of confining stress and two stress paths were also performed where confining stress was varied. Unfortunately the apparatus at present is unsuited to variation of confining stress which is a very slow manually controlled process and no more such paths were therefore included.

In Appendix A it may be seen that a number of paths where torsional shear stress is zero were performed. These, in effect, simulate triaxial stress conditions. Model parameters were therefore chosen to fit these particular results (21 paths) as well as possible and, then, tested against all 278 paths. Three models were compared: the new model, the Pappin model and the Kθ model.

The equations obtained were as follows: (strain in microstrain)

New Model: $\varepsilon_v = 260\ (\delta \ln p)^{.82}.\delta p^{.25} - 61\delta((\ln(\sigma_1/\sigma_3))^2).(\delta t + \frac{1}{3}\delta s)^{.28}$

$$\varepsilon_s = 194\ \delta \ln (\sigma_1/\sigma_3).(\delta t + \tfrac{1}{3}\ \delta s)^{.42}$$

Pappin: $\varepsilon_v = 600\ \delta p^{.30}(1 - 0.08\ (q/p)^2)$

$$\varepsilon_s = 950\ \delta(q/p).(\sqrt{(p_r^2 + q_r^2)}/p_m)^{.47}$$

Kθ: Elastic Stiffness = $.046\ \theta^{1.5}$ MPa

Poisson's Ratio = .35

where all symbols have been previously defined.

As explained in the previous section, the new model splits shear behaviour into separate planes and directions within a plane. Principal stress rotation therefore causes no special computational problems. On the other hand, Pappin's equation for shear strain involves the invariant q, which has direction varying as the principal stresses rotate. It also includes a stress path length term involving change in q. The procedure used here in computing predicted strains follows that adopted by Pappin for use in the SENOL computer program and described in his PhD thesis (Pappin 1979). In effect, the true invariant q is used but adjusted, again following a Mohr Coulomb failure equivalency, and the shear on horizontal and vertical planes is ignored when considering direction of q. The Kθ model is, of course, much simpler and is not complicated by principal stress rotation.

The results are presented in the same form as for the earlier triaxial data, as predicted against measured values. They are split into volumetric strain (figs 4.9, 4.10 and 4.11) and shear strain (figs 4.12, 4.13 and 4.14). The latter includes both triaxial shear strain (vertical strain less horizontal strain) and torsional (that induced by shear stresses on horizontal and vertical planes). These shears are not invariants; they are components of shear in the plane of the wall of the specimen. On all six plots the points relating to purely triaxial stress conditions are highlighted.

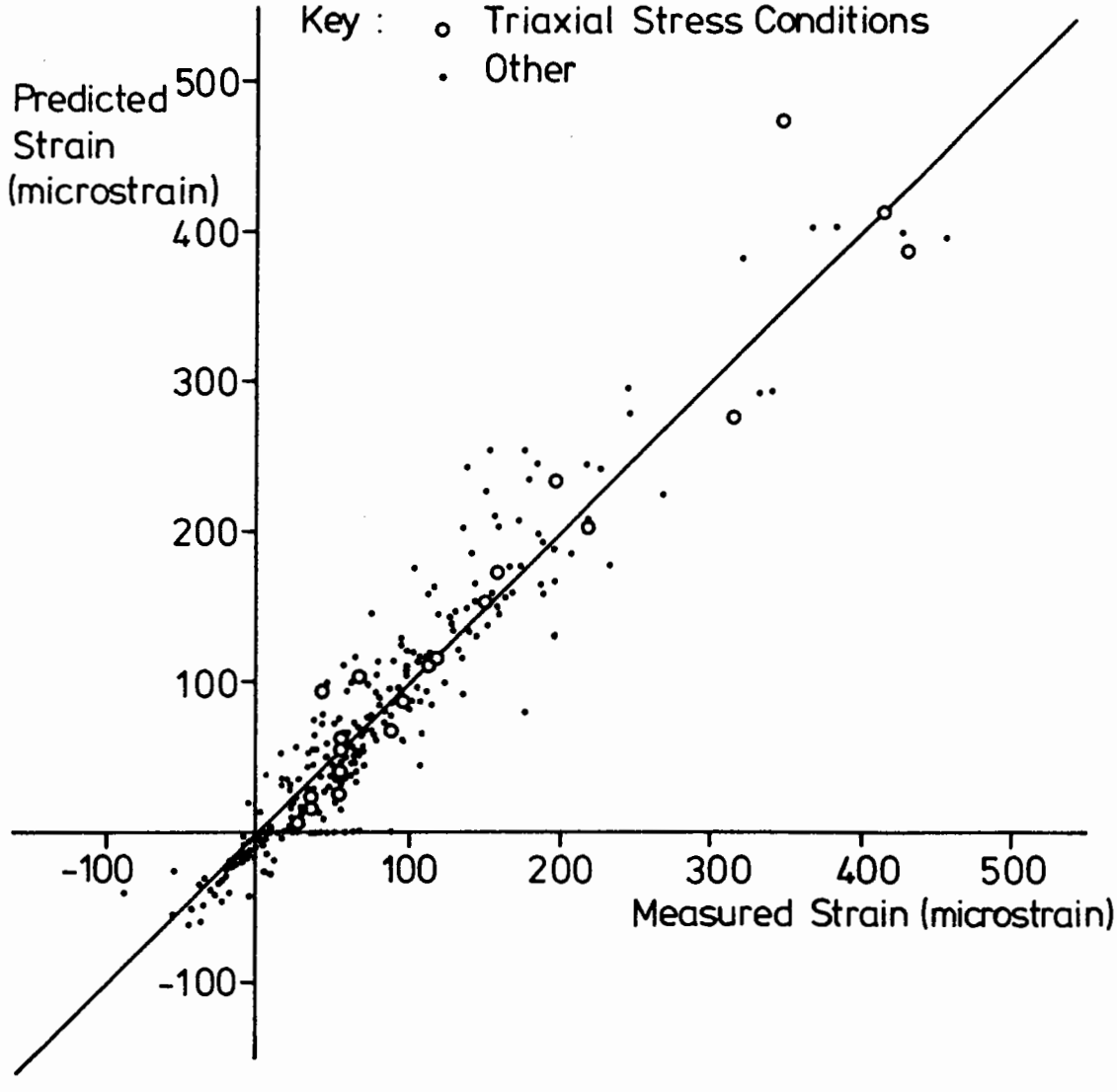

Fig. 4.9 Prediction of Volumetric Strain - New model
(data from Hollow Cylinder Apparatus)

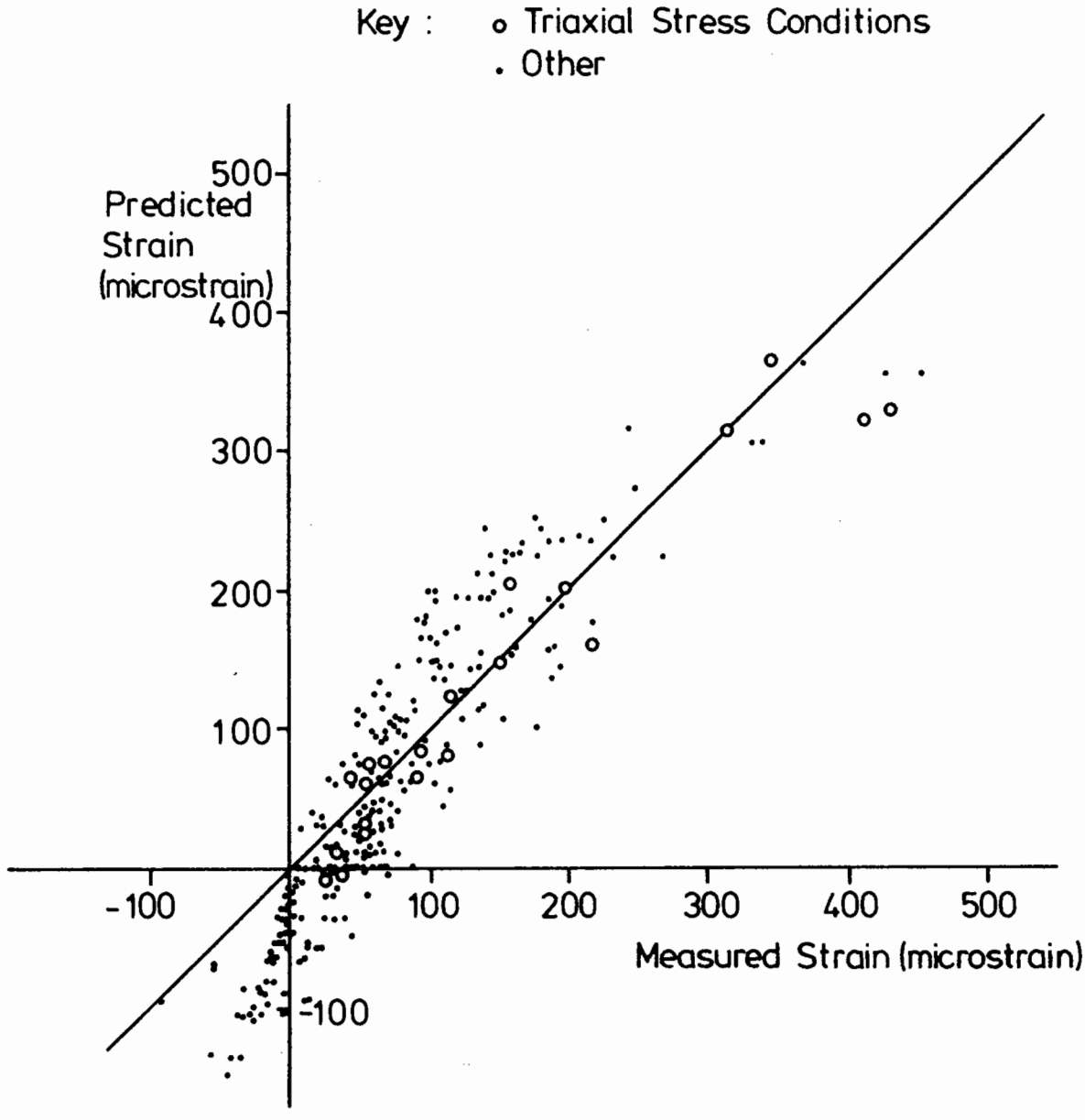

Fig. 4.10 Prediction of Volumetric Strain - Pappin model (data from Hollow Cylinder Apparatus)

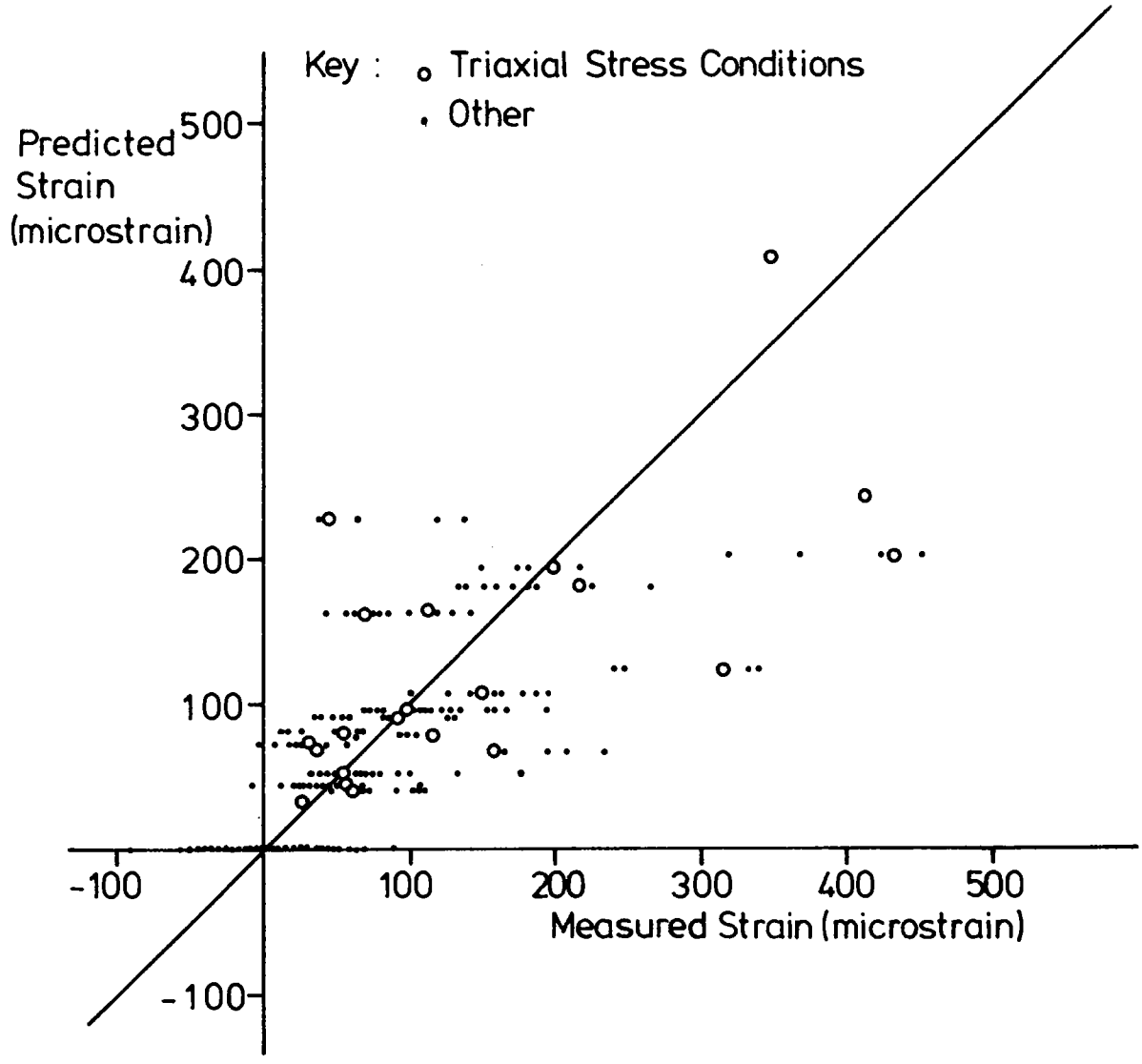

Fig. 4.11 Prediction of Volumetric Strain - kθ model
(data from Hollow Cylinder Apparatus)

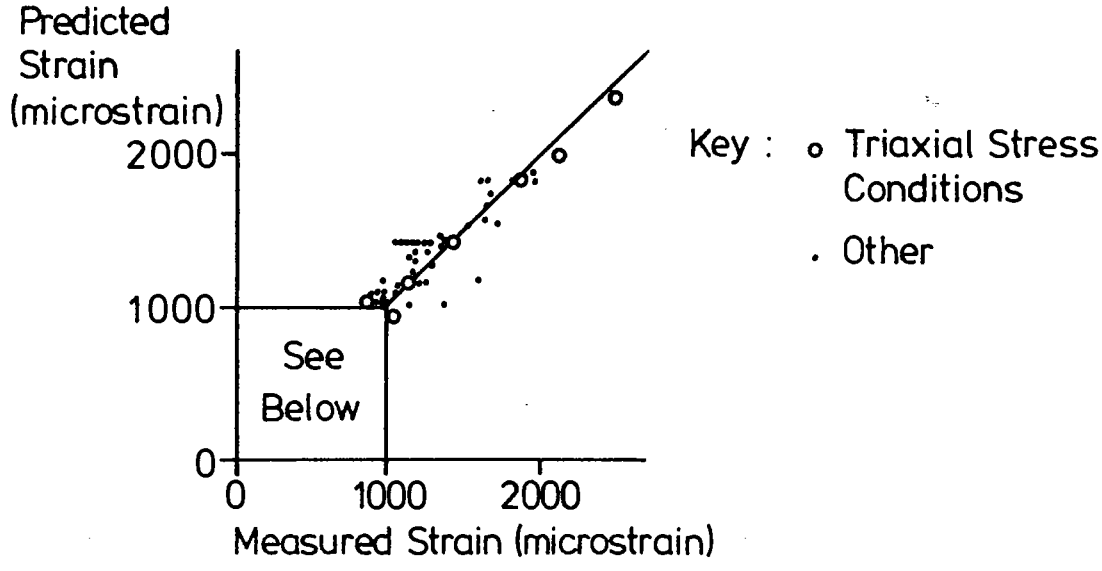

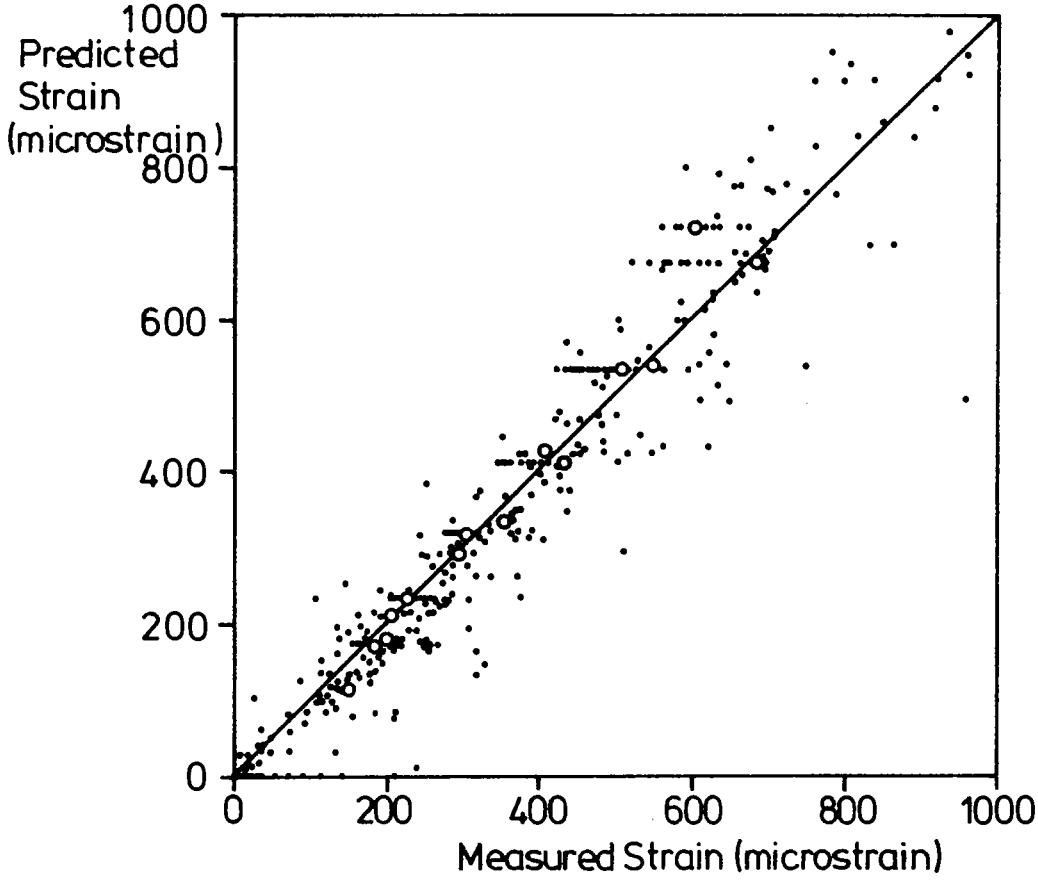

Fig. 4.12 Prediction of Shear Strain - New model
(data from Hollow Cylinder Apparatus)

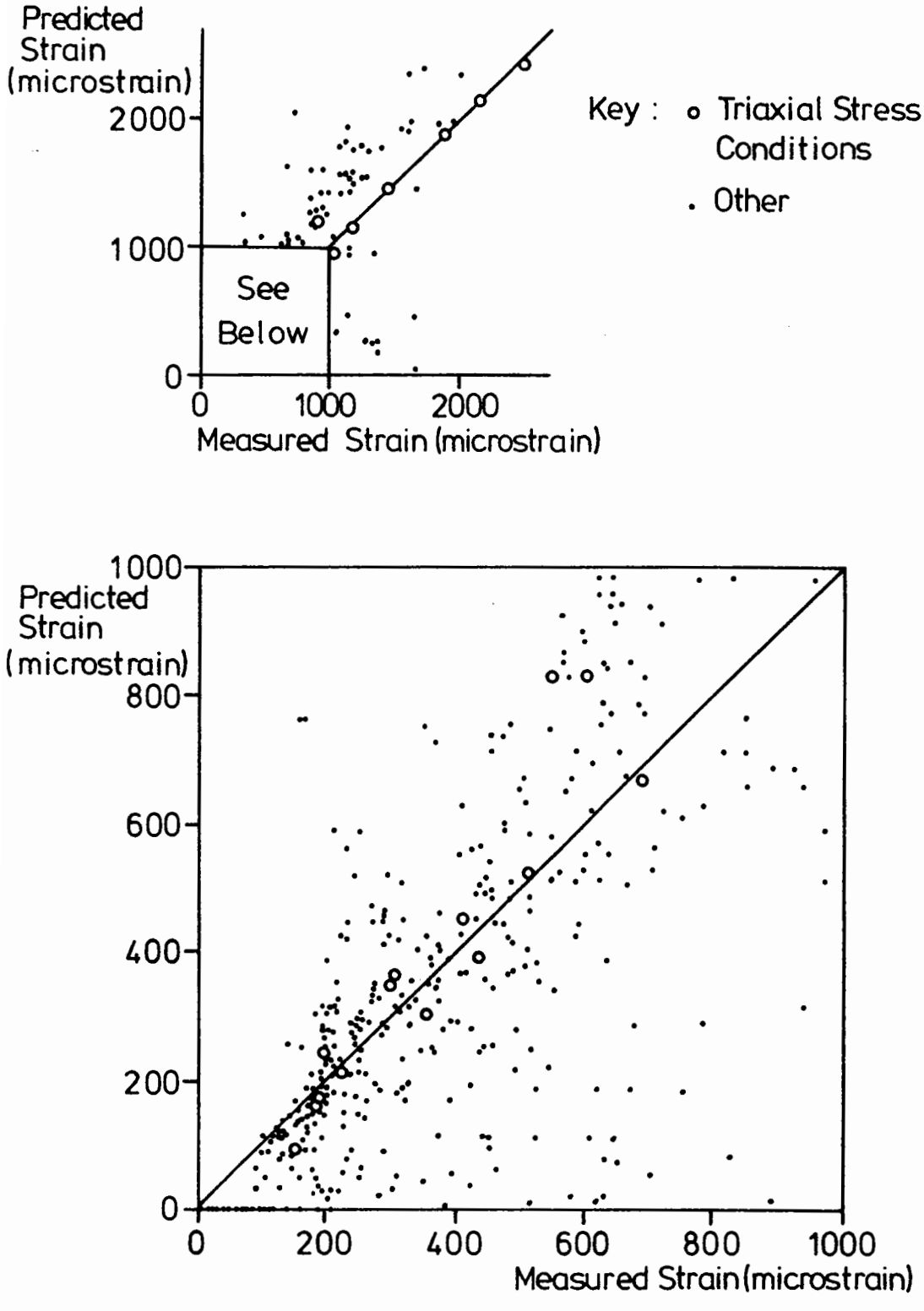

Fig. 4.13 Prediction of Shear Strain - Pappin model
(data from Hollow Cylinder Apparatus)

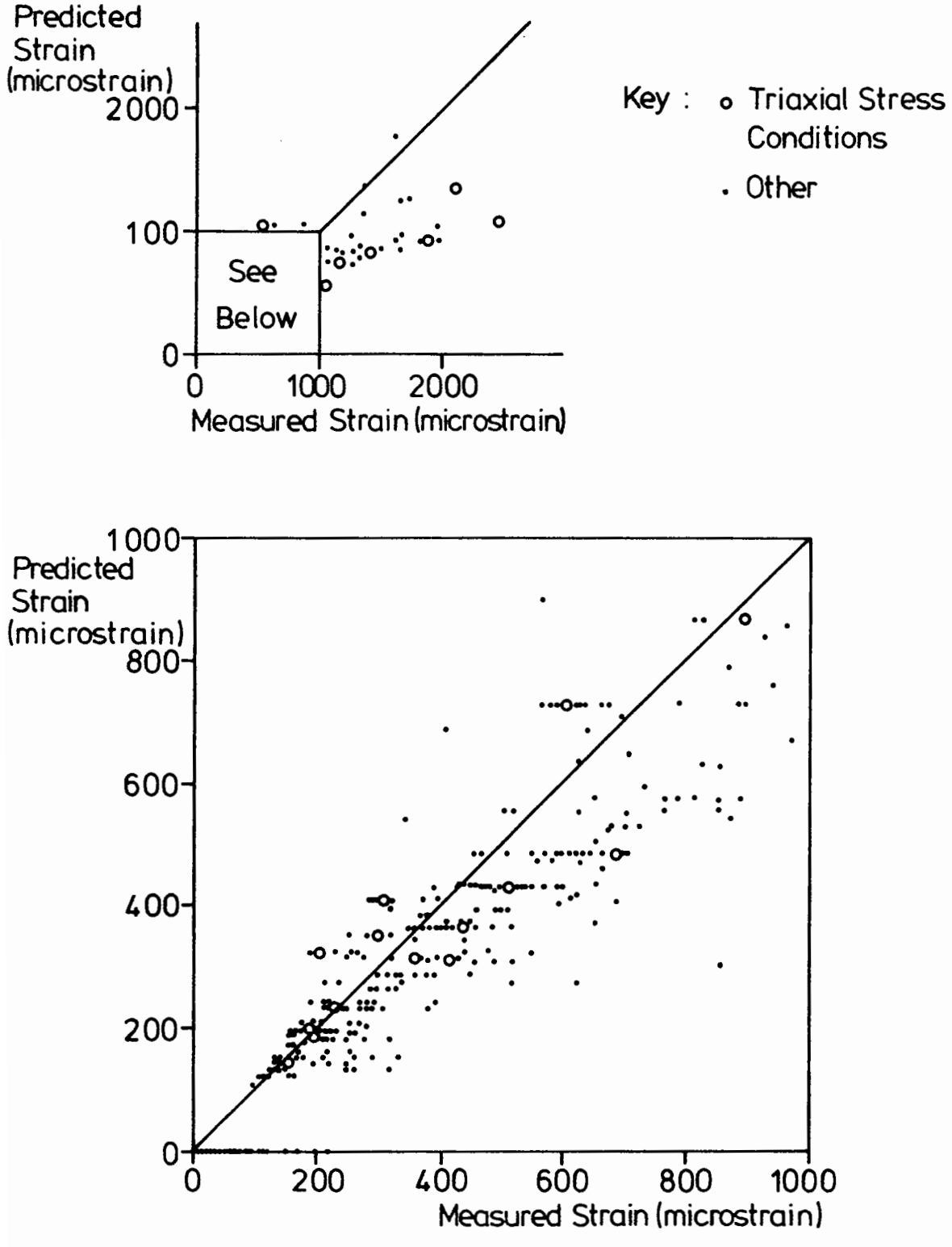

Fig . 4.14 Prediction of Shear Strain - kθ model
(data from Hollow Cylinder Apparatus)

A glance is sufficient to show that for volumetric strain the $K\theta$ model is not very satisfactory, whereas both the new model and Pappin's are much better, although the new model is distinctly more accurate, particularly in the negative strain region. Standard deviations from measured values are 39.2 microstrain (new model), 48.8 microstrain (Pappin) and 64.2 microstrain ($K\theta$). For shear the results are more dramatic. The new model is by far the best of the three and, in fact, Pappin's model is less good than the $K\theta$ predictions. Standard deviations are 88.2 microstrain (new model), 205.2 microstrain (K_θ) and 289.1 microstrain (Pappin). However, it is noticeable that the results relating to triaxial stress conditions are, once again, just as good for the Pappin model as for the new one, indicating that the improvement is in paths where principal stresses rotate.

Thus, it is possible to assess the relative performances of different models. However, a judgement on the absolute performance is more difficult, since it is complicated by all the built-in uncertainties, both in the normal variability of a particulate material and, also, in the errors possible in strain instrumentation and stress measurement. One known source of error stems from the 'slack' in the hollow cylinder apparatus torque system at zero torsional load, which leads to deviations in stress path where torque passes from positive to negative.

At this stage, therefore, no absolute judgement is given; it is sufficient to note that the new model appears to cope adequately with principal stress rotation. However, the following sub-section describes some very complex stress paths which have been used to explore as far as is presently possible the capabilities of the model.

4.2.3 Complex Stress Path Data

Although it has been demonstrated that the proposed model is capable of predicting strains over a range of stress paths, it will be noticed that all those covered so far have been straight line paths; ie there has been no out-of-phase variation of stresses. However, in many real situations, certainly in the case of a road foundation, this will not be the case. Clearly, the number of possible stress combinations which could be explored is infinite, even within the limitations of the triaxial and hollow cylinder apparatus, and it was therefore decided to analyse relatively few paths in some depth to ascertain whether it appeared probable that the model is more generally applicable than to straight line paths alone. One test in particular was intended to simulate as closely as possible the stress situation in a road foundation under a moving wheel.

It was noticed by O'Reilly (1985) that it was possible to use a stress-strain model of the form proposed by Pappin to predict not only the total strain between the end points of a path, but also the whole shape of the stress strain hysteresis loop. The procedure suggested is shown diagrammatically in fig 4.15. To find the strain at a stress level B (see fig) on the way from A to C it is simply equivalent to that for the stress path A B. On returning from C to A, the strain at B is given by that for the stress path C B. In this way it is possible to describe a hysteresis loop, which was shown by O'Reilly to match the actual measured response very well. Similarly, in the present work, it has been found that the new model is equally capable of predicting the shape of the hysteresis loop in general, although there are some paths, particularly those containing a large amount of volumetric strain due to shearing action, where the prediction is less good. Fig 4.16 shows a selection of stress-strain plots for straight line stress paths taken from hollow cylinder data, where the predicted hysteresis loop can be directly compared to the measured one. The stress paths are plotted as axial deviator stress against torsional stress, ie shear stress on horizontal and vertical planes. As can be seen, the strain predictions are generally very satisfactory.

When dealing with complex stress paths, where stresses are varied out of phase with each other it is difficult to define the beginning and end of the path, since it depends which direction of strain is to be considered. In the limit, two stress

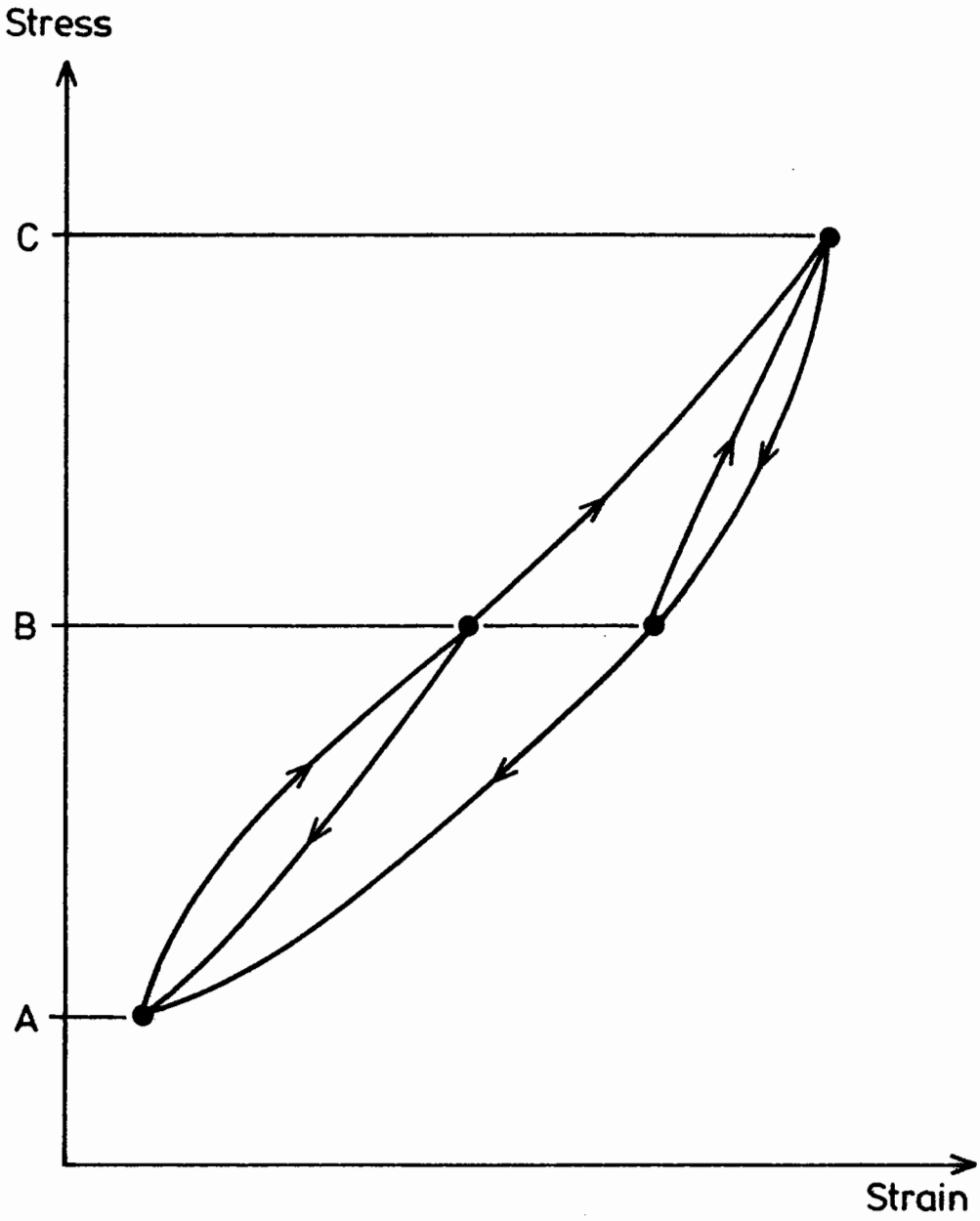

Fig. 4.15 Hysteresis Loop Prediction Method

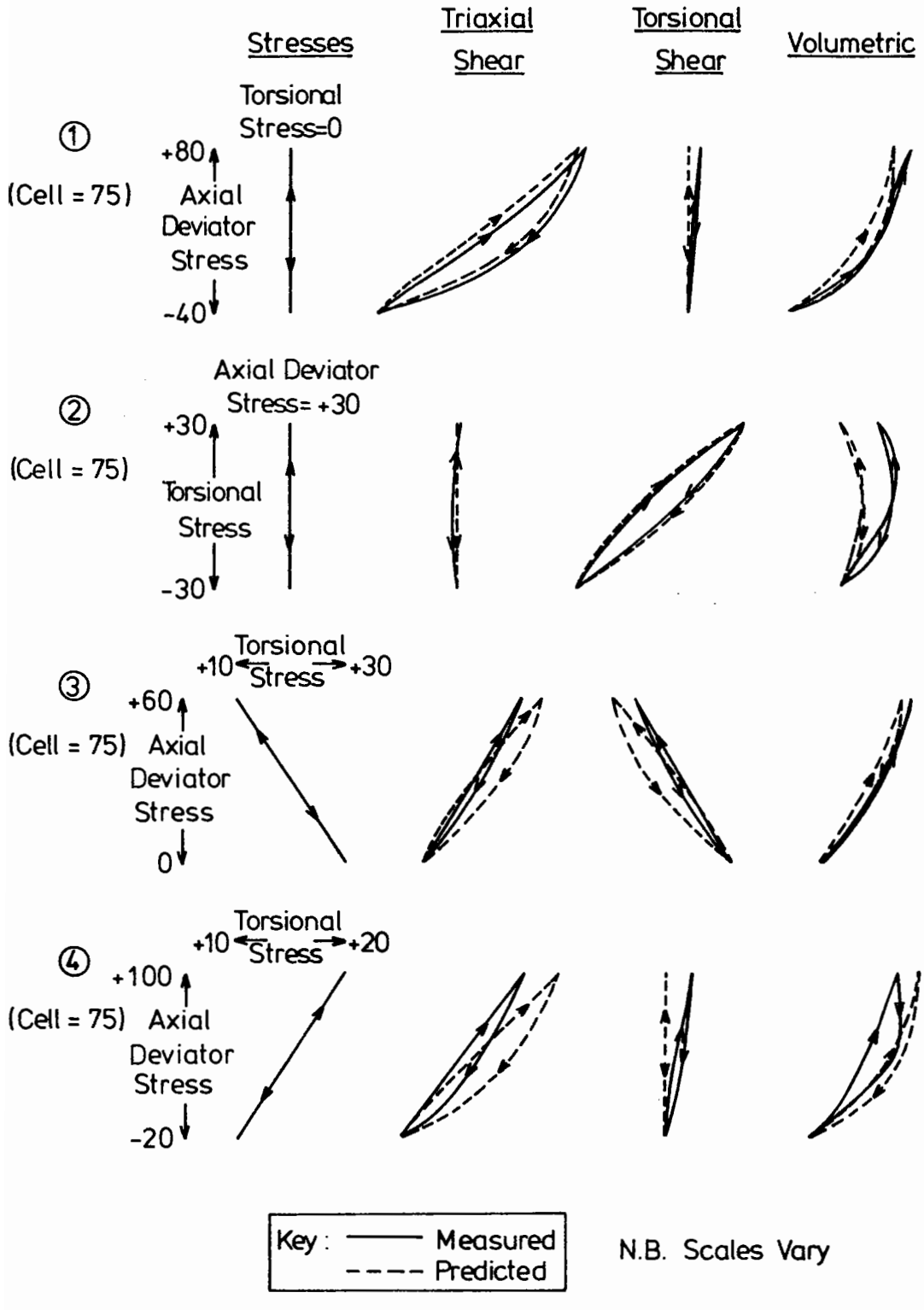

Fig. 4.16 Typical Hysteresis Loop Predictions

variables could be cycled 90° out of phase to produce a circular path if one stress were to be plotted against another. This section does, in fact, include such paths. The only way, therefore, to observe adequately the accuracy or otherwise of the predicted strain behaviour is to trace out the entire stress strain relationship, both measured and predicted curves, following the procedure shown to be satisfactory for straight line paths. Since, in general, a number of variables is involved, it was decided to plot all the relevant strains against one stress parameter. Fig 4.17 shows a selection of five stress paths, intended to be representative of the range of possible complex paths which the hollow cylinder apparatus is capable of applying. A glance shows that the predictions are remarkably good for almost all the strains involved.

The conclusion from the above evidence is that the model proposed here for elastic strain is capable of giving acceptably accurate predictions of strain for even the most complicated stress situations which laboratory testing devices can apply. Of particular interest is path 5 in fig 4.17, which is intended as a simulation of the type of stressing which occurs under a road, where the predictions are once more good. This is a strong

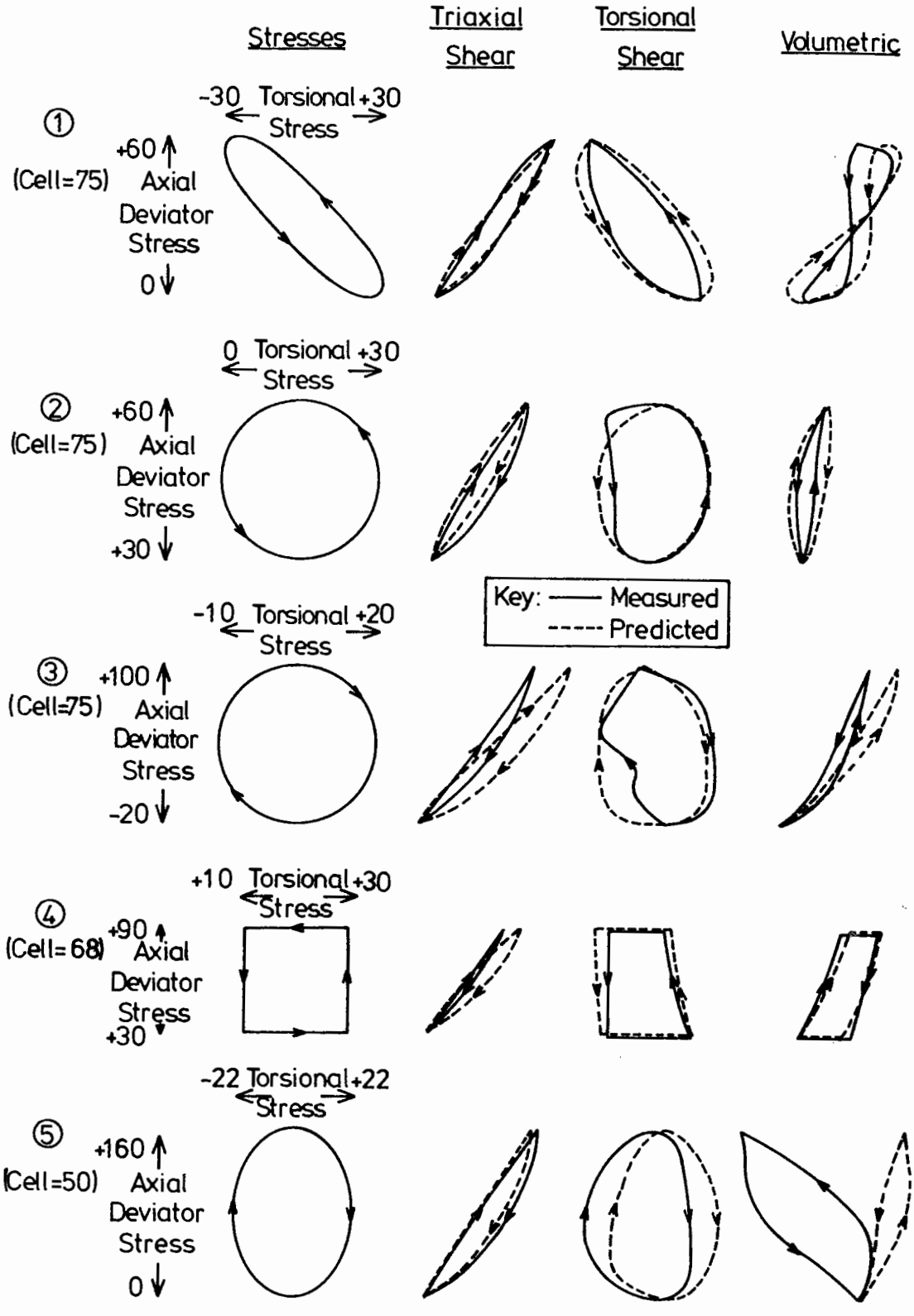

Fig. 4.17 Prediction of Elastic Strain for Complex Stress Paths

indication that the model is suitable for incorporation into a pavement analysis program.

4.3 PLASTIC BEHAVIOUR

The foregoing sections have concentrated on that part of granular material behaviour describing its elastic stiffness under repeated loading, clearly a very important aspect, governing the ability of a road foundation material to spread load. However, the second area of behaviour of critical importance concerns the accumulation of deformation within a material under cyclic loading, an area that was demonstrated by the example given at the beginning of chapter 2 and discussed there in relation to previous work on the subject.

Investigation of plastic strain accumulation poses more of a problem than that of elastic strain, since plastic behaviour appears to be greatly affected by previous straining of the specimen. This implies that each specimen will normally only yield plastic strain results from one stress path. Application of a second stress path will produce strains, but they will generally be affected by what has gone before. However, in an attempt to demonstrate some of the parameters influencing plastic shear strain accumulation, a specimen of dolomitic limestone was subjected to a number of different cyclic stress paths in a repeated load triaxial apparatus. Fig 4.18 shows the results as

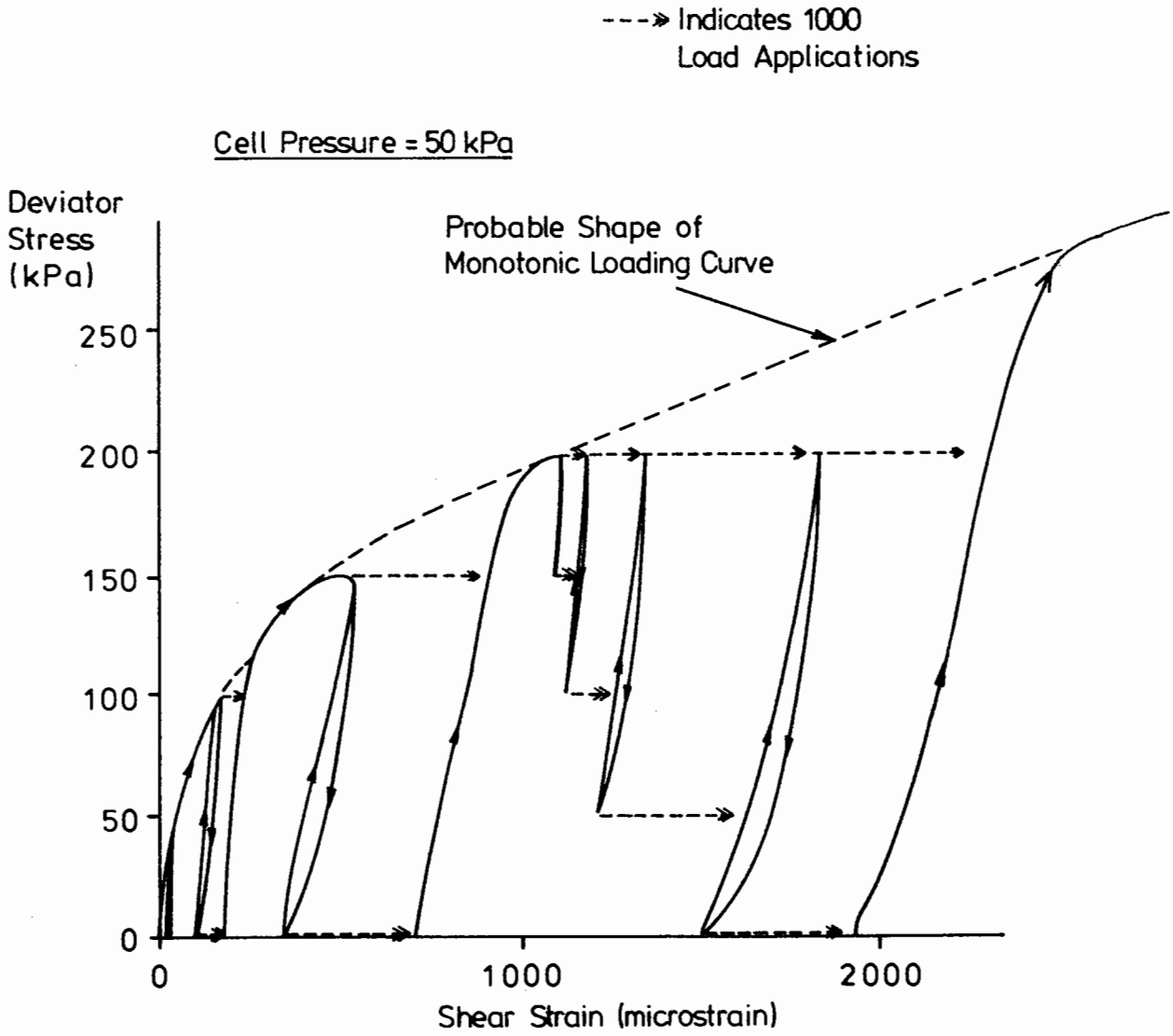

Fig. 4.18 Typical Plastic Strain Behaviour

deviator stress plotted against shear strain. The confining stress was kept constant. It will be noticed that the behaviour appears inextricably linked to the monotonic loading curve, which is repeatedly rejoined each time the deviator stress is increased. It is also evident that, comparing stress paths of equal length, those with a greater maximum deviator stress experience faster straining. Finally, it is equally clear that paths of greater length produce greater straining, though they may have the same maximum deviator stress. Reference to the section on plastic straining in chapter 2 shows that both these latter observations are fully in accord with the equation proposed by Pappin (eq 2.4), relating plastic shear strain to number of stress cycles.

4.3.1 Method of Investigation

Because of the potentially very time-consuming nature of this problem it was decided not to launch a full investigation into plastic strain until observation of early results provided clues as to the correct approach to be taken. Attempts were made to link the shape of the hysteresis loop in elastic behaviour with plastic strain accumulation rate, based on the assumption that the energy loss represented by the loop has to be the source of the plastic strain. However, this line was rejected when it was

realised that elastic stress-strain loops of similar size could be drawn from every part of stress space, from the very safest regions to the brink of failure, whereas the plastic strains arising would be very different. Another obvious anomaly was that volumetric hysteresis loops showing a negative energy loss component were commonly associated with positive plastic volumetric strains. To complete the case, chapter 5 will present results which show that elastic behaviour including the hysteresis loop is almost unaffected by the state of compaction of a material, whereas the plastic strain under cyclic loading is greatly affected.

Attention was therefore focussed again on the proposal made by Pappin for shear strain (eq 2.4). One aspect of his relationship which appeared slightly unsatisfactory was the fact that it was not asymptotic to failure: ie if the value of stress ratio q/p equalled the value at failure, the equation would still predict a finite plastic strain. Further testing revealed that the shear strain accumulation rate for one specimen on a stress cycle close to failure began to decrease initially, stabilised and then increased again. When plotted out it was noticed that the trough in strain accumulation rate coincided with the strain at which the monotonic loading curve peaked. This led to the suggestion

that the slope of the monotonic curve at a particular strain may be directly related to the shear strain accumulation rate and further examination of other results confirmed that this was a promising avenue to explore, rather than a stress ratio parameter such as q/p.

The other element in Pappin's equation which seemed open to question was the function of the number of cycles. Early observations suggested that a logarithmic function was usually appropriate for at least the first 1000 cycles, of the form:

$$\varepsilon = K \ln (N) + K' \qquad 4.12$$

where: ε = plastic strain

N = number of cycles

K, K' are constants

However, a series of tests performed on Mid-Ross sand involved variation in frequency of stress cycling from 0.1 Hz to 3 Hz and significant variation in shear strain accumulation rate with frequency was noticed. This presented problems in plotting the results since the constant K in eq 4.12 varied. Appeal was therefore made to a form of plot often used in assessing creep test results on various materials, a strain rate against strain graph. If eq 4.12 is differentiated with respect to N then the following results:

$$\frac{d\varepsilon}{dN} = \frac{K}{N}$$

therefore: $\ln \left(\frac{d\varepsilon}{dN}\right) = \ln K - \ln N$

$$= \ln K - (\varepsilon - K')/K \qquad 4.13$$

Hence, if eq 4.12 holds then so does 4.13 and a plot of the logarithm of strain rate ($d\varepsilon/dN$) against strain should yield a straight line. The advantages of such a plot are in two areas. When points of similar frequency are plotted and joined in a test where the frequency has been varied, then a set of parallel lines results. Also, it enables more than one plastic strain test to be performed and meaningfully assessed on the same specimen, assuming that earlier straining has no effect on the strain rate - strain characteristic. Fig 4.19 shows an assortment of test results on different materials and over different stress paths which demonstrates the use of the plot and the two advantages listed above. It can be seen that not all of them show straight line relationships, but they may none the less represent material characteristics.

The observations and developments listed above enabled a more comprehensive testing programme to be developed with the aim of producing a plastic shear strain model involving stress paths other than those from the triaxial apparatus. It was also anticipated that volumetric strain could be studied using a similar approach.

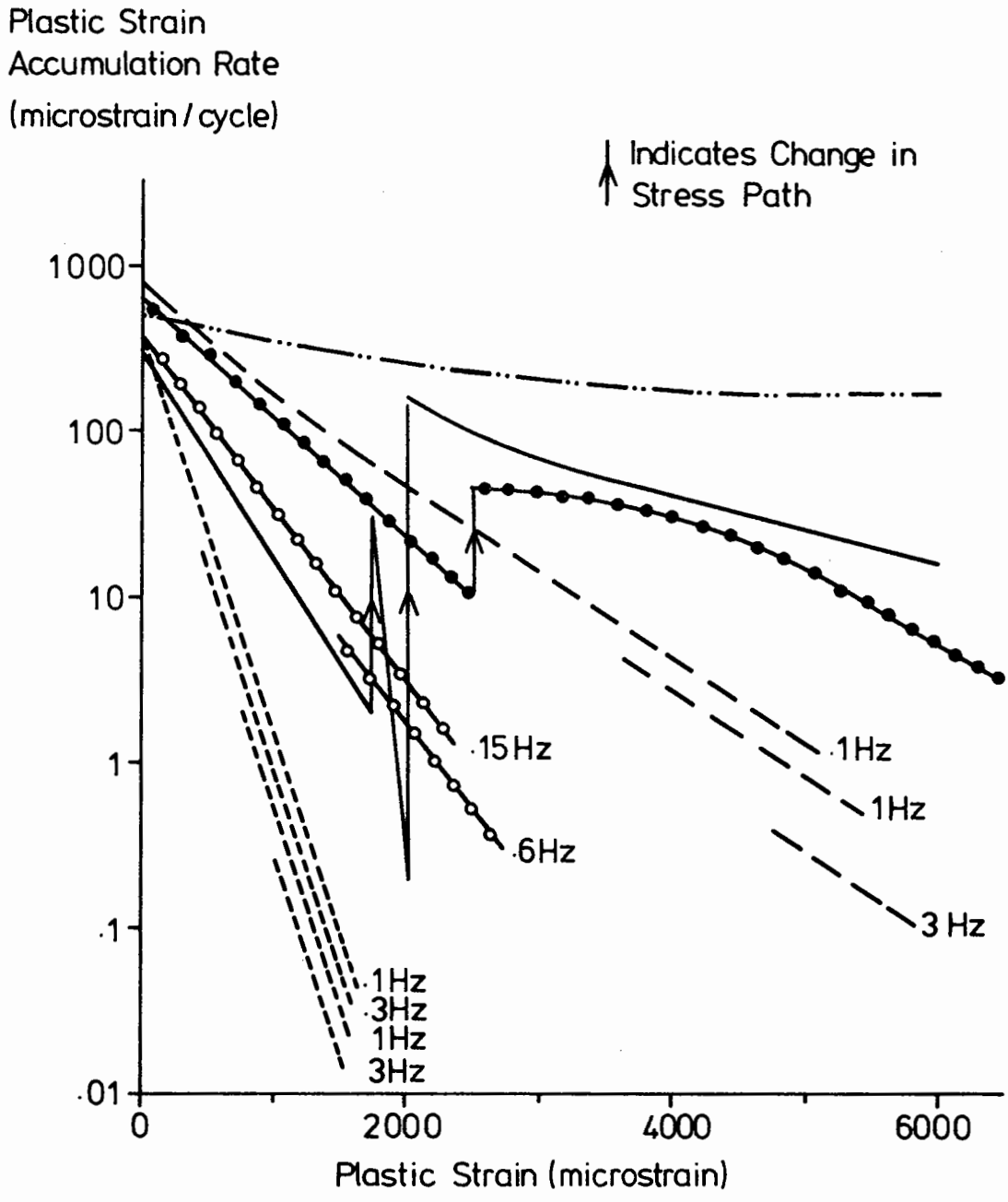

Fig 4.19 Typical Plastic Strain Results

4.3.2 Monotonic Loading Curves

With reference to fig 4.18, it is clear that, quite apart from any influence on strain accumulation rate, the first cycle of load is, in fact, part of the monotonic loading curve, if no strain has already taken place. It is, therefore, important to have a model which describes that loading curve. Various mathematical formulations have been used for shear strain (eg Duncan and Chang 1970), including power relationships. Consideration was also given to an elliptical formulation which appeared to model the curve quite well. However, the equation adopted was chosen for its apparently logical arrangement. It is as follows:

$$\frac{d\sigma}{d\varepsilon_s} = L\ (\sigma_f - \sigma) \qquad 4.14$$

where: σ = applied stress

ε_s = shear strain

σ_f = failure stress

L = constant

In the above, the slope of the curve is seen to be directly dependent on the nearness of the stress to failure, reaching zero as failure is reached. The obvious inaccuracy lies in the complete lack of post-peak strength loss but, since this area is of no practical importance in relation to road behaviour under multicyclic loading, this was felt to be no disadvantage. Integrating and rewriting eq 4.14 gives the following:

$$\varepsilon_s = \frac{1}{L} \ln \left[\frac{\sigma_f}{(\sigma_f - \sigma)} \right] \qquad 4.15$$

Whilst it will be appreciated that the purpose of this thesis on pavement foundation design is not to model monotonic behaviour, it is, none the less, an important factor contributing to modelling plastic straining under cyclic load. It would, therefore, be unfortunate if predictions based on the above equation were substantially in error. Fig 4.20 has been included, therefore, to compare measured monotonic shear behaviour with the predictions and it can be seen that, in these cases, they are visually quite acceptable. Determination of the constant L is slightly awkward. The "peak" strain (strain at maximum stress) cannot be used since the equation, being asymptotic at failure, predicts an infinite strain at maximum stress. For these plots, the point where the stress is 80% of failure has been arbitrarily chosen as the point, together with the origin, where predicted and measured values coincide.

In consideration of plastic volumetric strain, it will also be necessary to make reference to the slope of the monotonic loading line and a model for it has also to be chosen. The equation commonly in use when considering consolidation of clays and other particulate materials (eg Schofield and Wroth 1968) is logarithmic and of the same form as that used in this thesis for elastic behaviour, ie:

$$\varepsilon_v = \delta \, (\ln (p))$$

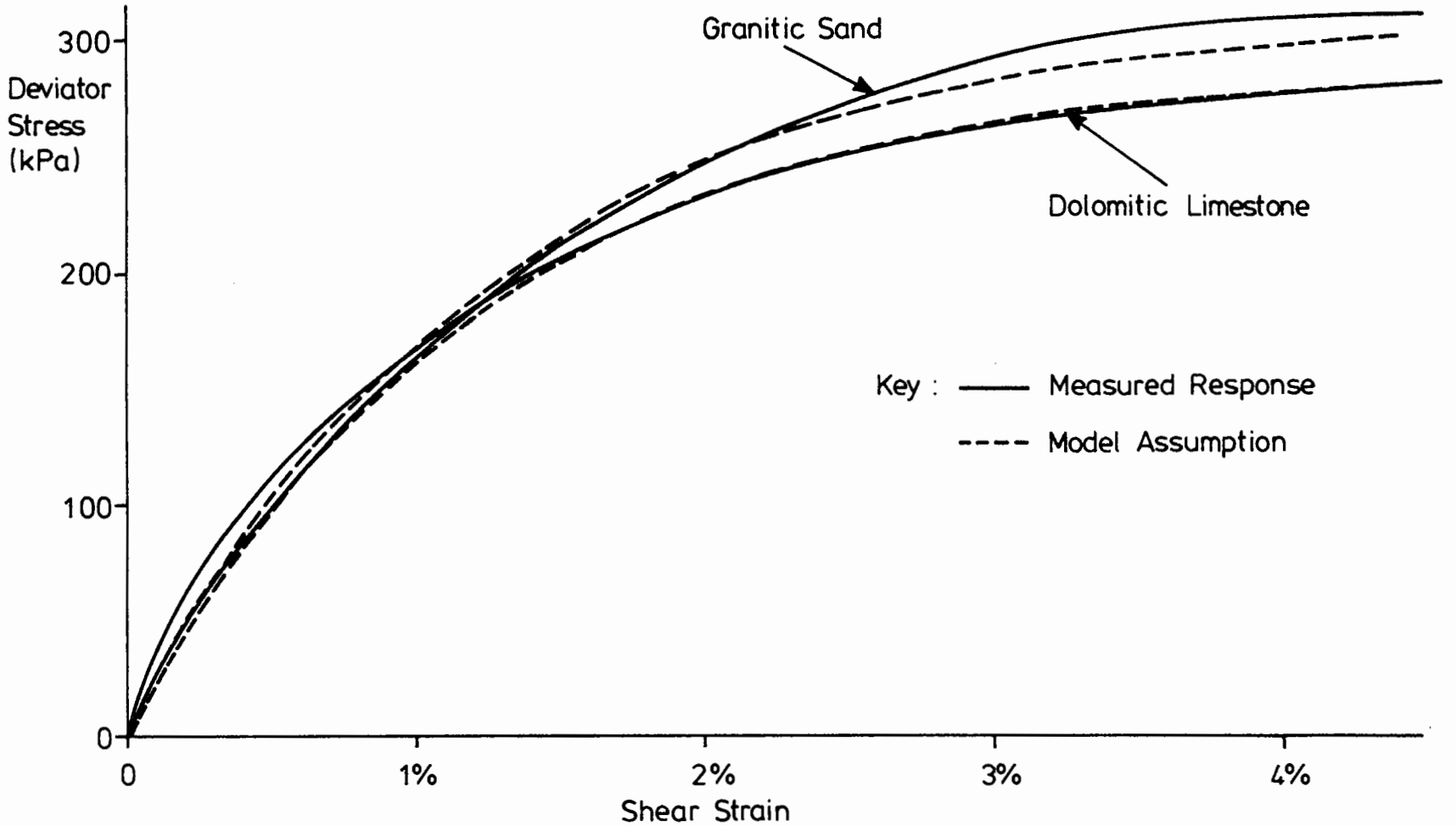

Fig. 4.20 Monotonic Loading Assumptions - Shear Strain

where: ε_v = volumetric strain

p = mean normal effective stress

δ means change in

A few monotonic volumetric compression tests were performed during the course of the present work, which confirmed that, even on initial loading, the stiffness increased with increasing stress level, but not to the extent of the logarithmic relation above. It was, therefore, decided, as an approximation, to use a straight line relationship. Fig 4.21 gives an indication of the errors involved in this assumption. This implied that the slope of the monotonic curve was a constant and that plastic volumetric strain under cyclic loading would, therefore, be unaffected by stress level.

4.3.3 Development of Shear Model

Having established the background equations, it is necessary to go through a few mathematical steps and to make a few assumptions in order to produce a plastic shear strain model in usable format. Equation 4.12 was noticed to be approximately correct in describing plastic strain accumulation. However, the observation has also been made that strain accumulation rate seems to be directly related to the slope of the monotonic curve at that strain. It is, therefore, proposed that, for shear, the quantity K in equations 4.12 and 4.13 should be replaced by a quantity inversely proportional to $L(\sigma_f - \sigma)$, the monotonic curve slope

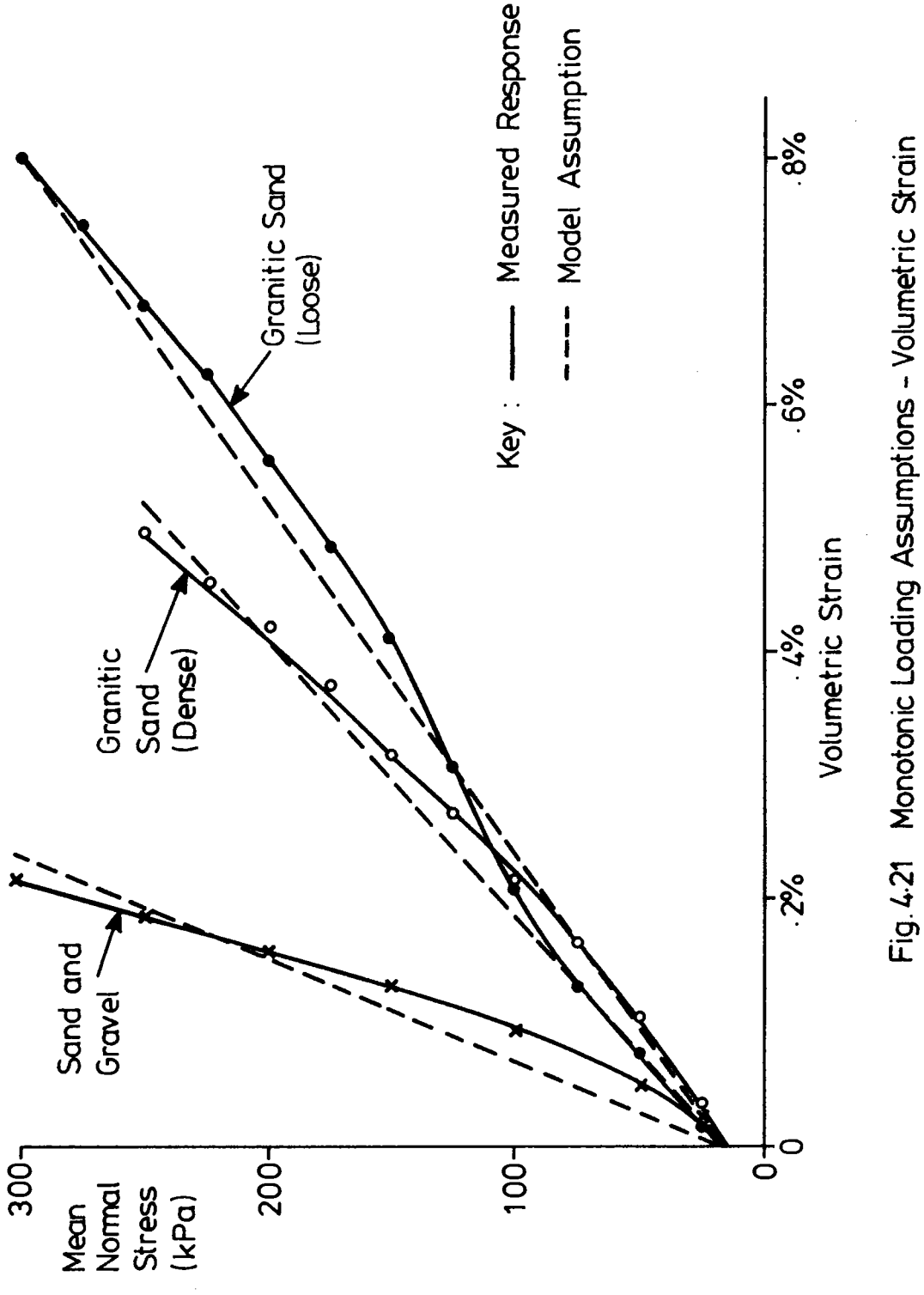

Fig. 4.21 Monotonic Loading Assumptions - Volumetric Strain

from eq 4.14. The equation actually proposed to replace equation 4.12 is:

$$\varepsilon_s = \frac{Z.\sigma_f}{L(\sigma_f - \sigma)} \ln (N) + K' \qquad 4.16$$

where: Z, K' are constants

differentiating: $$\frac{d\varepsilon_s}{d(\ln(N))} = \frac{Z.\sigma_f}{L\ (\sigma_f - \sigma)}$$

but from eq 4.15: $$\frac{\sigma_f}{\sigma_f - \sigma} = e^{L\,\varepsilon_s} \qquad 4.17$$

combining: $$\frac{d\varepsilon_s}{d(\ln(N))} = \frac{Z}{L}\, e^{L\,\varepsilon_s}$$

therefore: $$e^{-L\,\varepsilon_s}\, d\,\varepsilon_s = \frac{Z}{L}\ d\ (\ln(N))$$

integrating from 1st to Nth cycle: $$\frac{1}{L}\left(e^{-L\,\varepsilon_{so}} - e^{-L\,\varepsilon_s}\right) = \frac{Z}{L} \ln N$$

where: ε_{so} is the strain at 1st cycle (monotonic strain)

Now, ε_{so} can be substituted reusing eq 4.17:

$$e^{-L\,\varepsilon_s} = \left[\frac{\sigma_f - \sigma_{max}}{\sigma_f}\right] - Z \ln N$$

where: σ_{max} is the maximum stress of the stress path

therefore: $$\varepsilon_s = -\frac{1}{L} \ln \left[\frac{\sigma_f - \sigma_{max}}{\sigma_f} - Z \ln (N)\right] \qquad 4.18$$

Equation 4.18 is the form proposed in this research for cyclic plastic shear strain, although it still requires some slight modification. It can be seen that there are four constants involved. L and σ_f come from a knowledge of the monotonic curve and σ_{max} is a function of the stress path involved, leaving Z to be determined. Now, it has been shown from fig 4.18 that straining appears to depend partly on stress path length, as found by Pappin (eq 2.4). It is, therefore, necessary to replace Z by a term directly related to stress path length and the formulation of stress path length chosen is the same as that used in the elastic equation, ie $\delta t+\frac{1}{3}\delta s$ (section 4.1.1). Equation 4.18 therefore becomes:

$$\varepsilon_s = -\frac{1}{L} \ln \left[\left(\frac{\sigma_f - \sigma_{max}}{\sigma_f} \right) - \frac{1}{M_1} \left(\delta t + \tfrac{1}{3}\delta s \right) \ln (N) \right] \qquad 4.19$$

where: L, M_1 are constants

It is, of course, acknowledged that many assumptions have been made in taking the above mathematical steps, with limited supporting evidence. However, in section 4.4 it will be seen whether the model is capable of making reasonable predictions by comparison with test data. Firstly, a model for plastic volumetric strain needs to be developed.

4.3.4 Development of Volumetric Model

In the same way as for shear strain, the quantity K in eq 4.12 should be replaced by the slope of the monotonic loading curve. However, it was proposed in section 4.3.2 to use a straight line as an approximation to the actual curve for volumetric strain, and K can therefore remain as a constant, leaving only stress path length to be taken account of.

Stress path length for volumetric strain, however, is not straight-forward. It has been noticed in tests involving the hollow cylinder apparatus that rotation of principal stress has a sometimes dramatic effect on accumulation of volumetric strain (O'Reilly et al 1987), and the formulation for stress path length has to take account of this. Similar experiments involving principal stress rotation have been done using the Directional Shear Cell at University College London (Wong & Arthur 1985) and have found that very significant compressive volumetric strain can take place with no variation in mean normal stress, only rotation of principal stresses. Unfortunately the amount of evidence collected so far in this project is insufficient to be very confident of any proposal made, but it would seem that the stress path length should be the total summation of stress change in every direction. In a system of fixed axes, such as that used in the elastic model, this requires more than simply the change in each of three orthogonal normal stresses; it needs to take

account of shear perpendicular to those stresses. In fact, it is proposed that twice each shear stress change is added to the sum of the changes in three orthogonal normal stresses. This is mainly based on evidence from hollow cylinder tests, but has the logical basis that changing the maximum shear stress on a Mohr Circle plot (eg fig 4.1) imposes this change on both the principal stresses also. The result is that, for x, y, z axes, the stress path length for plastic volumetric strain is as follows:

$$\text{Stress Path Length} = \delta\sigma_x + \delta\sigma_y + \delta\sigma_z + 2(\delta t_{xy} + \delta t_{zx} + \delta t_{yz})$$

where the absolute value of each stress change is taken.

The equation for plastic cyclic volumetric strain therefore becomes (from eq 4.12):

$$\varepsilon_v = \frac{1}{M_2} (\Sigma\delta\sigma + 2\ \Sigma\delta t)\ \ln\ (N) + K' \qquad 4.20$$

where: M_2, K' are constants.

However, it will be noticed that there is no possibility from eq 4.20 that plastic volumetric strain could ever be negative, but it has on occasions been found to be so. Observations have led to the conclusion that a proportion of the plastic shear strain should be subtracted from eq 4.20 to take account of dilation due to shearing action. From an empirical rather than theoretical standpoint, it has been decided that a factor of one half is

appropriate. Equation 4.20 thus becomes:

$$\varepsilon_v = \frac{1}{M_2} (\Sigma\delta\sigma + 2\ \Sigma\delta t)\ \ln\ (N) - \tfrac{1}{2}\ \varepsilon_s + K' \qquad 4.21$$

One further amendment is required to eq 4.21: that is that the constant K' is ignored. The reason for this is that, unlike shear strain, volumetric strain does not appear to be tied to the monotonic curve in any way. To put it another way, the material 'remembers' how far it has gone in shear, but 'forgets' volumetrically, as soon as a few different stress paths have been applied. K' is, therefore, impossible to determine generally; it depends on stress history. The final plastic volumetric strain equation is thus:

$$\varepsilon_v = \frac{1}{M_2} (\Sigma\delta\sigma + 2\ \Sigma\delta t)\ \ln\ (N) - \tfrac{1}{2}\ \varepsilon_s \qquad 4.22$$

4.3.5 Frequency Effects

It was mentioned in sub-section 4.3.1 that accumulation of plastic strain has been found to be frequency dependent. The only firm data available to this research is contained in fig 4.19, which suggests an approximate dependency such that a tenfold frequency increase may lead to a **halving of strain rate** This order of magnitude has also been observed in recent tests on crushed carboniferous limestone but should still be taken as approximate only. The implication is that the constants M_1 (eq 4.19) and M_2 (eq 4.22) are frequency dependent and that this should be borne in mind when using data from laboratory tests in

pavement analysis.

4.4 PLASTIC BEHAVIOUR - CORRELATION WITH LABORATORY TEST DATA

Although a large number of repeated load tests has been done on many different materials, a series was performed specifically to aid the development of a plastic strain model on a 4mm down crushed granite, the same material as was used for proving the elastic model in section 4.2. The reason, as for the elastic testing, for the choice of this material was that it was small enough to enable hollow cylinder specimens to be prepared.

In all, 15 tests were performed, 9 in a triaxial cell and 6 in the hollow cylinder apparatus, on various stress paths. Density of specimen was deliberately varied, so that the failure criteria varied, thereby providing a broader test of model applicability. This meant that each specimen had to be taken to failure to determine the failure criteria applicable. Constants were chosen to give the best possible fit to the data, as follows:

$$L = 46$$

$$M_1 = 6.4 \text{ MPa}$$

$$M_2 = 250 \text{ MPa}$$

Unfortunately the dependency of monotonic volumetric behaviour on density was not recorded and the value of M_2 quoted could not be taken as appropriate for tests at low density. The first large source of error noted was in the strain expected after the first cycle. The measured and expected shear and volumetric strains, as well as the stress paths, are given in table 4.1, which shows that, particularly for volumetric strain, errors can be quite large. This is not seen as surprising, however, nor worrying. It was stated in sub-section 4.3.4 that the material appeared to 'forget' where it had reached in volumetric strain and no attempt was therefore made to model the first cycle correctly. The predictions for shear, it will be noticed, are consistently too high, which is almost certainly due to the fact that some straining took place during initial coupling up of the apparatus to the specimen. In fact, for test no. 11 in the hollow cylinder apparatus, the zero reading for the plastic strain test was taken after an elastic test programme had been performed, giving rise to a completely false first cycle prediction. In figs 4.22 and 4.23 it was, therefore, decided to compare the measured and predicted strains after the first cycle.

Fig 4.22 (a) and (b) shows some of the predictions for shear strain. Visual inspection is sufficient to show that they are of reasonable accuracy (error<.3%).It is clearly possible to follow the steepening curves applicable to some stress paths, very close to failure. Predictions for volumetric strain (fig 4.23) are not so good (errors as high as 1.2%). The

Table 4.1 Plastic Strain Predictions after One Load Application for Granitic Sand

Test Number	Stress Path (kPa)	Principal Stress Ratio at Failure	Volumetric Strain (%) (1 Application) Measured	Predicted	Shear Strain (%) (1 Application) Measured	Predicted
1	cell=50:q=0-150	7.00	-.23	-.50	.82	1.51
2	cell=50:q=0-150	7.58	.04	-.44	.67	1.32
3	cell=50:q=0-115	5.80	.31	-.47	.94	1.42
4	cell=100:q=0-295	7.26	.25	-.46	1.01	1.39
5	cell=25:q= 0-80	7.92	-.11	-.45	.40	1.35
6	cell=50:q=78-156	8.00	-.05	-.43	.97	1.28
7	cell=50:q=80-240	8.20	0	-.79	1.95	2.39
8	cell=50:q=140-300	8.46	-.20	-1.18	3.23	3.55
9	cell=50:q=170-330	8.60	-.15	-1.47	4.28	4.41
10	cell=50:Ax.Dev=0-160 τ = -21-+21	7.50	-.03	-.49	.82	1.47
11	cell=50:Ax.Dev=0-160 τ = 0	7.50	0	-.49	.36	1.47
12	Cell=65:Ax.Dev=0 τ = 0-40	7.50	.09	-.75	.54	2.26
13	Cell=50:Ax.Dev=0 τ = -35-+35	7.50	.20	0	-	-
14	Cell= 65:Ax.Dev=0-80 τ = 0	7.50	.04	-.15	.21	.46
15	Cell=65:Av.Dev=0-80 τ = -40-+40	7.50	.20	0	-	-

Key: Cell = Confining stress (Triaxial) or Internal vacuum (Hollow Cylinder)
q = Deviator stress (Triaxial)
Ax.Dev = Axial Deviator Stress (Hollow Cylinder) = $\sigma_v - \sigma_h$
τ = Torsional Shear Stress (Hollow Cylinder)
where Axial Deviator and Torsional Shear Stress are cycled together they are 90^o out of phase

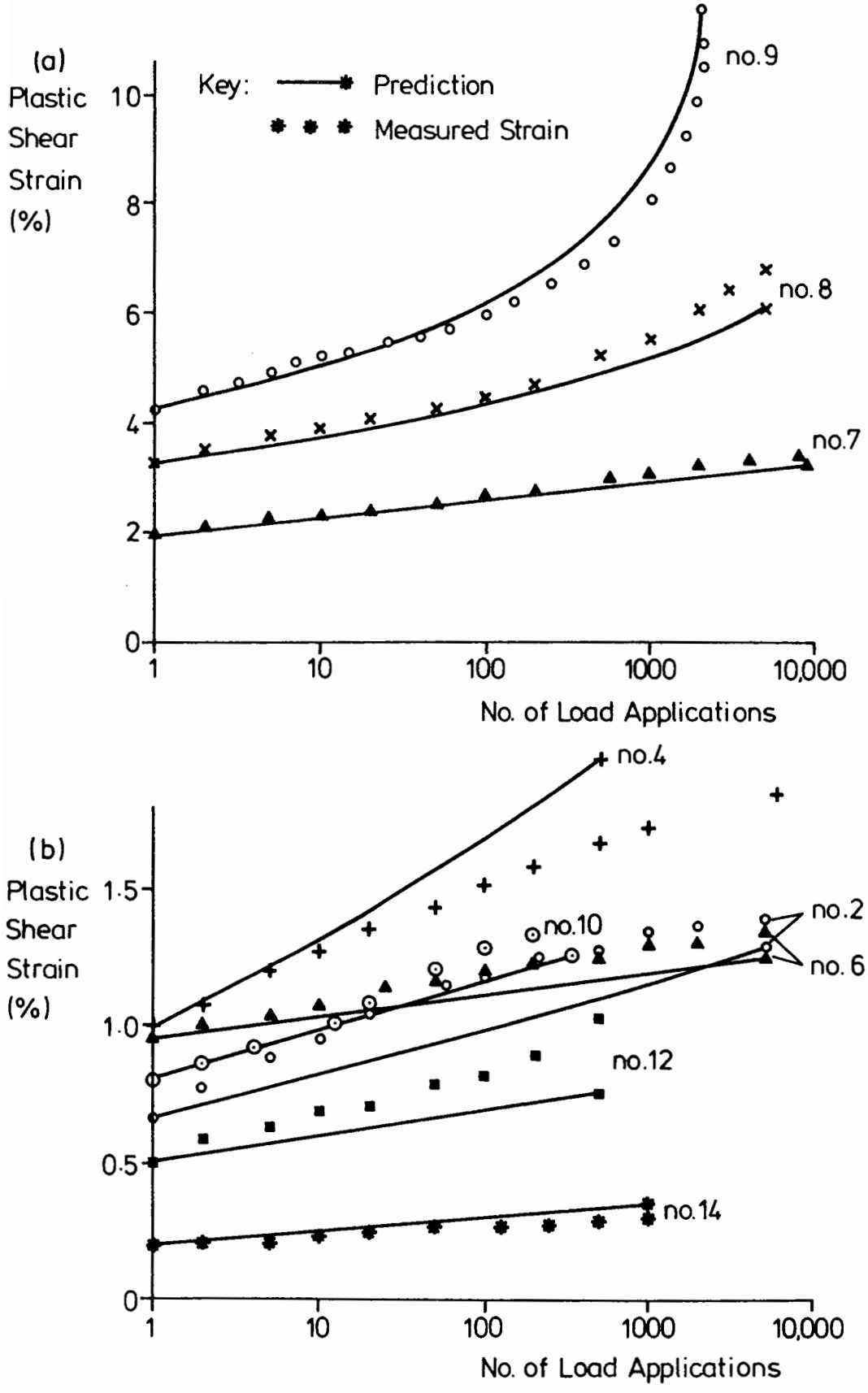

Fig. 4·22 Plastic Shear Strain Accumulation for Granitic Sand

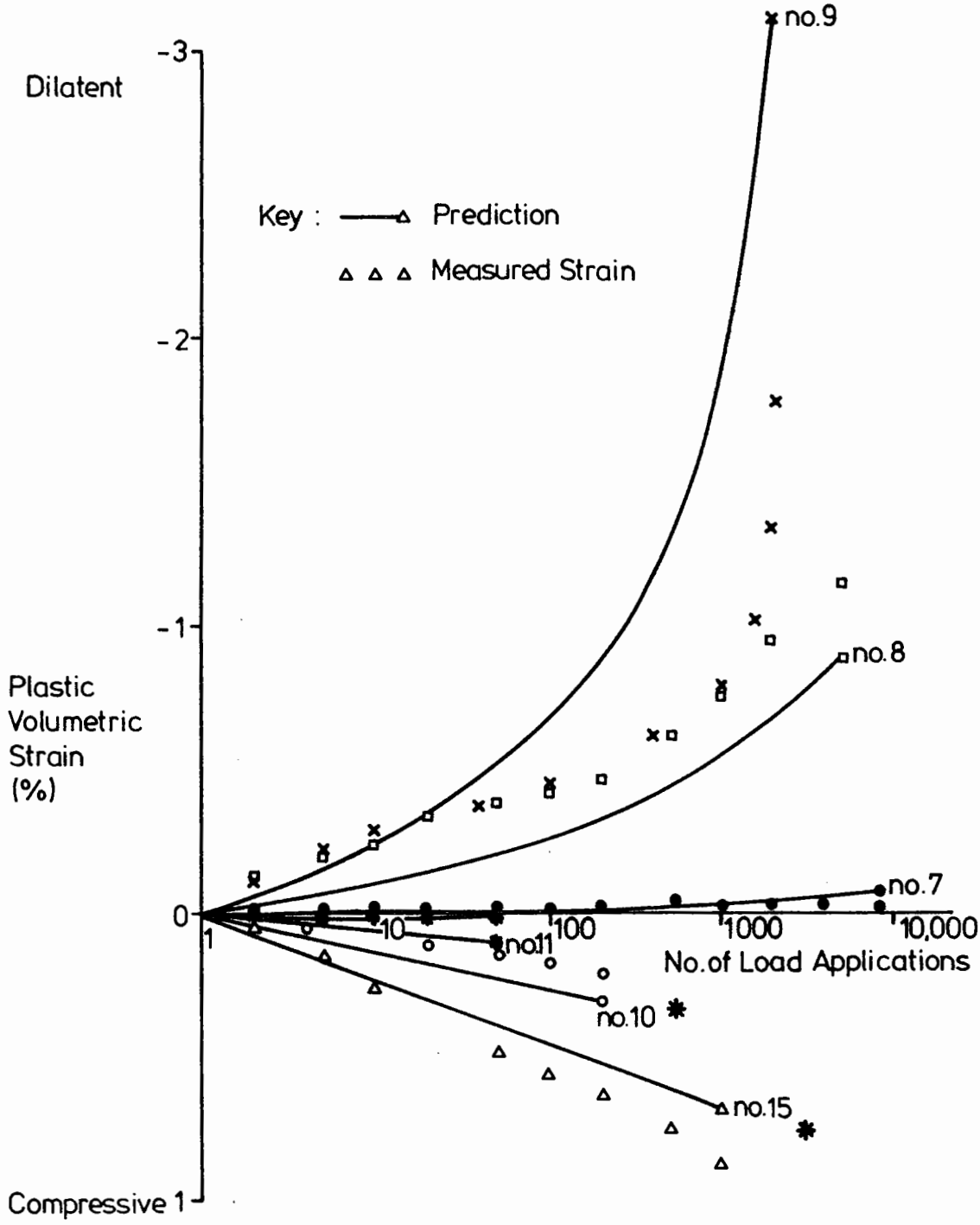

Fig. 4·23 Plastic Volumetric Strain Accumulation for Granitic Sand

proportional difference between test nos. 10 and 11 is modelled fairly well, simply by virtue of the increased stress path length for no. 10. It was this difference which first led to the realization that rotation of principal stresses has to be taken into account and the stress path length formulation used appears to be successful in doing this. In fact, the stress paths involving principal stress rotation have been highlighted in fig 4.23 with an asterisk and it can be seen that they are modelled as well as any other.

As has been stated, figs 4.22 and 4.23 show only a selection from the 15 tests performed, due to lack of available space. Those not plotted are not, in general, worse in prediction than those shown, but they group around the low strain region for both shear and volumetric behaviour.

It has been noticed, however, that several specimens of other materials do not conform quite so satisfactorily to the pattern shown above. In particular, it has frequently been found that the shear strain increase curve (fig 4.22) flattens off after 10^3 or 10^4 cycles, an occurrence not possible to model using the equations proposed here. This was certainly noticed by Pappin and is reflected in the function of number of cycles which he proposed. On the other hand, the steepening behaviour shown here (eg test no. 9) has also been observed (eg Brown 1974), including one of Pappin's specimens which approached failure. The conclusion is that use of the equations proposed here should be made with caution but that they are likely to give a useful guide

to plastic strain development under cyclic load.

4.5 SUMMARY

This chapter has dealt in some depth with proposals for new stress strain models for both elastic and plastic behaviour.

The models are formulated by splitting strain into shear and volumetric components, and by considering stresses and strains relative to a set of three orthogonal axes.

The basis and reasoning behind the choice of models have been thoroughly worked through.

For both elastic and plastic models, comparisons are presented between the predictions made using the equations developed and measured strains from both the repeated load triaxial and hollow cylinder apparatus. The match between predicted and measured strain has been found to be quite good. In the case of elastic modelling the new model is seen to be considerably superior to two other formulations presently in use. No direct comparison is made with any other plastic model.

In conclusion, a workable model of elastic and plastic stress strain behaviour has been developed for generalised stress conditions. Its further use is described in chapter 7.

CHAPTER FIVE

EFFECT OF MATERIAL VARIABLES

Chapter 4 has established a framework of elastic stress-strain relationships, and plastic strain equations, which have been shown to correlate quite satisfactorily with results from laboratory element testing for a limited number of different materials. This chapter will concentrate on determining the effect, on both elastic and plastic behaviour, of variations in the aggregate used. The variations covered will be the shape of the grading curve and the compactive state, for a particular type of crushed rock, the typical particle size and, finally, the type and source of aggregate. All tests will, at this stage, be dry however.

The aim of this investigation into the influence of these various material parameters is to determine the relative importance of each one in affecting each area of granular material behaviour and to demonstrate the findings in as simple a way as possible. It should, therefore, be evident by the end of the chapter just how important compaction is, what the effect of transgressing grading limits might be, and the relative merits, for example, of soft and hard rock aggregates, all in the dry state. Presentation of results will necessitate a considerable simplifying of the equations derived in chapter 4, although the constants pertaining to those equations will also be presented.

Also, the testing of such a large number of different materials requires a short, yet productive, test programme. The chapter will, therefore, start by describing a standard test routine and the logic behind it and will then proceed to present the results relating to each variable in turn.

5.1 STANDARD TEST ROUTINE

For a large number of tests, some on aggregates with particles as large as 40mm, the only suitable mechanical test available is the repeated load triaxial. Both the 150mm and 75mm diameter facilities have been used, as described in chapter 3. Specimens were not necessarily prepared in an identical manner, particularly where variation of compactive effort was to be studied, but in every case the mode of compaction was tamping by hand.@ Once each specimen was set up and instrumented, following the procedure in chapter 3, it was then subjected to the following programme of tests.

(a) Elastic tests on a series of 20 stress paths, as shown in fig 5.1. They are shown in p,q space, since such a system lends itself to the triaxial situation; p and q have been defined in section 2.2. It may be seen that 10 of the paths involve no deviator stress, whilst 10 do.

(b) Repeated load plastic testing on one stress path, more severe than any yet experienced, being cycling of the

@ This does not apply to the dolomitic limestone used as an example in Chapter 4, which was compacted on a vibrating table.

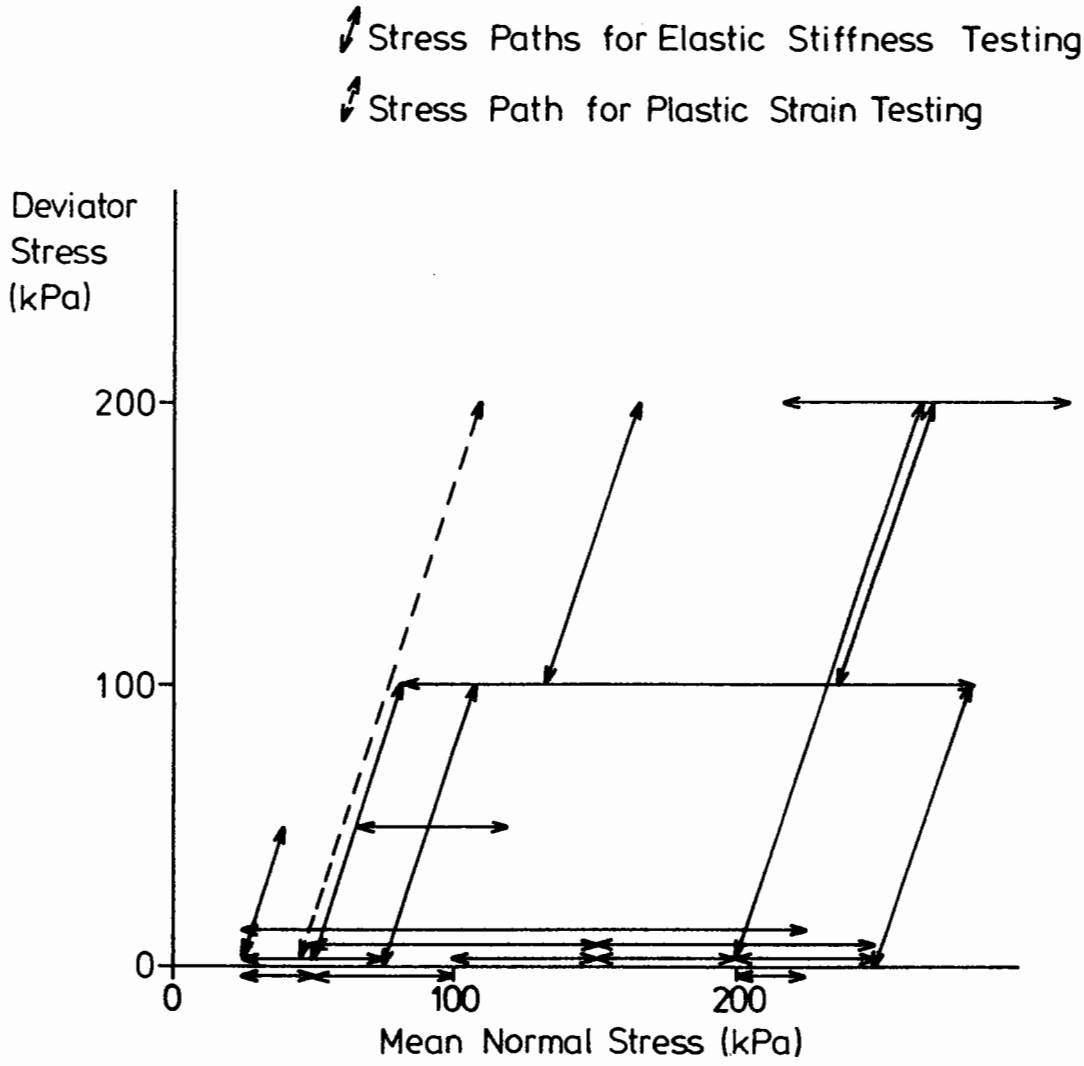

FIG. 5.1 Standard Stress Paths

deviator stress between zero and 200kPa at a confining stress of 50kPa, and at a frequency of 1 Hz.

(c) Raising the deviator stress slowly, at 50kPa confining stress, until continuous straining is occurring with no further deviator stress increase.

(d) Raising the deviator stress slowly, at nominally zero[@] confining stress, until continuous straining is occurring with no further deviator stress increase.

At every stage of testing, strain output is recorded from the axial and radial strain transducers, and converted to volumetric and shear strain. These strains are outputted directly onto an XY plotter, to record the elastic behaviour in phase (a) and the monotonic loading curves from phases (c) and (d). The voltage output from the transducers is also recorded by hand during phases (b), (c) and (d), and later converted to strain.

5.2 USE OF RESULTS

The above routine was developed so as to allow the determination of all the constants relating to the behavioural equations developed in chapter 4 but to require less than a day for each specimen to be set up, tested and dismantled. It is also easily possible to obtain a simplified set of behavioural parameters. The derivation of these numbers is described below.

@ Nominally zero implies no fluid pressure and a loose fitting membrane.

5.2.1 Elastic Behaviour

The results from phase (a) of the test routine are analysed in three stages:

(i) Volumetric strains for the 10 paths involving no deviator stress (fig 5.1) are plotted against change in ln (p), on logarithmic scales. Fig 5.2 is an example of such a plot, taking results for a sand and gravel. It can be seen that a set of equally spaced straight lines has been drawn, described by the magnitude of the change in p, and equation (1) shown inserted on the plot - describes the family of lines mathematically; this equation is of the form proposed in chapter 4 for compressive volumetric strain (eq 4.9). However, for the purposes of this chapter a simpler relationship is demanded, and also shown in fig 5.2 is a 45° dashed line, representing a best fit linear relationship between volumetric strain and change in ln (p). Equation (2) in the insert describes this line and the constant, in this case 500, is a type of non-linear inverse volumetric stiffness. Its inverse multiplied by 1000 will therefore be used as a compressive volumetric stiffness indicator.

(ii) The shear strains from the 10 paths involving non-zero deviator stress (fig 5.1) are then plotted against change in $\ln(\sigma_v / \sigma_h)$, where σ_v is the vertical stress and σ_h is

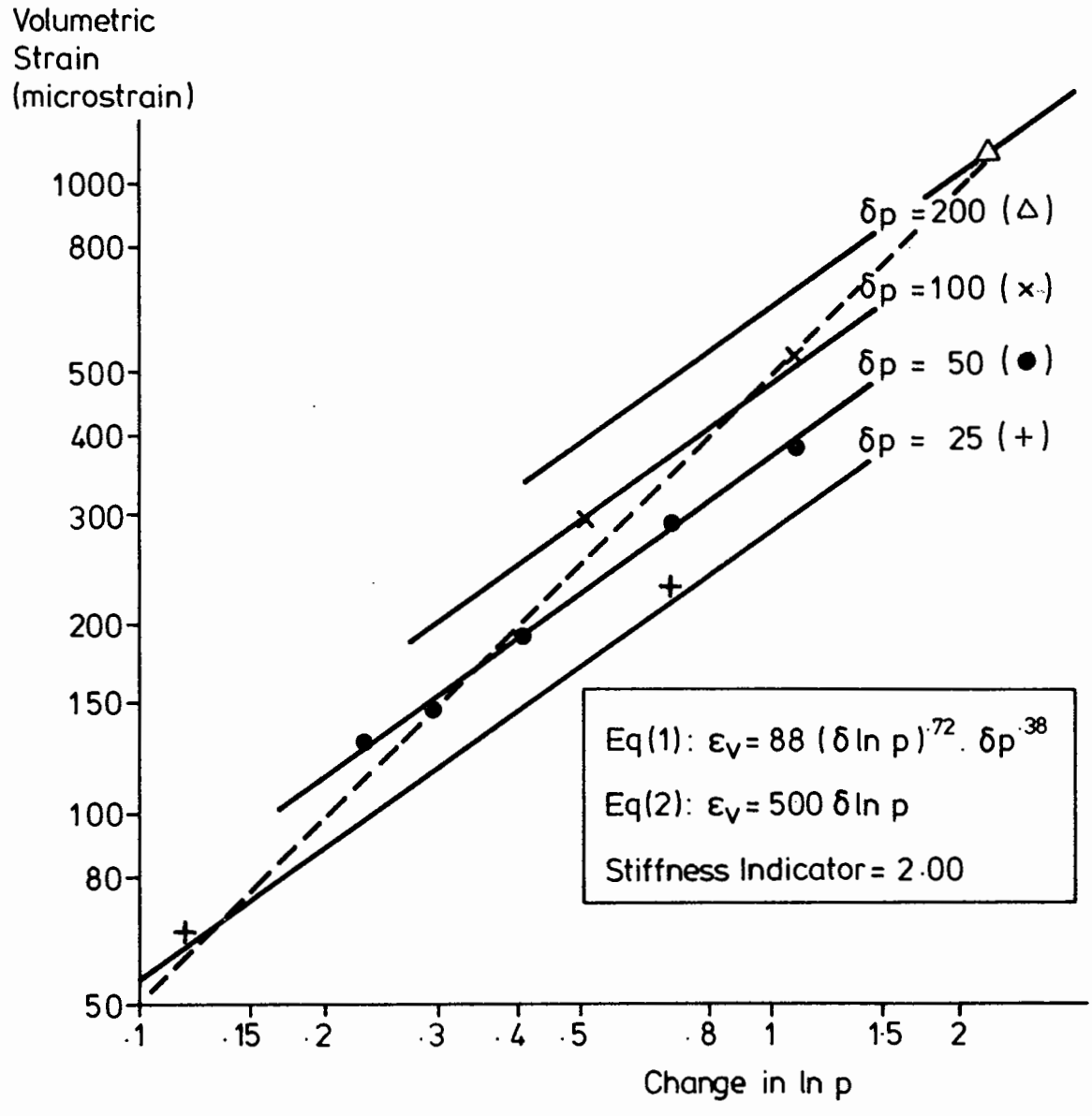

Fig. 5·2 Compressive Elastic Volumetric Strain Analysis for Sand and Gravel (Attenborough - Nottinghamshire)

the horizontal stress. Fig 5.3 shows the results for the same sand and gravel and, again, a set of equally spaced straight lines has been drawn. This time each line is described by the stress path length parameter, $\delta t + \frac{1}{3}\delta s$, (where $t=\frac{1}{2}(\sigma_v - \sigma_h)$ and $s = \frac{1}{2}(\sigma_v + \sigma_h)$), and equation (1) in the insert to fig 5.3 describes the family of lines drawn, following the form of eq 4.6. As for compressive volumetric behaviour, a 45^o best fit straight line is also shown and described mathematically by equation (2). This results in a single constant, the inverse of which multiplied by 1000 is used here as a measure of shear stiffness.

(iii) Finally, the volumetric strains predicted by equation (1) in fig 5.2 are computed for the second 10 stress paths, those involving non-zero deviator stress. The differences between the computed values and those measured are then taken and plotted against the change in the square of $\ln(\sigma_v/\sigma_h)$. This results in a graph such as that shown in fig 5.4 for the same sand and gravel. By this stage there is likely to be a certain amount of cumulative error, giving rise to a certain unpredictability in the form of results, but a straight line or family of straight lines can again be drawn, together with a best fit 45^o straight line (shown dashed). Equations (1) and (2) in the insert then describe the full and simplified behaviours respectively, in relation to volumetric strain due to

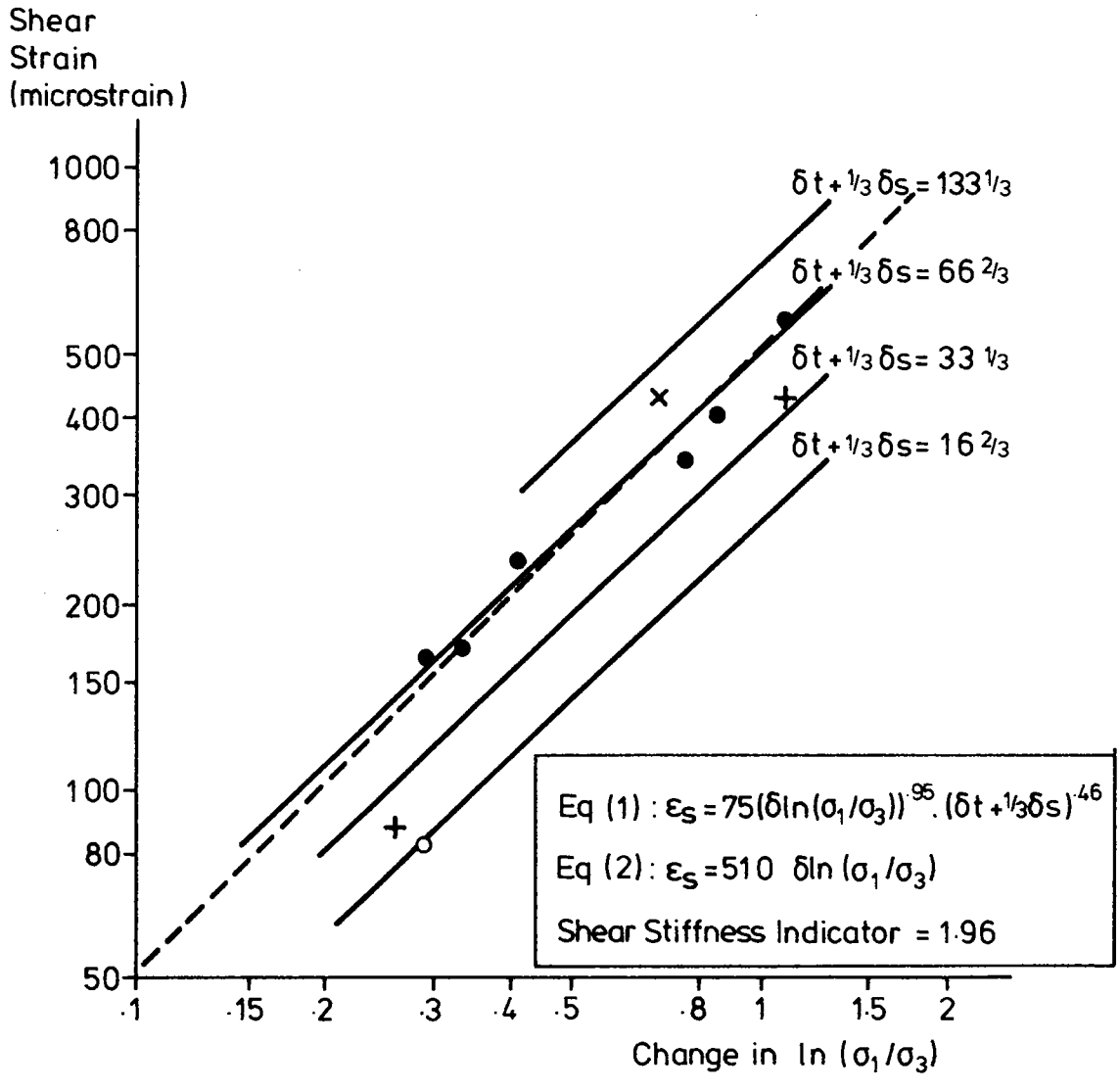

Fig. 5.3 Elastic Shear Strain Analysis for Sand and Gravel (Attenborough - Nottinghamshire)

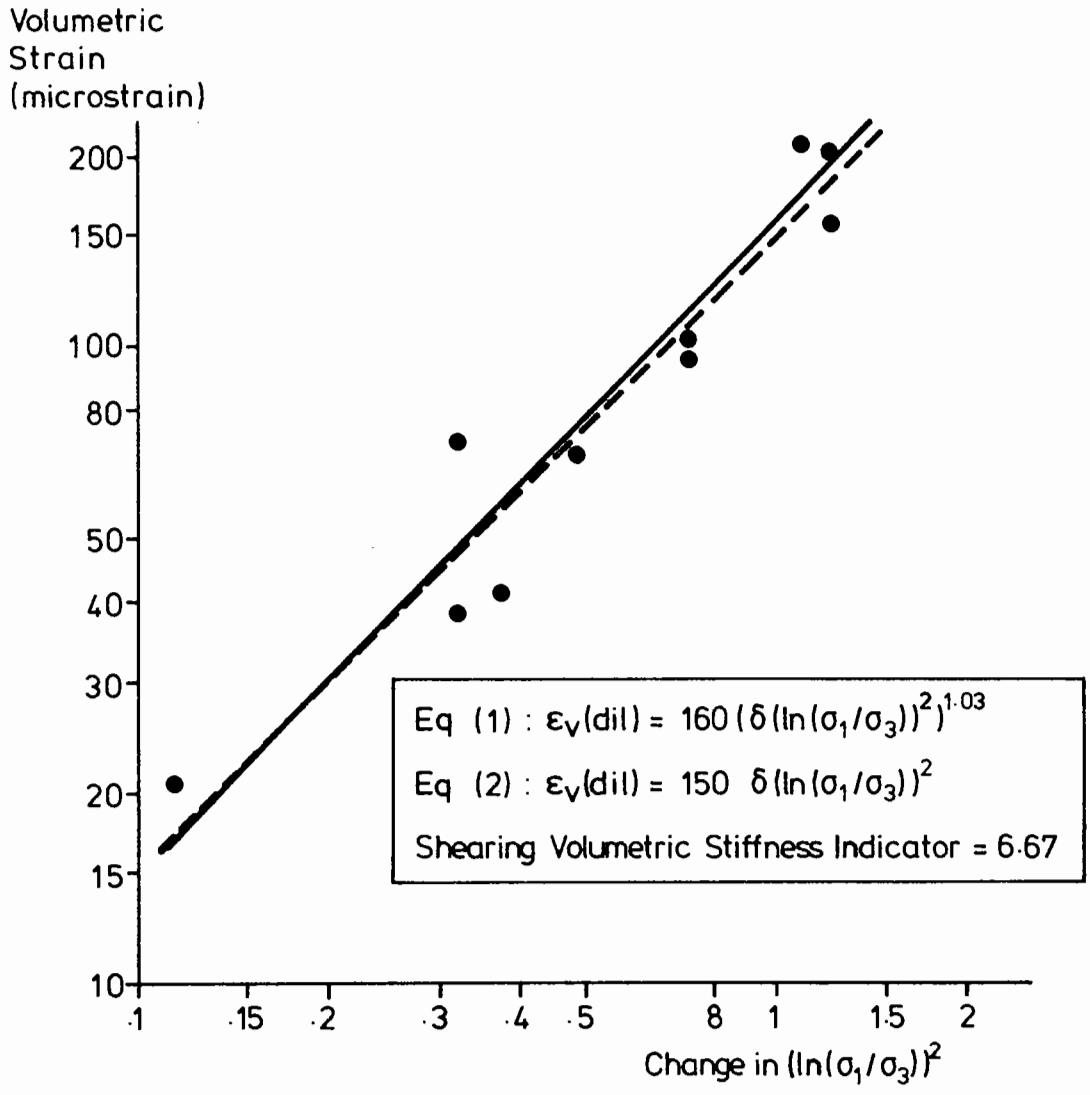

Fig. 5.4 Analysis of Volumetric Strain due to Shearing Action for Sand and Gravel (Attenborough-Nottinghamshire)

shearing action. The inverse of the constant in equation (2) multiplied by 1000 is used as a measure of the stiffness of the material volumetrically under shear.

5.2.2 Plastic Behaviour

To obtain the material constants used in chapter 4 to describe plastic behaviour, several steps are necessary:

(i) The results from test phases (c) and (d) are combined to describe a Mohr Coulomb failure line, shown in fig 5.5 for the sand and gravel, plotted as $(\sigma_v - \sigma_h)$ against σ_h . The intercept determined from phase (d), is commonly small, and the ratio σ_v / σ_h at failure relating to 50kPa confining stress may thus be used as a simple strength indicator or, alternatively, a ϕ value (friction angle) can be calculated.

(ii) The constant L in eq 4.15 is found by referring to the strain readings relating to the monotonic failure test in phase (c). It was found in chapter 4 that, if 80% of the failure stress was taken as the point at which eq 4.15 was constrained to give the correct shear strain, then the curve described by eq 4.15 would fit the data satisfactorily. This process produces a unique value for the constant L.

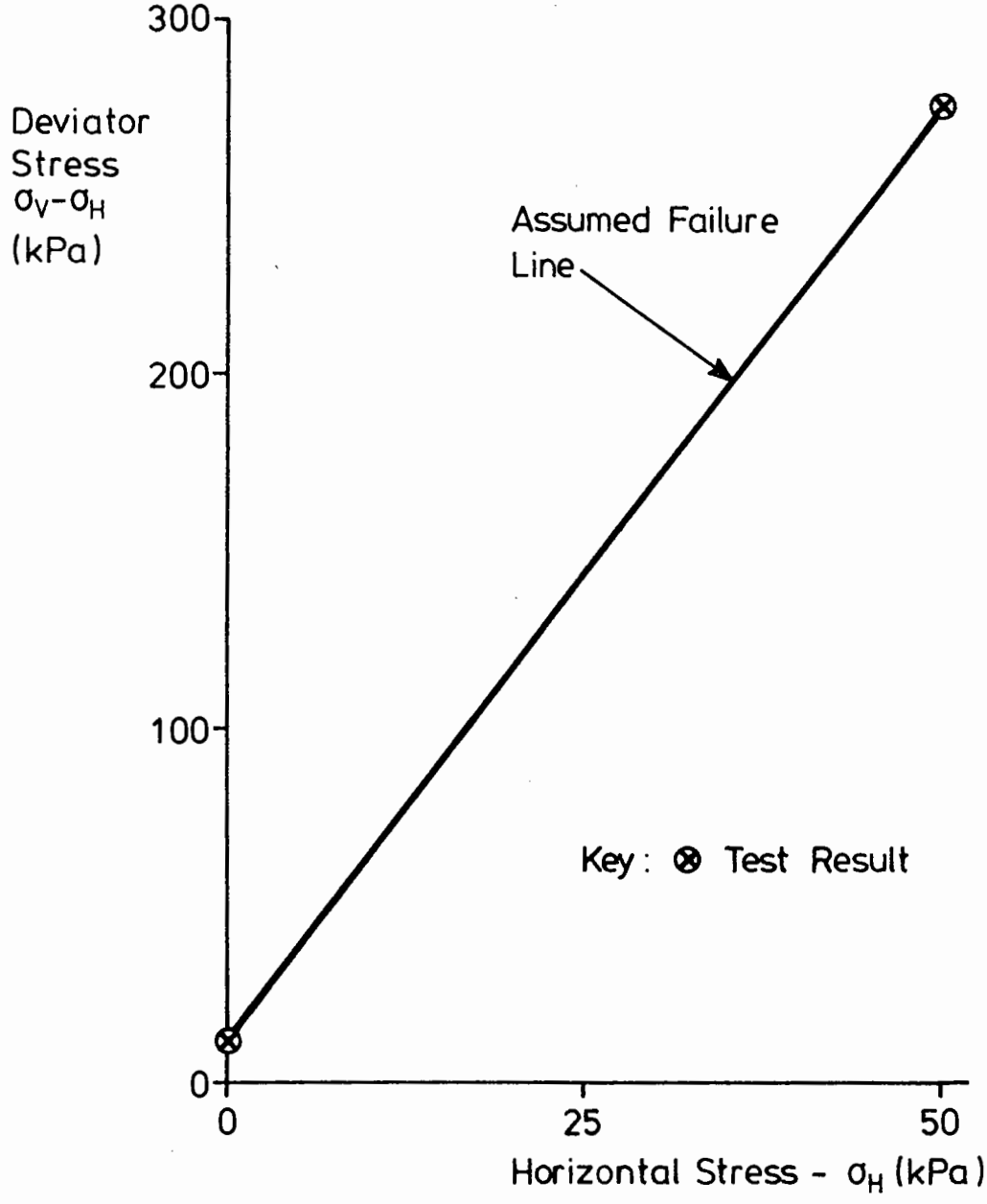

Fig. 5.5 Analysis of Failure Tests for Sand and Gravel (Attenborough - Nottinghamshire)

(iii) The final constant required to describe cumulative plastic shear strain is M_1 in eq 4.19. This is determined by taking the strain at 1000 cycles of load from phase (b) and choosing M_1 such that eq 4.19 gives that value, using the values of σ_f (failure stress) and L already obtained.

(iv) Plastic volumetric strain requires only one other constant, M_2 in equation 4.22, and this is simply determined by matching the measured volumetric strain at 1000 cycles.

Derivation of a simple quantity describing the susceptibility of a material to plastic straining under cyclic load is not easy, since a combination of parameters is involved. Thus, this chapter will use the plastic shear strain developed between the first and thousandth cycles of load in phase (b) of the testing, although, for some of the weaker specimens, this figure will have to be extrapolated since some tests were stopped early due to excessive straining. Use is also made in section 5.5 of the number of cycles to failure predicted by the plastic shear strain equation using the stresses in phase (b). It should be noted however that neither quantity gives a complete picture of plastic strain susceptibility.

5.3 EFFECT OF GRADING CURVE SHAPE AND DEGREE OF COMPACTION

This section details results from tests on a series of 21 specimens of dry dolomitic limestone, performed in the 75mm diameter triaxial apparatus (ref section 3.1.2). Apparatus size

(desirable in the interests of speed) placed an upper limit on the particle sizes which could be used and, in fact, all gradings tested had a maximum particle size of 10mm. Fig 5.6 shows the seven gradings tested. It can be seen that they form a family of curves described by the general formula shown in fig 5.6, differing only in the value assigned to the parameter 'n'. Alteration of this parameter achieves a spread of gradings from virtually single sized to very broadly graded. The only deviation from the theoretical gradings which was necessary was due to the fact that the proportions of size fractions less than 75 microns remained fixed, with a smallest particle size of around 1 micron. The logic behind the choice of gradings is that a property of the general formula in fig 5.6 is that the ratio of percentages passing any two size fractions, say d and d/2, remains constant whatever d. This is likely to be approximately the case in a material being crushed; ie if half the 20mm particles are crushed to smaller sizes, it is likely that half the emerging 10mm particles will be also, if they undergo the same process. Whether this argument is approximately valid or not, it is none the less true that the shape of the DTp type 1 grading envelope (Department of Transport 1986) for sub-base materials could be approximately represented by a curve of this family with n = 0.5 and d_{100} = 40mm.

At each of the seven gradings, it was decided to make up three specimens at very different levels of compaction. These were zero, 150 light blows per layer and 150 heavy blows per layer

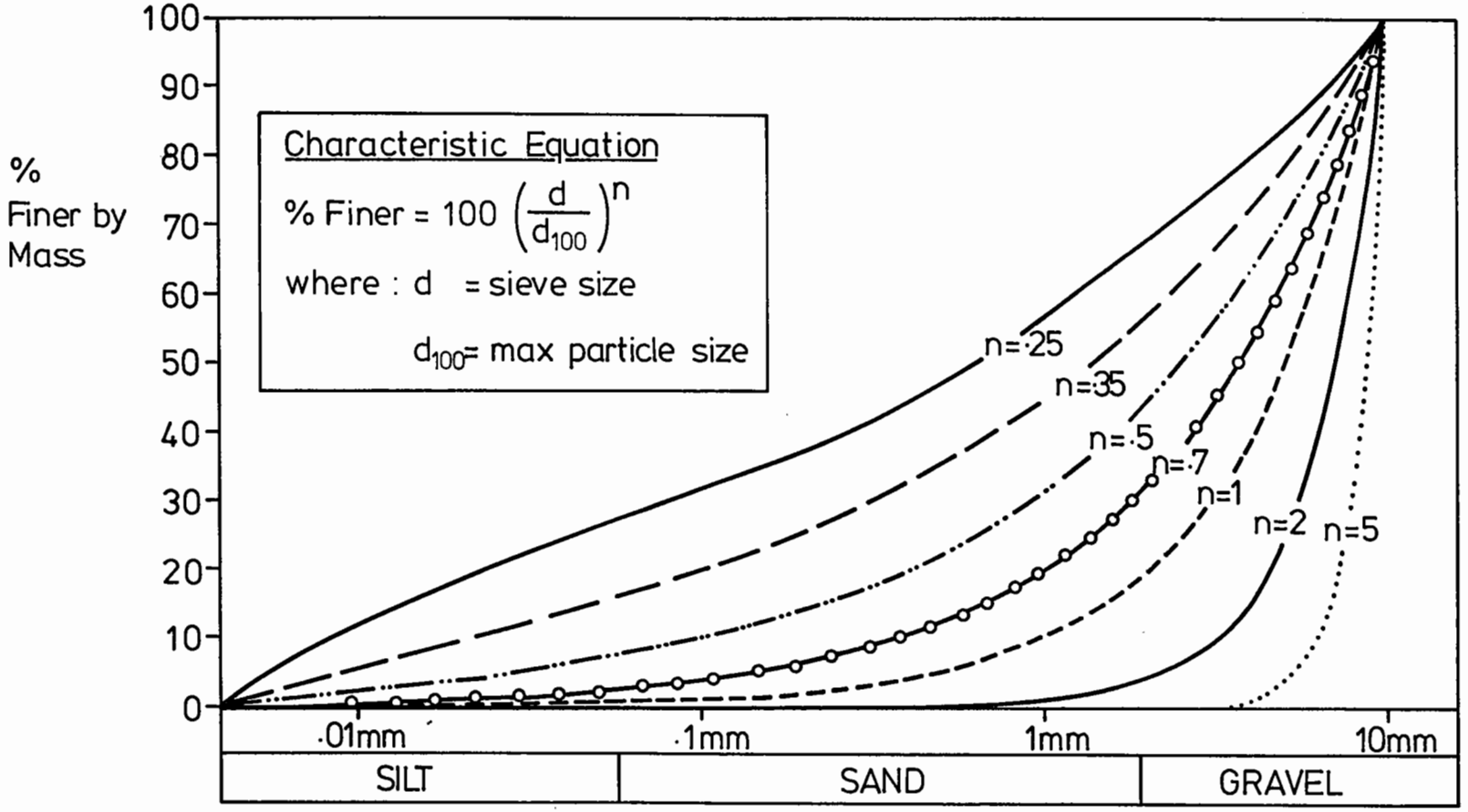

Fig. 5.6 Grading Variations Investigated

(both over 5 layers). Compaction was manual, giving rise to the possibility of some inconsistency in applied effort.

The dry densities achieved are plotted in figure 5.7. The first point to notice is that they all lie on smooth parallel curves and show little sign of any unexpected results due to inconsistent compaction. Otherwise the general form of fig 5.7 is not surprising. The difference in density between the different levels of compaction is fairly constant over the whole range of gradings. Generally, as the grading becomes broader the achieved densities increase, although there may be an optimum point at around n = .3, possibly due to deviation from the theoretical grading curves at the fine end.

Each specimen was subjected to the test routine described in section 5.1, except for the omission of part (d) for some specimens, and analysed according to the method outlined in section 5.2. The results will be discussed here, firstly in relation to elastic behaviour, then plastic.

5.3.1 Elastic Behaviour

Fig 5.8 shows plots of the variation of the three simplified elastic stiffness indicators described in section 5.2.1 against the grading parameter 'n'. (Constants for the full stress strain equations are given in Appendix B). Not surprisingly, there is some scatter but two quite interesting conclusions can none the less be made. Firstly, it is evident that the state of

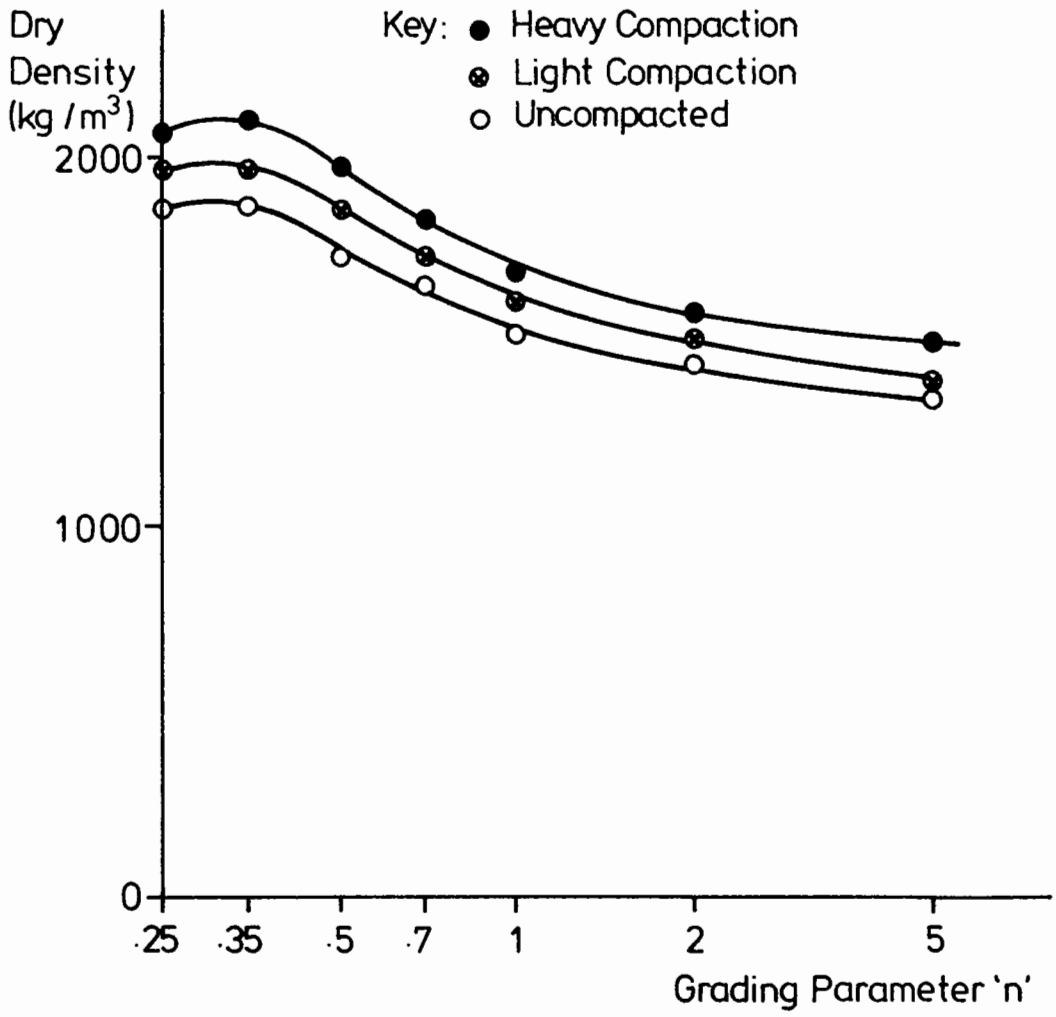

Fig. 5·7 Densities Achieved at Different Gradings

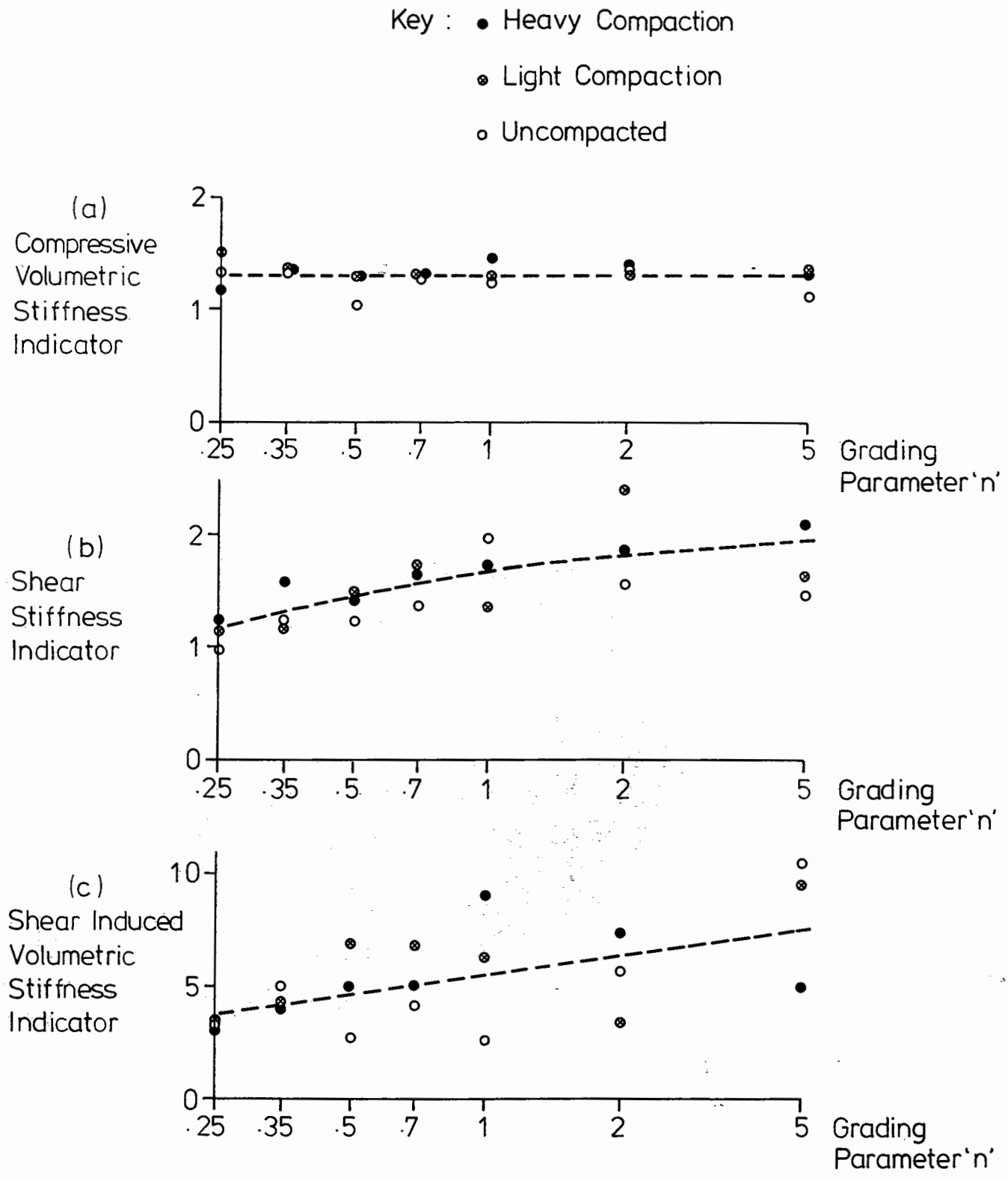

Fig. 5·8 Simplified Elastic Performance Indicators for Different Gradings

compaction has almost no influence at all, although some slight trend for the denser material to be stiffer may be seen in fig 5.8 (b) for shear stiffness. This is particularly interesting since the range of compactive efforts extends to zero. The amount of plastic volumetric strain which took place during elastic testing was monitored and never exceeded 1%, which is certainly far from sufficient to bridge the density differences shown in fig 5.7. Thus, this result is considered genuine.

The second conclusion is that the influence of grading is relatively slight, insignificant in fact in fig 5.8 (a) for compressive volumetric stiffness. Furthermore, the trend in fig 5.8 (b) and (c) is for the more uniform gradings to be stiffer, possibly up to a factor 1.5 to 1.8 between the two ends of the grading spectrum. The implication is that there is no relationship between voids content and elastic stiffness. To put it another way: packing fines into an aggregate will not improve its elastic stiffness; it may well reduce it.

In fact, both these conclusions were also made by Hicks (1970) after his tests on crushed rock, although his range of density and grading was much smaller. However he did observe that the effect of density on a partially crushed gravel was rather greater, indicating a possible material dependence in these relationships.

5.3.2 Plastic Behaviour

Fig 5.9 (a), (b) and (c) present the simplified parameters for shear strength and plastic straining under repeated loading described in section 5.2.2. (Constants for the full equations are given in Appendix B). Shear strength is shown in fig 5.9 (a) as a principal stress ratio (σ_v/σ_h). It can be seen that the effect of compaction is dominant, but that the more uniform gradings tend to be weaker as well. An optimum grading is hard to pick out, but it would certainly be toward the broadly graded end of the range. This effect is reinforced by the values of unconfined failure stress, determined in phase (d), section 5.1, which are plotted in fig 5.9 (b) for the heavily compacted specimens only. The test was not performed on the other specimens.

The parameter used as a simple indicator of resistance to cyclic plastic strain (ref. section 5.2.2) is plotted in fig 5.9 (c) Scatter is very much evident but still allows trends to be seen. Degree of compaction is clearly once more the dominant factor, the low values, indicating better resistance to straining, being for the heavily compacted specimens. The grading trend is complex but, for heavily compacted material, it appears that grading has little influence.

One point which is missing from the graphs, because it represented completely different behaviour from that of every other specimen, is that for the densely compacted specimen with

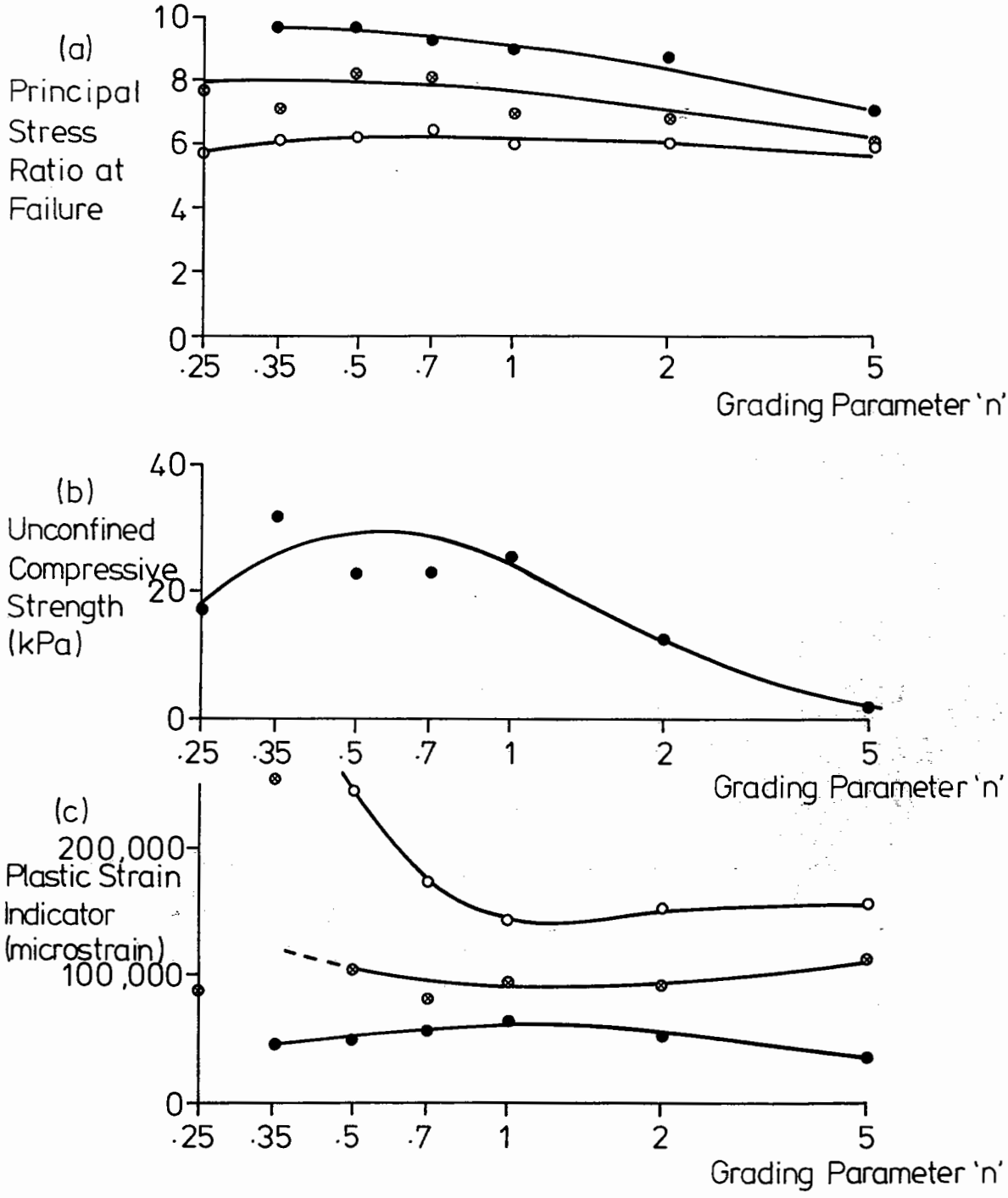

Fig. 5.9 Simplified Plastic Performance Indicators for Different Gradings

an n = .25 grading. As soon as the plastic strain cyclic stress path was applied, the specimen became rapidly less stiff and exhibited large plastic strains, such that the test had to be stopped. The exact reason for this is not known but it may relate to the importance of what has been termed a 'characteristic threshold' (Luong 1985), which, if transgressed repeatedly, leads to rapid failure. The only obvious difference between the results for this particular specimen and the others was that the plastic volumetric strain under repeated loading was negative, ie dilatent, whereas it was positive for all the others, and this may, in fact, be the trigger for the formation of failure planes. However, whatever the exact mechanism, the result underlines a possible danger in using an aggregate with very high fines content.

5.3.3 Summary

Several interesting facts have emerged above, which are summarised here. Compaction is seen as having almost no effect on elastic behaviour, but as being a dominant factor in reducing plastic strain and increasing shear strength. Grading has a relatively slight effect on elastic behaviour, the more uniform material being stiffer, but a more pronounced one on shear strength, where the more broadly graded material is stronger. The effect on plastic strain is not clear. It should be remembered that all the above results are for a dry material, and that the total picture may need amending when the effects of

water are included. This is seen in chapter 6.

5.4 EFFECT OF PARTICLE SIZE

One source of confusion in understanding granular material behaviour is that such a material is not really a continuum,@ but rather a mass of individual particles, each with its own unique properties of shape, roughness etc. This presents two possible problems. The first is that, as the number of particles across a specimen dimension, or through a pavement layer, becomes small, the approximation of the material to a continuum becomes less realistic. This may affect both elastic stiffness and plastic behaviour. The second problem is slightly different, being that different sized particles of a particular mineral may have different shape and surface properties. This second problem is, of course, likely to be material dependent.

Generally these questions do not arise in element testing of materials. A material is delivered from site and tested in an apparatus considered large enough for such effects to be negligible, ie such that the material may be treated as a continuum. However, testing of large material such as rock-fill demands answers to these questions. Work done by Marachi et al (1972) demonstrated that, if a rock-fill material was scaled down and the specimen size scaled down with it, then the monotonic loading curve would be similar to that for the full scale material in an appropriately larger specimen. In fact the shear strength was slightly greater for the smaller material.

@ Mathematical models of behaviour generally assume a granular material to be a continuum.

The stresses applied were the same. However, no repeated load testing was done.

Since the problem was seen as being an important one in enabling an improved understanding of granular material, three series of tests were performed in the triaxial apparatus to try to isolate the parameters relating to particle size effects. The test routines used were generally different from that described in section 5.1. This section will report briefly on each test series before summarising the findings as far as possible.

5.4.1 Tests on Single Sized Material

Accurate scaling of a graded aggregate containing fines requires the separation and recombining of all size fractions including those less than 75 microns. Since it is a time consuming procedure to achieve this for such small particles, the accuracy of scaling is often compromised in this area. However, single sized material presents no such problems, allowing a size range of at least two orders of magnitude to be explored. Several tests were, therefore, carried out on these materials in anticipation that the findings could also be applied to a graded aggregate.

It has been mentioned already that differences in shape and surface roughness between various size fractions are likely to be material dependent effects. Thus, four different types of aggregate have been investigated, namely granite, dolomitic

limestone, crushed concrete and steel slag, in the expectation that any trends common to all four are likely to apply equally to other minerals. Testing was performed in the 75 mm diameter triaxial apparatus on dry specimens which were each compacted using nominally the same compactive effort, that is 150 blows per layer over five layers. Blows were applied manually and it is possible that this may lead to some inconsistency. Either three or four size fractions were tested for each aggregate type, ranging from 75 microns, the smallest sieve size used, to 14mm.

The achieved compaction is illustrated in fig 5.10 which gives the results in terms of percentage of solid rock. This removes the discrepancies due to the different specific gravities of the four minerals. The results are interesting in that two of the four materials show a trend of decreasing density with decreasing particle size, whereas the trend for dolomitic limestone is reversed and that for steel slag is unclear. It can also be seen that some of the materials pack to a higher solid rock percentage than others. This is most noticeable at the fine end of the spectrum. The results serve as a strong indicator that different size fractions have significantly different average shapes.

The procedure chosen for these tests was a very simple one, since it was considered more important to cover a large number of specimens than to study each in depth. Two cyclic stress paths were applied, varying the confining stress with zero deviator stress. Thereafter the confining stress was held constant at 50kPa and three paths involving cyclic deviator stress applied.

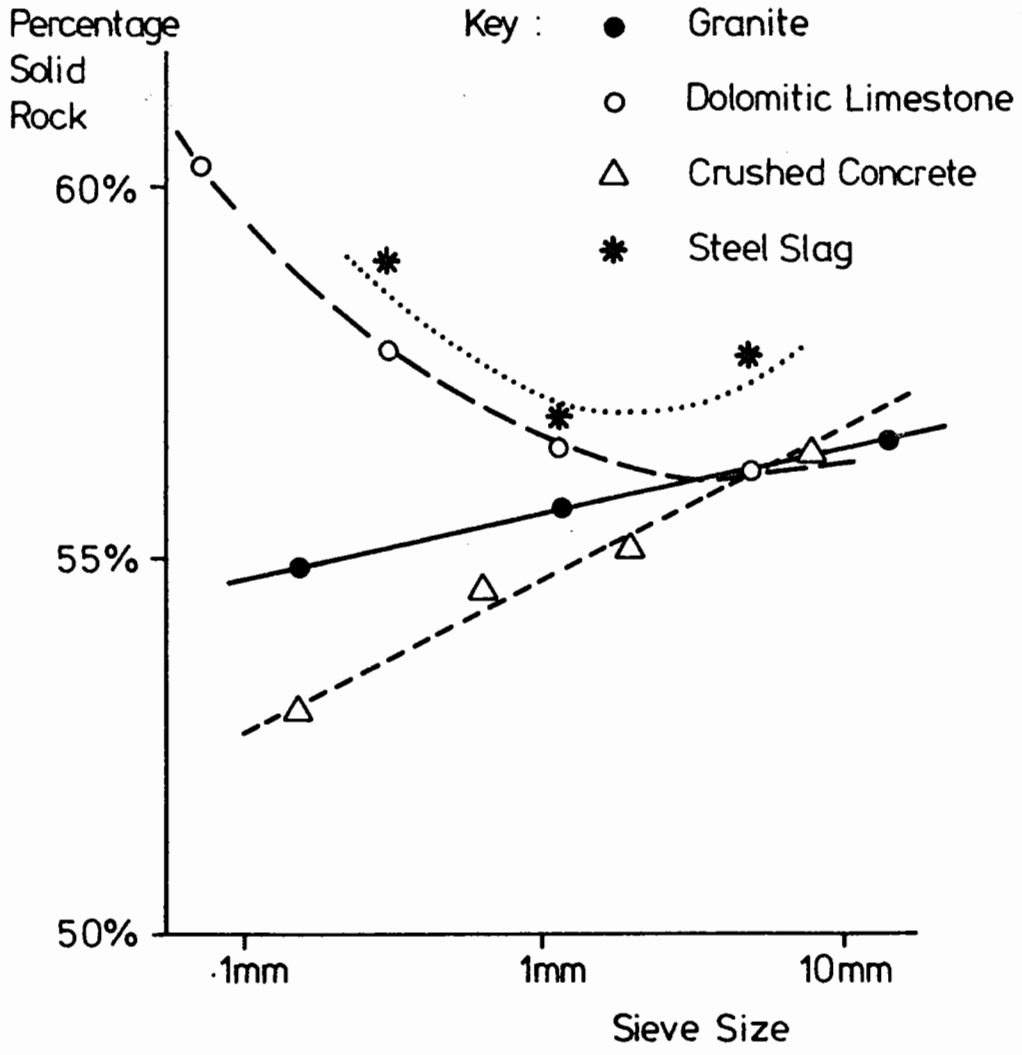

Fig. 5·10 Densities of Single Size Specimens

These five results enabled an idea of the elastic properties to be obtained. At the same confining stress a cyclic plastic strain test was done, the deviator stress cycling from zero to 150kPa 1000 times. Finally, each specimen was brought to failure by increasing the deviator stress, again at 50kPa confining stress. It was assumed from the results shown in Fig 5.9 (b) that all uniform materials would have a negligible unconfined compressive strength, and that a failure ratio could therefore be deduced directly. Unfortunately, there was a certain amount of deviation from the above test procedure. In particular, the tests on dolomitic limestone, although they involved a more comprehensive elastic test programme, did not include any cyclic plastic strain test. Also, the cyclic plastic strain test on 150 micron granite was performed on a less damaging stress path because of the material's weakness.

Since the number of elastic stress path tests was insufficient to obtain a full behavioural model, it was decided to work out an Elastic Modulus for each path and to compute an average as an indicator of material stiffness.

The plastic strain indicator chosen was the shear strain between the 1st and 1000th cycles. These two indicators and the principal stress ratio at failure are plotted in fig 5.11 (a), (b) and (c). Although the number of tests performed was limited and some scatter is evident, there are certain trends which emerge, as follows:

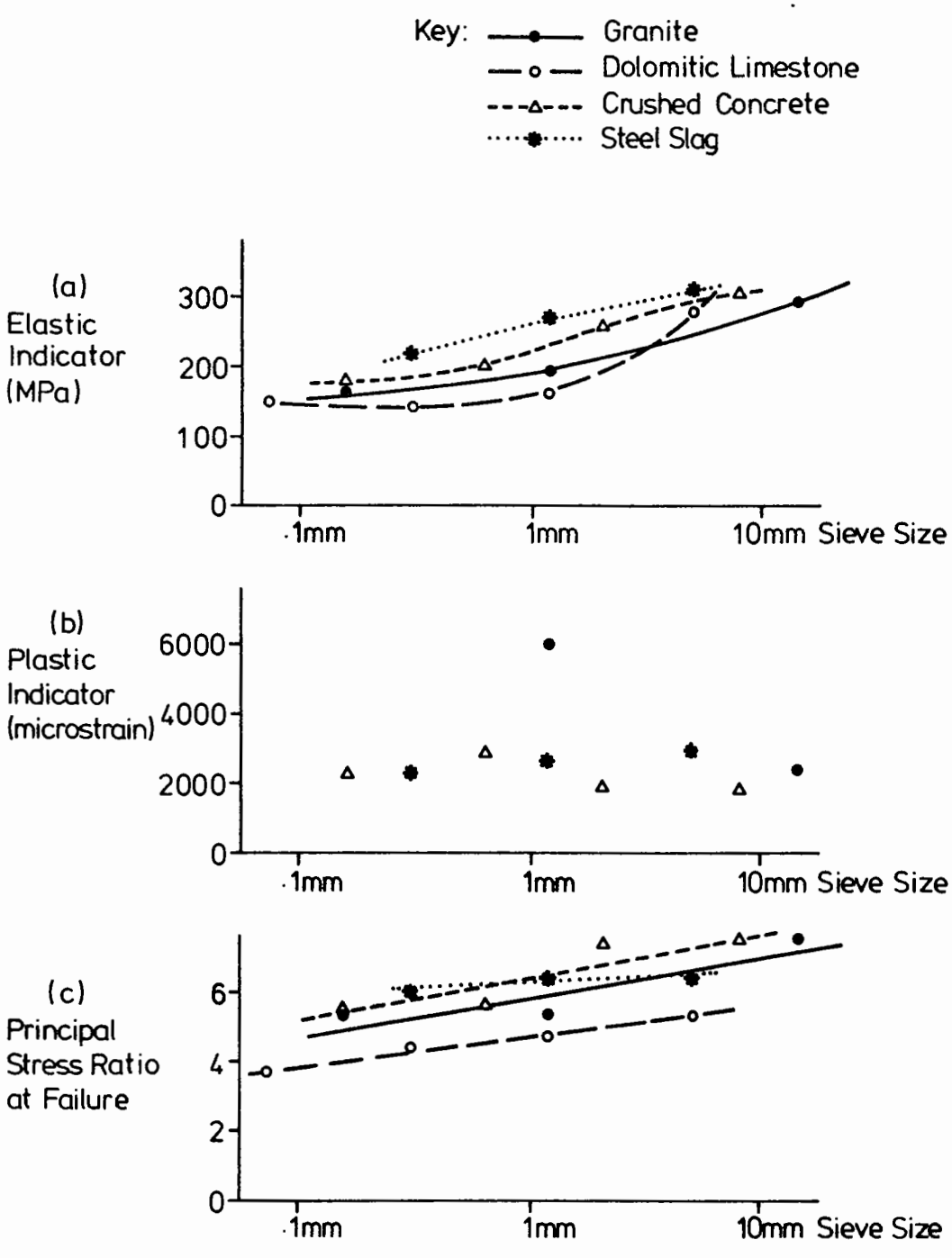

Fig 5.11 Mechanical Properties from Single Size Tests

(a) Elastic stiffness decreases with decreasing particle size, typically by about 25% for a tenfold size decrease.

(b) Shear strength decreases with decreasing particle size, typically by 15% for a tenfold size decrease.

(c) Cyclic plastic strain seems to remain fairly constant, although one result indicates otherwise.

The above points are approximately valid for the four minerals tested, giving a strong indication that they may be more generally applicable. In fact, testing carried out recently at Nottingham University on carboniferous limestone and granite (graded aggregate) has shown very similar trends. This was on material with a maximum particle size between 10 and 40 mm.

These tests, however, do not indicate whether it is purely the particle size which affects strength, stiffness and plastic strain or whether it is the ratio of particle size to apparatus size. The following sub-section details experiments designed to answer this question.

5.4.2 Tests on Graded Dolomitic Limestone

As soon as it became apparent that size effects might be of significance, a series of triaxial tests was devised to explore the influence not only of particle size but also of apparatus

size. The tests were performed on dolomitic limestone and the full size grading chosen was rather coarser than is allowed for a DTp type 1 material. Fig 5.12 shows the range of gradings explored, a one twentieth size material being the smallest used.

Three sizes of triaxial specimen were used, the 150mm and 75mm diameter devices described in chapter 3 and a small 37.5mm cell. Unfortunately strain measurement for this last apparatus was limited to measuring the vertical movement of the loading ram.

Test routines varied from specimen to specimen, since, at the time, it was not clear which aspects of behaviour could be most profitably explored. However, a confining stress of 50kPa was used throughout, except for the one twentieth size material where all stresses were reduced by a factor of ten. Deviator stress was raised in stages, and repeated cycling carried out at various levels, yielding an elastic response and also accumulation of plastic strain. Finally, the deviator stress was raised until its peak level was reached.

The intention at the time was to compact all the specimens to the same density in order to ensure maximum compatibility. Moisture was therefore added to some in order to assist compaction, since its possible effect in inducing negative pore pressure (ref chapter 6) was not yet fully realised. This introduces another variable which may render interpretation more questionable. None the less, the results are plotted in figs 5.13 and 5.14.

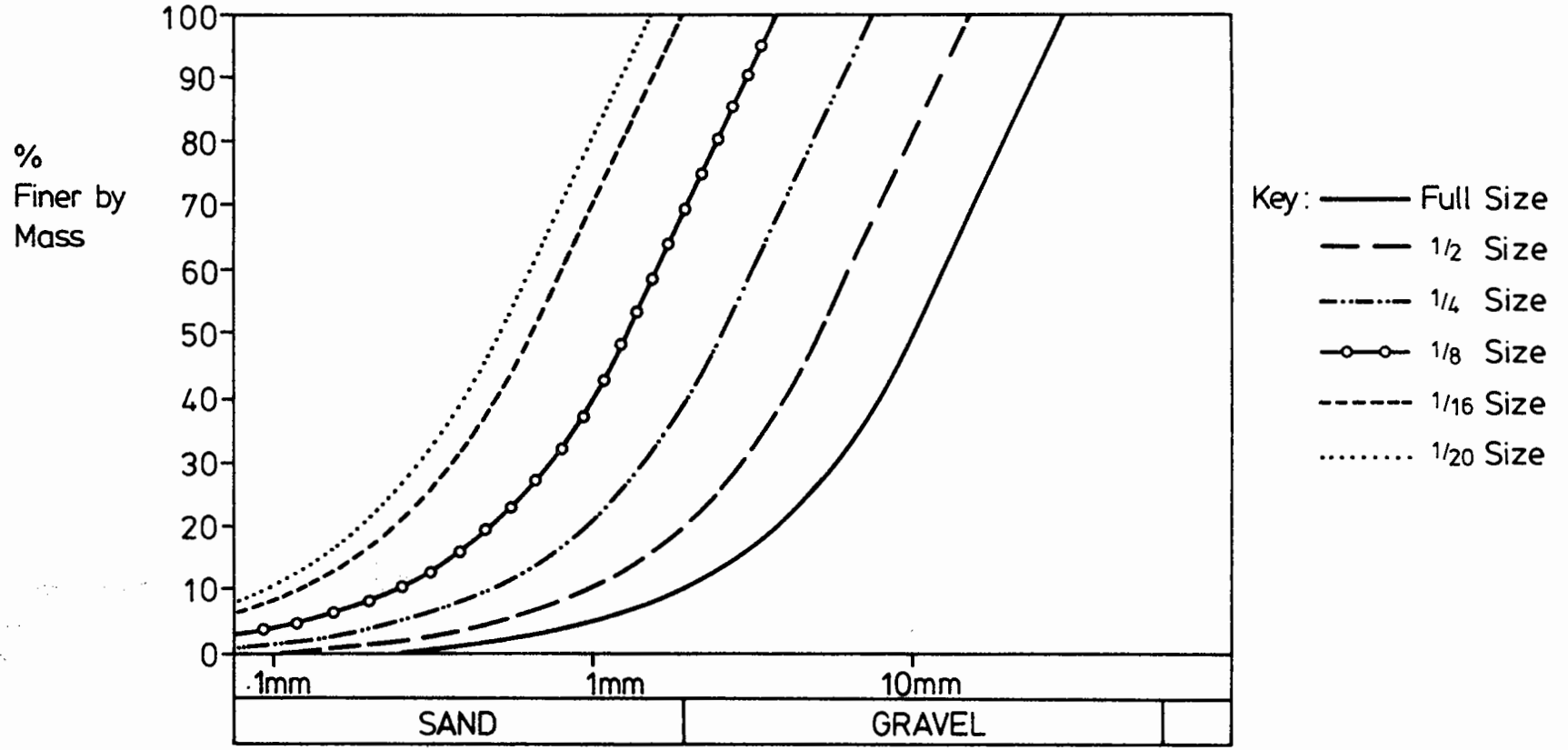

Fig. 5.12 Dolomitic Limestone Gradings Explored

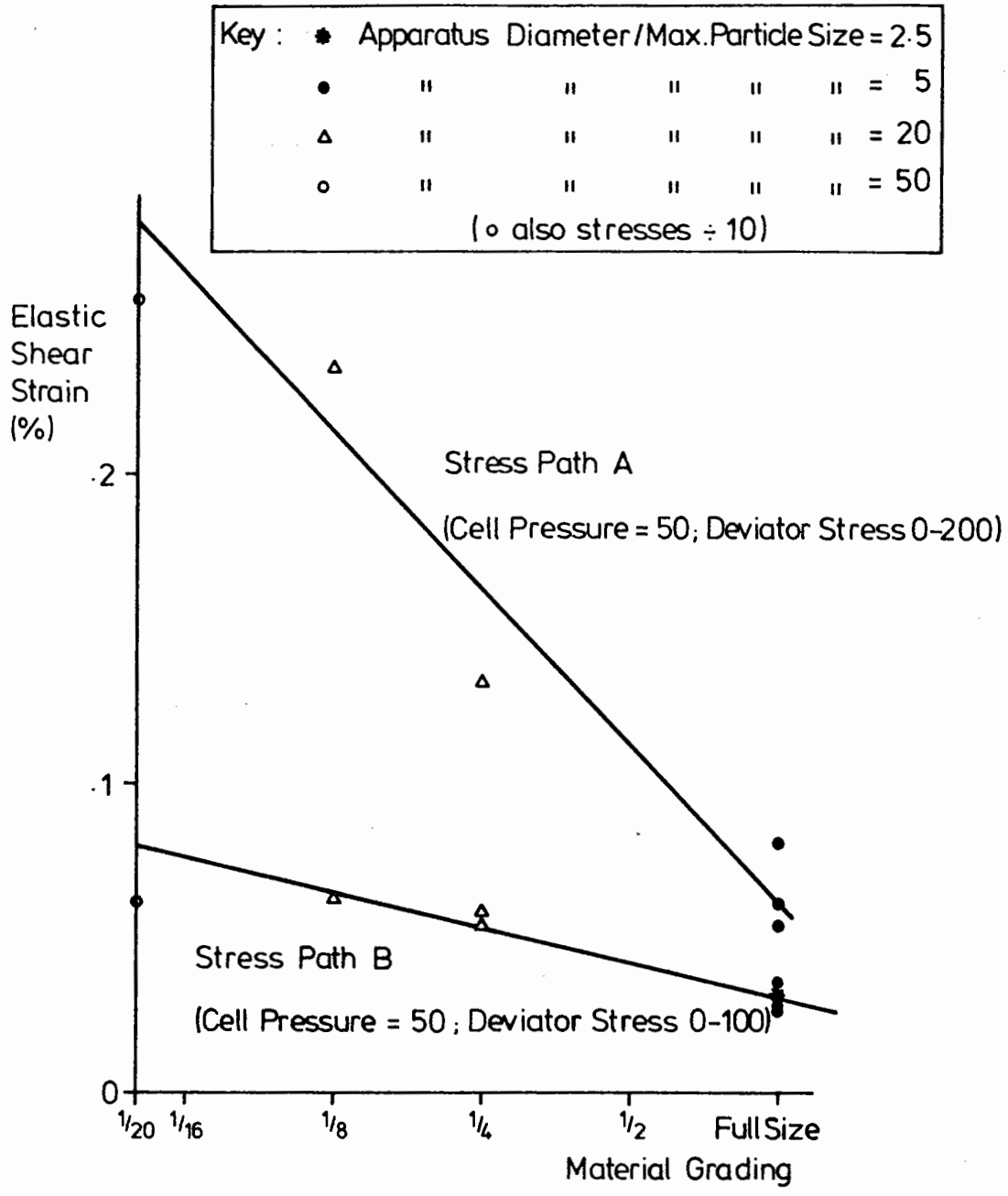

Fig. 5·13 Elastic Behaviour - Dolomitic Limestone Gradings

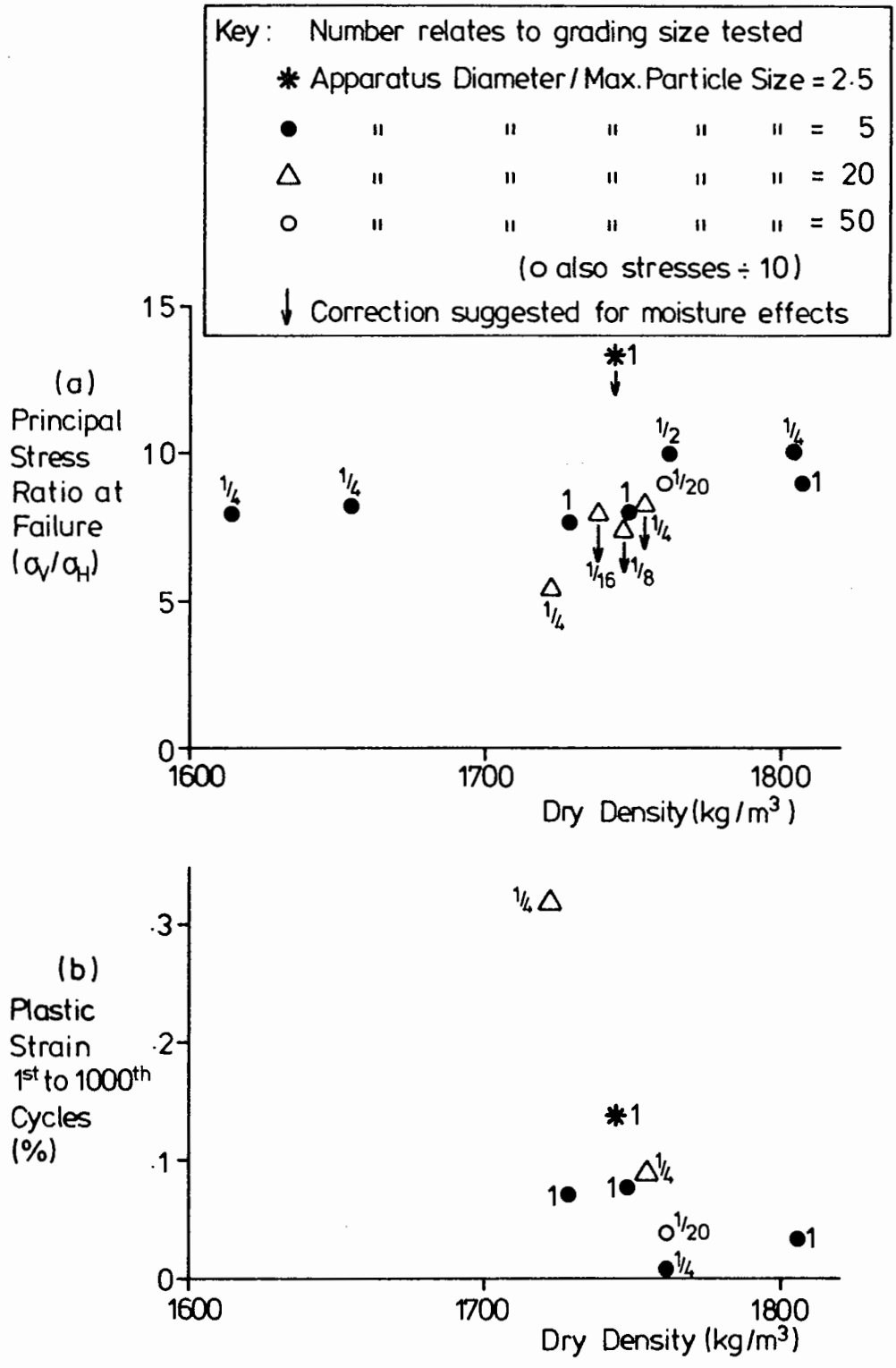

Fig. 5.14 Plastic Behaviour - Dolomitic Limestone Gradings

Fig 5.13 shows the elastic shear strain from two stress paths plotted against the size of the aggregate. Density and moisture content differences are ignored, since section 5.3 has already demonstrated the insensitivity of elastic behaviour to density variation and it is thought that any negative pore pressures would be small (ref section 6.2). It can be seen that apparatus size to aggregate size ratio appears to have no significant influence on elastic stiffness but that, as already shown in the previous sub-section, size of aggregate does: namely, smaller particles show more strain for a given stress path. Included are the results for the one twentieth size material at one tenth the stresses used for the other specimens. Not surprisingly, the strain measured is less than might be expected if the same stresses had been used because of the stress path length dependency typical of a granular material (ref section 4.1).

In fig 5.14, the principal stress ratio at failure and plastic strain between the first and thousandth cycles for stress path A (fig 5.13) are plotted against density . In neither case is the interpretation completely clear but, in the case of stress ratio at failure, (fig 5.14 (a)), it appears that it is the ratio of apparatus size to aggregate size which is of more significance than aggregate size alone. This conclusion becomes particularly likely if the corrections to moisture affected specimens suggested in the figure are made. Again the result for the one twentieth size material at one tenth stress is included and is seen to lie in the same band as the half size material at full stress, tested in the same apparatus. The results for plastic

strain under cyclic loading are rather more confused. Indeed it is not possible to draw any conclusions because of the scatter of results.

In summary, the conclusions from this test series are as follows:

(a) Elastic stiffness decreases with decreasing aggregate size, but is unaffected by apparatus size.

(b) Shear strength is controlled by the ratio of apparatus size to aggregate size, smaller ratios giving greater strengths.

(c) If, however, stresses are scaled down in proportion to aggregate size then shear strength, expressed as a stress ratio, remains unchanged.

5.4.3 Comparison with Delft University Tests

In a parallel research contract to the one described in this thesis, at Delft University in The Netherlands, a repeated load triaxial facility has been developed for testing specimens 400mm in diameter and 800mm high. An opportunity for comparing results from that apparatus with the 150mm diameter Nottingham facility was therefore sought and it was arranged to test two materials, a carboniferous limestone from the UK and a crushed concrete from Holland, in both devices. The testing at Delft was part of a series of tests, mainly on marginal materials, the results of

which are contained in Sweere et al (1987).

The test routine used was the standard Delft routine which involved cycling the deviator stress to progressively higher levels at a series of constant confining stresses and recording the elastic strains. Table 5.1 gives the stress paths used and the strains recorded for each material in both test facilities. It can be seen that there are some differences between the two sets of results but that, on average, the shear strains are comparable. The crushed concrete results are generally closer together, possibly because the grading control was better. In fact, the Nottingham crushed concrete results for shear average at 92.3% of those from Delft, whereas the limestone results average at 109.1%. This level of difference is not seen as significant, particularly since, in one case, the difference is positive and in the other negative, and the conclusion is that the same elastic shear stiffness is seen in both sizes of specimen.

The volumetric strain results are, however, completely different. The Delft tests showed a far greater dilatent strain for the limestone and a greatly reduced strain for the crushed concrete. These differences are disturbing and far greater than normal error margins would allow but, since they are in opposite directions, it is hard to draw any conclusions. All that can be said is that, though they highlight serious discrepancies, they do not indicate any influence of apparatus size.

Table 5.1 Elastic Strains - Comparison with Delft Tests

Stress Path	Carboniferous Limestone				Crushed Concrete			
	Delft		Nottingham		Delft		Nottingham	
	Shear	Vol.	Shear	Vol.	Shear	Vol.	Shear	Vol.
(1) Cell=12:q=0-24	237	-256	204	-34	177	68	127	17
(2) Cell=12:q=0-36	257	-155	287	-68	253	25	197	-6
(3) Cell=12:q=0-48	236	-99	361	-101	305	13	279	-42
(4) Cell=12:q=0-60	332	-197	428	-132	362	-32	342	-103
(5) Cell=12:q=0-72	428	-274	490	-160	414	-65	401	-177
(6) Cell=12:q=0-84	484	-489	547	-186	514	-101	468	-270
(7) Cell=24:q=0-48	218	-93	256	-10	231	98	199	2
(8) Cell=24:q=0-72	251	-60	361	-33	352	18	281	-40
(9) Cell=24:q=0-96	363	-8	454	-56	462	-1	379	-93
(10)Cell=24:q=0-120	432	-93	538	-77	520	-13	463	-161
(11)Cell=24:q=0-144	559	-332	616	-97	578	-95	551	-266
(12)Cell=24:q=0-168	604	-292	687	-115	676	-163	645	-360
(13)Cell=36:q=0-72	314	-97	293	6	304	101	275	-32
(14)Cell=36:q=0-108	403	-160	413	-10	496	146	385	-92
(15)Cell=36:q=0-144	546	-146	519	-25	492	-32	464	-149
(16)Cell=36:q=0-180	625	-244	615	-40	552	-108	553	-208
(17)Cell=36:q=0-216	772	-553	704	-54	700	-94	665	-301
(18)Cell=36:q=0-252	1017	-782	786	-66	787	-283	759	-453
(19)Cell=48:q=0-96	285	-72	322	19	313	133	317	-69
(20)Cell=48:q=0-144	297	-146	453	9	460	85	451	-140
(21)Cell=48:q=0-192	618	-256	571	-1	615	84	572	-205
(22)Cell=48:q=0-240	692	-467	677	-11	670	-50	668	-281
(23)Cell=48:q=0-288	883	-693	774	-20	773	-97	766	-383
(24)Cell=48:q=0-336	1144	-1120	865	-27	909	-206	907	-539

N.B. Strains given in microstrain.
Stresses given in KiloPascals
Cell = Confining Stress
q = Deviator Stress

5.4.4 Conclusions

Combining the three test series above, it is consistently clear that elastic behaviour is a material property and is independent of the size of apparatus used, although there will clearly be a great deal of scatter in the results if the ratio of apparatus to aggregate size becomes too small. It is also apparent from the first two test series that stiffness tends to decrease with decreasing particle size. Typically this appears to be about a 25% stiffness reduction for a tenfold size decrease.

The dolomitic limestone series indicates that shear strength is not an independent material property but that it depends on the apparatus used. Thus, it is the ratio of apparatus size to aggregate size which is the controlling factor. This in no way contradicts the finding in the first series that smaller particle sizes give reduced shear strength when tested in the same size apparatus. The relationship which emerges is that a tenfold increase in apparatus size to aggregate size ratio gives approximately 15% reduction in principal stress ratio at failure.

The implications from the tests described in this section may be seen in two areas. The first is that it is advantageous in road construction to use as large an aggregate as possible to obtain the best stiffness and strength properties. The second is that any attempted scale model of a road layer must take account of the way size affects different aspects of behaviour. Such a

model has already been described in Chapter 3 where it was stated that scaled down aggregate was being used in a reduced layer thickness under reduced stresses. The stiffness would therefore be less than the full size material but, because of the reduced stress path lengths involved, the strains may be similar. Strength, depending on ratio of particle size to layer thickness, would be unchanged. The model may, therefore, be a satisfactory simulation of the real situation.

5.5 EFFECT OF MINERAL TYPE

Although the test results quoted in chapter 4 and in earlier sections of this chapter have involved a number of different materials, there has as yet been no study of the influence of mineral type on the mechanical properties of an aggregate. This section, therefore, lists tests on several materials which could be used in road construction, many of them crushed rock at gradings within or near the DTp Type 1 grading envelope, but including some sands and gravels and other less commonly used materials. The aim was to cover as wide as possible a range of materials, particularly embracing different particle shapes and surface properties. Each material was subjected to a short visual and microscopic examination to establish the detailed make-up of its surface, as well as to categorise the shapes of different size fractions. A simple test was also performed to establish a ranking of surface friction properties. The test involved a particle, usually of approximately 20mm size, being loaded by a 2kg weight onto a rough surface, and the force

required to induce sliding being measured. This then yielded a friction angle. The materials investigated are listed in table 5.2 together with results of the microscopic examination, particle shape categorisation and measured friction angle, although it will be noticed that no information is given on two of the materials, which were not available at the time of the examination and friction test. The gradings are given in fig 5.15, where any not shown lie wholly within the DTp Type 1 limits.

Triaxial testing was carried out in the 150mm diameter apparatus on specimens compacted using nominally the same compactive effort, that is 150 blows per layer over 5 layers. Most specimens were dry; some were wet and, in those cases, the results were amended using the effective stress principle (ref chapter 6) to take account of negative pore pressures due to suction. The test routine used was that described in section 5.1 and the results were analysed according to the method in section 5.2.

Full results are given in Appendix B but, in this section, it is the simplified parameters suggested in section 5.2 which are used as a quick means of comparing the different minerals. Firstly, elastic behavioural parameters, compressive volumetric, shear and shear induced volumetric, are given in fig 5.16 (a) (b) and (c) respectively. As can be seen, the materials are ranked, the stiffest to the left, and the genus of material is shown by the

Table 5.2 Description of Materials Tested

Material (Source)	Shape		Surface Roughness		@ Friction Angle
	Large Particles	Small Particles	Large Particles	Small Particles	
1. Carboniferous Limestone (Dene-Derbyshire)	Angular	Sub-rounded to Sub-angular	Fairly Rough	Fairly Rough	32°
2. Carboniferous Limestone (ex A610 Kimberley Nottinghamshire)	Angular	Sub-angular	Slightly Rough	Fairly Rough	38°
3. Carboniferous Limestone (Chipping Sodbury-Gloucestershire)	–	–	–	–	–
4. Carboniferous Limestone (ex Wakefield Haul Road - Yorkshire)	Sub-angular	Sub-rounded	Slightly Rough	Slightly Rough	39°
5. Dolomitic Limestone (Whitwell-Nottinghamshire)	Angular	Sub-rounded to Sub-angular	Fairly Smooth	Slightly Rough	33°
6. Oolitic Limestone (ex A52 Friskney-Lincolnshire)	Sub-rounded to Sub-angular	Rounded to Sub-rounded	Fairly Rough	Smooth	38°
7. Oolitic Limestone (ex A52 Bicker-Lincolnshire)	Sub-angular	Rounded	Slightly Rough	Smooth	40°
8. Granite (Mountsorrel-Leicestershire)	Sub-angular to Angular	Sub-angular to Angular	Fairly Smooth	Fairly Smooth	27°
9. Crushed Concrete (Norfolk)	–	–	–	–	–
10. Crushed Concrete (The Netherlands)	Sub-angular	Sub-rounded to Sub-angular	Rough	Fairly Smooth	28°

Table 5.2 (cont)

Material (source)	Shape		Surface Roughness		Friction Angle @
	Large Particles	Small Particles	Large Particles	Small Particles	
11. Steel Slag (Scunthorpe-Humberside)	Sub-angular Angular	Angular	Very Rough	Fairly Rough	35°
12. Sandstone (Norfolk)	Sub-rounded to Sub-angular	Sub-rounded	Very Rough	Very Rough	30°
13. Sand & Gravel (Attenborough-Nottinghamshire)	Rounded to Sub-rounded	Rounded to Sub-rounded	Smooth	Smooth	25°
14. Sand & Gravel (South Wales)	Angular	Rounded to Sub-rounded	Fairly Rough	Smooth	38°
15. Sand & Gravel (Wymondham-Norfolk)	Rounded to Sub-angular	Sub-rounded	Smooth	Fairly Smooth	24°
16. Sand & Gravel (ex A52 Friskney-Lincolnshire)	Angular to Very Angular	Rounded	Smooth	Smooth	26°
17. Sand (Mid Ross - Scotland)	–	Sub-rounded	–	Fairly Smooth	–
18. Granitic Sand (Bardon Hill-Leicestershire)	–	Sub-angular to Angular	–	Slightly Rough	–

@ Note: Friction angle refers to the test described in the text rather than any other material property.

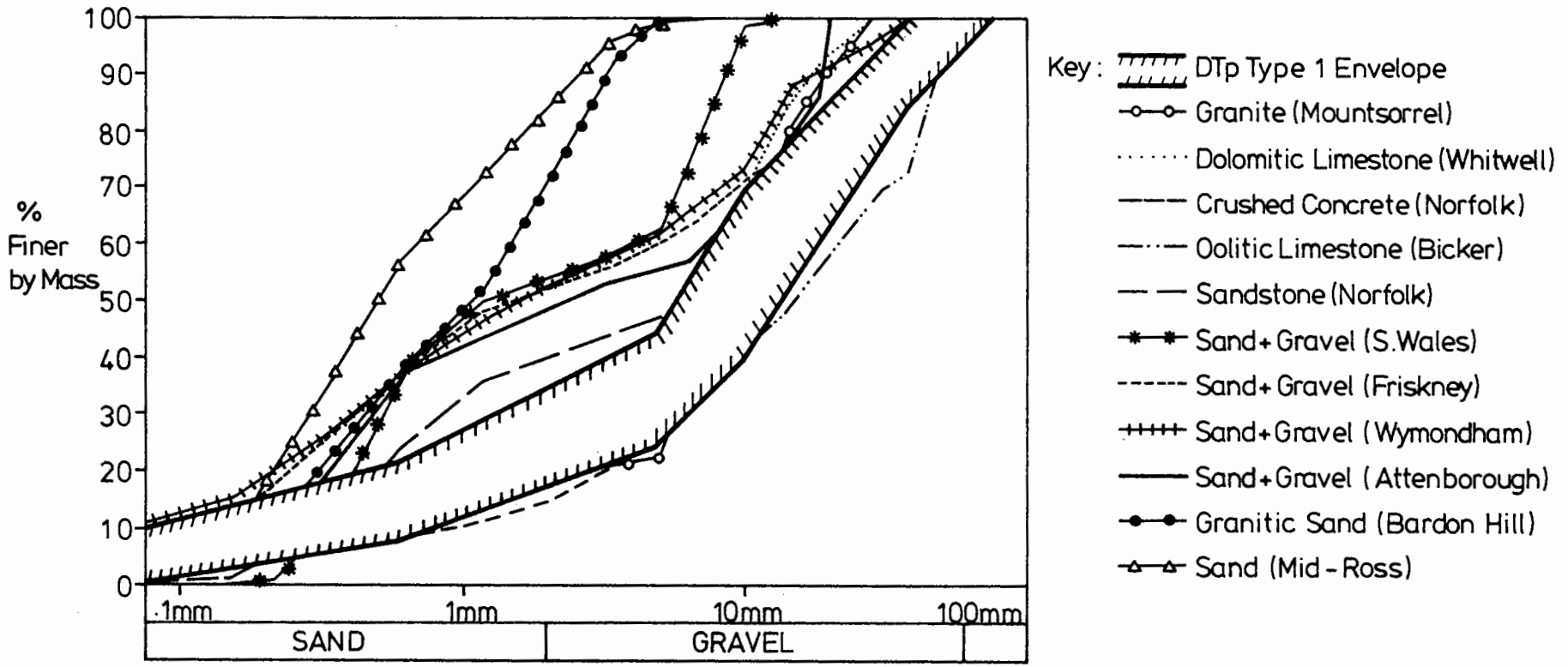

Fig. 5.15 Gradings of Materials Tested

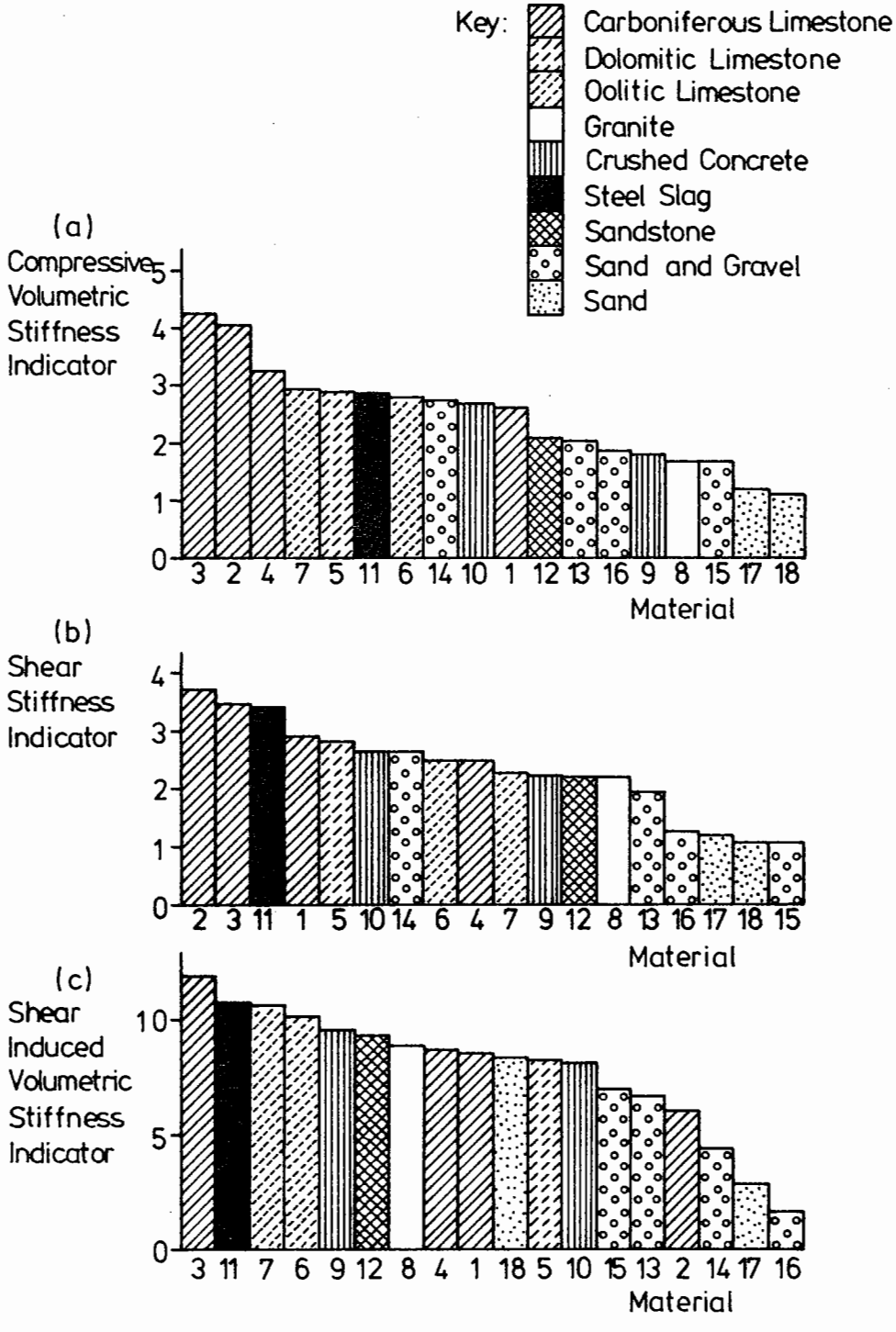

Fig. 5.16 Simplified Elastic Performance Indicators for Different Materials

shading used. Of the three graphs, it is (a) and (b) which are the most meangingful. It is immediately apparent that carboniferous limestone is a consistently stiff material with dolomitic limestone and steel slag also in the top few. Oolitic limestone is stiff volumetrically but not in shear. Crushed concrete is of average to poor stiffness, as is the sandstone. Granite@ and those materials classed as gravel are generally poor, although the material from South Wales is satisfactory: the two sands are consistently of very low stiffness.

Fig 5.17 (a) and (b) shows the other simplified results in the same way. Graph (a) gives the principal stress ratios at failure with a 50kPa horizontal stress; graph (b) gives the number of cycles to failure for the stress path (confining stress = 50kPa; deviator stress = 0-200kPa), predicted from the testing done and using equation 4.19. Here the rankings are rather different. Carboniferous limestone is still a good material, although not the strongest, with dolomitic limestone also in the same category. Steel slag is the strongest and has good resistance to cyclic load, but crushed concrete is also a very good material according to both indicators. Also in the top group is the sandstone. However, oolitic limestone joins the sands and gravels in the weakest group and with poor resistance to cyclic load. Granite@ is fairly strong but also has poor resistance to cyclic load.

To return to table 5.2, it is interesting to observe whether there is any correlation between the physical properties

@ Note: Only 1 granite material was tested and the results may not be representative of other materials in that group.

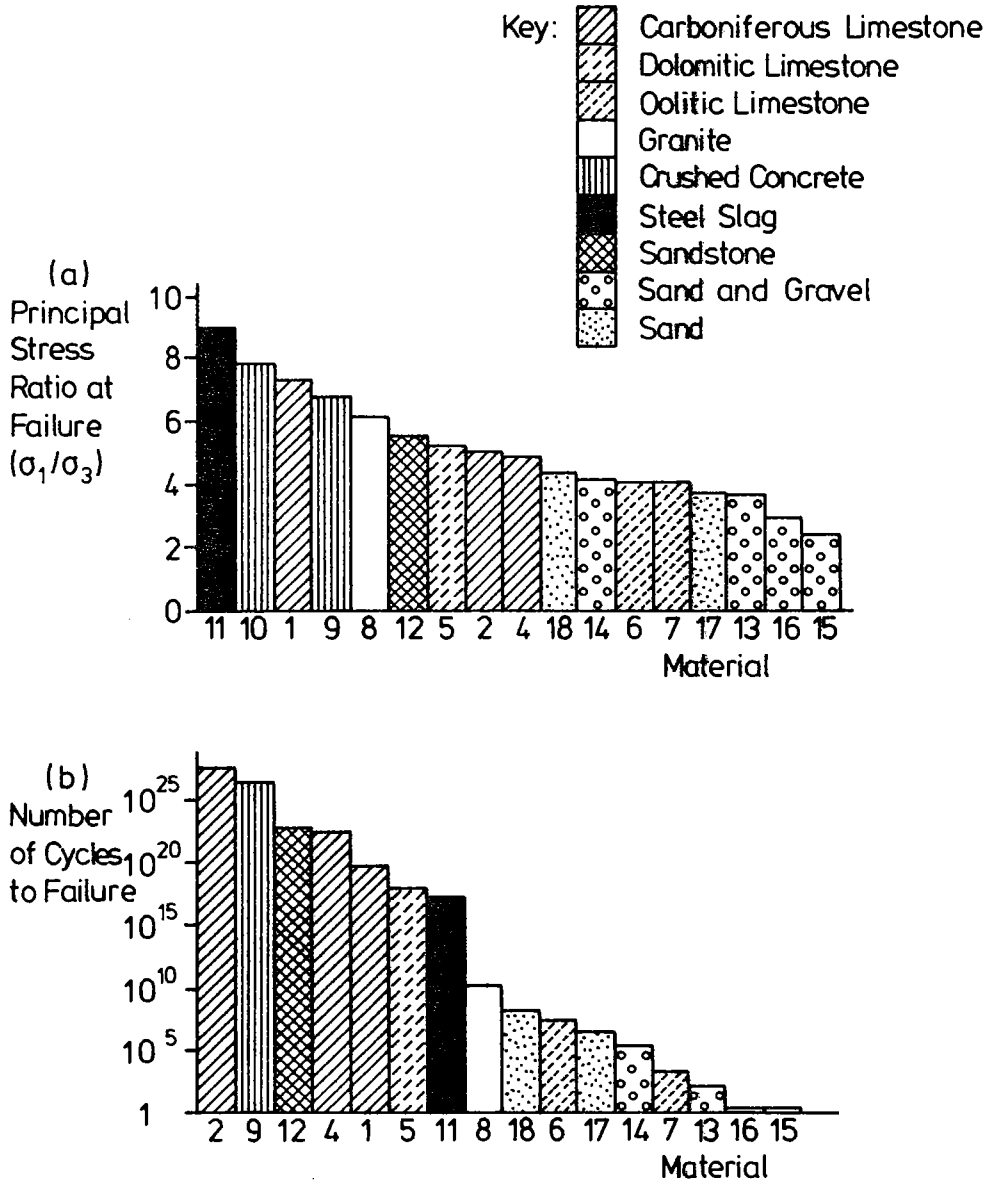

Fig. 5.17 Simplified Plastic Performance Indicators for Different Materials

Note: The number of cycles to failure plotted is extrapolated from the data and should not be taken as accurate. It is intended as a means of ranking the materials.

described in the table and the mechanical properties established from triaxial testing. Firstly, it is apparent that a description 'rough' applied to an aggregate does not necessarily imply that the angle of friction will be high. This means that the angle of friction is dependent on aspects of the surface rather different from those investigated visually, possibly crystal shape. However, it is quite noticeable that there is a considerable degree of correlation between angle of friction and elastic stiffness, particularly volumetric stiffness.

The second area where correlation is noticeable is shear strength, which appears to be dependent on a combination of angularity and roughness in the larger particles. This supports conclusions by Roner (1985) who studied particle shape effects in relation to railway ballast.

For example, steel slag has sub-angular particles described as very rough and is the strongest material; the sandstone is also very rough but has sub-rounded particles and is less strong; crushed concrete is rough and sub-angular giving it high strength; carboniferous limestone from Dene quarry is only fairly rough but is angular and, therefore, also has high strength. Other limestones and granite are also angular or sub-angular but are relatively smooth and are less strong. The sands and gravels tend to be smooth faced and therefore weak. The exception is the material from South Wales which has rough angular particles but, as can be deduced from the grading curve (fig 5.15), it is, in

fact, the smooth smaller sizes which control behaviour; larger particles are lost in the mass of finer material.

There is some difference between the rankings for strength and cycles to failure, for which, at present, no explanation has been found in terms of physical properties, but, in general, those materials that are strong also give good resistance to cyclic load. The same physical criteria of angularity and roughness of the larger particles may, therefore, be applied to indicate probable resistance to cyclic load. Possibly roughness is of more significance in resisting cyclic load, particularly if the relative performances of granite and sandstone are compared.

In summary, the stiffer materials are those with the best surface friction properties (microtexture). Of the materials tested, all the limestones performed well as did steel slag. Crushed concrete was average, and sandstone, granite, sands and gravels were generally poor. Angularity and roughness (macrotexture) both contribute to strength and resistance to cyclic load. Steel slag, crushed concrete, sandstone, carboniferous and dolomitic limestone were all good materials; granite was average; oolitic limestone, sands and gravels were poor.

A final point to make is that hardness and resistance to crushing do not appear to be of much importance in influencing mechanical properties. For example, the sandstone was very soft and crumbly but showed very good strength and resistance to permanent deformation. Similarly both oolitic limestones were soft but had

good stiffness. Conversely many of the sands and gravels and the granite were very hard but performed very poorly. This point, together with the others mentioned above will be taken up again in chapter 10 where road foundation design is discussed.

CHAPTER SIX

EFFECT OF MOISTURE

It will be remembered that the results quoted in chapter 5 were all for dry material. However, it would clearly be inappropriate not to consider the often extremely deleterious effects of moisture when investigating the behaviour of road foundation layers. The importance of drainage is often stressed in discussing road design and the reasons behind this require careful study.

The great break-through in the treatment of water in a soil or granular material was made by Terzaghi (1936) when he introduced the concept of effective stress. The effective stress is the stress taken by the granular material matrix, which is found by subtracting the pressure in the pore fluid (commonly a mixture of air and water) from the applied total stress. The assumption made is that the area of contact between particles is a negligible part of their total surface area. This effective stress principle is universally used with great success, both where pore pressures are positive and also for negative pore pressure or 'suction'. It is commonly applied to problems where the pore fluid is assumed to be 100% water, but has been shown (eg Pappin 1979) to apply equally well to the partially saturated state. Such a well tried and established principle may, therefore, be applied to the road foundation situation with great

confidence.

However, assuming the truth of the effective stress principle, there are other questions to be answered, such as the sensitivity of permeability and suction to grading and degree of compaction, and moisture content. Also it is necessary to investigate whether there might be any other effects due to moisture as yet undiscovered. Testing has therefore proceeded on three fronts. Initial tests were done to confirm the applicability of the effective stress principle; a series of tests on specimens of the same seven gradings and same material type as in section 5.3 was done; several site materials have been tested at site moisture contents and their behaviour observed. This chapter will, therefore, present results in these three areas and finally summarise the findings.

6.1 TO CONFIRM THE EFFECTIVE STRESS PRINCIPLE

Early in the course of this research a test was performed on a crushed granite specimen at a DTp Type 1 grading with the dual aims of proving the capability of the 150mm triaxial apparatus in dealing with 'wet' materials and also proving the effective stress principle. The apparatus capabilities have been described in chapter 3: this section will look at the test results. Testing was done in three stages, as follows:

(i) The specimen was made up dry and a series of stress paths applied to it, in order to establish elastic stress strain

equations for the dry material. At the time, the equations derived were of a form similar to Pappin's (eq 2.2 and 2.3) but, for consistency, they have been amended to follow the pattern proposed in chapter 4.

(ii) Water was introduced into the specimen through the bottom platen, while a vacuum was applied through the top, until water rather than air emerged at the top. No back pressure was applied. A series of stress paths was again applied and the strains and pore pressures measured. At this stage the pore pressure coefficient B (Skempton 1954) was about 0.5, indicating partial saturation only.

(iii) Water was passed continuously through the specimen in the manner described for stage (ii) for several hours. A back-pressure of 200kPa was then applied to the specimen, and a further series of undrained elastic tests performed. Strains and pore pressures were again measured. The pore pressure coefficient had by then reached in excess of 0.9, indicating near full saturtion.

The equations developed for the dry material were then applied to the effective stresses measured during phases (ii) and (iii); ie measured pore pressure was subtracted from the confining stress to give an effective value. This provided predictions of shear and volumetric strain, which are compared to the measured values in fig 6.1. The equations used are also given in the insert to fig 6.1. It can readily be seen that the predictions match the

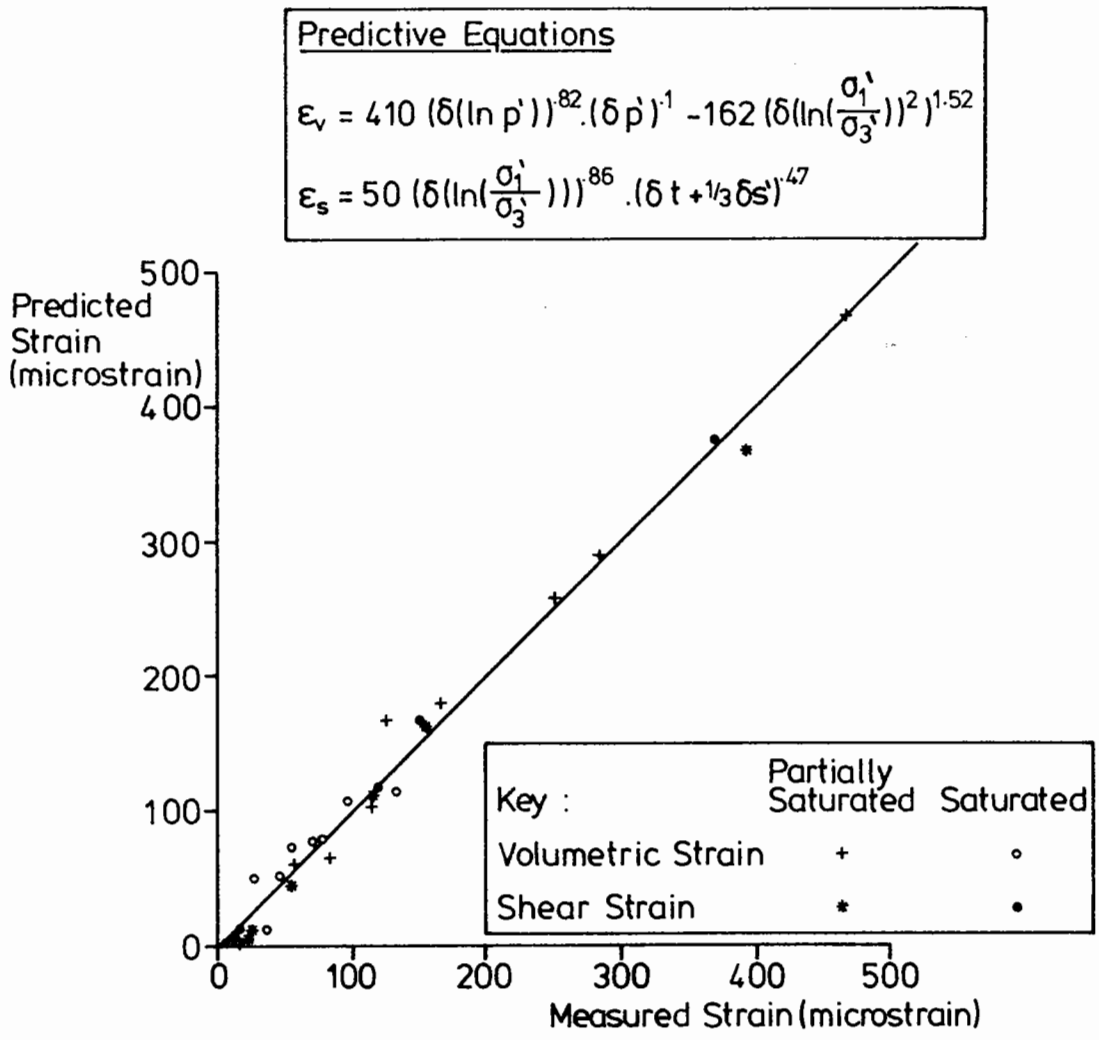

Fig. 6.1 Predictions using Effective Stress Principle

measured values very satisfactorily, thus providing further evidence that the effective stress principle is valid for both partially and fully saturated materials. It should, of course, be remembered that this test was only for one material, a granite, and that only elastic testing was done and, also, that only positive pore pressures at high moisture contents have been evaluated. The following sections will look at other tests and describe how lower moisture contents have been dealt with.

6.2 TESTS AT DIFFERENT GRADINGS

Particularly in relation to the development of negative pore pressure and to permeability, it was felt to be important to investigate effects from changing the shape of the grading curve. A series of tests was, therefore, carried out on specimens of crushed dolomitic limestone at the same seven gradings as were explored in chapter 5 (section 5.3), shown in fig 5.6. Several aspects of the effects of moisture were investigated, and they are detailed in the following sub-sections.

6.2.1 Permeability

The study of permeability in relation to grading is a subject which has been neglected in the past. Several researchers have proposed formulae relating permeability to the percentage passing one or more sieve sizes (e.g. Hazen 1892, Juang and Holtz 1986), but it would appear that they have all been derived from tests on sands and silts and cannot be applied with any confidence to a

broadly graded crushed rock. Tests by Biczysko have revealed, however, just how sensitive permeability is to relatively small shifts in grading curve shape (Biczysko 1985), showing a hundredfold difference between the two limits of the Department of Transport Type 1 envelope. His paper shows how drainage properties could be radically improved by a small change in grading specification. Unfortunately, in this research, only a very limited amount of permeability testing has been done owing to lack of time and because a parallel project has been initiated at Nottingham University with the aim of studying the whole area.

None the less, each of the specimens involved in the grading and compaction study in chapter 5, was also subjected to a permeability test after the completion of mechanical testing. Ordinary tap water was used under a head of 700mm and readings taken once a steady state of flow had been achieved. The results, which are given in fig 6.2, should be treated with some caution, since there were problems with clogging of a porous stone, which may have artificially lowered the values for the most broadly graded material. Also, at the most open gradings, the pipework may not have been of sufficient diameter to cope with the flow, thus again artificially lowering the result. However, it is considered that the permeabilities shown are likely to be of the correct order of magnitude.

It is evident that there is an enormous spread of results between the two extremes of the grading spectrum, and that the state of

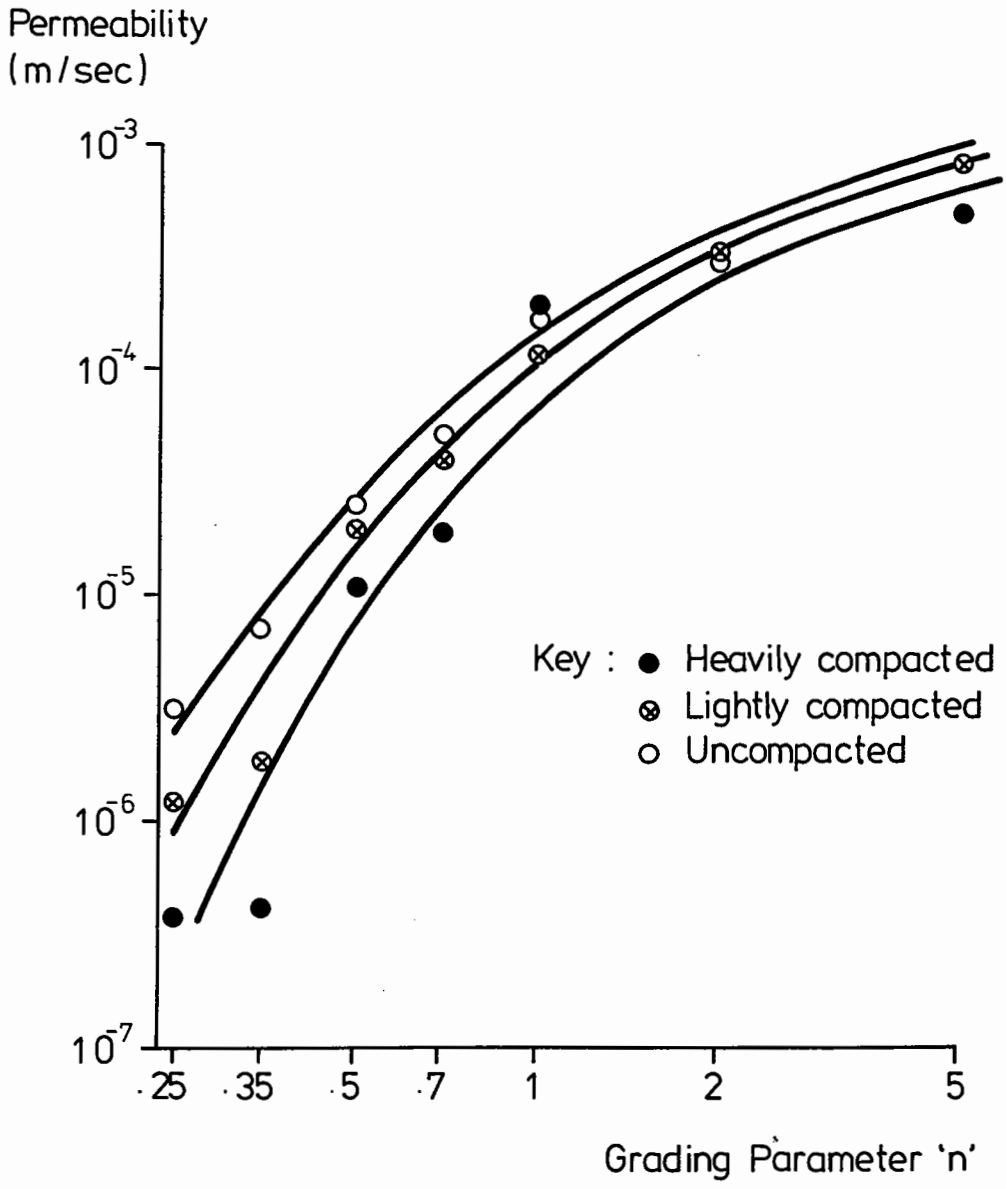

Fig. 6·2 Effect of Grading and Compaction on Permeability

compaction has a secondary but significant effect. Clearly the implications, of grading curve shape particularly, on drainage properties and on short term dissipation of pore pressures under a wheel load are very great indeed, and their consideration should certainly influence the design of an aggregate grading.

6.2.2 Compaction

It is common knowledge that, for a given compactive effort, the moisture content of a granular material has a direct bearing on achieved dry density. The reason for this dependency is less well known but suggestions will be made here to explain it. In order to explore the area, five of the seven gradings in fig 5.6 were compacted at different moisture contents into a 75mm diameter 150mm deep mould, in five layers. Compaction was achieved by hand tamping, with the same nominal level of compaction being applied in all tests. This is, of course, not a standard test and therefore will not yield standard results but they will be comparable with each other. The two most uniform gradings were excluded because of their inability to retain water.

Fig 6.3 shows the results of achieved dry density against moisture content. The shape of the curves is a familiar one, although the portion at very low moisture content is often excluded from practical testing. It can be seen that density falls from a relatively high level when dry to a low point, before rising again to a maximum at the point commonly termed

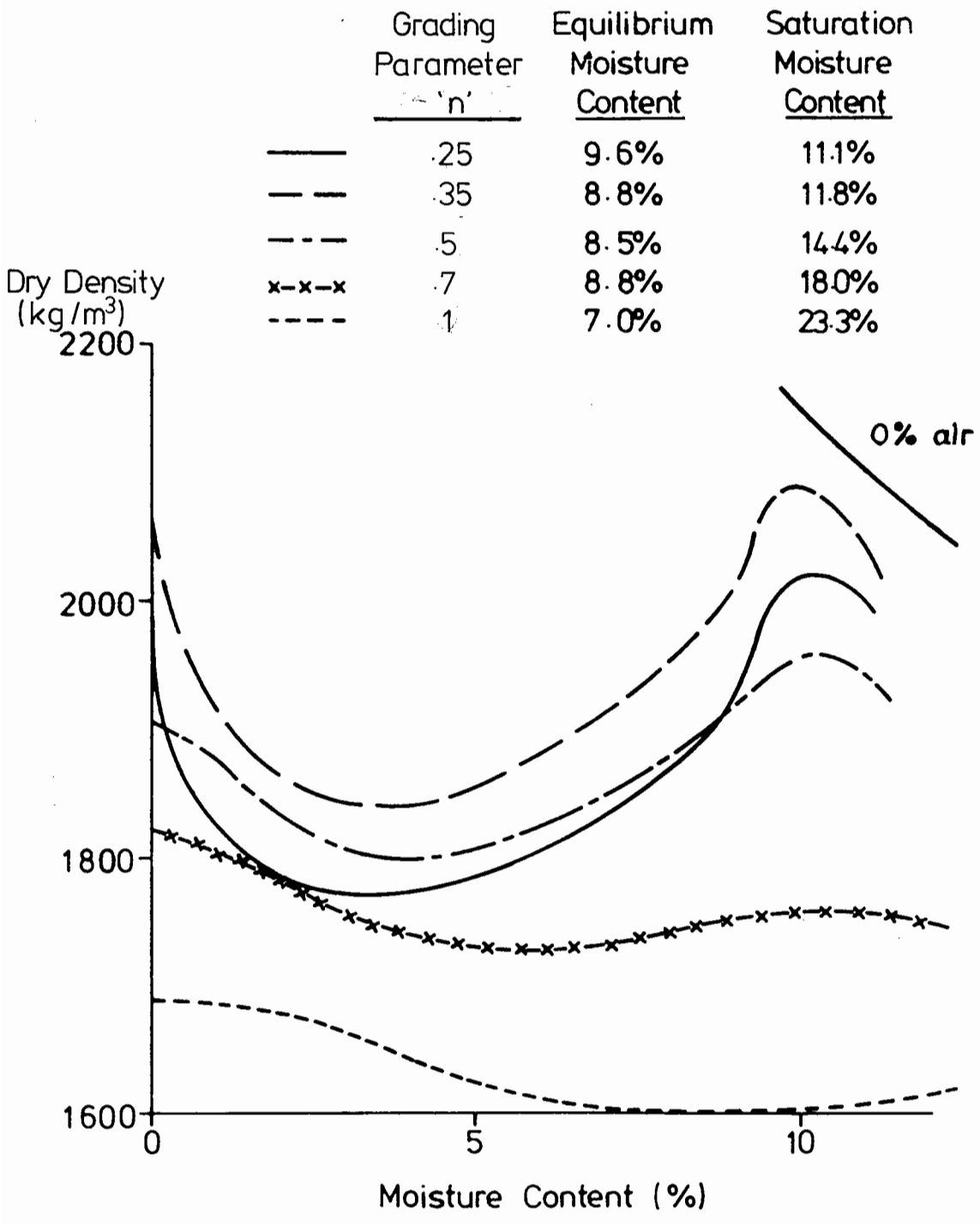

FIG. 6.3 Compaction Curves

'optimum moisture content'. Finally it drops away again as the zero air voids line is approached. In general, it is the optimum moisture content that is aimed for in road construcion, which, if achieved, would clearly result in a state very near saturation, ie close to zero air voids, particularly for broadly graded material.

The reasons for this moisture content dependency should, it is considered, be sought in the development of pore pressures. Dry material allows no pore pressure development. As the moisture content is increased, negative pore pressures will develop due to surface tension effects at the air-water interfaces, thereby binding groups of particles together and inhibiting movement towards tight packing. Further increase in moistue will see a point of maximum negative pore pressure being reached, after which the number of air voids reduces, giving less air-water interface area, less surface tension and, therefore, greater achievable density. Eventually, if the proportion of air becomes very small, then, not only is there no chance of negative pore pressure, but the strains induced under compaction loading will lead to positive pore pressures. This will effectively ease inter-particle movement and allow a dense state of compaction to be achieved. However, if even more water is added, then the void space has to increase again to allow for it and densities will reduce.

If the above explanation is true, then a glance at the curves is sufficient to indicate that negative pore pressure will be at its maximum at between three and five percent moisture content for most of these materials, but that moisture contents at or above optimum are likely to lead to positive pore pressures, the effects of which are discussed in section 6.4.

6.2.3 Suction - Negative Pore Pressure

The compaction curves in fig 6.3 allow deduction of the existence of negative pore pressures at low moisture content. So do experiments with standing columns of granular material such as those described by Dawson (1985). However, suction is not an easy quantity to measure directly, particularly in an aggregate containing large particles, and it was therefore decided to employ an indirect technique.

Fig 5.9 (b) has already given values of unconfined compressive strength shown by the seven gradings here being investigated, and values of 'failure ratio' σ_v/σ_h for σ_h = 50kPa can be seen in fig 5.9 (a). These results were for dry material. If a specimen of one of these materials is made including water, negative pore pressure is induced due to suction effects, and this negative pore pressure will lead to an equivalent increase in effective stresses, both vertically and horizontally. If an unconfined triaxial compression test is then performed on that material, an increased strength will be recorded which reflects these positive horizontal effective stresses. Assuming that the slope of the

failure line in effective stress terms is unchanged by the presence of water, the level of negative pore pressure acting can be deduced.

This procedure has been followed for specimens at the finest four gradings from fig 5.6, at moisture contents approximating to the 'low points' of the compaction curves in fig 6.3. The compactive state used was the densest of the three explored in section 5.3, since unconfined compression strength data was not available at other densities. The values of deduced negative pore pressure are plotted in fig 6.4.

It can be seen that values range from zero to about 7kPa at the finest grading. Such numbers look small but could have a significant effect in each of the following two areas:

(i) A positive horizontal effective stress at the surface of a granular layer enables a much larger vertical stress to be carried before failure is reached; ie improved trafficability.

(ii) For drainage considerations 1kPa repesents a 100mm head of water and, since road drains are commonly only a few hundred millimetres below sub-base level, a small negative pore pressure could greatly inhibit drainage from taking place.

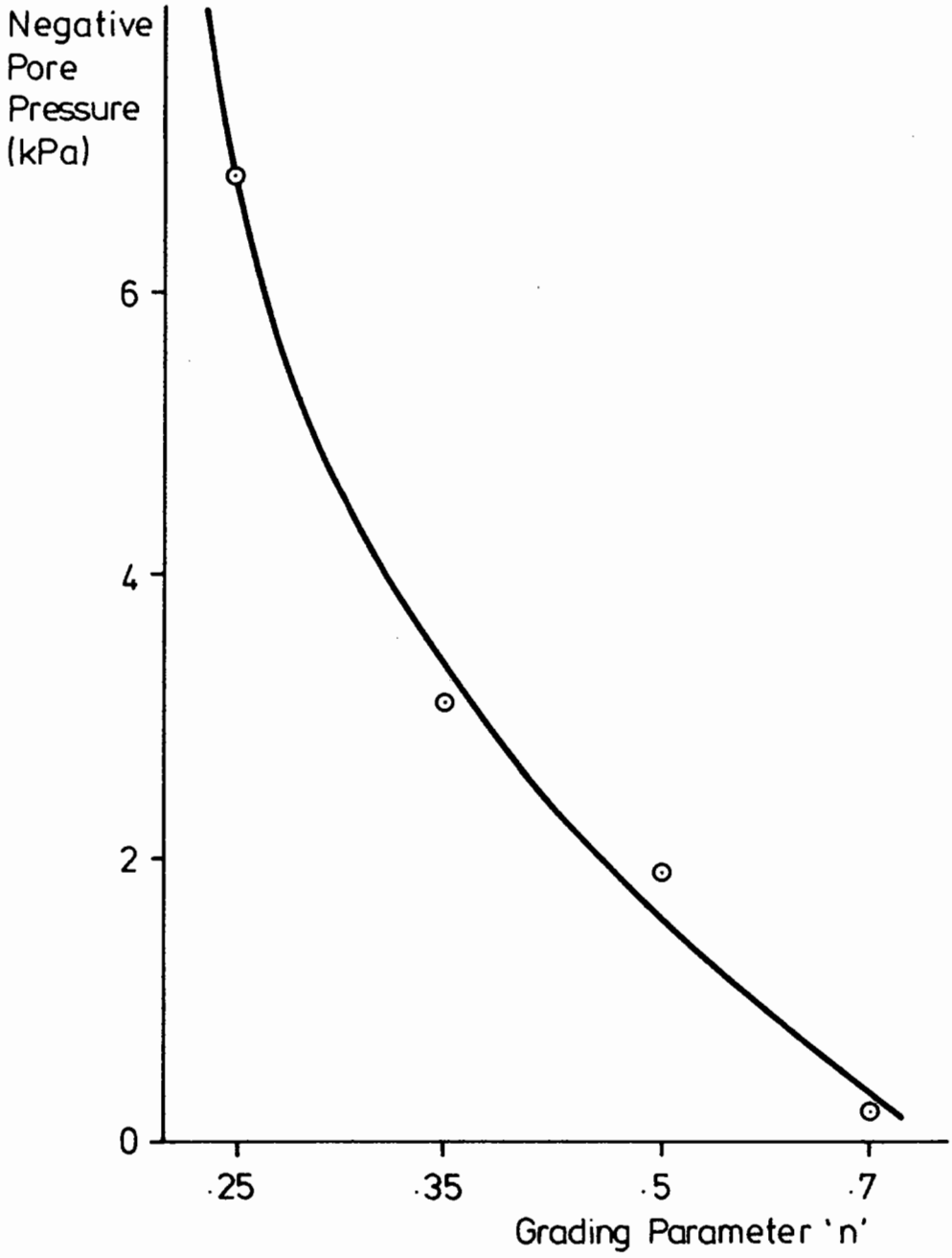

Fig. 6.4 Deduced Negative Pore Pressures due to Suction

This brief look at suction cannot do more than indicate its possible effect. There are, inevitably, complications due to differences between wetting and drying, cementation and possibly other effects. Some of these will emerge in the following sub-section detailing elastic tests on wet material.

6.2.4 Elastic Testing

From the above, it was expected that a wet specimen might well behave more stiffly than a dry one due to the effect of suction. It was therefore decided to test a series of specimens and observe the changes in elastic response as the moisture content was varied. The apparatus used was the 75mm repeated load triaxial facility (section 3.1.2), which enables moisture to be added or taken away through both the top and bottom platens. Moisture content was assessed by monitoring the weight of the whole triaxial cell, including specimen.

In all, five specimens were tested, three at the n = .5 grading (fig 5.6) and one each at n = .35 and n = .7. An elastic test programme, consisting of ten stress paths, was devised to assess the stress-strain behaviour. The paths are shown in p,q space in fig 6.5. It was decided to perform the test programme after each change made in moisture content. Four of the specimens were made in a dry state, compacted in the same way as the densest group described in section 5.3, and one of the n = .5 gradings was compacted at around optimum moisture content, but to the same dry density as those compacted dry. In adding and subtracting water,

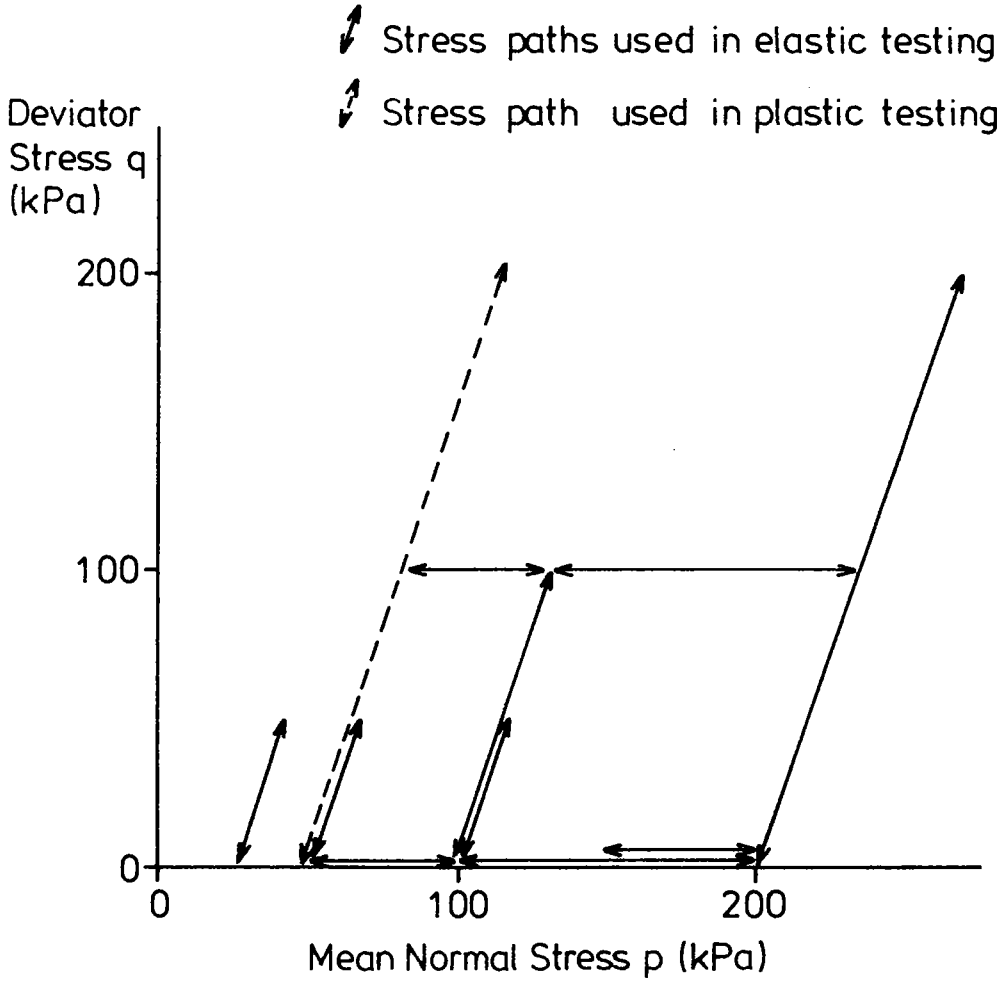

Fig. 6.5 Stresses Applied During Moisture Investigation

the aim was to create no disturbance among the aggregate particles, and a low head of about 400mm was therefore used. Water was added through the top platen, so as to percolate through the specimen under gravity, and was subtracted through the bottom platen.

Fig 6.6 shows the results for all five specimens, plotted as the variation of an elastic stiffness value. Although, as has been shown in great detail in chapter 4, granular material is far from being linear elastic, it was decided that the only way of attempting a direct stiffness comparison between specimens was to select an Elastic Modulus value. In fact, an average of the moduli resulting from the ten stress paths in fig 6.5 was computed and it is that value that is shown in fig 6.6. It should be remembered, however, that the number itself is not a fundamental property of the material.

Superimposed upon the paths in stiffness/moisture content space, shown in fig 6.6, is a band inside which the behaviour generally falls. It can be seen that two distinct areas of behaviour exist. The first, while the specimen is being intially 'wetted up', is fairly flat, indicating little change in stiffness with increasing moisture content. The second area relates to subsequent drying out and rewetting, and forms a much steeper line, rising to a very high stiffness indeed in a fully dried out specimen. This is clearly a more complicated and slightly different situation from the expectation of a simple relationship

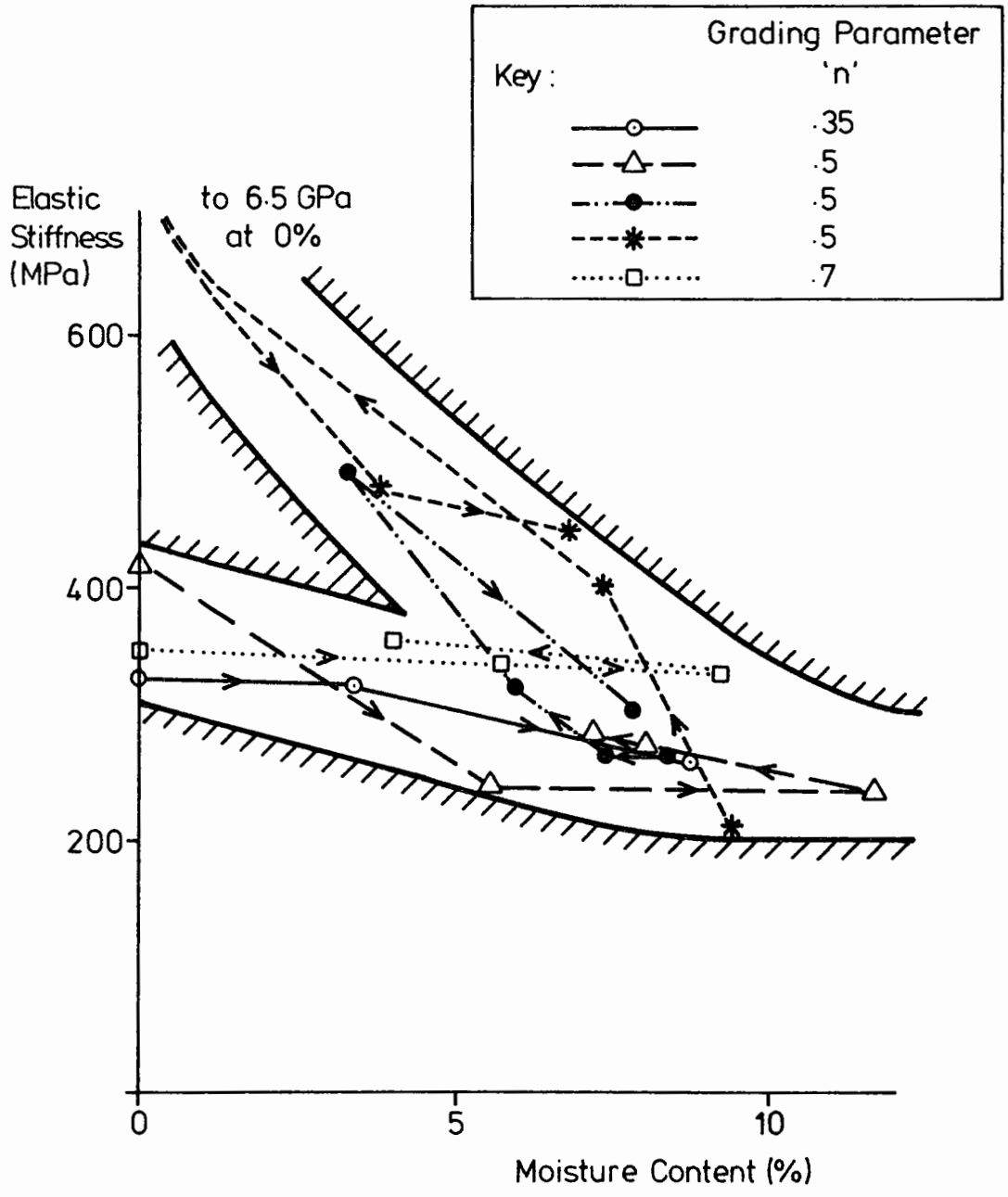

Fig.6·6 Effect of Moisture on Elastic Stiffness

Note: The hatching shown does not represent a limit to behaviour. It is added as an aid to understanding the results.

between moisture content and negative pore pressure due to suction.

The explanation suggested here can be summarized as follows:

(a) The flat section of fig 6.6, pertaining to initial 'wetting up' may be due to the air-water interfaces being curved in the same way as is shown by water rising up a dry capillary tube. This may, in fact, lead to positive rather than negative pore pressure and could explain the slight stiffness reduction as water is added intially.

(b) The steep section is probably due to the air-water interfaces being curved in the opposite sense, as by water retreating down a capillary tube. This section is that most likely to be of practical significance, since granular material in a road foundation is generally wet from the time it is laid. It indicates that, as the moisture content is reduced from a certain level, in this case around 10%, negative pore pressure is induced and stiffness increased.

(c) As moisture content is reduced to very low levels, it is probable that cementation takes over from the effects of negative pore pressure as the dominant means of increasing stiffness in the limestone material. Such an explanation accounts for the very high stiffness apparent at zero moisture content.

It should be noted that none of the above suggestions violates the principle of effective stress, but they do imply that the pore pressure exerted by a partially saturated material is not easy to predict. In this case, the phenomenon of cementation means that it is impossible to separate out the values of negative pore pressure operating. However, it is certain that the most favourable elastic properties are found in a material that has been wet but has dried out since. This point is discussed in section 6.4, and is also applied in chapter 10 to road foundation design.

Unfortunately, it has not been possible in this project to extend this study to other materials, but negative pore pressure measurement has been made in pavement foundation layers (eg McInnes 1984) revealing it to be a real and important effect.

6.2.5 Plastic Testing

The tests described here take a similar form to those for elastic behaviour above. The problem however is that a plastic test is a non-return situation; ie testing irrepairably changes the specimen. However, it had been noticed in section 4.3 that a graph of strain accumulation rate (shear strain per load cycle), plotted logarithmically against shear strain generally produced a smooth and often approximately straight line. It was therefore decided to make up specimens dry, to begin a plastic strain repeated load test and then add water at intervals during the

test, observing the effect on shear strain behaviour. All seven gradings (fig 5.6) were tested in this way, and all showed the same sort of behaviour. Fig 6.7 shows three of these tests on very different gradings of material.

It can be seen that, as water is added, there is a sudden jump in strain accumulation rate but that it then decays on a line parallel to its original characteristic. The phenomenon is repeated on subsequent increases in moisture content but to a lesser extent.

This behaviour is unlikely to be due to pore pressure, since the same effect is noted for both uniform and broadly graded material. It may, therefore, be some form of lubrication, enabling easier slippage of stone against stone, although research in the past has not shown any evidence for this. However, it should be realised that, although the phenomenon appears dramatic in fig 6.7, showing an instantaneous tenfold increase in strain rate, it really only amounts to a jump of a few tenths of a percent of strain, being the horizontal separation of the lines. This, it is felt, is not likely to be of much significance in the long term.

6.3 TESTS ON SITE MATERIALS

Materials have been obtained directly from road sites on a number of occasions during the course of this project, mainly in

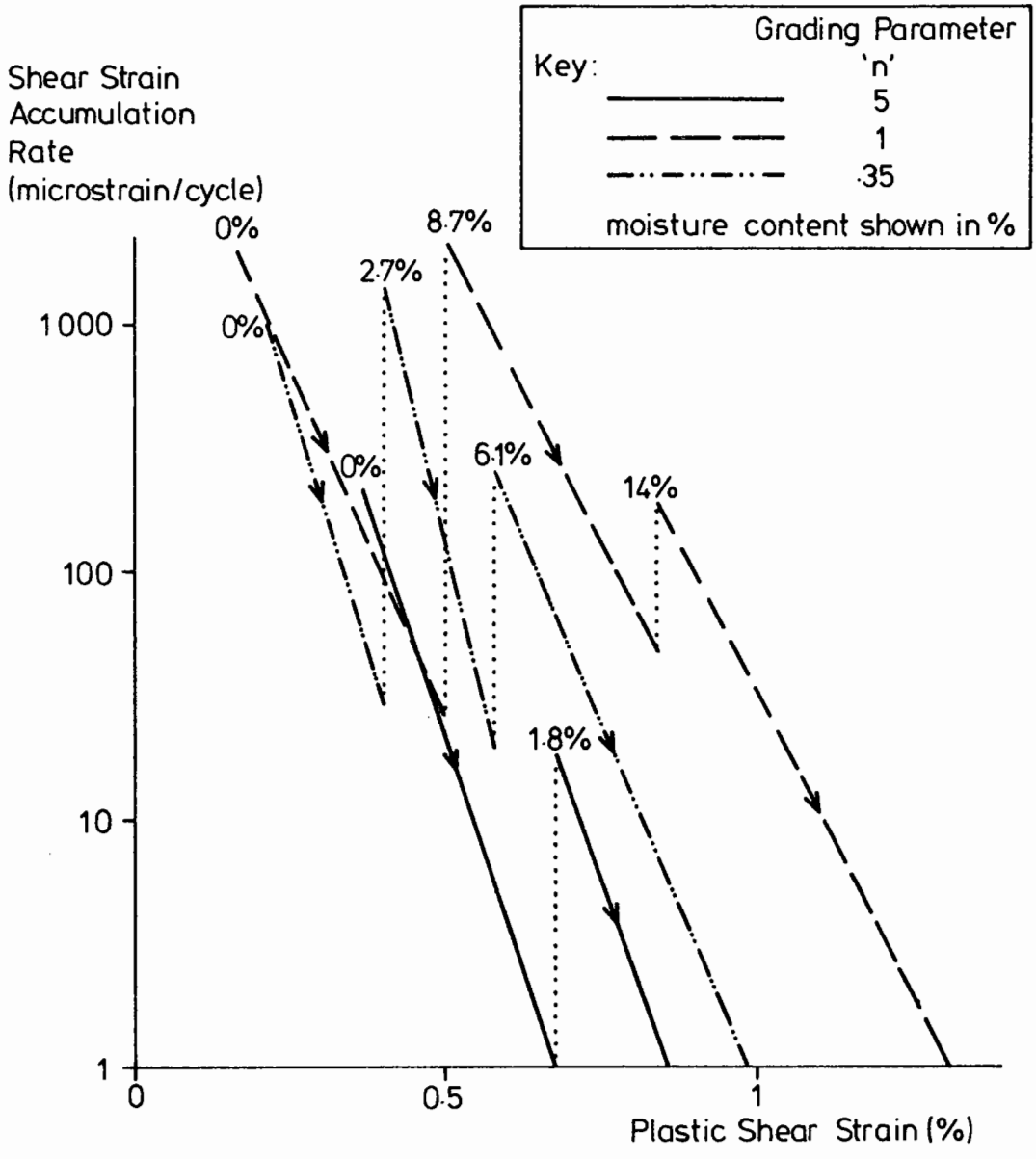

Fig. 6.7 Effect of Moisture on Plastic Behaviour

connection with the testing described in chapter 9, and in each case the material was tested at the site moisture content. It was not, of course, possible to obtain an undisturbed sample of material, as might be possible for clays, so it was always necessary to recompact each specimen, attempting to obtain the same density as on site. The testing procedure followed was the same as that described in section 5.1.

In each case, it was noticed that the material could sustain an unconfined compression of many tens, sometimes hundreds of kiloPascals. In order to assess the contribution of negative pore pressure, a second specimen of each material was made dry, and an unconfined compression test performed. In each case, this second test produced a lower strength value. This enabled a value of negative pore pressure acting at site moisture content to be deduced, in the same way as for the specimens described in sub-section 6.2.3. These values are listed in fig 6.8, and it may be seen that they range up to 25kPa. The grading curves are also shown in fig 6.8 for five of the six materials involved, and it is evident that the gradings with high fines contents show higher levels of negative pore pressure. No quantitative assessment is really possible because the moisture contents are not comparable, but the trend is clearly in agreement with the results from sub-section 6.2.3. A high fines content can mean high negative pore pressures and, therefore, improved mechanical properties.

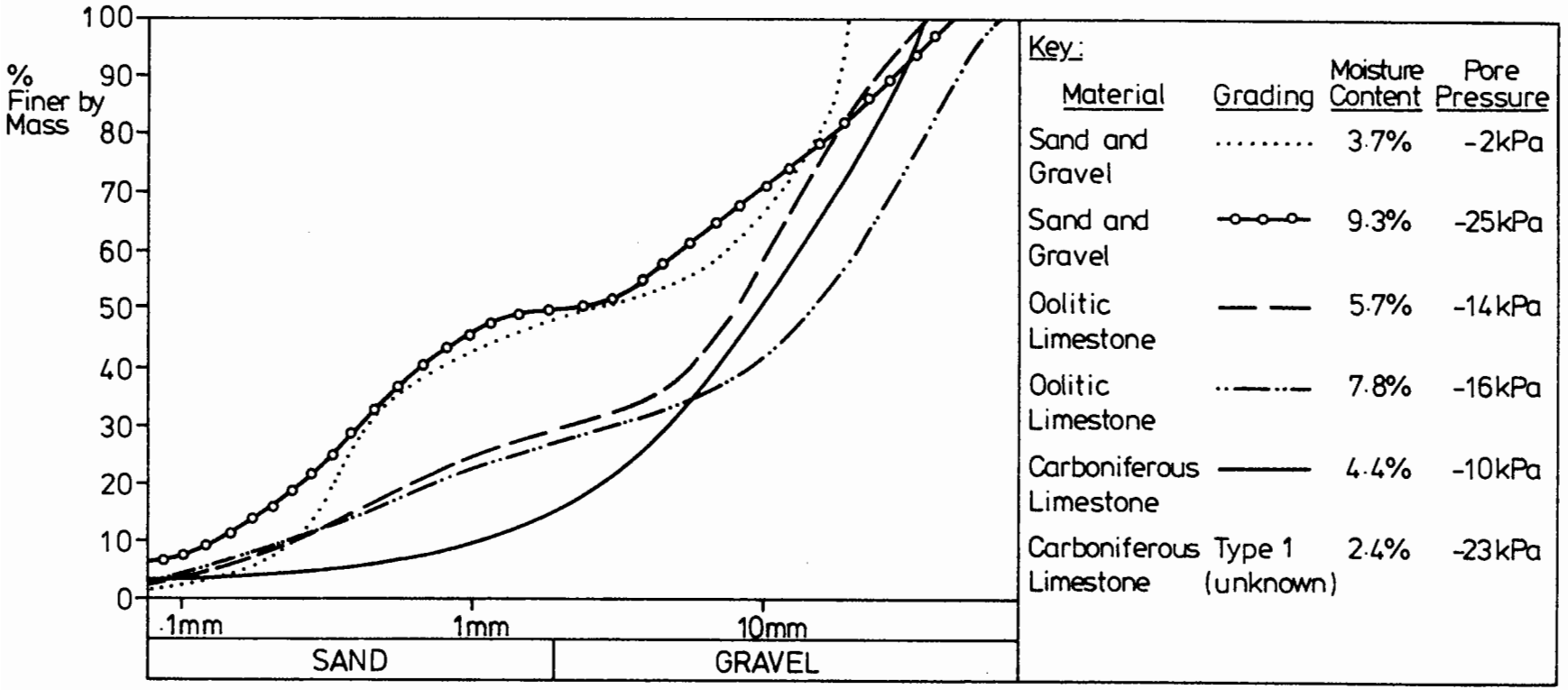

Fig. 6·8 Materials from Site Displaying Suction

6.4 DISCUSSION

It is the practice in road construction all over the world, even in very dry countries, to add water to aggregates in order to improve the density achieved by compaction. Figure 6.3 shows that, indeed, it is possible to establish a moisture content at which density can be optimised. It was also demonstrated in chapter 5 that degree of compaction is a critical factor in producing a strong material with good resistance to plastic strain. These points will form the basis for the study of compaction in chapter 8 and are assumed by every road engineer. It is thus inevitable that an unbound aggregate will contain water from the start of its life as part of a road foundation. Indeed, it is likely to be at a high degree of saturation, since the maximum on the compaction curve tends to represent a low air content. However, the way in which that moisture content increases or decreases with time depends on the material properties, contruction practice, drainage design and many other factors.

If the material is of low permeability, or it is exposed to wet weather conditions, or drainage is poor, or any combination of these, then the moisture content may increase and approach full saturation. Alternatively, if permeability is high, drainage is good and the material is protected from the weather the moisture content is likely to decrease. Section 6.1 has demonstrated the applicability of the effective stress principle at high moisture contents, where positive pore pressures were generated. Clearly

the danger from such high moisture contents in a road is that transient loading from a vehicle will induce positive pore pressures. This reduces effective stresses and may lead to increased elastic and plastic strains, implying an increased tendency for the road to both crack and rut. Extreme cases of positive pore pressure can be seen occasionally in the phenomenon of pumping where water and fine material are ejected under pressure through cracks in the surfacing material as a vehicle passes. Examples of this have been reported by Roy (1981) and Grace (1981), and it has invariably been accompanied by other signs of failure.

A reduction in moisture content, however, has been shown in this chapter to lead to the development of negative pore pressure due to suction, which, in turn, leads to improved mechanical properties and, therefore, to a greater service life for the road. It has also been shown that it is the more broadly graded materials, those with high fines content, that exhibit the highest levels of suction. These materials clearly have the potential to have very good mechanical properties indeed. Unfortunately, they are the least permeable and, therefore, most likely to become saturated. Chapter 10 discusses this dilemma further in connection with road design.

CHAPTER SEVEN

PAVEMENT ANALYSIS - THE GRANMAT PROGRAM

The previous three chapters have concentrated on resolving the mechanical behaviour of an isolated 'portion' of granular material, and expressing it in terms of all the many variables involved. This chapter begins to apply this knowledge to the particular engineering problem posed by a road pavement. Unfortunately, the problem is a complex one, due to the interaction of various different materials with widely differing properties and this necessitates the use of a computer if a detailed analysis is to be performed.

Chapter 2 has outlined briefly some of the computing tools currently available in pavement analysis. Many involve use of linear elastic theory for all materials (eg BISTRO), others contain some degree of non-linearity (eg GAPPS7). All are useful in appropriate situations. However, having developed a set of new stress-strain equations, it was decided that the only possible courses of action open were either to substitute the new equations into an existing program, or to write a completely new one. The only possible existing program which might have been developed was SENOL (Brown and Pappin 1982), an iterative finite element program written at Nottingham University to take account of Pappin's proposed stress strain equations. This option was examined but eventually rejected for the following reasons:

(a) The type of finite element used in SENOL is fairly primitive.

(b) The program was very difficult to follow, particularly the necessary aids to convergence on the solution.

(c) Very substantial alteration would be necessary.

Of the three reasons given, (c) is probably the most important, since it implied that the writing of a new program might take less time than the development of SENOL. It was therefore decided that a new program should be written, called GRANMAT (GRANular MATerial), and the following sections detail its development from the initial idea through to checks on its accuracy.

7.1 THE AIMS OF GRANMAT

GRANMAT, as its name implied, was to be a program which concentrated on the role of granular material in a pavement. Particular care would be taken to model the granular material in as realistic a way as possible, using the equations developed in chapter 4. It had been noted that linear elastic analysis programs seemed to cope very adequately in situations where upper layers of bitumen- or cement-bound material were thick, ie where the granular material had little influence on stresses and strains in the rest of the pavement. Tam (1987) has observed how hard it is to back-analyse the stiffness of a granular material under thick upper layers, because that stiffness has so little

influence. The need, which both SENOL and now GRANMAT have attempted to meet, is to analyse realistically situations where surfacing layers are thin or even non-existent and the granular material forms the main structural layer.

Using both the elastic and plastic equations from chapter 4, it was hoped to compute both the transient stresses and strains under a wheel load and the contribution made by the granular material to rut development. These two aspects are included in both SENOL and GAPPS7, although the methods and equations used are very different (see section 2.4). SENOL has a problem, however, in analysing completely unsurfaced granular pavements.

One final aim was that GRANMAT should take account of pore pressures both negative, at low moisture content, and positive, at high moisture content. It would therefore have to model the development and dissipation of pore pressures over the duration of a load pulse. This would, it is believed, be a unique facility.

A restriction accepted was that it would analyse a three layered structure only.

7.2 PROGRAM DESCRIPTION

A complete listing of the program is contained in Appendix C, written in BASIC, together with a list of variables.

Having decided how to treat the granular layer, the question was how to treat the other layers.

Surfacing, being only thin, was relatively less important to model correctly, and linear elastic theory was seen as being quite adequate. In fact, GRANMAT treats the surfacing as a plate in elastic bending, allowing no volumetric strain. The subgrade is always a very important element. Tam (1987) has described how great an improvement is made to stress-strain analysis, once non-linearity of the subgrade is included. Various models of subgrade behaviour are available and it was decided that it would be prudent to allow options in GRANMAT, such that the user could decide between a choice of three. The three models chosen were:

(i) Linear Elastic - there may often be inadequate data to allow any other.

(ii) K - θ model

(iii) Loach model - the latest development at Nottingham University (Loach 1987).

The remaining decisions concerning assumed properties of the pavement were less hard but, for completeness, they are listed below.

(i) A rigid layer is assumed below the subgrade (= bedrock)

(ii) A non-slip condition is imposed on both the subgrade/granular and granular/surfacing interfaces.

(iii) A zero shear stress and zero radial displacement condition is imposed at a three metre radius in the granular material, and at a greater radius in the subgrade, depending on thickness.

(iv) An axi-symmetric situation is assumed.

The following sub-sections describe each aspect of the program in turn.

7.2.1 Analysis Type

After several attempts at solving the entire problem exactly in one step, it was decided, for relative ease of programming, to embark on an iterative alternative, using a discreet point analysis. The program therefore generates a grid of points, such as that shown in fig 7.1, covering the whole of the granular base and subgrade, out to the boundaries set for the problem. The spacing close to the load can be set as desired by the user but it is automatically increased radially and vertically.

At all times the program retains in its memory a value for each unknown stress and displacement at each point in the grid. The iterative process is one of continuous updating of these values

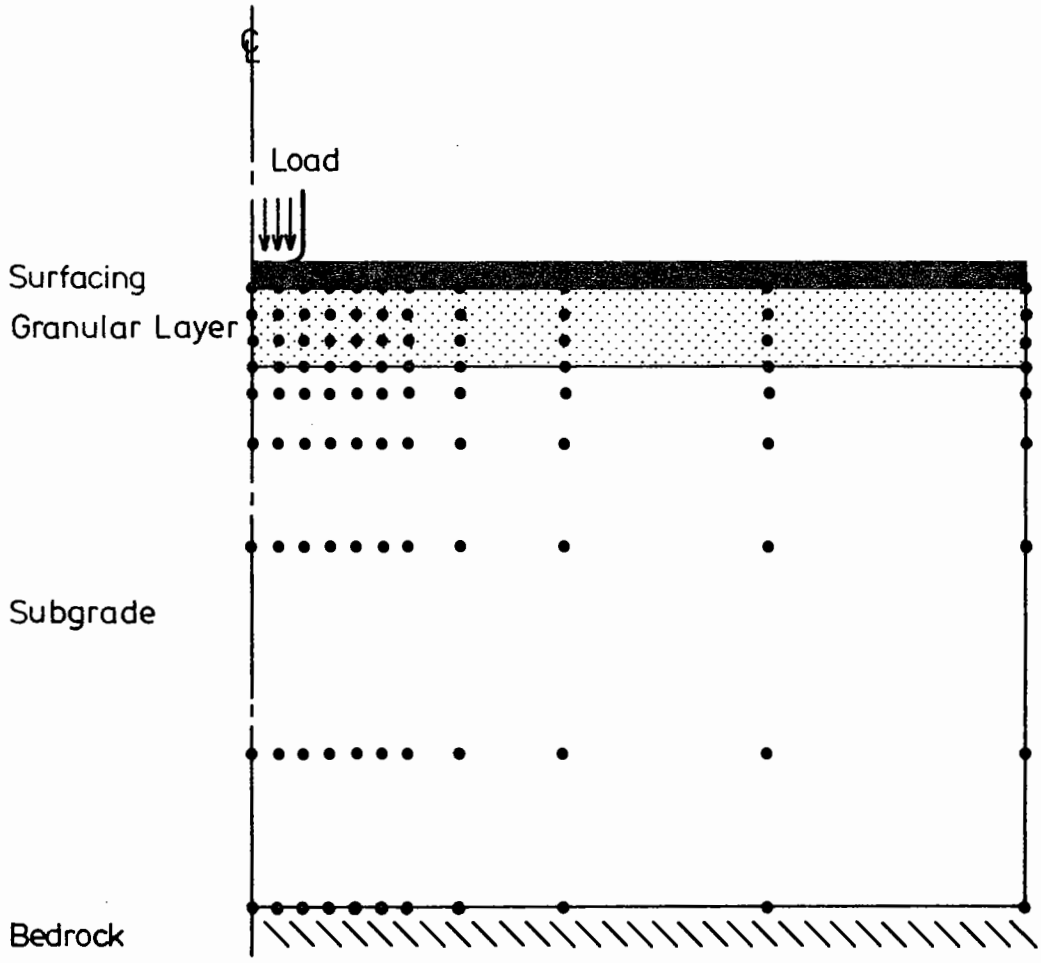

FIG. 7.1 Typical GRANMAT Array

by solving equations relating the variables to each-other. For instance, during a certain stage in the program, new values will be computed for vertical stress in the granular material at each point, using an equation in terms of other stresses and strains. In the next stage these new values of vertical stress will be used in the calculation of new values of radial stress. And so the process continues with the aim that the correct answer, where all equations at every point are satisfied, is approached. At a certain stage during each iteration, the program will move to the subgrade to calculate stresses and displacements there and, at another stage, it will solve for the surfacing layer as well. Pore pressure build-up and water flow are also dealt with at an appropriate stage.

7.2.2 Details of the Iterative Process

At every point, there are six unknowns which the program is trying to find correct values for.

These are as follows:

σ_v = vertical stress

σ_r = radial stress

σ_t = tangential stress

τ = shear stress in the (r,z) plane

mv = vertical displacement

mr = radial displacement

The strains at a point, shear and volumetric, can all be written

in terms of the differential of displacements mr and mv. Linking these six unknowns are six equations. For the granular base, four come from the elastic stress strain relationships developed in chapter 4. Three are for shear strain in various directions, and follow the form of equations 4.6 and 4.7, as follows:

$$\tfrac{1}{2}\left(\frac{dmr}{dr} - \frac{dmv}{dz}\right) = A\left(\delta \ln\left(\frac{\sigma_v}{\sigma_r}\right)\right)^B \times (\text{Stress Path Length})^C \qquad 7.1$$

$$\tfrac{1}{2}\left(\frac{mr}{r} - \frac{dmr}{dr}\right) = A\left(\delta \ln\left(\frac{\sigma_r}{\sigma_t}\right)\right)^B \times (\text{Stress Path Length})^C \qquad 7.2$$

$$\tfrac{1}{2}\left(\frac{dmr}{dz} + \frac{dmv}{dr}\right) = A\left(\delta \ln\left(\frac{\tfrac{1}{2}(\sigma_v+\sigma_r)+\tau}{\tfrac{1}{2}(\sigma_v+\sigma_r)-\tau}\right)\right)^B \times (\text{Stress Path Length})^C \qquad 7.3$$

where: A,B,C are constants

δ means 'change in'

Stress Path Length is different for each equation, following the pattern of eqs 4.6 and 4.7.

There is another 'sense' of shear strain, that describing the difference between vertical and tangential strain, but it is rendered redundant, in theory, since the differences between vertical and radial (eq 7.1) and radial and tangential strain (eq 7.2) have already been expressed. The fourth stress-strain relationship is that for volumetric strain, which follows the form of eq 4.11, as follows:

$$-\frac{mr}{r} - \frac{dmr}{dr} - \frac{dmv}{dz} = D\left(\delta \ln(\sigma_v+\sigma_r+\sigma_t)\right)^E \cdot \left(\delta(\sigma_v+\sigma_r+\sigma_t)\right)^F \qquad 7.4$$

$$- H\,\Sigma\left(\delta\left(\left(\ln\frac{s+t}{s-t}\right)^2\right)\right)^J$$

where: D,E,F,H,J are constants

s,t are stress terms explained in chapter 4.

In fact, at the time of writing, a stress path length multiplier was allowed for in each of the dilation terms summed at the end of eq 7.4, although it has not usually been found necessary in describing material behaviour.

The final two equations come from considerations of equilibrium, and are as follows:

$$\frac{d\tau}{dz} = \frac{d\sigma_r}{dr} + \frac{\sigma_r}{r} - \frac{\sigma_t}{r} \qquad 7.5$$

$$\frac{d\sigma_v}{dz} = \frac{d\tau}{dr} + \frac{\tau}{r} \qquad 7.6$$

These last two equations are, of course, valid for the subgrade as well as for the granular material.

The first four, however, have to be replaced by equations expressed in terms of bulk and shear moduli G and K, thereby becoming:

$$\tfrac{1}{2}\left(\frac{dmr}{dr} - \frac{dmv}{dz}\right) = G\delta(\sigma_v - \sigma_r)/2 \qquad 7.7$$

$$\tfrac{1}{2}\left(\frac{mr}{r} - \frac{dmr}{dr}\right) = G\delta(\sigma_r - \sigma_t)/2 \qquad 7.8$$

$$\tfrac{1}{2}\left(\frac{dmr}{dz} + \frac{dmv}{dr}\right) = G\delta\tau \qquad 7.9$$

$$-\frac{mr}{r} - \frac{dmr}{dr} - \frac{dmv}{dz} = K\delta(\sigma_v+\sigma_r+\sigma_t) \qquad 7.10$$

The values assigned to the bulk and shear moduli depend on which of the three subgrade options for Elastic Modulus the user has chosen. For each, however, a Poisson's Ratio of 0.4 is assumed in the program.

The three choices of formulation for Elastic Modulus are as follows:

(i) Linear: E = constant

(ii) K - Theta: $E = K_1 \theta^{k_2}$

$\theta = \sigma_v + \sigma_r + \sigma_t$

K_1, K_2 constants

(iii) Loach: $E = \frac{1}{3A} q_r \left(\frac{p_o}{q_r}\right)^B$

p_o = initial mean normal stress (unloaded)

q_r = deviator stress

A,B are constants

Option (iii) is undoubtedly the most realistic if sufficient data is available for determining the constants.

Now that the basic unknowns and equations have been described, it is possible to draw up a flowchart showing the way GRANMAT sets about solving for them. This is shown in fig 7.2. The bulk of the program is seen to be taken up with solving for the above six

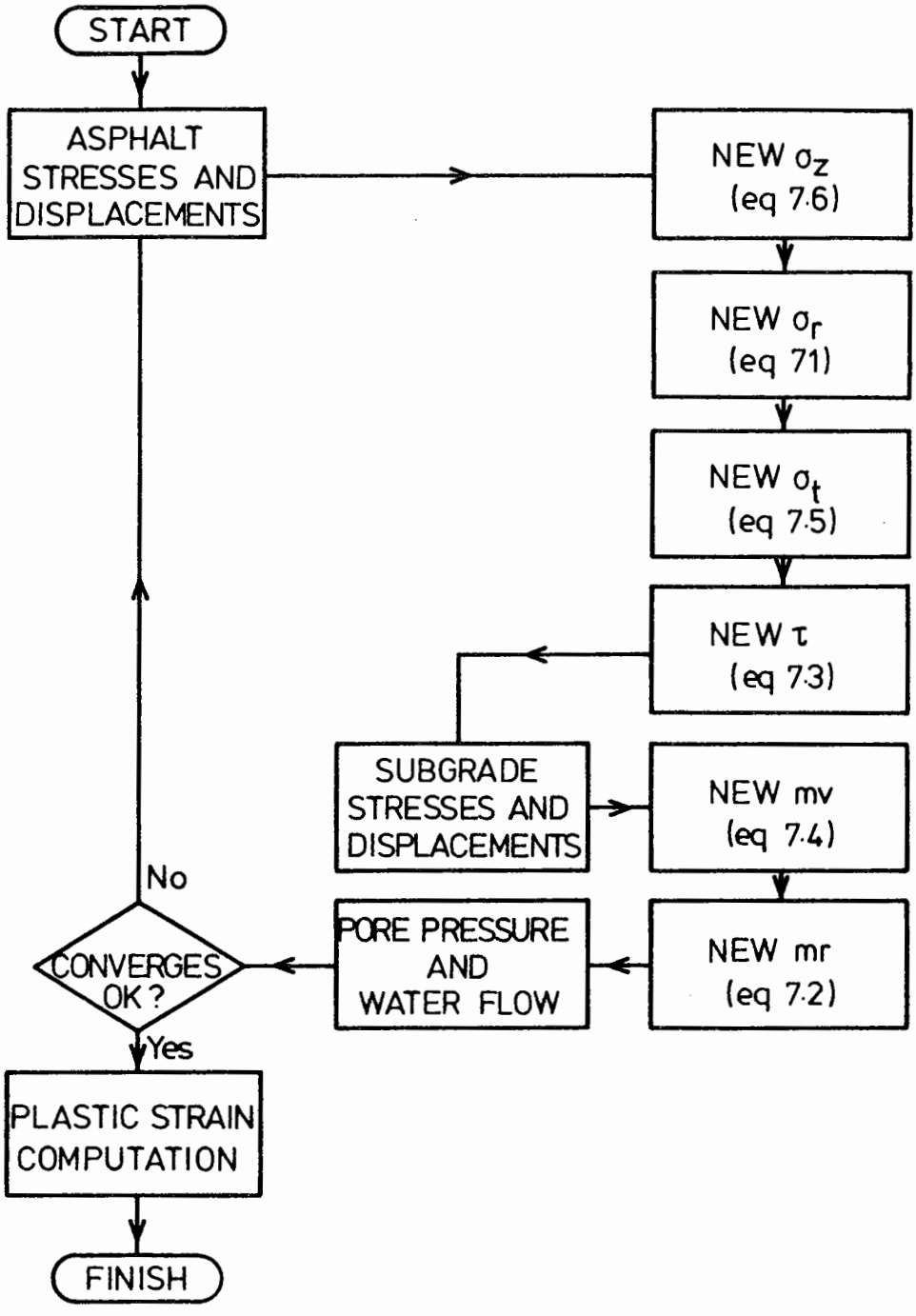

Fig. 7.2 Flowchart for GRANMAT

unknowns in the granular base and subgrade. A step is shown at the beginning of each iteration for solving the stresses and strains in the surfacing. Since it is treated as a plate in bending, this is a fairly simple procedure involving curvatures, bending moments and shear forces, enabling the deflections calculated at the top of the granular base to be related to a revised vertical stress distribution at that level.

One problem which may be seen is that all the equations 7.1 to 7.10 contain elements in differential form. Thus, it is commonly necessary to work out the rate of change of a quantity with respect to either depth or radial distance, at a particular point. This is achieved in a fairly crude way by subtracting the value at the previous point from the value at the next point and dividing by the distance between them. This is acknowledged to be a source of error.

During each iteration, the absolute values of the changes in each of the six unknowns at every point are summed, and the total, termed a convergence indicator, gives a measure of the rate of convergence. This number is then used to determine whether to continue iterating or not. In fact, as is commonly the case in iterative programs, a little help is needed to 'point' the program in the direction of convergence rather than divergence or oscillation. GRANMAT takes the following measures to aid convergence.

(i) Having solved for a particular unknown, the program then permits the value of that unknown to change only by a fraction of that which the solution demands.

(ii) Vertical downwards displacement is constrained to decrease radially.

(iii) Vertical stresses are adjusted to balance the live load plus overburden.

(iv) Radial and tangential stresses are not permitted to oscillate.

(v) Radial displacement has to be outward.

(vi) During the final ten iterations, once the convergence criterion has been met, the unknowns are permitted to vary by ever-decreasing proportions, thereby rendering oscillation less likely.

The convergence criterion is an upper limit on the indicator described above, which depends on grid size and applied load, and has been set by experience. Even when this has been met, it is still possible that the value of any unknown may be in error, since an iterative process such as that used here can never be said to be complete. A decision has to be taken however to end the process at some point.

7.2.3 Accounting for Moisture

GRANMAT allows a choice of two moisture states in the granular base, either very wet, meaning levels of saturation where positive pore pressures could develop under transient loading, or 'less wet', where the user can stipulate a level of negative pore pressure due to suction if he considers it appropriate. This second choice is simple to deal with. The effective stress principle is assumed to operate and the negative pore pressure is simply added to all the total stresses (except shear) to give effective stresses. It should be noted that the results are outputted in effective stress terms also.

A near saturated condition, however, gives rise to a much more complicated situation. As the material starts to take the load, there is a tendency for volumetric strain to take place, ie compression or expansion of the pore space. Since water has a very high bulk modulus compared with air, it resists this tendency, the more strongly as degree of saturation is increased. The effect is to develop pressure in the pore fluid rather than to allow volumetric strain to take place. This pore pressure then influences the effective stresses in the granular material structure. The situation is further complicated by the fact that the load is not applied instantly and, depending on material permeability, this will allow pore water flow and a dissipation of pore pressures before maximum load is reached.

This problem is dealt with by GRANMAT in a stage inserted into the iterative process at the end of the cycle, just before the check for convergence, shown in fig 7.2. The process of stress and displacement computation is performed normally, using effective stresses and, then, when the pore pressure stage is reached, the program examines the computed volumetric strains. The water in the pores is assumed to be incompressible, so that all volumetric strain has to take place in the pore air, which is assumed to behave as a perfect gas at constant temperature. This means that pressure is inversely proportional to volume of air. The program then allows the pore pressure to rise, causing pore air compression, but at the same time reducing effective stresses and thereby also reducing the desire of the granular matrix to compress. These two effects are balanced at each point, and all the resultant pore pressures used in the next iteration to compute effective stresses. Of course, in the case of full saturation, there is no pore air to pressurize, and pore pressure has to rise until the granular matrix has no desire to compress at all.

In order to model the dissipation of pore pressure during load application, GRANMAT applies the load in 50 increments, when the very wet moisture state is being analysed. A triangular load pulse is assumed, so that a fiftieth of the load is added at the start of each of the first fifty iterations, and only after that is the convergence indicator consulted.

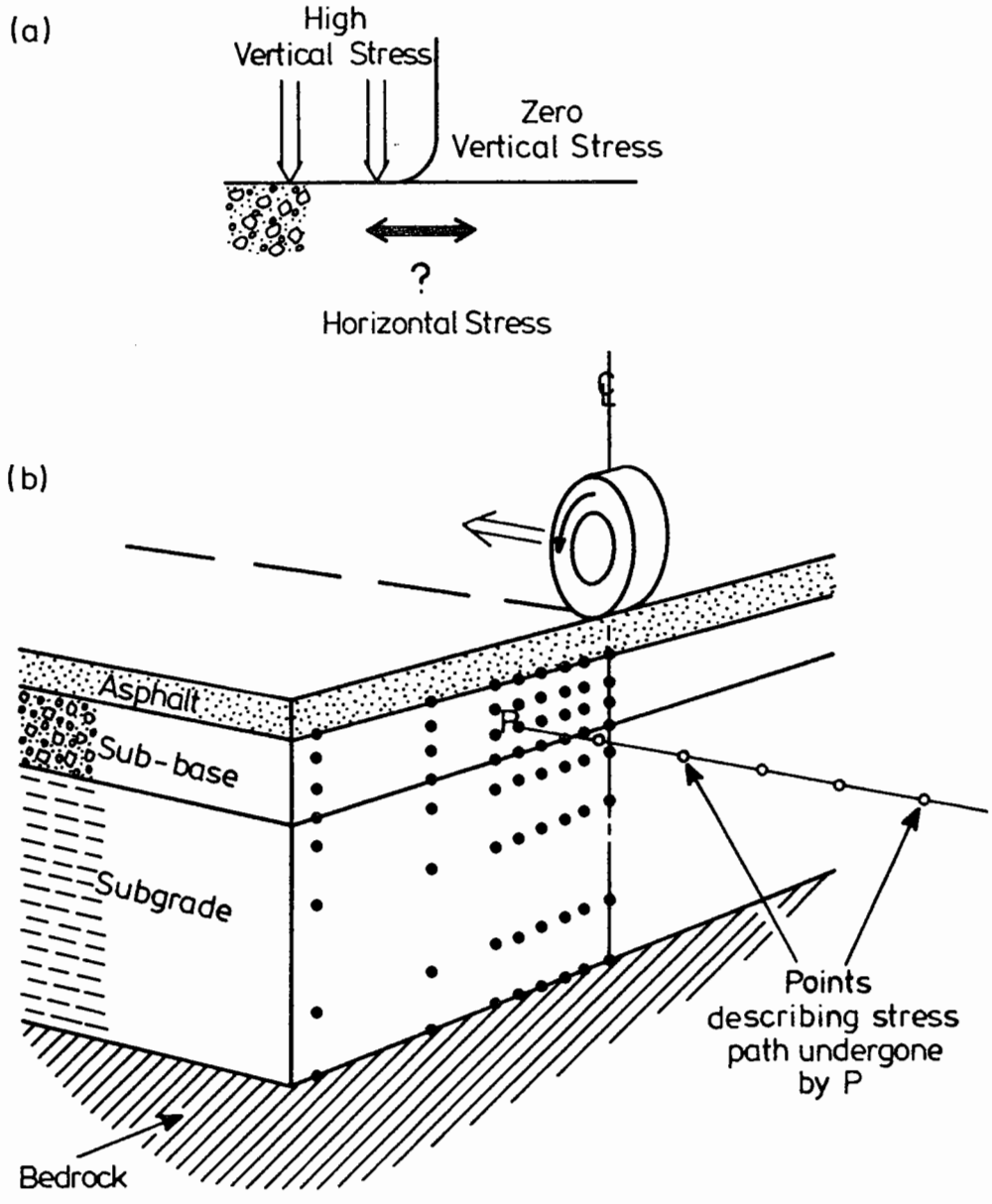

Fig. 7.3 Illustrations to GRANMAT Solution Techniques

The load pulse duration is stipulated by the user, and dissipation of pressure is permitted during the first fifty iterations, each of which lasts for one hundredth of the total pulse duration. This is achieved by constructing elements around each point in the grid, and allowing water to cross the element boundaries in proportion to pressure difference, boundary area and permeability. This, of course, alters the pore volume in each element, and this is taken into account in computing pore pressures in the next iteration. Since it is the peak load situation that is to be analysed, no further water flow is allowed after the first fifty iterations. Thus, an approximate modelling of pore pressure dissipation may be achieved.

7.2.4 The Unsurfaced Condition

In a linear elastic analysis of a layered structure such as a road, tensile forces can always be observed at the surface, just outside the loaded area. This presents no problems in material bound by bitumen or cement, but gives rise to a dilemma if the surface material is unbound. It is usually assumed that such a material can only support stress in one direction if a certain level of compressive stress is also applied perpendicularly. Such are the assumptions implicit in the Mohr Coulomb failure criterion, and every other criterion generally applied to granular material, and they certainly leave no room for tensile forces. This dilemma is illustrated in fig 7.3(a). The vertical stress imposed by the load demands a horizontal stress to support it, but how can such a horizontal stress act unless there is a

vertical stress outside the loaded area.

In fact, it has been demonstrated by the tests reported in chapter 5 that a graded aggregate can take stress in one direction with zero stress perpendicularly, of the order of 20 or 30kPa commonly. This intercept on a Mohr Coulomb failure diagram is believed to be due to particle interlock. This property goes some way toward answering the dilemma shown in fig 7.3, but there is still the unsatisfactory situation of an infinite stress ratio at the surface which, according to the shear strain equations used by GRANMAT (eqs 7.1, 7.2, 7.3), should give rise to infinite strain at the corner of the load.

It is believed that the real solution is to be seen in that a granular material is not a continuum, and that it is therefore meaningless to talk of the stress state in a very small area around the edge of the load since the problem has become one of individual particles. Clearly the strength and stiffness of an individual particle is that of solid rock, which is far greater than that of the granular mass. Section 5.4 has indicated that the smaller the ratio of 'problem size' to particle size, the more the strength of a material increases. However, as was seen in that section, the relationship is a complex one. GRANMAT therefore introduces the concept of a 'single particle depth', being the depth of material which has to be allowed before the laws of continuum mechanics can be assumed to apply.

This is an arbitrary cut-off. At smaller depth, the material is treated as being stiff and strong enough not to contribute to deformation; at greater depth it is assumed to be an isotropic continuum. It has been termed 'single particle depth', since it is considered that the diameter of a single particle, possibly approximately the sieve size where 60% of the material passes, is appropriate. However, the user can stipulate the dimension he thinks suitable.

By such means GRANMAT can arrive at a solution for stresses and displacements in an unsurfaced pavement structure, although it is acknowledged that the method is only approximate.

7.2.5 Plastic Strain Computation

Plastic strains are only considered once the elastic solution has been found. The stresses predicted by the elastic solution are then used to derive plastic strains. However, several assumptions have to be made. GRANMAT takes a fundamentally different approach to that found in such as the GAPPS7 program, where plastic strain occurs because stresses and strains are allowed to redistribute themselves during each load application. Thus, under the load, the material climbs marginally higher up the monotonic failure curve under each successive load application, leading to plastic strain. It is assumed that no plastic strain takes place, unless the stresses change.

GRANMAT, however, follows the line taken by SENOL, where stresses do not change from one load application to the next, but plastic strains accumulate according to a model developed from laboratory tests. SENOL, of course, uses the shear strain model proposed by Pappin (Brown and Pappin 1982), whereas GRANMAT uses the equations developed in section 4.3.

The first dilemma is that the elastic analysis is performed on an axi-symmetric problem, whereas a rut is fundamentally a plane strain problem, since there can logically be no plastic strain longitudinally; ie the road does not get longer or shorter with time. GRANMAT therefore considers a planar grid of points forming a transverse section through the road. Each point is assumed to undergo a stress path, under every passing wheel, equivalent to the stresses on a longitudinal line through that point, considering a static wheel. Fig 7.3 (b) attempts to illustrate this. The program converts the radial and tangential stresses on that line to transverse and longitudinal, so that a stress path is defined in terms appropriate to rut development for each point.

In order to develop a rut, it was decided that the shear strain due to the difference between vertical and transverse stresses, combined with volumetric strain, would be the appropriate quantities to consider. These stem from equations 4.18 and 4.22 and may be written as follows:

$$\varepsilon_s = \frac{-1}{L} \ln \left[\frac{\sigma_f - \sigma_{max}}{\sigma_f} - \frac{1}{M_1} \left(\tfrac{1}{2}\delta(\sigma_z - \sigma_{tr}) + \tfrac{1}{6}\delta(\sigma_z + \sigma_{tr}) \right) \ln N \right] \quad 7.14$$

$$\varepsilon_v = \frac{1}{M_2} (\delta\sigma_z + \delta\sigma_r + \delta\sigma_t + 2\delta\tau) \ln N - \tfrac{1}{2}\varepsilon_s \quad 7.15$$

where: L, M_1, M_2 are constants inputted by the user.

σ_f is the failure stress, dependent on stress state and the failure criteria inputted by the user.

σ_{max} is the nearest approach to failure.

$\sigma_v, \sigma_r, \sigma_t, \sigma_{tr}, \tau$ are vertical, radial, tangential, transverse and shear stresses.

N is the number of load applications.

δ means the 'absolute value of change in'.

It will be noticed that the stress path length for volumetric strain is given in axi-symmetric terms. This is done for the sake of simplicity, and should result in a very similar number to one expressed in transverse and longitudinal terms.

The program goes through the stress path for each point, looking for stress path length and nearest approach to failure, then calculates the shear and volumetric strains, converts them to vertical and transverse displacements and outputs them as described in the following sub-section. The negative component of shear, ie that where transverse stress exceeds vertical, is computed separately from the positive and is subtracted from it. Displacements are outputted assuming no plastic strain in the subgrade and a completely pliable surfacing layer, neither of which are likely to be true, and this should be realized in assessing the results.

In the above, the shear strain due to difference between vertical and longitudinal stress has been ignored. In fact, if this is calculated, it is generally found that some longitudinal strain is predicted. As mentioned above, this is not physically possible and the only way seen here to 'explain it away' is to suggest that the initial longitudinal stresses, ie those in the unloaded state, increase sufficiently to stop it happening. This phenomenon has been termed 'shakedown' (Sharp 1983) and has been investigated and found to be very likely by Selig et al (1986) in relation to ballast in rail-road tracks. This will be further discussed in chapter 8. Examination of the transverse plastic displacements predicted also tends to show very unlikely high displacements distant from the load and it is considered probable that these are also resisted by transverse stress increases, in the same way as longitudinal.

7.2.6 Input/Output Format

GRANMAT has been designed to run on a microcomputer and has, therefore, been given an interactive form. Once the RUN command is given, the user is asked for details of the structure to be analysed, summarized as follows:

(a) Title.

(b) Layer thicknesses and grid size.

(c) Elastic stiffness of surfacing (if any).

(d) Granular base parameters: ie the constants involved in both elastic and plastic behavioural equations.

(e) Subgrade model type and associated constant(s).

(f) Material densities; Initial stress ratio (K0 = σ_h/σ_v) in the base; Applied load and loaded area.

(g) Moisture Condition (Very Wet/Less Wet)
If very wet: Permeability, Degree of saturation and Pulse Duration.
If less wet: Negative pore pressure due to suction (if any)

(h) Output type: (Full/reduced; printer/screen)

Once input is complete, a summary of it is printed on the screen for the user to check. If he is satisfied, he presses a key and the program runs; if not, the input can be repeated. As the program runs, it prints the convergence indicator for each iteration onto the screen. The number can usually be seen to be reducing in value, although the first fifty iterations of a 'very wet' run do not produce meaningful values, since the load is being increased each time. As soon as the convergence criterion has been met and the final ten iterations performed, the results are printed as determined in (h) above by the user.

If full output is required, the input details above are given followed by values of vertical, radial, tangential and shear stress, and vertical and radial displacement, printed for each point in the grid, together with the grid dimensions. Pore

pressures are printed for each point in the granular base. Plastic deformations are then given, vertically and transversely at every point in the base, for 1, 10, 100, 1000 etc load applications, either till 10^8 applications or till premature failure is reached. The exact number of load applications to failure is also printed.

If reduced output is required, the computer prints the following only:

(i) A summary of the pavement details supplied by the user.

(ii) Tensile strain at the base of the surfacing layer (if any).

(iii) Compressive vertical strain at the top of the subgrade.

(iv) Vertical displacements at the surface, together with radial grid dimensions.

(v) Vertical stress at the top of the subgrade.

(vi) Rut depth at 1, 10, 100, 1000 etc load applications, either till 10^8 applications or till failure.

(vii) Number of load applications to failure.

7.2.7 Program Summary

GRANMAT is a 3 layer pavement analysis program, designed to run on a microcomputer. It treats the surfacing layer as a plate in bending, and is not therefore appropriate for thick surfacing situations. The surfacing can be reduced to zero if desired. The second layer is granular, and uses the equations developed in chapter 4 in governing its mechanical properties. The lower layer is the subgrade, with 'bedrock' assumed beneath it. Three choices of subgrade model are available, being linear elastic, K - theta and that developed by Loach (1987).

The program is interactive, allowing the user to enter details of the pavement to be analysed directly. A grid of points is set up, of size determined by the user, and an iterative process is followed to calculate elastic stresses and displacements at each point. Once a convergence criterion has been met, the iteration ends. Run time for this process is commonly about five minutes on a Tandon AT computer. The program allows either negative pore pressure due to suction or the development of positive pore pressures under transient loading to be considered.

Finally, plastic strains in the granular base layer are computed, but not in any other layer. Output can be either a full list of all the stresses, strains and pore pressures computed, including plastic displacements at intervals, or else a reduced list of key quantities. The choice is made at input time by the user.

7.3 ASSESSMENT OF VALIDITY OF OUTPUT

The various assumptions and approximations made by GRANMAT have been brought out already but the following is a list of the more important ones.

(a) The situation modelled is axi-symmetric.

(b) Stresses and displacements are computed at discreet points rather than for the whole space.

(c) An iterative technique is used to converge on the solution, but the exact solution is never reached.

(d) Loading rate effects are taken into account with regard to pore pressure development and dissipation but not with regard to bitumen viscosity or system inertia.

(e) Plastic strain is computed in the granular layer assuming a completely elastic subgrade and a perfectly pliable surfacing layer.

Of the above points, (a) is a defect which is shared with every other analysis program commonly in use; (b) and (c) represent areas where it is undoubtedly possible to improve the accuracy of the solution and suggestions are made in chapter 11 on these lines. Point (d) has been the subject of research by a number of workers. Mamlouk and Davies (1984) have written an analysis

program which takes account of inertial effects and indicates their importance in relation to such testing devices as the Roadrater, where the pavement is effectively resonated. However, Tam (1987) has shown that, under normal traffic loading, the effect of inertia is very small, of the order of one or two percent, and it is not seen here as a major source of error. The viscous nature of bitumen is well known to cause a loading rate dependency but it is assumed that the surfacing stiffness chosen by the user is selected as appropriate to a particular loading rate and, indeed, a particular loading temperature. The final point, (e), undoubtedly means that the plastic displacements computed will rarely be realistic, and accuracy is further reduced by any errors in the elastic stresses.

With so many uncertainties, it was clearly necessary to perform a number of checks on GRANMAT to establish to what extent the output should be believed. The most useful are direct comparisons between predicted and measured stresses and displacements and some of these are described in this section. A comparison has also been attempted with other analysis programs.

7.3.1 Pavement Test Facility

The Nottingham pavement test facility has been in use for several years for the direct checking of design ideas by trafficking a small section of pavement (Brodrick 1977). It is standard practice to include instrumentation for stress and strain

measurement, details of which are given by Brown and Brodrick (1977). In particular, the results from one pavement were used in assessing the output from the SENOL program (Brown and Pappin 1982), and it was decided to measure GRANMAT against the same set of results. The pavement consisted of 50mm of bituminous material of comparatively low stiffness, approximately 170mm of crushed carboniferous limestone and a Keuper Marl subgrade of about 5% CBR, extending to a depth of 1.5m. The limestone was the same as that tested by Pappin and referred to in chapter 4, although the presence of about 3% moisture renders a certain amount of suction likely. In fact, a negative pore pressure of 20kPa has been assumed when running GRANMAT. Space limits the amount of data that can be presented, so fig 7.4 shows the relative values of computed and measured stress and strain at just two levels in the pavement in vertical, transverse and longitudinal directions.

In assessing fig 7.4 it should be remembered that it is never possible to be absolutely certain of the measured values. The pressure cells, in particular, although installed with care, are very sensitive to the exact stone distribution around them. This is demonstrated by the vertical stress results where both SENOL and GRANMAT ensure that their predictions, whether right or wrong, are in equilibrium with the applied load. The measured values in the sub-base, however, imply a load almost twice as great as that actually used, indicating substantial error. Any looked for correlation must therefore be substantially qualitative. On this basis both SENOL and GRANMAT predict

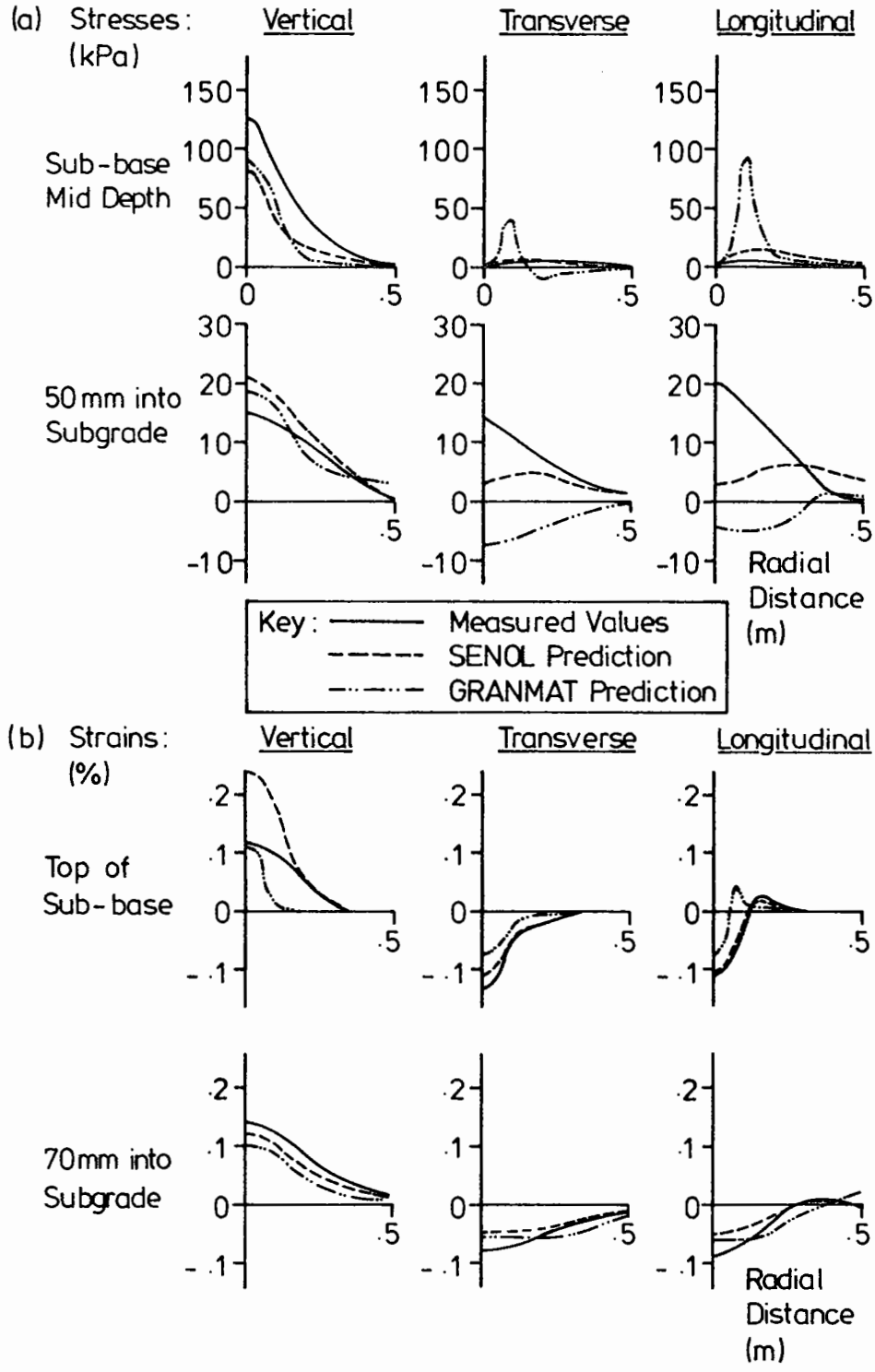

Fig.7.4 Comparison of Measured and Computed Stresses and Strains from Pavement Test Facility

vertical stress satisfactorily but there are significant discrepancies evident in the transverse and longitudinal results, particularly for GRANMAT. The peak shown in the sub-base by GRANMAT is totally absent from the measured results. The strain predictions from both programs are consistently more acceptable, probably reflecting the greater confidence to be placed on strain measurement. However GRANMAT substantially underpredicts sub-base vertical strain away from the load centre line and SENOL greatly overpredicts at the load centre.

More recently a series of pavements has been tested in the pavement test facility to examine the effect of geosynthetic membranes at different levels. This has also yielded stress and strain data which have been compared with GRANMAT predictions based on laboratory testing of the materials involved. Table 7.1 lists the relevant values for the two pavements so far analysed. In the first case, where a poor sand and gravel base was used under 30mm of bituminous mix, the predictions from GRANMAT were reasonable, although the quantity of instrumentation was relatively limited. In the second case , where a much better quality crushed limestone was used, the strains were greatly underpredicted. When it was realized that the base was close to saturation, the program was rerun for saturated conditions, but with little change in predicted strain.

These results demonstrate the use of GRANMAT, with its facility for dealing with saturated conditions, but warn against possible

Table 7.1 Pavement Test Facility Checks on GRANMAT

Stress in kPa Strain in microstrain	Pavement 1 (30mm Bituminous) 100mm Sand & Gravel 2% CBR Subgrade)		Pavement 2 (30mm Bituminous 150mm Crushed Limestone 2.5% CBR Subgrade)	
	Predicted	Measured	Predicted	Measured
Vertical Stress Top of Subgrade	51	51	26	50
Vertical Strain Mid Sub-base	950	2200	950	4100
Vertical Strain Bottom of Sub-base	-	-	550	1650
Vertical Strain Top of Subgrade	13600	6850	7653	6650
Vertical Strain Lower in Subgrade	3725	3200	1100	4550
Longitudinal Strain Bottom of Bituminous	2700	3050	480	4100
Transverse Strain Top of Subgrade	1350	3350	350	2400

errors in horizontal stresses and vertical strains.

7.3.2 Data from Site Instrumentation

In a parallel project to this at Nottingham, an experimental road has been designed and constructed, containing instrumentation similar to that in use in the pavement test facility. The road has only recently been opened to traffic, which consists of large wagons containing colliery waste material, and only one set of pressure cell readings has so far been taken under traffic loading. The pressure cells concerned form a group of eight at mid depth in the granular sub-base with pairs of cells measuring vertical, longitudinal and transverse stresses and a pair measuring stress at 45^{o} to the vertical and longitudinal directions. By such an arrangement the whole stress state is defined if a wheel passes directly over the instruments.

The pavement construction at that point consists of 210mm of bituminous material with stiffness approximately known, 370mm of crushed limestone sub-base which has been tested in a triaxial apparatus, and a compacted weathered rock subgrade becoming firmer rock at fairly shallow depth. A linear subgrade stiffness of 100MPa was chosen over a thickness of just 2m for purposes of analysis. The wagon load was not known exactly but from an approximate knowledge of tyre pressure it was assumed to induce 600kPa over a 150mm radius contact area. Variation between wagons was also not known but may have been small since they were all of the same capacity and make. The situation was further

complicated by the fact that most of the wagons did not follow the line of instruments perfectly.

GRANMAT was used to predict the values of peak stress which would occur during the pass of a wagon at various distances laterally from the wheel path. The results for predicted and measured stress are given in table 7.2. In two instances bracketted figures are included to illustrate the effect of an error in assessing the offset of the wheel from the instrument since this was only done by eye. The first pleasing point to note is that the stresses are of the same order of magnitude. The horizontal stress prediction is consistently higher than the measured value, whereas the vertical and 45^{o} stresses are commonly in good agreement. An exception is pass J where a very high vertical stress was measured, far higher than pass H which was supposedly similar. One reason for this may lie in dynamic loads induced by the vehicle suspension giving substantial variation from the mean, but this is only speculation. The fact that horizontal stress prediction is high supports the same observation from the pavement test facility, but may reflect the difficulty of installing horizontally acting pressure cells as much as any program deficiency. The data quoted here is the first trickle only from this site and it is hoped that the instrumentation installed will eventually provide a large and very useful supply.

Table 7.2 Prediction of Sub-base Stresses at Wakefield using GRANMAT

Wagon Pass	Offset from Pressure Cells (mm)	Stress Directions Measured	Maximum Stress Change Predicted by GRANMAT (kPa)	Maximum Measured Stress Change (kPa)
A	100	Transverse	40	17
		Transverse	40	11
B	0	Longitudinal	50	28
		Longitudinal	50	22
C	200	Longitudinal	35	22
		Longitudinal	35	17
D	300	45°	60	79
		45°	60	66
E	0	45°	114	93
		45°	114	91
F	600	45°	9	21
		45°	9	20
G	300	45°	60	33
		Vertical	51	61
H	0 (200)	45°	114 (77)	52
		Vertical	70 (64)	64
I	300 (400)	45°	60 (32)	23
		Vertical	51 (21)	16
J	0	45°	114	79
		Vertical	70	151

7.3.3 Surface Deflections under the Falling Weight Deflectometer

The falling weight deflectometer is described more fully in section 9.2.1. It is a testing device which applies a measured load over a known circular area and records the surface deflections at various radial distances from the load. Loading is applied very rapidly by the dropping of a weight to simulate the passing of a vehicle. Chapter 9 details its use on unbound pavement layers but it provides an opportunity to test computations of surface deflection. Fig 7.5 shows measured and computed deflections from testing at two sites, two different situations being shown at each site. At both sites a layer of granular material covered the subgrade directly. Specimens of the granular materials were removed and tested in the triaxial apparatus to establish parameters for use in GRANMAT; subgrade stiffnesses were estimated. The falling weight deflectometer deflections are in each case an average of several different test positions.

Clearly the computations are of the right order of magnitude, but the consistent feature is failure to predict the steepness of the deflection bowl near the load. This leads to underprediction at the centre becoming overprediction at half a metre radius or so, and roughly correct again at large radial distance. As explained in section 7.2.4, the method for dealing with the unsurfaced condition in GRANMAT is pragmatic and approximate and may well be the cause of some of the observed discrepancy, but it does at

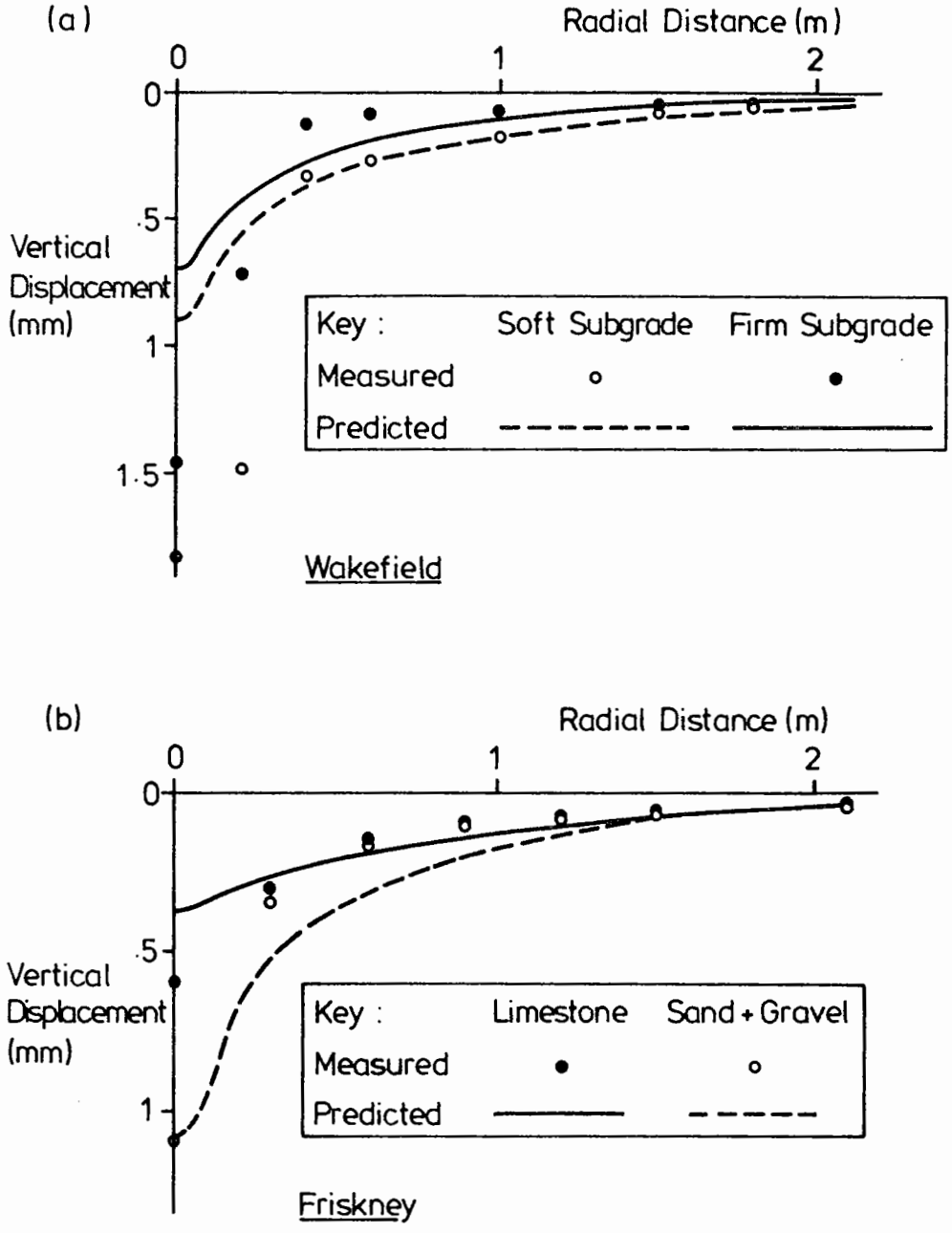

Fig. 7.5 GRANMAT Prediction of F.W.D. Bowls

least allow a rough computation to be performed.

7.3.4 Comparison with BISTRO

Because the parameters required in the granular material analysis performed by GRANMAT are dissimilar to any others, direct comparison with other analytical methods is difficult. In an attempt to overcome this a version of the program was written to use the same iterative discreet point approach but to allow a linear elastic stiffness to be used throughout. The same convergence criterion as before was used. The situation analysed was a 2m thick layer of stiffness 100MPa loaded at 500kPa over a 150mm radius. For comparison the linear elastic multi - layer program BISTRO was also used to solve the same problem.

Table 7.3 is presented to show the two sets of results and the way in which they diverge. Near the surface the vertical strains given by GRANMAT are significantly higher near the load but lower at larger radial distance: at 0.5m depth this has been reversed with GRANMAT giving far lower strains near the load but higher at greater radial distance. This ties in with the stress distributions at 0.5m depth which shows that GRANMAT has allowed the load to spread far wider than BISTRO. This may show the root of GRANMAT's inability to predict the steep deflection bowls resulting from the falling weight deflectometer.

BISTRO is assumed here to be an accurate tool for linear elastic

Table 7.3 Comparison of BISTRO and GRANMAT

Strain in microstrain Stress in kPa	Distance from centre of load (m) 0	.1	.2	.3	.5	.9	2.1
Surface Vertical Strain							
BISTRO	1410	1410	14	14	13	11	3
GRANMAT	2200	2210	150	100	20	0	0
Vertical Strain at 0.5m							
BISTRO	621	567	434	286	92	4	1
GRANMAT	160	160	125	125	45	25	5
Vertical Stress at 0.5m							
BISTRO	61	56	45	31	13	2	0
GRANMAT	26	26	21	21	6	4	0

analysis: it has been used for a number of years and gives very similar answers to other linear elastic programs. This implies that the iterative technique used by GRANMAT and the constraints imposed to ensure convergence can induce serious error and this is seen as a major problem which requires further development work. It seriously limits the reliance which can be placed on analysis using the program.

7.3.5 Summary

From the above comparisons it is clear that GRANMAT in its present form is likely to give rise to error. However, the results appear usually to be of the correct order of magnitude and the features of pore pressure allowance and unsurfaced analysis may well be very useful. It is thought that the source of error is largely in the discreet point approach and the iterative technique, both of which should be developed further or replaced.

CHAPTER EIGHT

COMPACTION

The foregoing chapters have concentrated on laboratory and computational work in relation to pavement foundation layers. At this stage a fairly brief look is taken at the practical aspect of producing the product on site, before proceeding in chapter 9 to look at in-situ testing methods. Since this project has not included much practical investigation on the subject, a large part of the chapter will be concerned with bringing together the results of other research in the field, particularly those arising from the International Conference on Compaction in Paris in 1980. However, the one site trial that has been performed will also be alluded to . No attempt is made to cover the whole field. Rather, the following sections will pick out a few aspects of compaction study which appear particularly relevant.

8.1 AIMS AND ACHIEVEMENTS OF COMPACTION

It has doubtless been the experience of road builders and users for millennia that when the stones forming a road are compacted together well then such a road will be durable and not susceptible to rutting. This valid observation has led by stages to the present situation where powerful compaction plant is employed to achieve the maximum possible density in a granular foundation layer. The gradings produced by crushing plants are

of a form which allows a very high percentage of solid rock to be attained in a well compacted aggregate. Indeed, in South Africa the national specification for top quality granular road base is couched in terms of solid rock percentage. In complete contrast, railways have always been founded on nearly single sized ballast which is completely uncompacted until the first train passes over it; compaction then occurs under traffic. Thus the aim of achieving maximum density in a road layer is certainly open to question.

However, chapter 5 has clearly demonstrated the influence of level of compaction in reducing the plastic strains to be expected from a granular material. In a road situation this implies a reduced rut depth, clearly desirable. Chapter 6 has then illustrated the well known dependency of achieved density on moisture content and has confirmed the existence of an optimum moisture content where maximum density is achieved. This was illustrated by fig 6.3. This, then, is the target commonly aimed at by road builders in the belief that, by such means, the best possible state is achieved. Unfortunately chapter 6 has also pointed out that compaction at this optimum moisture content generally leaves the material in a nearly saturated condition, giving rise to the possibility of serious problems at a future date due to the generation of positive pore pressures.

Leflaive and Schaeffner (1980) have presented a study on the effect of compaction at various depths within a granular layer compacted using a vibrating roller. Fig 8.1 reproduces some of

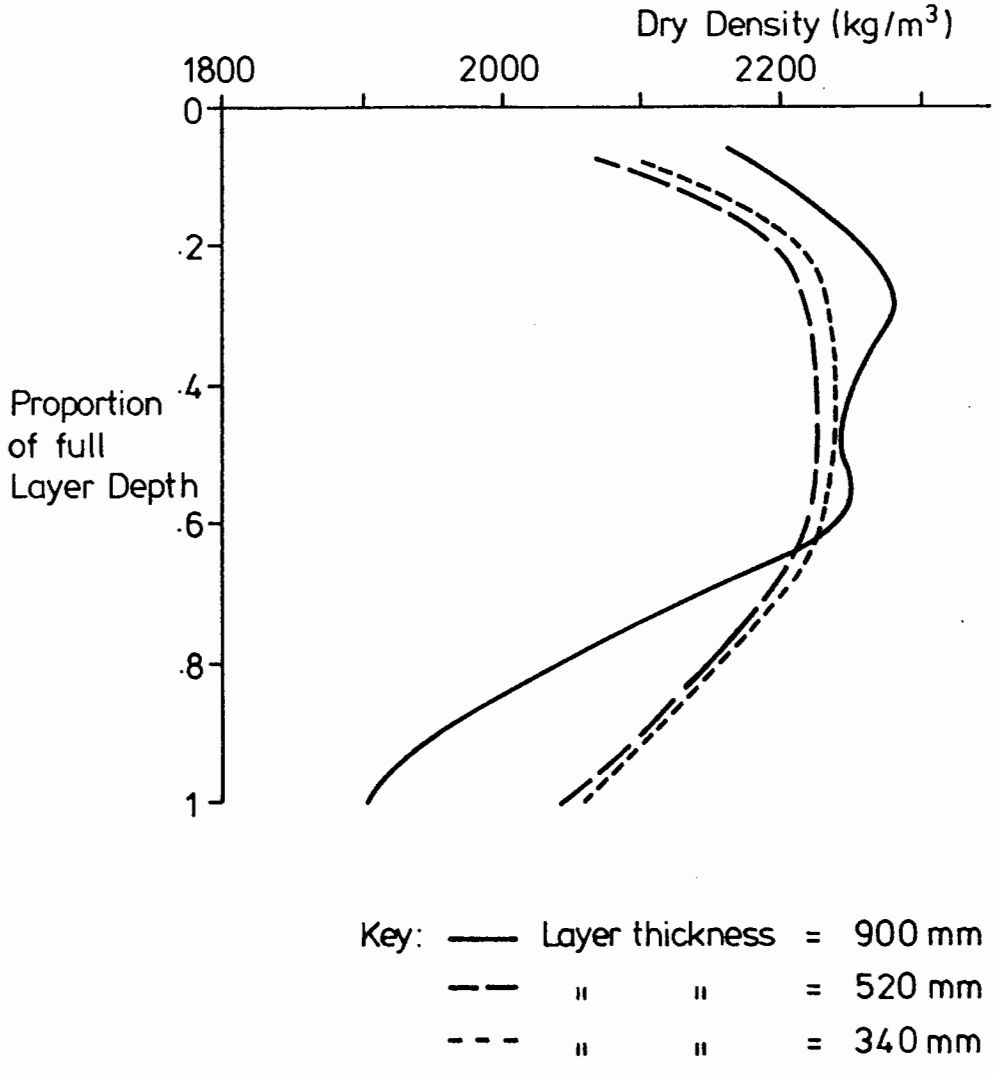

Fig. 8.1 Variation of Density with Depth
(after LeFlaive and Schaeffner 1980)

their results relating to gravel layers and it is clear that, even for the thinner layers, the density distribution is far from uniform. In particular, there is a loose region near the surface and poor compaction towards the base of the layer. If the differences in density shown in fig 8.1 are compared with the differences shown in fig 5.7 between uncompacted and heavily compacted laboratory specimens at the same grading, it is clear that the undercompaction revealed by fig 8.1 is likely to be very significant. Care should therefore be taken when using density results obtained at the surface and they should not necessarily be taken as wholly representative.

Current compaction practice can therefore be summarised as leaving a granular layer in a dense but nearly saturated state, with a low density region at the base of the layer and possibly one at the top.

8.2 EFFECT OF SUBGRADE SUPPORT

Valeux and Morel (1980) have described a series of full scale compaction tests using a vibrating roller on 200mm and 300mm gravel layers using different subgrade suppport conditions. Fig 8.2 (a) is taken from their paper and shows the very considerable differences in average layer density to be expected over three different subgrades. The subgrades range from a cement stabilized gravel to a weak silt. Here it can clearly be seen that a method specification which ignores the support conditions

(a) (after Valeux and Morel 1980)

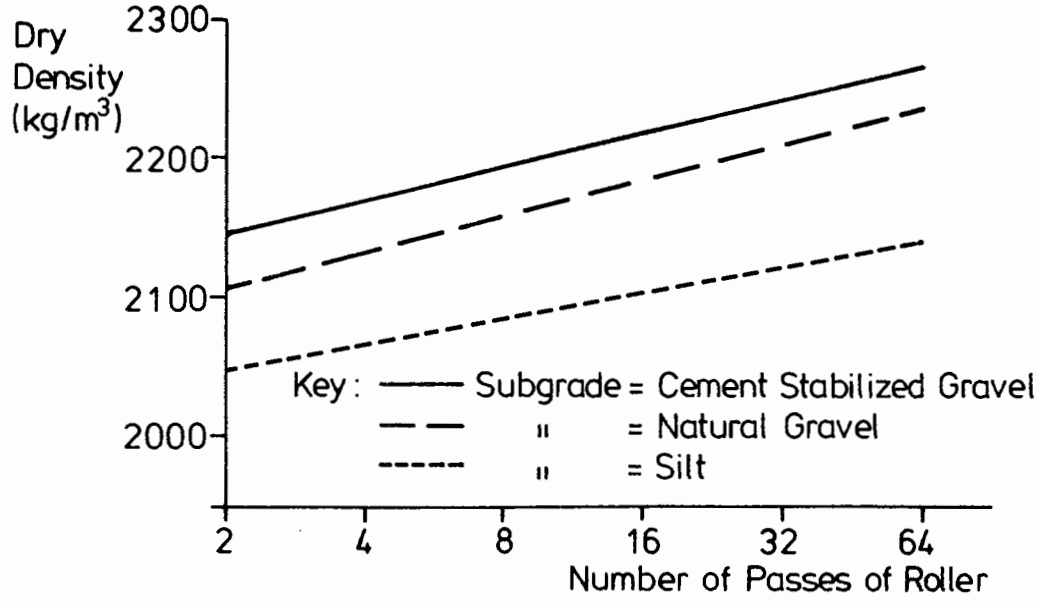

(b)

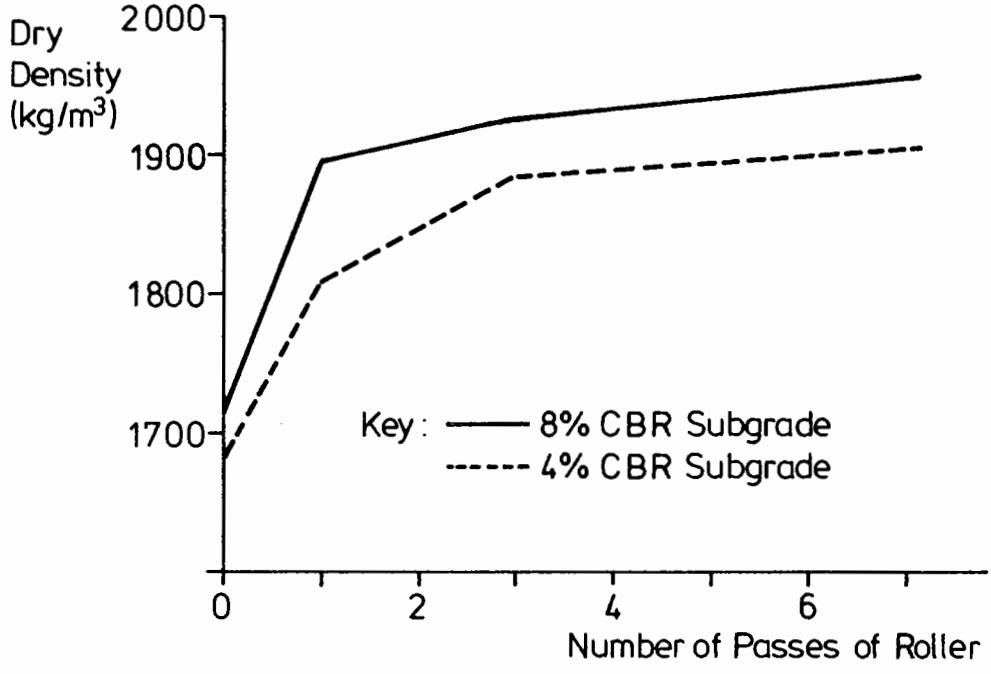

Fig. 8.2 Effect of Subgrade on Achieved Density

will be inadequate and will not ensure high density. The figure gives the average density of the layer but Valeux and Morel have shown that the density difference is not restricted to any one part of the layer.

In the one compaction trial performed during this research, which is described fully in section 9.3.2 in relation to in-situ testing, it was possible to compare two strips of granular sub-base differing only in their support conditions. The measured density results during compaction are given in fig 8.2 (b), where it may be seen that the two supports were approximately of 4% and 8% CBR (ref section 9.2 for CBR definition). Once again a clear difference between the two densities, both of which are the average of three points taken at the surface using a nuclear density meter in backscatter mode, can be seen. Reference to chapter 5 indicates that such density difference is likely to lead to considerable difference in both the strength and resistance to plastic strain of the granular layer.

8.3 OVERCOMPACTION

The word overcompaction is part of a road engineer's vocabulary, but may mean different things on different occasions. In the trial referred to in the previous section and described in section 9.3.2, the elastic response of the ground was monitored during rolling using an instrument called a Terrameter, marketed by Bomag Ltd (ref section 9.2.5). This instrument indicated that, in the weak support region, the stiffness of response began

to reduce after the first couple of passes even though the density was still increasing slightly. Such behaviour may represent the beginning of a type of overcompaction and may be linked to the phenomenon described in section 5.3.2 of exceeding a 'characteristic threshold' for the material. Further compaction might therefore lead to a weakening and reduction in stiffness even though density may not actually reduce.

Perhaps a more common manifestation of overcompaction is the case where the material becomes saturated, either because the moisture content is higher than optimum or because an excessive amount of compaction has been used. This leads to the development of positive pore pressures and a temporary weakening of the material. The danger here is that, in a material rich in fines, the water does not drain away and conditions of near saturation prevail both during laying of the surfacing and after completion. This can mean that an overlying bituminous layer cracks under the roller due to lack of support from the granular material.

These two manifestations of overcompaction are both dangerous and to be avoided. Both are likely to occur in cases where a broadly graded aggregate with a relatively high fines content is used, such as a material at the fine end of the DTp type 1 envelope, and are almost inconceivable for more uniform materials.

8.4 INFLUENCE OF ROLLER SPEED

It appears that the most efficient way of increasing the density of a granular material is to apply repeated loading to it rather than simply to compress it statically. This has certainly been borne out by laboratory testing (Brown and Ansell 1980) and is also evidenced in practice. Thus a vibrating roller, applying many load applications, requires relatively slight weight to achieve the same densities as a heavy static roller. The repeated loading achieved by a static roller comes from rerolling the same spot, implying that, whatever the roller speed, one load application is delivered on each pass. The vibrating roller, however, delivers a certain number of load applications per unit time and will therefore achieve less per pass at any one spot the faster it travels.

Fujii et al (1980) have investigated the speed factor in a slightly different way by measuring the transient stresses developed in the ground under a roller. They found that the stresses under a vibrating roller dropped significantly (by up to 40%) as the speed of travel was increased from 0.4m/sec to 1.2 m/sec. Conversely, every other type of roller showed stress increasing as speed increased. No results for achieved density are presented, but it might logically be expected to correlate with applied stress level.

8.5 STRESS DISTRIBUTION AFTER COMPACTION

It has been suggested (e.g. Uzan 1985) that compaction of a granular material induces residual horizontal stresses which may be greater than the vertical stress due to overburden. This is based both on in-situ measurement in layers of retaining wall back-fill and also on a theoretical analysis. The latter indicates that the elastic stiffness of a granular layer, being stress dependent, would not achieve a realistic value unless some horizontal residual stress were assumed. The same type of theoretical study has been done analysing results from the Nottingham pavement test facility, which indicated that the transient stress measurements would be impossible, ie beyond failure, unless a residual horizontal stress were assumed (Thom and Brown, 1985), in that case about 30kPa. Sharp (1983) developed a theory by which "shakedown" is allowed to occur in a granular material under repeated load. This means that residual stresses are set up within the material to minimize the amount of plastic deformation that occurs. The concept has been pursued by Selig et al (1986) who measured quite high residual horizontal stresses in a sand layer under repeated load, building up as the number of load applications increased.

In the light of such evidence it was decided to try to measure residual stress in a granular layer under compaction. It was noted that previous efforts using conventional pressure cells had been unsuccessful, so it was decided to construct a new cell with frictional faces formed by sticking pieces of stone to the sides.

The cell was successfully made and calibrated, and proved by compacting it into an aggregate in a box, where the horizontal stress recorded matched that measured at the side of the box. It was then used on several occasions, both on site and in the pavement test facility, at various depths in granular material, both longitudinally and transverse to the roller motion. However, the experience on each occasion was that, although transient stresses might be high, they always disappeared almost completely as the roller passed on. The maximum residual stress recorded after a pass from a vibrating roller was around 2kPa but rose to about 5kPa under a static roller on one occasion.

Recent work at Delft University has had similar results, implying that compaction is not responsible for the sort of residual stresses which have been expected, certainly not when vibrating rollers are used. This may be because the vibrations effectively destroy any stress contacts that would otherwise form between particles. However, the argument for the existence of such stresses is strong and it appears likely after the work of Selig et al (1986) that it is, in fact, the traffic loading that forces the accumulation of residual horizontal stress. This has been referred to in section 7.2.5 in relation to the calculation for rut development used in the GRANMAT program and satisfies the conceptual demands of 'shakedown' theory.

8.6 CONCLUSIONS

This chapter has highlighted a few aspects of compaction which are of relevance to this project. The influence of roller speed and support condition has been shown to render the application of a method specification for compaction control rather inadequate for ensuring high density. It also emphasizes the dangers in assuming at the design stage that a certain density can be achieved. Similarly, the density distribution through a layer has been shown to be far from uniform, a fact not usually accounted for in design. The dangers of excessive moisture and of excessive compaction have also been alluded to.

CHAPTER NINE

FIELD MEASUREMENTS

Previous chapters have concentrated on the properties exhibited by various granular materials in various states and on their incorporation into a road structure. If a chosen design were followed exactly and the correct procedure of laying and compacting complied with, then it might be possible to assume that a pavement layer would perform satisfactorily. Indeed, the practice commonly followed in the UK (Department of Transport 1986) is to use a 'method specification', whereby the supervising authority attempts to check that the correct materials are being used and laid in the stipulated fashion. If all is in order then the pavement layer is assumed to have the properties desired by the designer.

However, problems inevitably occur, either in the design stage or during construction, and disputes as to the suitability of a layer are always likely. In such a case it is possible to argue that the contractor either did or did not follow the method specification but, if it were feasible to test the layer in-situ, such matters might be more easily resolved. In fact, if the specification included the final properties of the layer, in terms of meaningful tests, then the whole situation would be much clearer. Of course, certain tests are at present often carried out by a prudent supervising authority to assist his

judgement as to the acceptability of a layer, but they do not usually form part of an end product specification.

This chapter will assess some of the tests currently possible in-situ, will attempt to identify which property each test is measuring and will make suggestions as to when each test might be appropriate. Five site trials have been performed during the course of this project with the principal aim of checking the various tests against each other. These will be described after an initial discussion of current practice and of the available testing devices. Results will then be presented and discussed before conclusions are drawn.

9.1 REVIEW OF CURRENT PRACTICE

With the advent of the nuclear density meter, it is now a relatively simple matter to obtain values of dry density and moisture content for a granular material and such testing is commonly done. If the nuclear device is not trusted, and there are certainly problems in calibrating it for different materials, then the sand replacement method is also available, although somewhat slower and more laborious. If a compaction test has been performed in the laboratory, then site data on density and moisture content can be compared with the optimum values from the laboratory.

Samples from site are sometimes removed for grading analysis since it is often found that the grading after laying and compaction is rather finer than beforehand.

One test which is recognized worldwide by road engineers is the California Bearing Ratio (CBR). The test itself is in theory suited to either field or laboratory conditions and involves the loading of a 50mm diameter rigid plate until a penetration of 1.27mm (1/20 inch) into the material is achieved. The ratio is given as a percentage of the performance a particular rock in California. It is usual to remove material from site to a laboratory, where a machine can apply the load at a specified and constant strain rate onto a portion of material in a 150mm diameter mould. In the case of non-cohesive material, such as a granular pavement layer, it is necessary to recompact it into the mould before commencing the CBR test.

The problem with the sort of aggregates used in road construction is clearly that they consist of large particles, often as large as a CBR loading plate, and that the test may therefore not give meaningful answers. Many authorities in the UK have, therefore, decided to adopt the plate bearing test as a field equivalent to the CBR (Plate 7). It is essentially a similar test. A plate of between 150mm and 750mm diameter is loaded, usually by jacking against a heavy vehicle, and the deflection measured. The test is generally stopped when the CBR deflection of 1.27mm is reached and, by means of a conversion equation, an equivalent CBR is derived. The plate bearing test is particularly widely used for

testing lower sub-base or capping layer and the subgrade itself, where material quality is commonly specified in terms of CBR. Day (1981) describes the use to which the test is generally put, as well as its origin in the US Corps of Engineers.

Use of a proof roller is sometimes made, with the aim that any undercompacted areas can be readily spotted and dealt with. The advantage is its capacity to test virtually the entire surface area of a pavement layer in a reasonably short time.

9.2 TESTING DEVICES AVAILABLE

Besides those mentioned in the previous section, there are now several in-situ testing devices available, some very sophisticated, others quite simple, all of which can reveal something about the state of a pavement layer. The instruments investigated in this research are briefly described in this section, together with some background information on their interpretation.

9.2.1 Falling Weight Deflectometer

The Falling Weight Deflectometer (FWD) was developed in France (Bretonnière 1963) and is now quite widely used, in Europe particularly, as a road testing tool. It is a relatively sophisticated and expensive machine involving computer control and data acquisition as well as sensitive measuring devices (see

Plate 8).

The model available to this project was a Dynatest 8000, described by Sørensen and Havyen (1982), jointly owned by the University of Nottingham and a local firm of pavement consultants (SWK Pavement Engineering). It is a trailer mounted machine controlled by a microcomputer housed in the towing vehicle. The principle is that a weight is raised and dropped onto a loading platen in contact with the ground. Both weight and drop height can be varied according to the load to be applied. The duration of the load pulse is typically of the order of 25 to 50 milliseconds, which fairly realistically simulates the pulse exerted by a moving vehicle. The applied pressure is usually between 400 and 800kPa, representing a heavy vehicle wheel. Deflections are measured by seven geophones which are positioned at the loading plate and at adjustable distances radially to a maximum of 2.1 metres. The geophone is a velocity transducer which uses computer integration to arrive at a maximum deflection, the accuracy of which is stated by the manufacturer as being $\pm$ 2 microns.

Thus, a test using an FWD yields an applied load and a set of surface deflections forming a bowl shape. It is then possible to use a pavement analysis program to find the combination of layer stiffnesses which provides the best theoretical fit to the deflected bowl. More than one such back-analysis procedure has been devised, including a program called ELMOD which is provided by the manufacturers. However, Tam (1987) has demonstrated that

there are significant deficiencies in the program and has designed his own, called PADAL, which uses the multi-layer linear elastic analysis program BISTRO (ref section 2.4) as a sub-routine. Although use of such a linear elastic program means that a granular layer will not be modelled totally accurately, Tam has incorporated a means of dividing the subgrade into five layers which can have different stiffness values, thus enabling a certain degree of non-linearity to be included. It is PADAL which will be used in this chapter in back-analysing FWD results.

The large majority of FWD testing has been done on finished roads and the stiffness values applicable to each layer calculated. Testing on an unbound material can present problems if one of the geophones is positioned over a loose stone and experience has shown that the occasional impossibly high or low deflection measurement does occur. However, the majority of tests described in this chapter produced satisfactorily shaped deflection bowls. Those which showed obvious error have been ignored. It was noticeable that compaction commonly took place under the FWD loading platen and it was therefore usual to take the last of at least four drops as being representative of elastic behaviour. Where a full back-analysis of the deflection bowl is not done, this chapter makes use of the modulus of reaction (load/central deflection) as a measure of response.

9.2.2 Clegg Impact Hammer

In contrast to the FWD, the Clegg hammer is small, simple, manually operated and relatively inexpensive, and it is designed to assess an unbound material. It was developed by Professor Clegg (Clegg 1976) in Australia and has since been a source of worldwide interest, mainly because of its simplicity and ease of operation. Plate 9 shows the instrument. The principle is similar to that of the FWD in that a weight (4.5 kg) is dropped through a known distance (450mm) onto the ground. The contact area is a circle of 50mm diameter. However, instead of recording the applied force and resulting deflection, an accelerometer is used and the maximum deceleration at impact is displayed as a multiple of 10 x gravity. It is recommended that the last of four drops at each point should be used, that being a largely elastic situation.

Using Newton's second law, since the mass of the dropped weight and the acceleration at impact are known, it is possible to obtain a contact pressure (assuming even pressure distribution). This reveals that, for a Clegg impact value (CIV) of 50 (= 500 g), the contact pressure is about 11MPa, more than ten times the greatest pressure likely from a vehicle. A CIV of 50 is typical for a compacted sub-base layer.

Further calculation is also possible but assumptions become unrealistic. For instance, if the ground is assumed to be an isotropic linear elastic half space and ground inertia is

ignored, and the mass is assumed to fall freely through a vacuum to the ground, then the following equations can also be deduced using the laws of linear elasticity and Newton's second law.

$$\text{Pulse Duration} \approx 50/(\text{CIV}) \text{ msecs} \qquad 9.1$$

$$\text{Elastic Modulus of Ground} \approx 1/10\ (\text{CIV})^2 \text{ MPa (depending on Poisson's Ratio)} \qquad 9.2$$

$$\text{Maximum Deflection} \approx 90/(\text{CIV}) \text{ mm} \qquad 9.3$$

Comments as to the applicability or otherwise of these formulae will be made in the light of actual results, but it is worth noting that the assumptions of linear elasticity and zero ground inertia are significantly erroneous. Also the very high contact pressures may contribute to unrealistic stiffness values.

Clegg (1976) also developed a CBR conversion curve, based on tests on a number of laboratory specimens, the formula for which is:

$$\text{CBR} = .07\ (\text{CIV})^{2.21} \qquad 9.4$$

Experience with the Clegg hammer is very limited at present and insufficient work has been done to date to establish the exact meaning of a CIV number in terms of the mechanical properties of the material being tested. What may be said is that it appears to measure the elastic response of the ground in some way.

9.2.3 Dynamic Cone Penetrometer

The test performed by a dynamic cone penetrometer (DCP) is completely different to that of the FWD and Clegg hammer. It involves driving a cone through the ground or pavement layers under the action of a 10kg weight dropped through 500mm against an anvil. Plate 10 shows the apparatus owned by Nottingham University in use, although many other designs exist. Though the principle of operation is simple, it is a much more awkward piece of equipment to transport and use than the Clegg hammer. Two people are generally required to operate it and, if many tests are to be done, considerable expenditure of effort is needed in repeatedly raising the 10kg weight. One other problem, which has occurred on the Nottingham University model and has also been reported on other models, is that many of the threaded connections holding the apparatus together tend to be seriously loosened by the impact of the weight on the anvil.

However, if the above problems are satisfactorily attended to, use is straightforward. Readings of penetration are taken every few blows, depending on how resistant the material is. These readings can then be converted into blows per centimetre and plotted against depth. One of the advantages of such a test is that it is usually possible to obtain layer thickness by noting the depths at which abrupt changes in penetration rate take place.

Very little experience with the DCP has been obtained to date in the UK but it is relatively widely used overseas, particularly in the developing world, where more sophisticated mechanised versions are sometimes used. Kleyn and Savage (1982) report that the DCP can be very successfully used in establishing criteria to be used in pavement design.

9.2.4 Plate Bearing Test

The basic test has been described in section 9.1. However, certain adaptations have been made by some users which have been the subject of investigation in this country, particularly by some of the County Council Highways Laboratories. In particular, it is standard practice in West Germany to load the plate, unload it and then reload it. A stiffness of response is obtained for both the first and second loadings and limits are set on the absolute value permissible for the second loading as well as the ratio of the two stiffnesses. The theory is that the second loading is almost entirely elastic and will therefore give a good measure of the elastic stiffness of the pavement, whereas the ratio of the two stiffnesses is a measure of how well the layer has been compacted; ie a ratio near one implies very little plastic strain on first loading and, therefore, good compaction.

Since no plate loading equipment is owned by Nottingham University, it has been necessary to use the results of tests performed by various authorities on a basis of mutual co-operation. Lincolnshire County Council has been of particular

assistance in this matter and results have also been gratefully received from Nottinghamshire County Council and the West Yorkshire Joint Waste Management Board.

9.2.5 BOMAG Terrameter

One of the recent developments by BOMAG for monitoring compaction is the Terrameter (Kirschner 1986 (a)). It is a device which is fitted to a vibrating roller and its main use so far is to maximise the efficiency of use of compacting plant. The Terrameter records the acceleration vector in the vibrating drum continuously and, by means of computer controlled sampling of the output, it computes a value of effective power transmitted to the ground, termed the w-value (omega value). This w-value can be seen directly on a meter in the operator's cab and also recorded continuously on a chart recorder if desired. The Terrameter also has the facility for comparing an averaged w-value from one pass with that from the next, thereby indicating whether further passes are likely to produce any improvement in compaction.

BOMAG have performed several trial compactions using the device (eg Kirschner 1986 (b)), and have shown that it is generally capable of identifying the point where further compactive effort is of no avail. They have also observed a few situations where the w-value reaches a peak after one or two passes and then decreases again, indicating a stiffness reduction in the response of the ground. This phenomenon appears to represent over-

compaction, discussed in section 8.3, and provides another example of the Terrameter's capabilities. Perhaps the most impressive testimony to its sensitivity is the ability of the machine to detect stiff or soft inclusions, even at a metre or more depth.

This chapter describes one trial, carried out in conjunction with BOMAG, which was designed to increase understanding of the meaning of the Terrameter output.

9.3 DESCRIPTION OF SITE TRIALS

9.3.1 A610 Kimberley Bypass

Kimberley bypass is a dual two lane road six miles north-east of Nottingham and the contract, during which the testing was done, involved reconstruction of the east bound slow lane, which was previously a wet-mix macadam base construction overlying a relatively thin sub-base and soft clay soil. Premature signs of failure had necessitated the complete reconstruction of the pavement. Because of the soft nature of the subgrade, 600mm of soil was replaced by approximately single sized (150mm) limestone rock-fill, and above that the sub-base was 150mm of crushed limestone type 1 material. Testing was carried out mainly at top of sub-base with a few tests being done on the rock-fill also.

Nottinghamshire County Council, who were the Client and supervising authority for the contract, provided equipment and

staff for conducting plate bearing tests, nuclear density and moisture content evaluation. The University made use of its FWD, DCP and Clegg hammer. Testing was carried out at seven points on the sub-base and two on the rock-fill, although not all devices were used at each point.

9.3.2 Wakefield Haul Road

A paved haul road has recently been constructed for the transport of colliery waste materials to a reclamation area in the Calder Valley near Wakefield. It was, in fact, designed as an experimental road and is divided into sections of different construction detail, as well as incorporating some in-situ instrumentation. Some of the results from the instrumentation have been referred to in section 7.3 as evidence in assessing the GRANMAT computer program. The trial described here took place during construction over a 25m length on an embankment approximately 7m high, constructed out of material taken from a cut on another section of the road. The fill material was a mixture of very weathered siltstones, sandstones and mudstones and was of variable quality, but a minimum CBR of 4% was achieved.

The trial involved some preliminary testing at formation level, ie top of fill, and the compaction and testing of a nominally 240mm thick layer of type 1 sub-base. The compacting equipment used was a BW213 single drum wheel drive vibrating roller,

supplied by BOMAG and fitted with a Terrameter.

The other testing done consisted of plate bearing tests performed at formation and finished sub-base levels by the supervising authority who were the West Yorkshire Joint Waste Management Board and FWD, Clegg hammer and nuclear density tests performed by the University at various stages before, during and after compaction. The test section was divided into three strips, one of which was compacted using a lower amplitide of vibration than the other two.

9.3.3 A52 Friskney Realignment

The contract which provided the opportunity for testing was a major realignment of a particularly winding section of the A52 between Boston and Skegness in Lincolnshire. Lincolnshire County Council offered the opportunity to test the capping layer material at locations already covered by plate bearing tests. The site was one with very uniform subgrade of soft wet clayey silt, with a water table close to formation level. A fabric was used as a separator between the silt subgrade and the overlying pavement construction which involved a capping layer of at least 500mm thickness. Two very different materials had been used as capping layer; a natural sand and gravel, and a local crushed oolitic limestone. Fortunately it was possible to test both.

Apart from the plate bearing tests performed by the County Council, tests were also performed with the FWD and Clegg hammer.

Unfortunately the DCP was damaged at an early stage and provided no useful results. One aspect which could be important is that many of the plate bearing tests had been carried out one or two months previously during much worse weather conditions and may, therefore, not be directly comparable to the FWD and Clegg hammer results.

9.3.4 A52 Bicker Realignment

This was a very similar site to the one described above at Friskney. It involved the construction of several sections of new road on the A52 between Grantham and Boston. The subgrade was also a soft silt; a fabric was also used above it; testing was also carried out on top of a capping layer material. On this occasion, however, plate bearing tests had only recently been carried out by Lincolnshire County Council and were of much more certain use. Also the DCP was fully operational and was used in conjunction with the FWD and Clegg hammer. Only one capping layer material was used, a crushed oolitic limestone containing particles up to 150mm in diameter.

9.3.5 A46 Dunholme Bypass

Another site under the control of Lincolnshire County Council, Dunholme bypass was a new road being built over variable subgrade, but stiffer than at Friskney or Bicker. Testing was carried out both directly on capping layer material (nominally

500mm thick) and also on the overlying 150mm of sub-base. Both were of dolomitic limestone, but with different gradings. Plate bearing tests and nuclear density measurements were carried out by the County Council and, once again, FWD, DCP and Clegg hammer testing was performed by the University. In fact, a second Clegg hammer, provided by Cambridgeshire County Council, was also used by way of comparison.

9.4 ANALYSIS OF RESULTS

It is not possible in the space available to discuss every detail of the measurements taken, but it is hoped in this section to bring out every important trend or interdependency between instruments which has been found and, thereby, to isolate the meaning and usefulness of each test. The conclusions will be highlighted in section 9.5. Since different tests were performed at each site under different conditions, it was considered that the most useful approach would be to draw out the results relevant to each instrument in turn, although some overlap is inevitable.

9.4.1 Falling Weight Deflectometer

The point has been made in section 9.2.1 that the FWD is a test for measuring elastic stiffness. Tam (1987) has given a very up-to-date account of its use, illustrating its capacity for isolating the stiffness values appropriate to each layer. This capacity, therefore, is clearly the area to be explored in

relation to the unbound materials comprising a road foundation. Two of the sties, Bicker and Dunholme, were not of any special interest for FWD back analysis. Bicker contained no significant material variability and the results were therefore, not surprisingly, all fairly similar. Dunholme included both capping layer and sub-base testing but, since the two materials were very similar, it is once again not easy to use the results to make any point. The other three sites, however, will be used. At Wakefield, over the area tested, there were two distinctly different areas of subgrade, one significantly softer than the other. The approximate CBR values from static cone and Clegg hammer testing were 8% and 4%. An average FWD bowl was therefore computed for each area, simply the mean of all the relevant results, and the back analysis program PADAL used to calculate the sub-base and subgrade elastic stiffnesses. The result is shown in Table 9.1 and it is immediately clear that the difference between the two cases is in the subgrade. At Friskney a comparison of two very different granular materials over similar subgrade was possible, being sand and gravel on the one hand and oolitic limestone on the other. Again the resultant stiffnesses are shown in Table 9.1, where the capping layer has been analysed in three different ways, being considered as one, two or three layers of different stiffness. It is apparent that the subgrade is of similar stiffness in each case whereas the limestone is stiffer than the sand and gravel, at least on average.

Table 9.1 Elastic Stiffness Moduli back - calculated from FWD Tests (in MPa)

Location	Sub-base	Capping Layer/Rock-fill			Top of Subgrade
Wakefield					
Subgrade CBR 8%	66				100
Subgrade CBR 4%	55				56
Friskney					
Sand & Gravel (1 Layer)			104		80
(2 Layer)		99		161	83
(3 Layer)		133	46	500	79
Limestone (1 Layer)			213		113
(2 Layer)		257		106	112
(3 Layer)		454	48	500	108
Kimberley					
On Sub-base	466		166		206
On Rock-fill			63		166

However, the different stiffnesses that arise depending on how many layers are used in analysis are also evident. It appears that it is in the upper portion of the layer that the difference between the two materials is seen. Indeed, for the two layer case the lower layer is stiffer for the sand and gravel, and the 500MPa for the lowest of three sub-layers is an upper bound set by the program and does not represent identical behaviour. It is probably unwise to attempt an explanation for the distribution of stiffness revealed here, because the main reason is probably that the program is attempting to use a linear elastic solution to fit a fundamentally non-linear material. However, some logic may be seen in that two things lead to high apparent stiffness in a granular material; high mean normal stress and low stress change. These two may be found at the top and bottom of the layer respectively. In the same way the reason for the slight difference in subgrade stiffness between the two cases may be that the stress change induced under the sand and gravel is greater than that under the stiffer limestone. The results from Kimberley (table 9.1) also show a large difference in capping layer stiffness between the two cases which is likely to be due to the different stress conditions involved.

In summary, the FWD can be used on granular material to separate out the stiffnesses of different layers but it is probably not wise to try to sub-divide a layer since the resultant stiffnesses are not likely to be realistic. The actual linear elastic moduli obtained should be used with caution because of the large dependence on stress conditions.

9.4.2 Dynamic Cone Penetrometer

Since the test performed by the DCP is basically a failure test as the cone is continuously driven into the ground, it was thought likely that, for a given material, correlation might be sought with density on the grounds that strength of a granular material depends on density (ref section 5.3). Unfortunately, only one site where both density and DCP measurements were taken involved large density difference, that being Kimberley, and only three points were explored. None the less these results are plotted in fig 9.1, together with those from Dunholme, although the latter cluster rather meaninglessly in one area. This is clearly a subject that demands further data before the case is proven, but it is felt probable that the DCP may be used as an indirect way of determining the state of compaction. Indeed, it may be preferable to a direct density measurement because of the latter's sensitivity to variations in grading (see fig 5.7).

9.4.3 Plate Bearing Test

It has been stated that there are various ways of using and interpreting the plate bearing test, but in the trials described here it is the single loading to the CBR deflection of 1.27mm which has consistently been used. This is then converted to a CBR value. It was noticed that, as for the DCP, the CBR value was also responsive to density change, a not surprising observation since the majority of the deformation induced by the

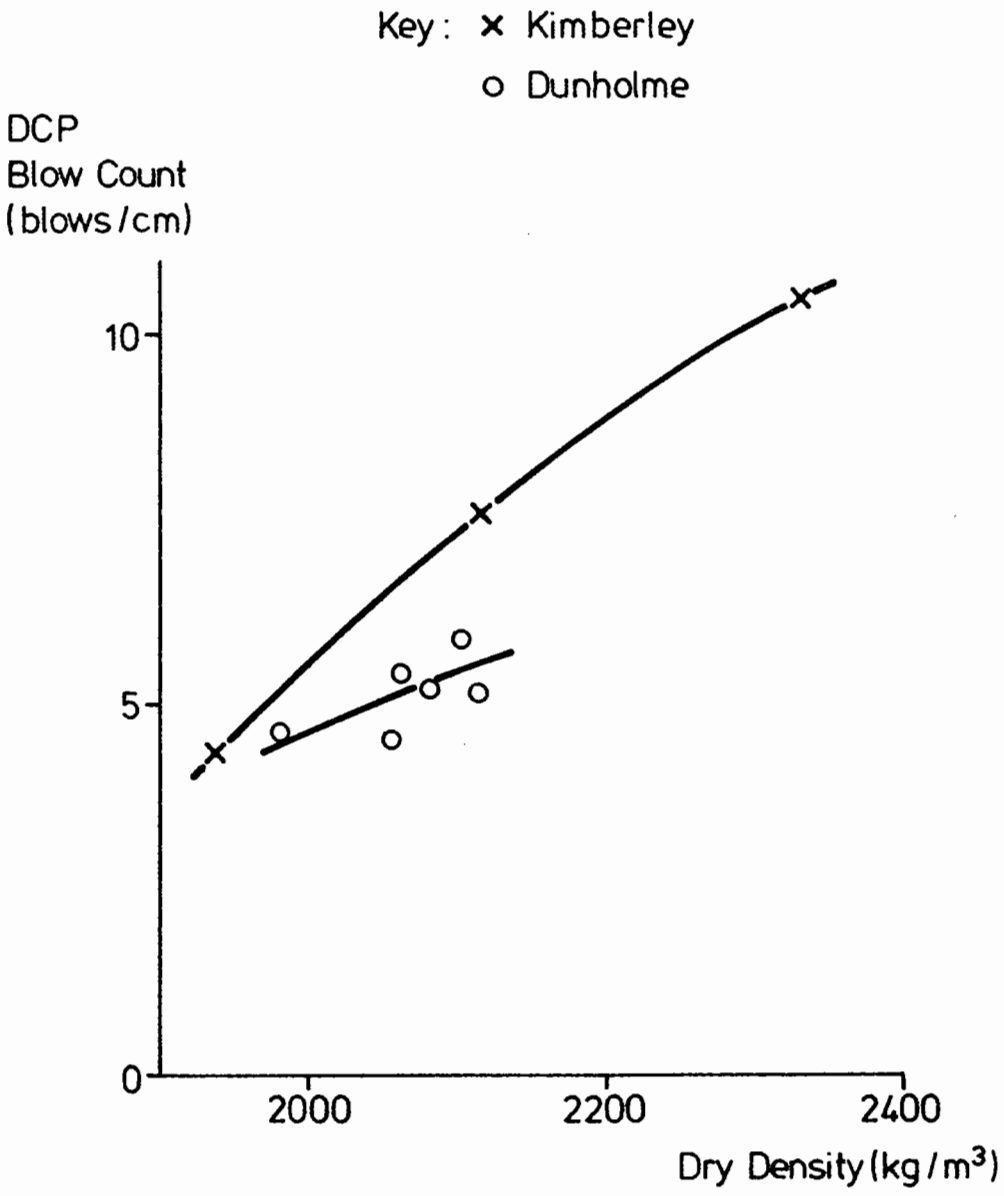

Fig. 9.1 Correlation of DCP with Density

test is plastic and irrecoverable. This is illustrated by fig 9.2 where plate bearing CBR is plotted against DCP blow count for the three sites where both tests were used. It can be seen that there are a few rogue points but that, for a given material, some correlation exists. However, in the same way as the FWD, the plate bearing test is inevitably also affected by the subgrade stiffness since it uses a similar sized loading plate. This may account for some of the exceptions to the general correlation with the DCP and render interpretation of the test more difficult.

It had been hoped to study during this project the method of loading and reloading the plate, as employed in West Germany, to determine its possible advantages, but it has unfortunately not been possible to establish sufficient data. Many such tests have been performed by Lincolnshire County Council but there has generally been no comparative data from other tests. However, it may be that it is possible not only to determine the degree of compaction of a material but also to ascertain whether further densification is possible, or whether the subgrade is too soft. Therefore, such an extension to the test appears extremely desirable.

The present practice of loading until a specified deflection is reached is also seen here as being unfortunate in that, since the same pressure is to be expected in each location under a heavy vehicle wheel, the same pressure should therefore be applied in each test (say 500kPa). This would allow a more direct

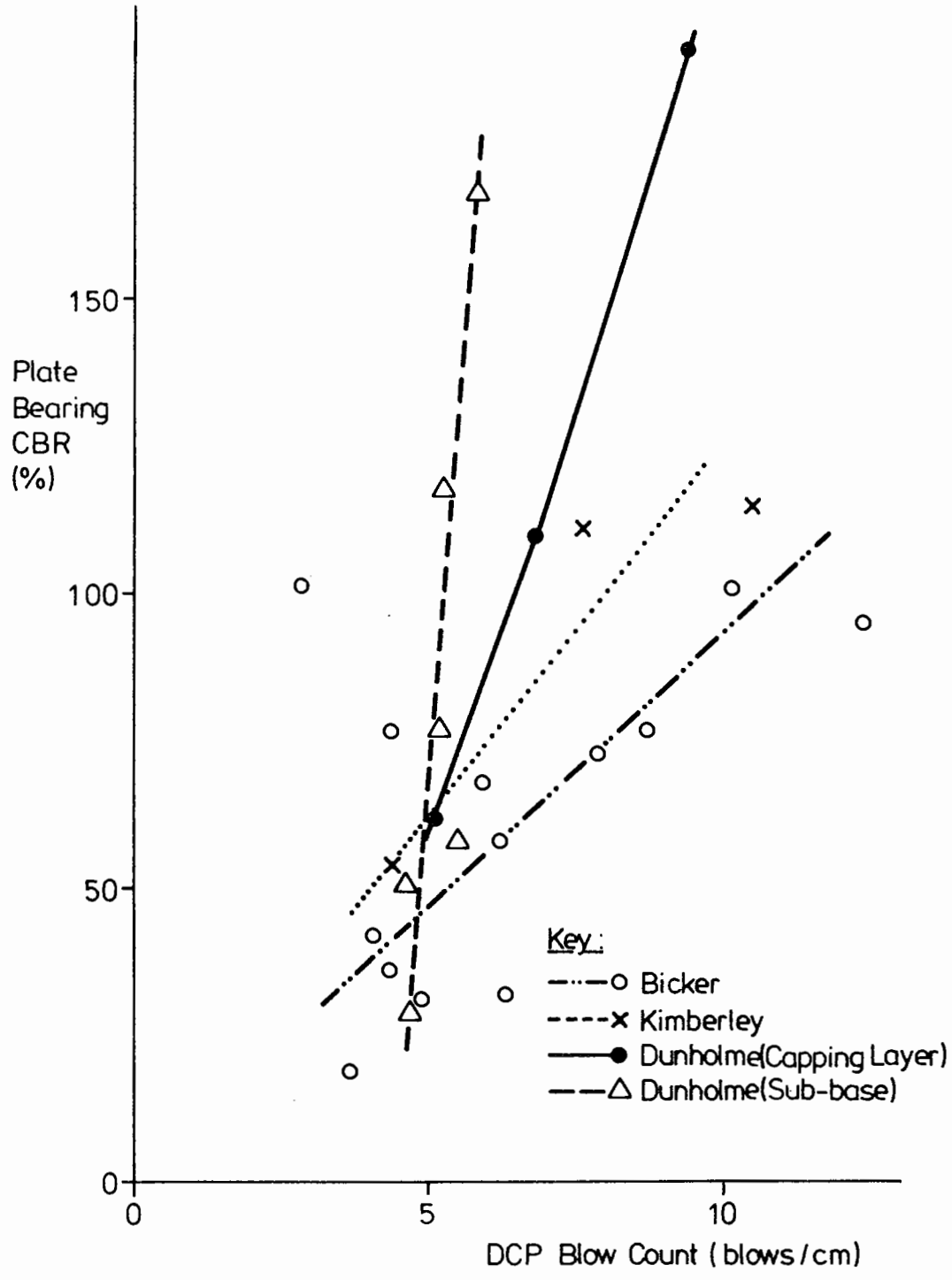

Fig. 9.2 Correlation of Plate Bearing CBR with DCP

comparison between tests.

In summary, much could be done to improve the test, but in its common UK form the resultant CBR value correlates substantially with density and therefore with DCP blow count.

9.4.4 Clegg Impact Hammer

The suggestion was made in section 9.2.2 that Clegg Impact Value (CIV) was a measure of elastic response, operating on a similar principle to the FWD. It was therefore decided to look for correlation between the two instruments. However, it was rapidly realized that the CIV was very sensitive to the exact position of the test, probably because of the small area of pressure application in relation to aggregate particle size. This gave a large scatter of results and meant that correlation between tests on a material of fairly uniform elastic properties was hard to prove. In an attempt to overcome this, four CIV values were taken at points immediately around each FWD test position and then averaged. The results are shown in fig 9.3, where both FWD modulus of reaction and CIV are plotted against dry density or, in the case of Bicker, DCP blow count since dry densities were not available. The first point to make is that neither CIV nor FWD modulus can be said to depend greatly on density, although CIV values for the highest density area are slightly greater than the least dense. However, it can be seen that some correlation between CIV and FWD modulus exists. The peaks and troughs on the

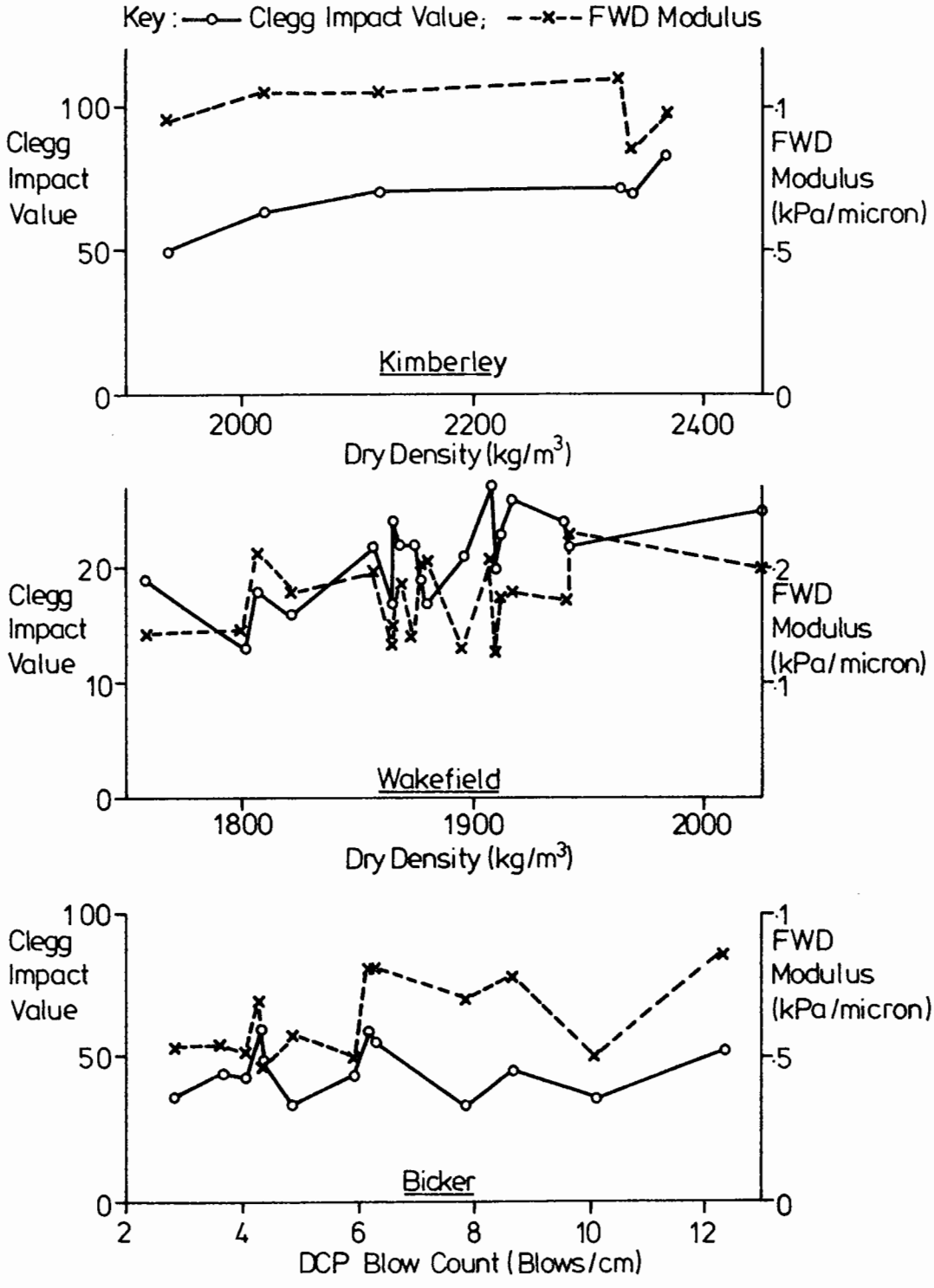

Fig.9.3 Clegg Hammer and FWD Correlations

plots commonly coincide although the correlation is far from 100%. This reinforces the view that the CIV is largely a measure of elastic stiffness. Information from two of the sites is not shown because of space restrictions: at Friskney similar correlation could be seen on both the sand and gravel and the limestone: at Dunholme there was very little material variation and no correlation was observed.

The question which then required answering was whether the Clegg hammer could be used as a cheap and far less precise alternative to the FWD. It was noticed at Wakefield that the same CIV values were obtained over the area of firm and soft subgrade, implying that the test was only influenced by the top layer. However, when the contact pressure deduced from Newton's second law was used in a GRANMAT analysis (ref chapter 7), the material parameters being taken from laboratory tests, it was found that the subgrade should have been of significant influence. Also the deflection expected by GRANMAT was much greater than the estimate given by equation 9.3. Although no proof is given, the reason for this discrepancy is thought to be in the use of a static analysis program (GRANMAT). A calculation using the pulse duration given in equation 9.1 reveals that a modest CIV of 30 or 40 would induce inertial stresses of tens of kilopascals in the ground which would effectively resist deformation and assist in protecting the subgrade. This effect might, in fact, make the Clegg hammer even more useful since it would not be influenced by lower layers; ie it might be a direct stiffness test of the top pavement layer. Unfortunately, it has not been possible to

experiment on sufficient different materials yet but the theoretical relationship in eq 9.2 is certainly not applicable since it relates to very high stress conditions and ignores ground inertia. Another point which does emerge from comparing results is that the level of suction operating in the ground has a large influence. None the less, fig 9.4 is included to compare CIV with laboratory determined stiffnesses at one selected stress level. It may be seen that considerable correlation is evident for the limited number of materials tested, but the elastic stiffness modulus shown should not be taken as realistic. Some of the scatter may be due to the presence of suction in the material on site but not in the laboratory.

It has been suggested that the Clegg hammer should be modified to use a larger contact area and lower contact stresses and a device on these lines called a Dynoplaque has been developed in France specifically for testing unbound materials. It is true that the scatter problem should diminish and a stiffness at more appropriate stress levels may be found, but the problems of lower layer influence return. If a unique relationship between CIV and measured elastic stiffness could be proved, then the Clegg hammer would be a very useful instrument, in spite of the scatter problem.

To summarize, the Clegg hammer gives a measure of elastic stiffness and is influenced only by the top few centimetres, but shows serious scatter due to its small contact area. It shows

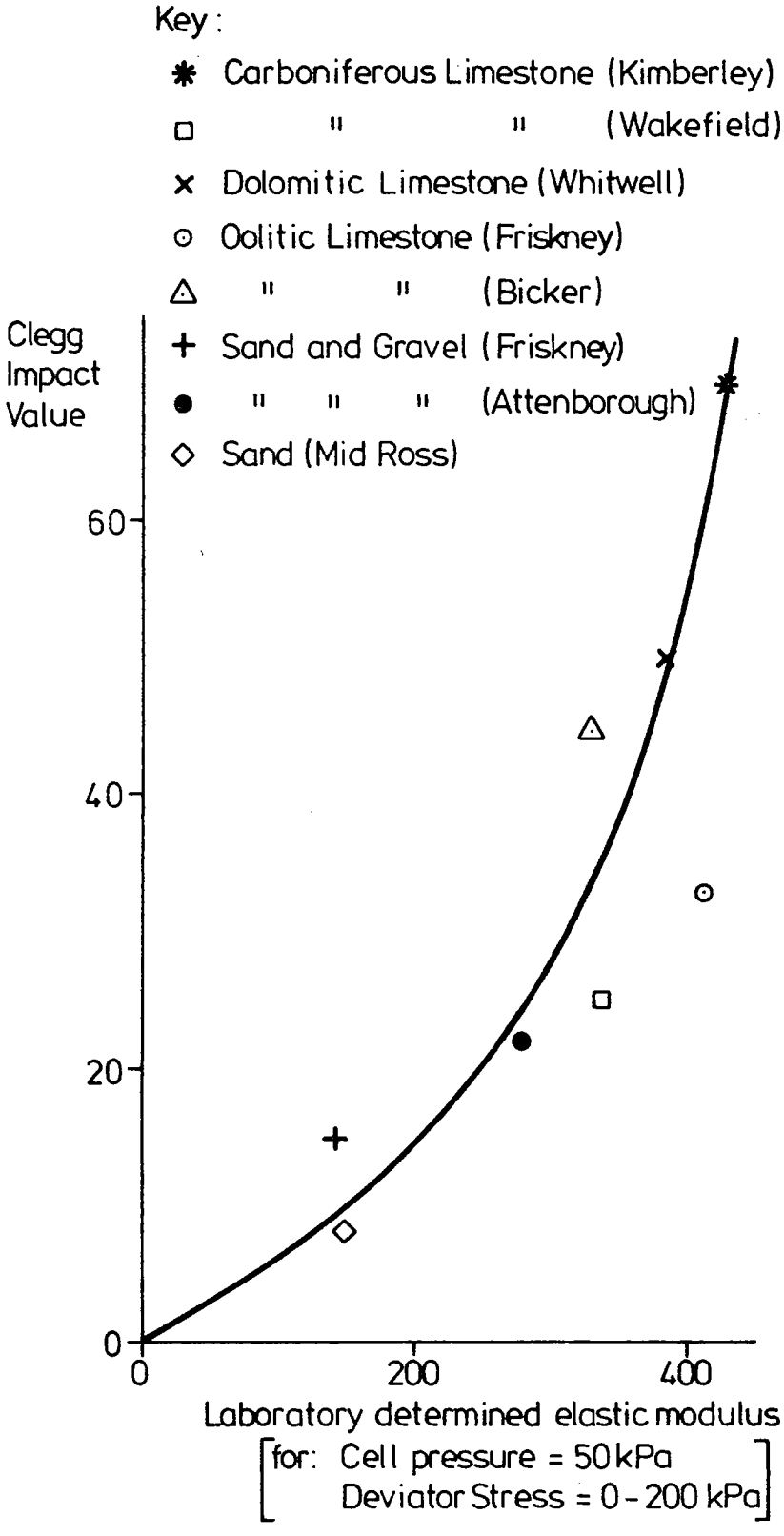

Fig. 9.4 Relationship between Clegg Impact Value and Elastic Stiffness

some density dependence but should not be used as a measure of CBR.

9.4.5 BOMAG Terrameter

The single trial performed as part of this project using the Terrameter was at Wakefield. The trial area was split into three strips (A,B and C) of 25m length each. A large part of strip C was over relatively soft subgrade, referred to in connection with achieved density (section 8.2) and with respect to FWD back analysis. The test procedure was, firstly, to roll the subgrade and obtain an w-value output from the Terrameter, then to lay the sub-base and compact it recording the w-value during the first, second, fourth and sixth passes. Strip A was vibrated at low amplitude, strips B and C at high amplitude. Other tests, including density measurement, were performed at intervals before, during and after compaction. Fig 9.5 attempts to show a complete record of Terrameter output for all three strips.

The w-value record for the subgrade can be seen as variable over very short distances, but it is clear that a large section of strip C produced significantly low values, which correlated well with low stiffnesses obtained by the Clegg hammer (CIV $\approx$ 16: elsewhere $\approx$ 22). If the traces recorded during compaction of the sub-base layer are inspected, it may be seen that many of the peaks and troughs superimpose well on each other and on the subgrade output, although error is to be expected because of the difficulty in ensuring the same line being taken by the roller in

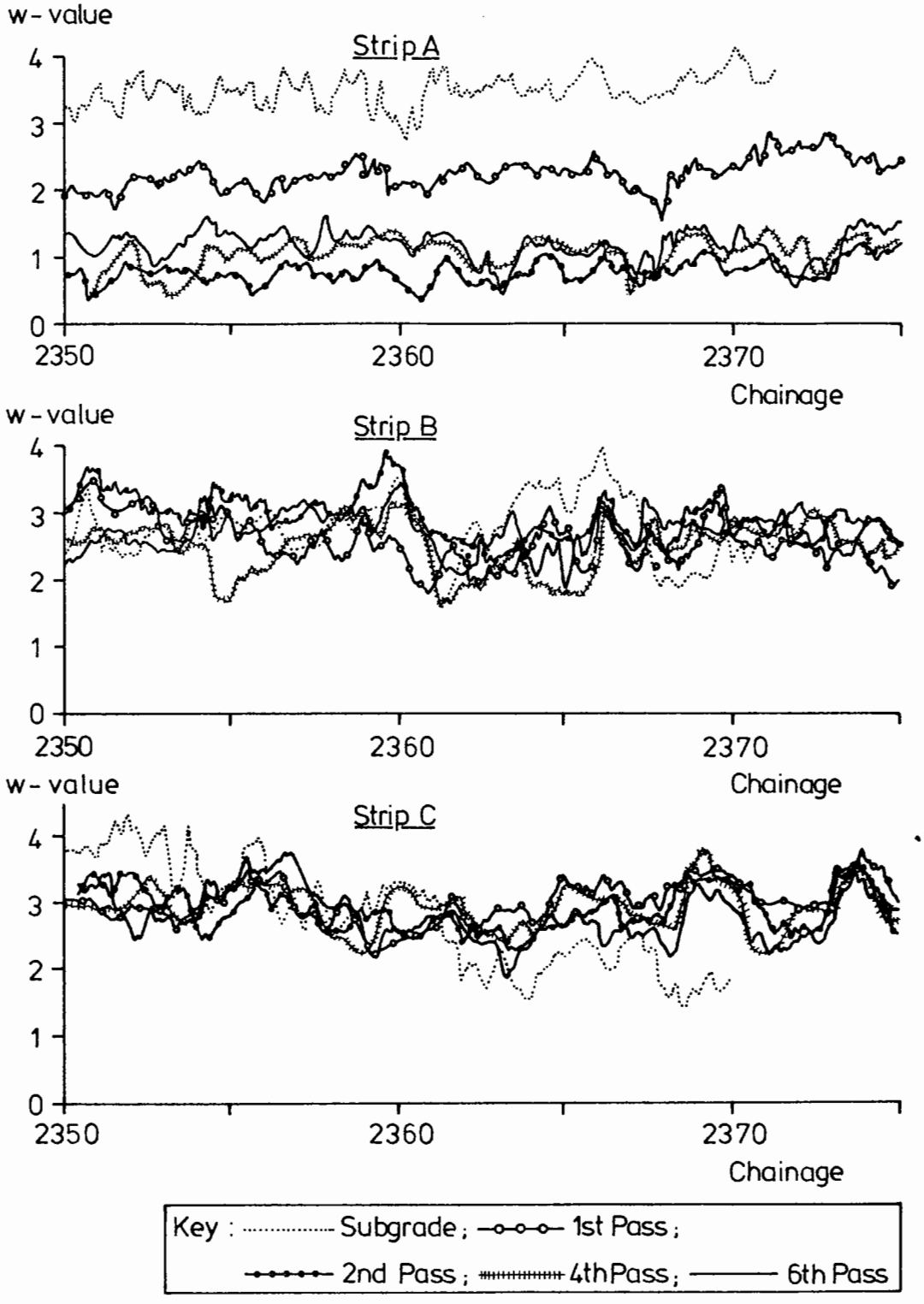

Fig. 9·5 Output from Terrameter

consecutive passes. This implies that the fluctuations in output are not random but repeatable and therefore represent genuine changes in ground response.

To consider each strip separately: the first pass of strip A should be ignored since it was accidentally vibrated at high amplitude. Subsequent passes reveal a generally increasing w-value. On strip B, however, vibrated at high amplitude, the w-value cannot be seen to improve at all on average. This is also the case for part of strip C but, where the subgrade is soft, the w-value actually decreases slightly from one pass to the next. In all cases the density was increasing with every pass.

It is clear that the phenomenon illustrated by the area of soft subgrade on strip C is overcompaction. Planes of failure were probably being developed by the roller, thus leading to a less stiff response even though the overall density was increasing. Strip B represents the case where optimum compaction has been achieved and further passes of the roller serve no purpose; they might eventually lead to overcompaction as in strip C. In strip A, the continuing increase in w-value implies that compaction is not yet complete.

As explained in the instrument description section, the Terrameter contains a facility for comparing the averaged w-value on one pass with that from the previous pass. By such means an operator can identify the time when the roller has achieved all

that it can and where further passes might lead to overcompaction. If a choice of vibration amplitudes is available, it will also enable him to select the most appropriate. It may even be possible to stipulate on a particular site the averaged w-value which should be achieved if compaction is to be considered satisfactory.

9.5 Conclusions

Five testing devices have been used, compared and analysed and the following are the major conclusions:

(a) The FWD can be used on granular material with success and enables the elastic stiffnesses of individual layers to be computed. It is likely to be a useful tool in trouble-shooting situations though it should be remembered that the resultant granular material stiffnesses are stress dependent.

(b) The DCP blow count correlates with density for a given material.

(c) The plate bearing CBR correlates with density for a given material.

(d) The Clegg hammer measures the elastic stiffness of the top few centimetres of material, but is susceptible to serious scatter in measurements. It is also slightly density

dependent.

(e) The Terrameter can be used to control compaction such that the point when no further compaction is desirable can be determined.

CHAPTER TEN

DESIGN CONSIDERATIONS

Because the function and behaviour of granular road foundation material has not been well understood in the past, it is not surprising that a very empirical approach to its design has always been taken. Once it is general experience that use of a particular material with a certain thickness gives good results, then its use is included in a design guide. Differentiation between high and low quality material has been made and is presently exemplified by the categories of type 1 and type 2 sub-base contained in the DTp Specification for Highways (1986), as well as the more open classification of capping layer material.

The TRRL report LR 1132 (Powell et al 1984) contains the most up-to-date guide to road foundation design presently used in this country. In it the whole foundation up to top of sub-base is seen as a dual purpose construction. Firstly, it has to bear the weight of construction traffic, which is generally the most onerous duty and, secondly, it has to perform satisfactorily as part of the finished road. According to the quality of subgrade, a capping layer may be necessary to increase the CBR (ref section 9.1) at formation. Once that is decided upon, the thickness of

sub-base necessary depends on the quantity of construction traffic expected.

Certain properties are assumed in current granular road foundation design. The sub-base is assumed to be sufficiently stiff not to overstress either the upper layers or the subgrade. It is also assumed to be sufficiently permeable to drain away any excess water that may arrive. However, as chapters 5 and 6 have shown, both stiffness and permeability are quantities that may well vary from one material and grading to another. It would clearly be of benefit if such properties could be ensured scientifically rather than assumed to apply to every type 1 sub-base material.

Previous chapters have supplied an understanding of granular material which it should be possible to use in design. Chapter 5 has revealed the very small effect that a quite considerable change in grading is likely to have on both elastic stiffness and plastic straining and that density affects plastic straining but not elastic stiffness. It has shown that aggregates containing larger particles are both stiffer and stronger. Finally, it has given an insight into which minerals are likely to be stiffest and which are likely to resist plastic straining. Chapter 6 has highlighted the dependence of permeability on grading, as well as the likely levels of suction which could exist. The dangers of saturation of a material of low permeability have been made clear. In chapter 7 a tool has been designed in GRANMAT which enables the effects of changes in various parameters on the whole

pavement to be studied. Chapter 8 has examined what can be achieved by compaction of a layer and chapter 9 has examined ways in which it may be possible to test the properties of a granular layer once it is laid.

In this chapter it is proposed to present the results of several 'GRANMAT runs', examining the influence of various parameters, particularly the stiffness, strength and thickness of granular base, on the pavement as a whole. Having established the importance or otherwise of each relevant parameter, it is the intention to determine the materials, gradings, thicknesses etc which are appropriate to various design conditions. Finally, it is hoped to make suggestions for appropriate tests and checks to ensure that the as-laid product is satisfactory.

10.1 RESULTS FROM GRANMAT

Since there are infinite combinations of layer thickness and stiffness possible in a pavement structure, not to mention all the other variables of load, initial stress conditions and moisture, it was decided to use GRANMAT to analyse five standard structures, representing various types of pavement, and then to explore the effects of varying each parameter in turn for those five structures. The structures chosen are detailed in Table 10.1.

Table 10.1 Standard Pavements Analysed

	Asphalt Thickness	Base Thickness
Pavement 1	0	300mm
" 2	0	800mm
" 3	50mm	400mm
" 4	100mm	200mm
" 5	200mm	200mm

Asphalt Stiffness	5 GPa
Base Stiffness Equations (ref eqs 4.6 and 4.11)	$\varepsilon_s = 80\ \delta\ln(\sigma_1'/\sigma_3').(\delta t + \frac{1}{3}\delta s')^{0.4}$ microstrain
	$\varepsilon_v = 75\ (\delta \ln p')^{0.8}.(\delta p')^{0.4} - 150\ (\delta(\ln(\sigma_1'/\sigma_3'))^2)^{1.2}$ microstrain
Base Failure Condition	$\sigma_1' = 30 + 9.\sigma_3'$ kPa
Base Plastic Parameters (ref eqs 4.19 and 4.22)	$L = 80.5$
	$M_1 = 8$ MPa
	$M_2 = 1200$ MPa
Base Suction	10 kPa
Base Permeability	0.0001 m/sec
Subgrade Stiffness Equation	$E = \frac{q_r}{0.3}\ (\frac{p'}{q_r})^{1.5}$
Depth to Bedrock	5m
Applied Pressure	600 kPa
Radius of Loaded Area	125mm

The effects of variation of the eight most important parameters are shown in figs 10.1 to 10.8. In the cases of stiffness and strength of the granular base (figs 10.4 and 10.5) more than one of the constants describing granular material behaviour has been varied although only one is plotted on the horizontal axes. Since it is clearly not possible to present the full output of stresses and displacements for each run, four key quantities have been selected and are plotted in each figure. They are the surface deflection under the centre of the wheel load; the maximum tensile strain at the base of the surfacing layer, critical for crack control; the maximum vertical subgrade strain, often critical for rut control; and the number of load applications till failure occurs within the granular base. Of these, the last should not be looked upon with great confidence, but should serve as a useful indicator of the relative performances of different structures. The following points summarize the main findings from figs 10.1 to 10.8, some of which are already well established facts:

(i) Contact pressure from a wheel (fig 10.1) has a greater than linear effect on subgrade strain, although it is less dramatic in its effect on asphalt tensile strain. Excessive contact pressure leads to early failure in the granular material.

(ii) Asphalt stiffness (fig 10.2) appears relatively unimportant, having very little effect on either asphalt tensile strain or subgrade strain for the pavements

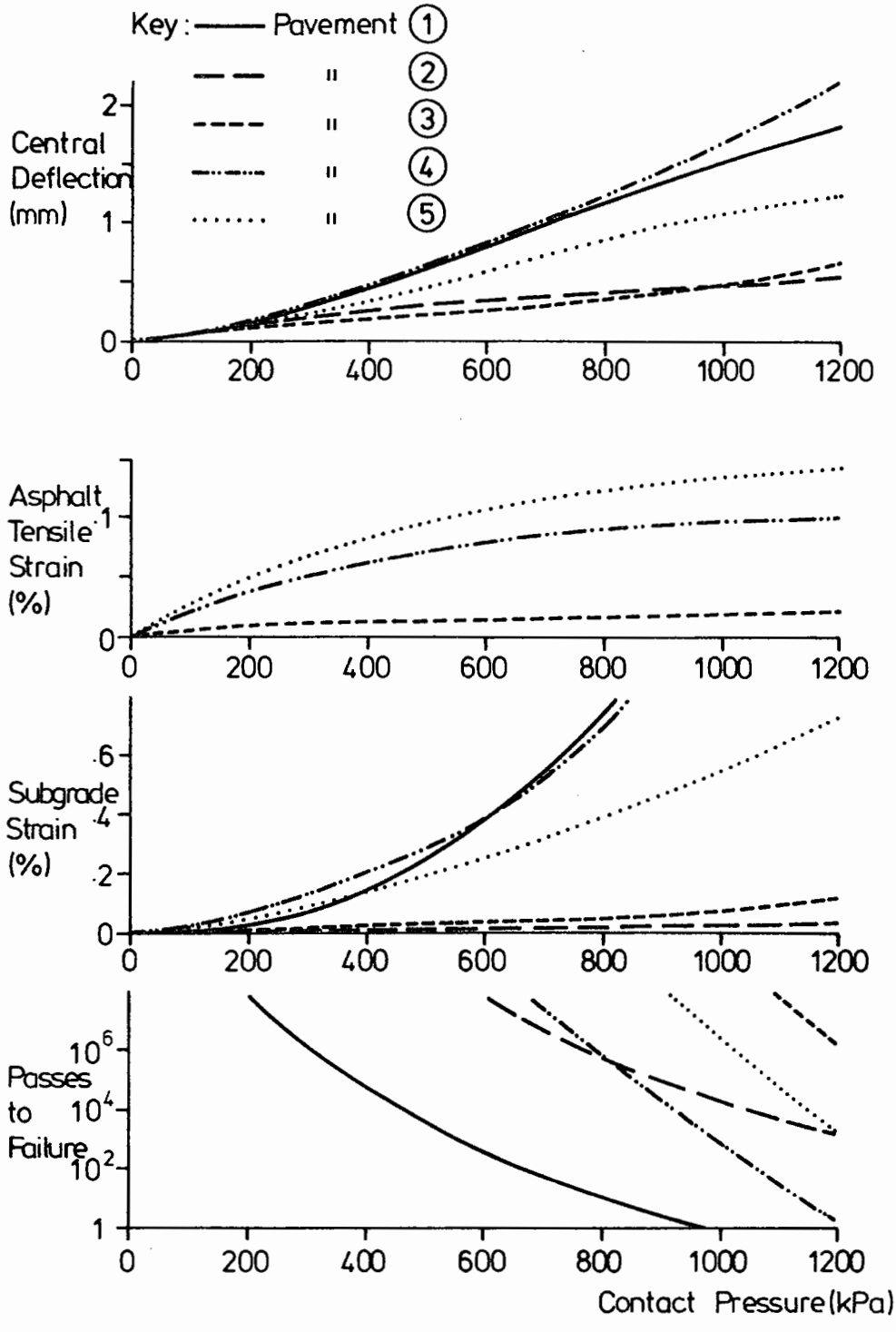

Fig. 10.1 GRANMAT Results - Contact Pressure Variation

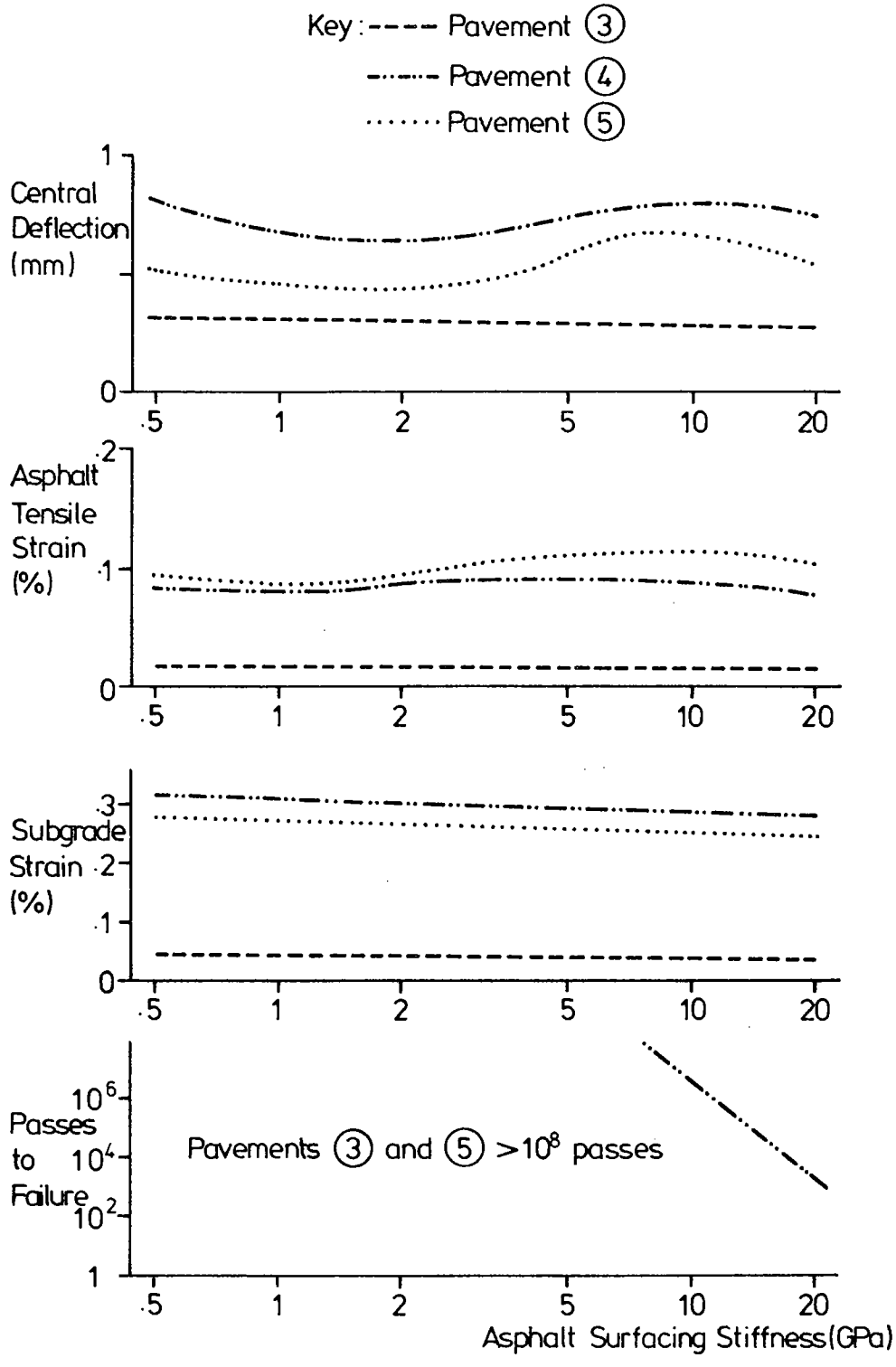

Fig.10.2 GRANMAT Results - Asphalt Stiffness Variation

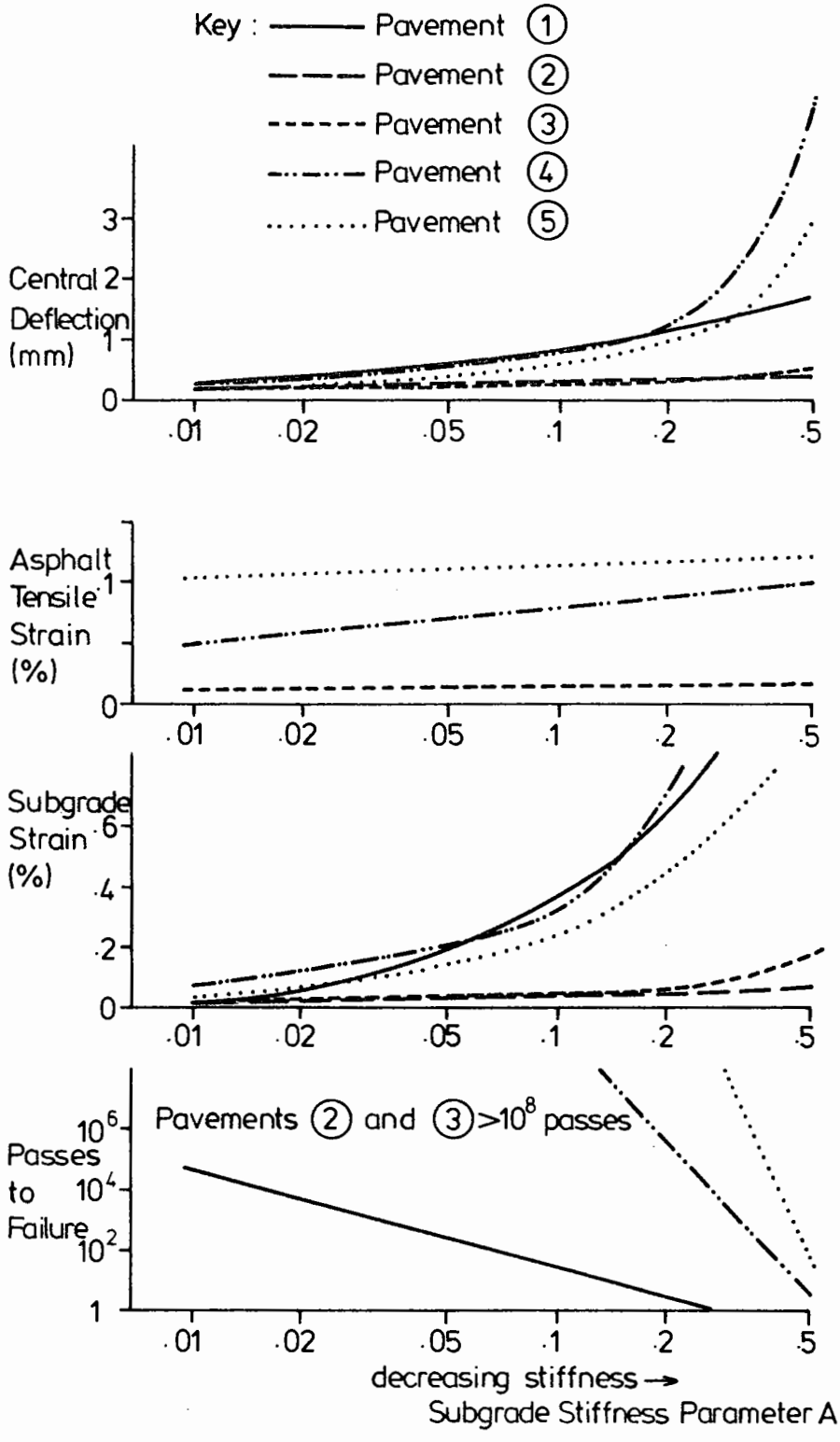

Fig. 10.3 GRANMAT Results - Subgrade Stiffness Variation

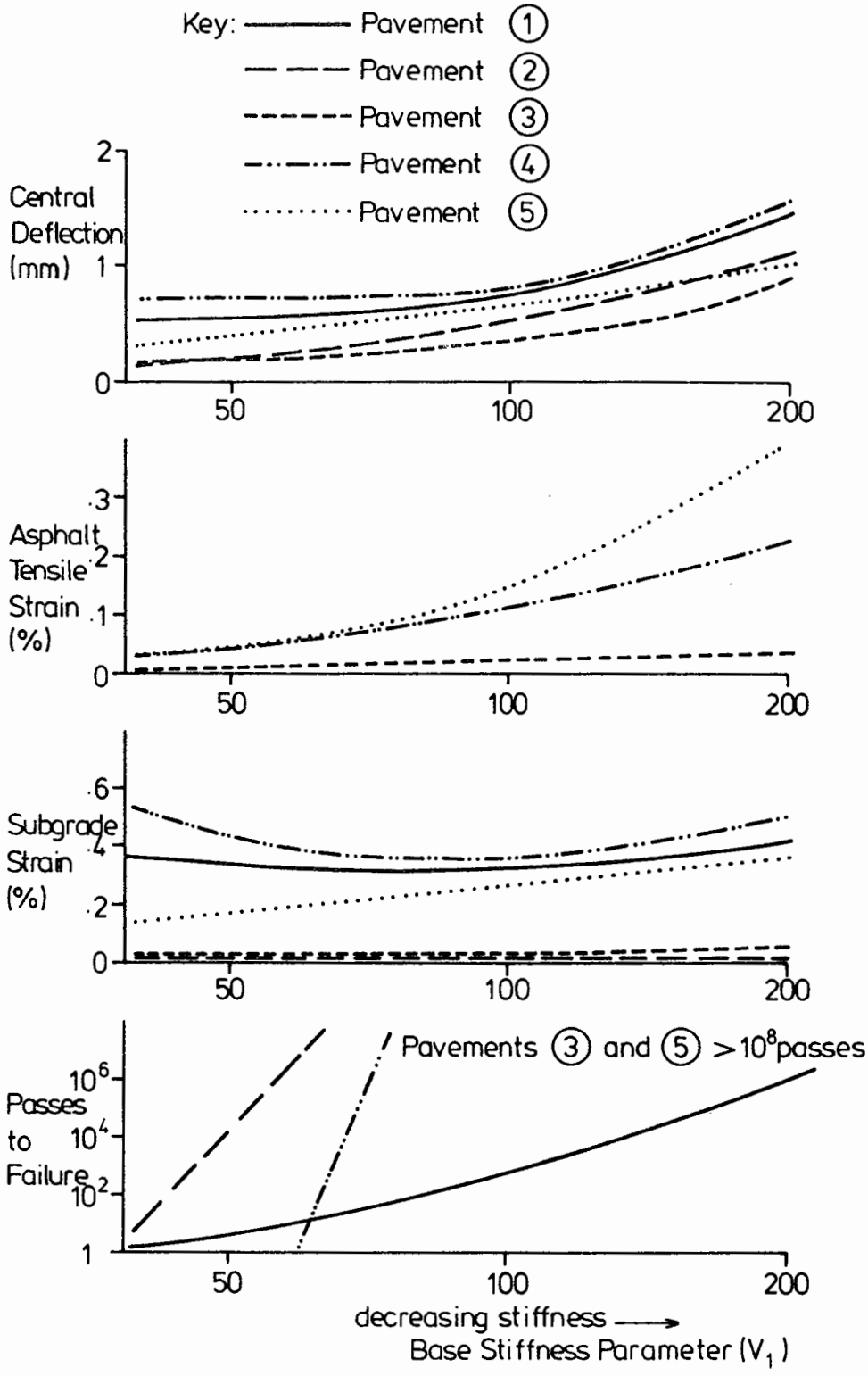

Fig. 10.4 GRANMAT Results - Base Stiffness Variation

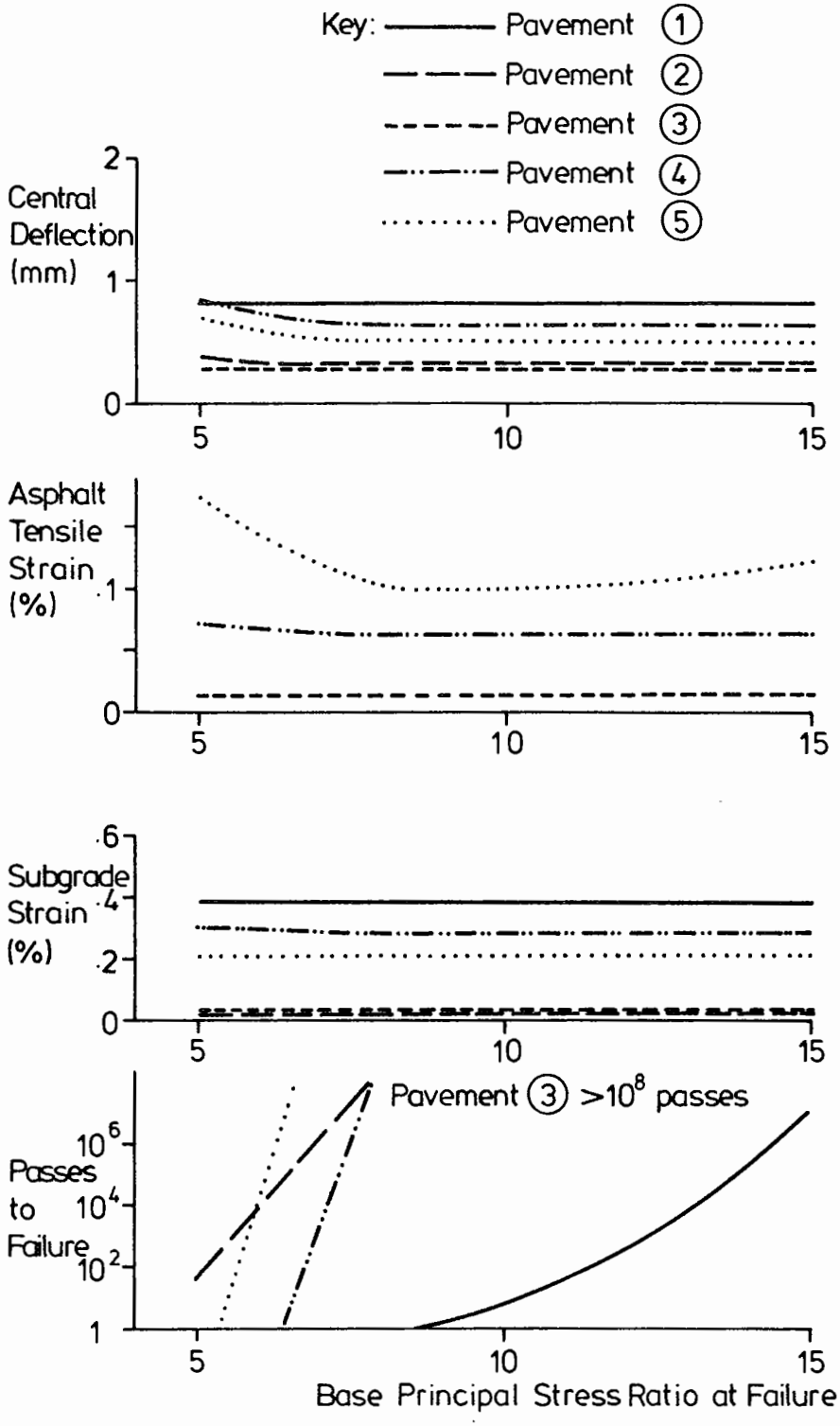

Fig.10.5 GRANMAT Results - Base Strength Variation

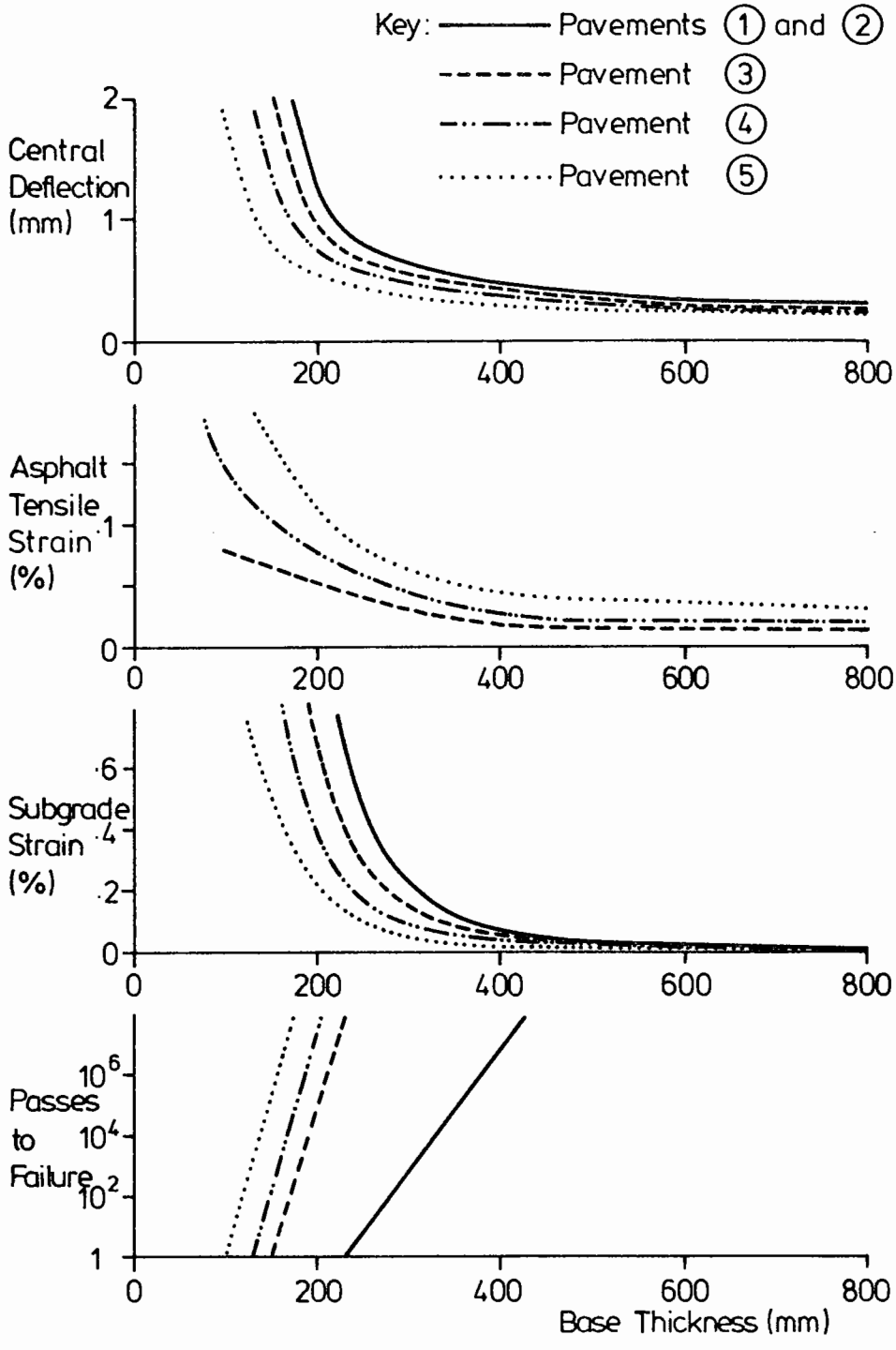

Fig. 10·6 GRANMAT Results - Base Thickness Variation

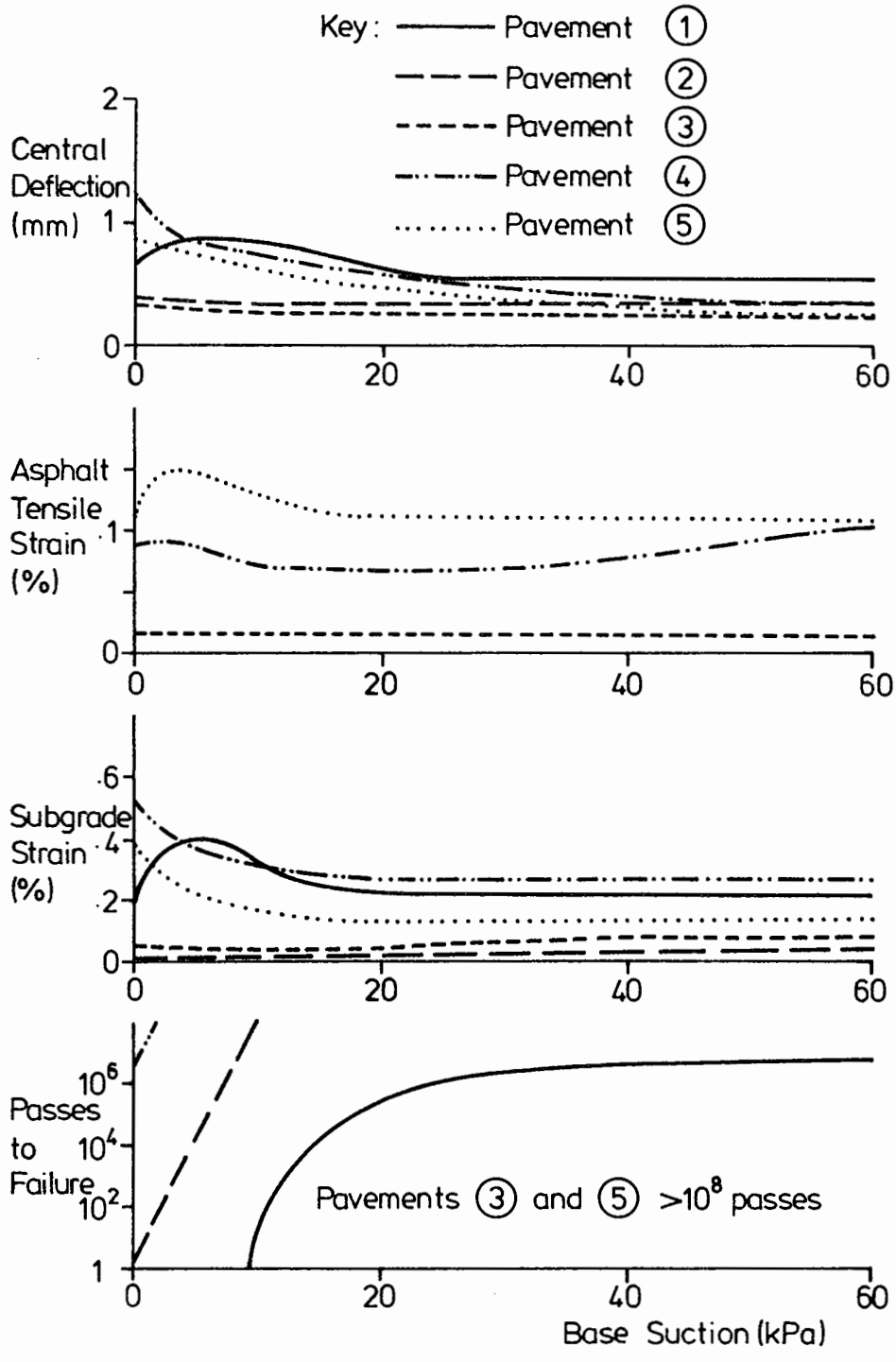

Fig. 10.7 GRANMAT Results - Base Suction Variation

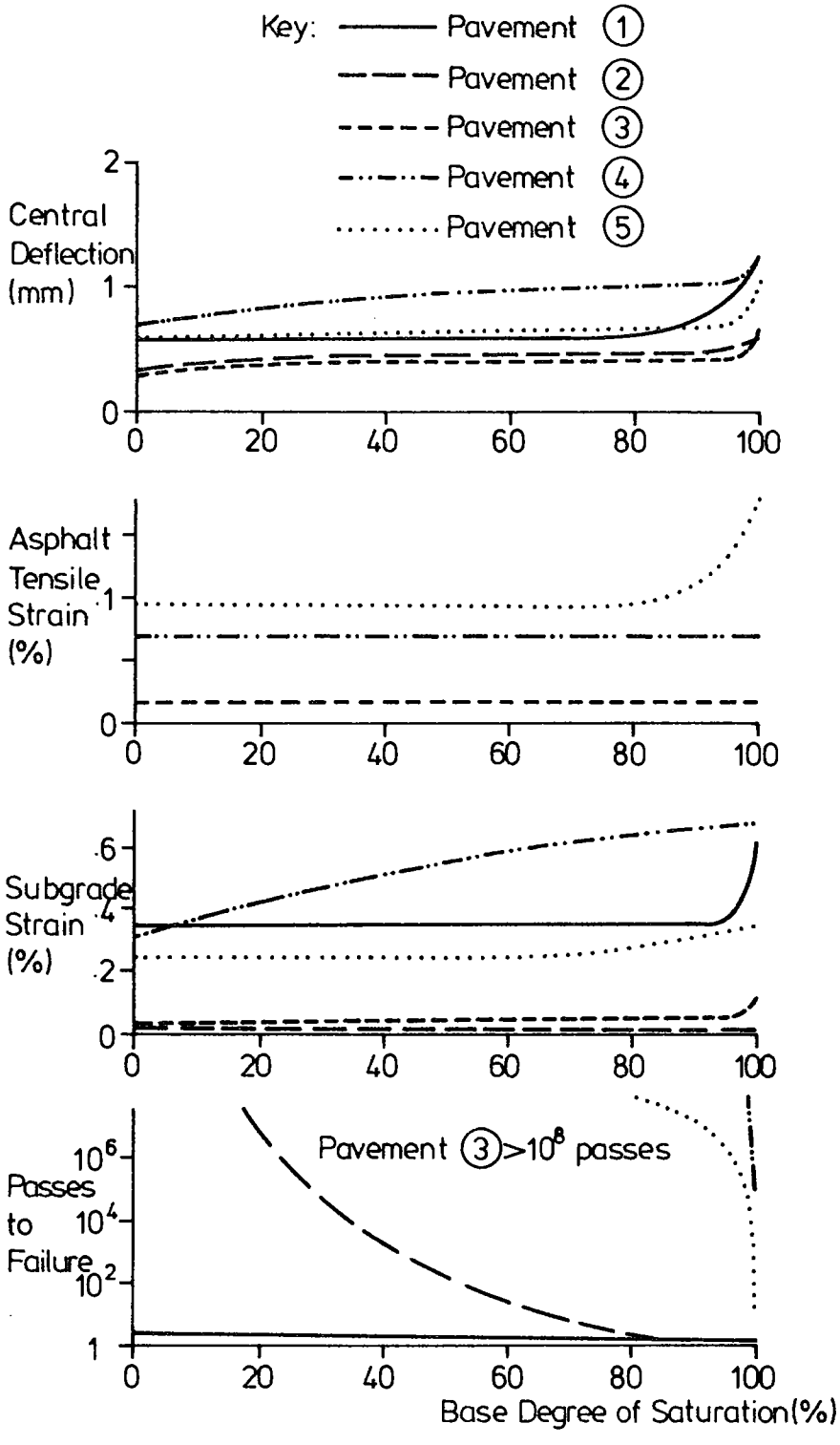

Fig. 10.8 GRANMAT Results - Degree of Saturation Variation

investigated. It does however reduce the tendency of the granular material to fail early in pavement 4.

(iii) Subgrade stiffness (fig 10.3) has a not surprising effect on subgrade strain, but has very little influence on asphalt tensile strain for the three surfaced pavements. Since a stiff subgrade imposes less shear stress on the overlying material, it consequently reduces the likelihood of granular layer failure.

(iv) Base stiffness (fig 10.4) has a relatively slight effect on subgrade strain, even for the weakest structure. In fact the biggest influence was found for the most thickly surfaced pavement. It does, however, have a very significant influence on asphalt tensile strain and on susceptibility of the base to failure.

(v) Base strength (fig 10.5) has no significant influence on either asphalt tensile strain or subgrade strain. However, it is extremely important in preventing granular material failure.

(vi) Base thickness (fig 10.6) is seen to be crucial, particularly in limiting subgrade strain, but also in reducing asphalt tensile strain and in preventing base failure.

(vii) A high level of suction (fig 10.7) within the granular base is clearly useful in reducing subgrade strain, but it is much more important in preventing failure of the base itself.

(viii) The results for variation in the degree of saturation (fig 10.8) are presented but, as explained in chapter 7, are not wholly trusted. They do, however, indicate that, as full saturation approaches, the subgrade and asphalt tensile strains tend to increase and failure within the base becomes more likely.

10.2 APPLICATION TO DIFFERENT DESIGN CONDITIONS

This section will make use of the results from GRANMAT quoted above to examine the design requirements associated with four widely differing situations, ranging from a short term haul road to a heavily trafficked highway. The means of achieving those requirements will then be examined.

10.2.1 Short Term Haul Road

The type of situation envisaged here is the construction phase of a surfaced road or a short term access requirement, where typically up to 1000 standard axles are expected. Clearly the dangers are rutting failure occurring in the granular material or, alternatively, in the subgrade. Depending on the subgrade quality a certain thickness of granular material is required

(fig 10.6) to limit the subgrade strain and, therefore, the possibility of rutting failure at that level. Base strength and stiffness (figs 10.4 and 10.5) are unimportant in their effect on subgrade strain, but strength can be seen as particularly important in preventing failure in the granular material. Clearly the expected load (fig 10.1) will also greatly affect design.

In conclusion, the granular material property of most importance here is shear strength. Neither thickness nor stiffness, nor subgrade quality, can assist significantly in preventing failure within the granular material, although a certain thickness is required to prevent subgrade rutting.

10.2.2 Long Term Unsurfaced Road (or Surface Dressed)

Such a road would not be common in the UK, but would be normal in many parts of the world. Many of the same considerations apply as in the previous case, including the fact that base stiffness is relatively unimportant. Base strength is still vital in preventing early failure and, according to fig 10.3, a stiff subgrade is of assistance in this area. Depending on subgrade stiffness, a certain thickness of granular base is necessary (fig 10.6), greater than in the first example because of the larger number of axles to be catered for, in order to limit the subgrade strain.

However, because this is a long-term situation, the effects of moisture should be carefully considered. In many climates it may be possible to use a granular material rich in fines and to assume a very high base suction for the greater part of the year and, as fig 10.7 shows, this is very effective in preventing failure within the base and also reducing subgrade strains. It may thus be possible to use a material of lower intrinsic strength and rely on suction. However, in locations of higher rainfall, a high fines content inhibits drainage, leading to the possibility of saturation and the consequences evident in fig 10.8. Therefore a freer draining material should be used.

10.2.3 Thinly Surfaced Road

Probably the large majority of roads in the developed world fall into this category, with up to 100mm of bituminous surfacing. Generally all the considerations necessary for the second case are also valid here. Base strength is still vital in preventing rut development at that level, since the granular material is still the main structural layer; the surfacing will deform relatively easily. A reduced base thickness is possible (fig 10.6) but not by much. However, asphalt cracking is now a possible problem. Fig 10.2 indicates that asphalt stiffness is not very important, but the parameter which has by far the greatest influence on asphalt tensile strain is seen as base stiffness; subgrade stiffness has little influence here.

As for the previous example the same moisture considerations are important.

10.2.4 Heavily Trafficked Road

The examples from which figs 10.1 to 10.8 were drawn do not really extend to this situation, where bituminous or concrete surfacing in excess of 200mm might be expected, but some comments are possible. Sub-base thickness is clearly not so important, although a certain small thickness will usually be required to limit subgrade strain. Failure within the granular material is not a real possibility, implying that strength is not important. However, on the basis of fig 10.4 granular material stiffness is still likely to be critical in limiting asphalt tensile strain.

In consideration of moisture, it appears that suction is not likely to be of great benefit, whereas positive pore pressures may lead to excessive strains. A sufficiently permeable grading should therefore be used.

10.2.5 Summary

Unfortunately it has not been possible to quantify the above comments with sufficient confidence in this project. Further development or rewriting of the GRANMAT program, particularly in the permanent deformation area, may lead to sufficiently precise answers upon which to base specific design proposals. Clearly correlation is also required with data involving the use of

subgrade strain and asphalt tensile strain criteria such as the Nottingham design method (Brown et al 1985). The potential strengths of design based on GRANMAT are in the area of possible rutting failure within the granular material for unsurfaced and thinly surfaced roads, and in the isolation of the effects of positive or negative pore pressures within the material. It is hoped that development in the near future will enable a fuller realization of potential.

At present, it is possible to use the asphalt tensile and subgrade strains and to design thickness and stiffness requirements for a granular base but, for the establishment of design charts, many more program runs would be necessary than have been performed to date.

10.3 ACHIEVEMENT OF GRANULAR MATERIAL REQUIREMENTS

The present method of specifying granular material in the UK is in terms of grading, rock or material type, plasticity and a crushing test, the 10% fines test. Other requirements are durability and frost resistance, which are not covered by this project. There is currently no specified way of testing directly to ensure that a material has sufficient strength and stiffness.

The investigation into different gradings (section 5.3) has revealed that the variation of stiffness with grading is very slight for a given maximum particle size, the more uniform

material being slightly stiffer. However, particle size effects have been shown to be significant (section 5.4) such that a 75mm maximum size material may be say, 10% stiffer than a 37.5mm material. Therefore, size should be as large as possible if stiffness is important, within the practical constraints of laying and compacting the layer. However, section 5.5 has revealed very considerable difference between different material types, with all types of limestones generally stiff whereas other materials, particularly granite, are less good. Sands and gravels can also be seen to have low stiffness. A dependence on microtexture has been indicated. In fact, a friction test, isolating microtexture properties, is seen here as being a useful tool in distinguishing between different minerals in relation to stiffness properties.

Material strength has been shown (section 5.3) to be grading dependent to some extent, with the highest strengths being for a grading curve roughly of the DTp type 1 shape or slightly finer. However, so long as the material is nowhere near uniform, the variation is not very great. As with stiffness, particle size has an effect, the larger sized material being stronger. Also the mineral type dependency is considerable, the limestones not being quite so dominant, particularly the softer ones, but with crushed concrete, steel slag and sandstone all in the top group. In this case it appears to be the angularity and macrotexture of the stones which is important, the rougher more angular materials performing better. Good compaction is also crucial.

The following summarizes these points:

(i) High stiffness (useful in limiting asphalt tensile strain) requires as uniform a grading as possible, as large a particle size as possible and good frictional micro-texture.

(ii) High strength (useful in preventing failure within a granular base) requires a broad grading, as large a particle size as possible, good angularity, a rough macrotexture and good compaction.

10.4 SUBGRADE TREATMENT

It has already been shown that a soft subgrade increases the danger of rutting both in the subgrade itself and also in the granular material (fig 10.3). This necessitates a thick granular layer in order to reduce the stresses at subgrade level. The lower part of this granular layer, being under lower stress can be of comparatively low grade material, as is intended in the use of a capping layer in UK road construction. Such use of a capping layer may be seen as a form of subgrade treatment.

However, chapter 8 has brought out the point that the density achievable in a compacted granular layer is greatly influenced by the support conditions. It would not, therefore, be possible to achieve high density in a capping layer overlying very soft material and in the sub-base or base layers the effect of the

soft subgrade would certainly still inhibit compaction. It may therefore be a viable alternative to stabilize the subgrade with either lime or cement, thus creating a much firmer platform upon which to compact the granular material. The higher densities achieved would reduce the likelihood of permanent deformation within the base and, of course, a stiff layer at the top of the subgrade would reduce subgrade strains and resist permanent deformation at that level. The total thickness of granular material required would therefore be much less.

10.5 TREATMENT OF MOISTURE

The importance of drainage has been one of the most frequently stressed axioms in road design. Yet it is still not always taken seriously. The damaging effect of positive pore pressure build-up in a granular material has been demonstrated in fig 10.8 and experienced in practice far too frequently. However, there are a few practical design steps which can virtually eliminate the possibility of it ever happening.

(i) Design a granular material to have a relatively free draining particle size distribution. Many techniques for computing permeability given a grading curve have been proposed (eg Juang and Holtz 1986); however, according to Biczysko (1985), a material with grading at the coarse end of the DTp type 1 envelope should be of very adequate permeability.

(ii) Ensure sufficient drainage outlet for water in the granular material to side drains. Too often roads have been constructed as if in a trench with nearly impermeable sides.

(iii) If a relatively coarse material is to be used, a geotextile is recommended at top of subgrade level if the soil is fine grained, to act as a separator and avoid contamination of the aggregate.

(iv) Seal the road surface as well as possible, and design sufficient crossfall to allow water to run off quickly. This is particularly important for roads with no bituminous surfacing.

Although the above points are valid for climates where significant rainfall is expected, there may be situations where excess water is never a problem, in which case broader grading may be desirable so that suction is generated and a stronger pavement results.

10.6 SPECIFICATION

It is not the function of this section to write an all purpose specification for a granular road layer, but rather to consider the various ways in which it might be desirable to write it in different situations. It is, of course, necessary to consider

the practical feasibility and cost implications of any test or restriction which one may wish to introduce, as well as its purely technical merit. Section 10.2 has already indicated that properties which are completely unimportant in one case become very important in another and it is thus inappropriate to write one specification for all cases since many perfectly valid alternatives are then excluded. This point is currently being made by many organisations in the UK who see their product as being suitable for inclusion into a road structure where the current DTp specification excludes it. The recent Transport and Road Research Laboratory report RR 64 (Earland and Pike 1986) has made the point that many sands and gravels behave as well as crushed rock under certain circumstances, yet are presently excluded. Again, economic arguments are often foremost in that an area may not have any local sources of acceptable material and alternative sources are therefore sought. Reuse of waste materials is both economically and ecologically desirable but often not allowed in a specification.

The approach taken here is, therefore, to attempt to isolate the parameters which really are important in a particular case and to see whether a specification may be written in those terms. To consider the grading first, it has been stated that there is a broad range of gradings from the coarse half of the DTp type 1 envelope and coarser for which the mechanical properties of an aggregate are relatively unchanged. If the uniformity coefficient falls below about 10 then the shear strength begins to fall, but it should be remembered that this is not always

important, particularly if there is to be a very thick bound layer above and the material is of sufficient quality to stand up to construction traffic anyway. Conversely, if the uniformity coefficient exceeds about 80 then the stiffness begins to decrease, but this is only important for surfaced roads. Perhaps a more important restriction is that imposed by permeability where, to ensure sufficient permeability, a grading coarser than the mid-line of the type 1 envelope (uniformity coefficient = 50) should be chosen and an upper limit on material passing 75 microns of, say, 6% is desirable. Of course, in climates where water is not a problem this can be relaxed and a high fines content even stipulated to ensure high suction, but the band where uniformity coefficient lies between 10 and 50 is seen as generally suitable. However, it is important that the shape of the particle size distribution curve is of a form such that the material is not too gap graded; ie the bulk of the particles should be large to give optimum mechanical properties. The actual limits on maximum particle size are dictated to some extent by the necessity of compacting the material in layers but, if compaction can be adequately performed, particles up to 100mm should be acceptable. The lower limit depends on how vital strength and stiffness are seen in the particular pavement. For instance, if the actual rock type to be used is of high quality then a smaller maximum particle size may be allowed, whereas if it is a marginal rock large particles may be essential. To illustrate the above suggestions fig 10.9 is included to show possible grading limits. The existing DTp type 1 limits are also

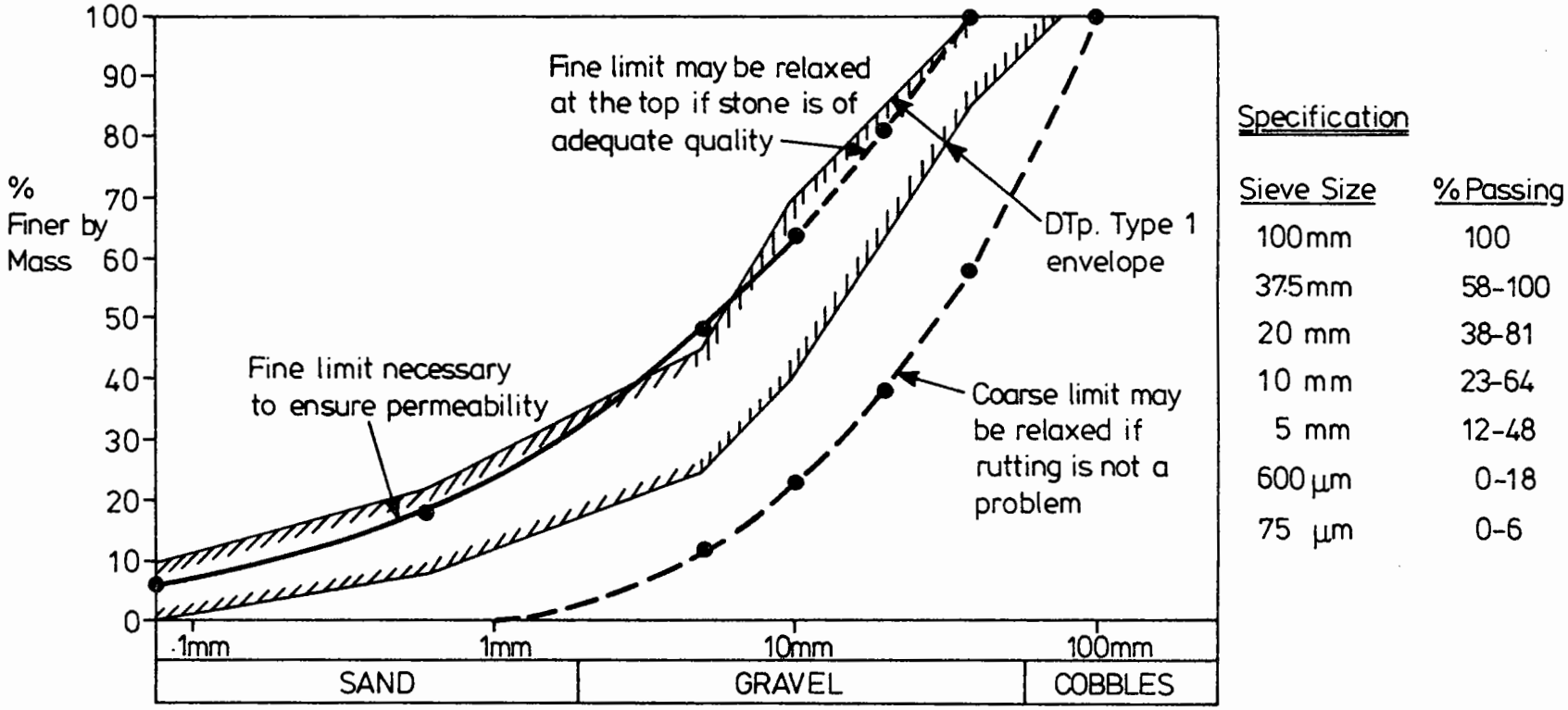

Specification

Sieve Size	% Passing
100 mm	100
37·5 mm	58–100
20 mm	38–81
10 mm	23–64
5 mm	12–48
600 μm	0–18
75 μm	0–6

Fig. 10·9 Suggested Grading Specification

shown and it may be seen that the suggested specification is rather wider but may necessitate the discarding of fines from the naturally outputted material of a mechanical crushing plant. One further point is to repeat the recommendation that, for those relatively coarse materials, a geotextile is specified as a separator between subgrade and granular base whenever soft fine grained soil is encountered. If no geotextile is available a thin layer of sand is likely to be suitable. McCulloch (1981) has investigated the problem of contamination from the subgrade soil and it is clear that it should be avoided.

The next subject which may require specification is the mechanical properties to be expected from a particular rock or other mineral. The limits of any test done must here be left flexible because they will depend on how strong or stiff a material needs to be in a particular case. Two approaches are seen as possible. The first is an actual stress strain test on the aggregate such as might be done in a simplified triaxial device or a shear box. Whichever were chosen, the test should include repeated loading at different stress levels to investigate stiffness and a failure test to obtain a shear strength. If such a simple and relatively cheap, yet sufficiently accurate, device could be made as a standard it would be ideal in that, if a material met the specified strength and stiffness criteria, then grading limits could be relaxed so long as permeability was ensured.

The second approach, if no direct mechanical test were available, would be to test individual particles for the shape and texture properties relevant to elastic stiffness and shear strength. A friction test would determine the quality of microtexture, affecting stiffness, possibly a simple sliding test as performed on the materials covered by section 5.5, or even a pendulum test. The latter test is already used to determine the skid resistance exhibited by different road surface materials, but may be equally applicable to determining the elastic stiffness of an aggregate.

To establish the shear strength and associated resistance to plastic straining, the only method seen possible, apart from direct mechanical testing, is to determine the angularity and visible surface roughness of the larger particles in an aggregate. Such a test would necessarily be susceptible to operator dependency, which is slightly unfortunate, but would allow rapid prediction of the likely ability of an aggregate to withstand rutting failure.

Although it is seen as important that a specification should be aimed at the properties of strength and stiffness which directly affect the performance of a road, it should always be remembered that in particular cases one of these two may be relatively unimportant, allowing a relaxation in the specification.

Of the other material properties commonly specified, a limit on plasticity is clearly useful in ensuring a free draining material but is probably not important if the proportion of fine material

is very small anyway (say < 3% passing 75 microns). The frost heave test certainly represents an attempt to prevent a real problem, although questions as to the suitability of the present test remain, but it may be that the use of a rather more uniform grading than is currently usual would reduce the scale of the problem. Use of a soundness test, currently under discussion, presents two problems: the development of a meaningful test and the establishment of aggregate soundness as an important property. Until both are achieved the inclusion of such a test in a specification would be unwise. Finally, no evidence has been found in this project to support the use of an aggregate crushing test although, in cases where crushing could substantially reduce permeability, it may be necessary.

Having chosen an appropriate aggregate, it is then necessary to ensure that it is laid correctly. Current practice is usually to specify a test whereby an optimum moisture content for compaction is found. The material is then laid within certain limits. Since the grading recommended in this section is relatively coarse, the influence of moisture content on achieved density is likely to be reduced. However, assuming that granular material strength is required, not necessarily the case if thick bound layers are involved, then the practice of obtaining an optimum moisture content and using it is seen as sensible. The test involved should include a realistically high level of compaction and should certainly not require the exclusion of any but the largest particles, and the modified vibrating hammer compaction

test (BS 5385) has been found to perform very well. It is recommended that the moisture range specified should be mainly to the low side of optimum, perhaps exceeding it by half a percent only, since the dangers of excess water are real.

The next problem is to ensure that sufficient compactive effort is used to obtain high densities. A method specification stipulating a certain number of passes and layer thickness depending on roller type and weight, such as is presently employed by the DTp in the UK, could be worked but is very rigid, takes no account of subgrade support conditions, and is very hard to supervise. The instrument described in section 9.2.5, the BOMAG Terrameter, is clearly a possible future alternative, since it appears to give a good indication of whether further compaction would be useful. It is in use at present with certain contractors who wish to optimise their use of plant, but it is possible to foresee a time when it might provide an on-site checking tool as well. The actual output value which would be used as a control bound would almost certainly vary depending on subgrade quality and the type of granular material used and would need to be established by a trial at an early stage. Of the other instruments examined in chapter 9 in detail, the dynamic cone penetrometer was the only one which correlated with density variation alone. However, as explained, the test is not quick, it requires two operatives and it tests only one specific point at a time. It may, however, be useful as a tool by which disputes over compaction are settled, although it has the further drawback that, if a geotextile is being used, then care has to be

taken not to puncture it. The direct measurement of density is seen as a last resort since the variability of tests using the sand replacement method is well known and the problems of calibrating a nuclear density meter for a particular aggregate are also sometimes great.

Since elastic stiffness has been shown not to depend to any great extent on compaction, the in-situ measuring devices which respond to stiffness variation, that is the sophisticated falling weight deflectometer and the simple Clegg impact hammer, are not seen as useful in checking a granular layer. The stiffness should have already been ensured by material choice. If, however, any particular problem arises, either with regard to granular layer or subgrade stiffness, then the falling weight deflectometer is an ideal tool. As explained in chapter 9, the Clegg impact hammer can also be useful in this regard. The plate bearing test is seen as unduly cumbersome, although at present it has the advantage that it is possible to check for low density and also to observe areas of soft subgrade. However, its early replacement, at the very least by a well designed dynamic cone penetrometer, is recommended and the possibility of using a Terrameter or similar device is seen as a very desirable option.

On large sites, where economics allow, a proof roller has some of the qualities of the Terrameter since it covers the whole area, not only specific points, and enables easy observation of undercompacted areas. However, it is not so sensitive to

variations in support condition and is seen as second best.

Unfortunately, although some of the recommendations contained in this section could be applied immediately, particularly those relating to grading, there are many areas where a test requires development and a certain amount of further work is necessary. These areas will be highlighted in chapter 11 where the future is discussed.

CHAPTER ELEVEN

CONCLUSIONS AND RECOMMENDATIONS FOR FUTURE WORK

For convenience, this chapter has been divided into five sections relating to different aspects of the work described in this thesis. In each section the principal results and conclusions are listed, followed by discussion of possible future work. It is inevitable, in view of the wide ranging nature of the project, that there are a number of specific areas where further investigation or development is desirable and this has necessitated the use of further sub-sections in some cases.

11.1 LABORATORY FACILITIES

(i) The Nottingham Hollow Cylinder Apparatus has been commissioned, developed and effectively used.

(ii) A Miniature Pavement Tester (c. one tenth scale) has been designed, constructed and commissioned.

11.1.1 Hollow Cylinder Apparatus

The present Nottingham apparatus is restricted in that the level of confining stress which can be applied is limited to less than one atmosphere, ie the capacity of a vacuum pump. Control of

confining stress is also manual and very slow, making cycling almost impossible. A useful development, therefore, would be to construct a cell wall around the specimen which would allow a relatively incompressible fluid to be used as the confining medium, both internal and external to the specimen wall. Connections to both internal and external voids would allow independent stressing; the stress levels attainable would be satisfactorily high and rapid alteration of stress would be possible. Furthermore, if pressure were to be applied through a servo-hydraulically controlled piston, then rapid and controlled stress cycling could be achieved.

The other area which could usefully be improved is control and data acquisition. The present analogue system should be replaced by a computer. This would allow a complex elastic testing programme to be performed in a matter of hours rather than the several days presently necessary. If the pressure application arrangements suggested above were also made, the computer would enable extremely complicated stress paths to be applied fairly easily and allow more rigorous testing and possible improvement of both elastic and plastic strain prediction techniques.

11.1.2 Miniature Pavement Tester

Although commissioned, the miniature pavement tester has not yet been put to serious use. It is considered likely, however, that it may prove a useful tool for the rapid checking of design concepts. The possibility of including a scaled down asphaltic

surfacing should be considered, together with possible ways of displacement monitoring beneath the surface of the pavement. Variations in base thickness and grading, subgrade stiffness etc could be rapidly explored and the results used in conjunction with theoretical predictions. The four track facility enables the damage factor associated with different loading stresses to be investigated also.

11.1.3 A Simple Laboratory Test Device

It appears possible that there may be a need for a simple and relatively cheap device for the rapid mechanical testing of granular materials. It would certainly be feasible to design a cheap repeated load triaxial device using air as the confining medium and an air pressure ram to apply axial deviator stress. However, one of the drawbacks is that no easy way of measuring radial strain is seen and such measurement would be vital. An alternative is the confined compression test, currently used in New Zealand (Bowling 1980). Here the material is compacted into a thin walled metal cylindrical mould and stress applied to the top surface. Repeated loading using an air pressure ram is once again possible and measurement of vertical displacement is straightforward. However, it is also possible to strain gauge the mould walls, allowing knowledge of the radial strain in the material and also the radial stress, assuming the dimensions and properties of the metal mould are known. Clearly, the disadvantage is that there is no independent control of radial stress, but the simplicity of the concept and the approximation

to conditions in a road are seen as considerable advantages and worthy of detailed study.

11.2 MATERIAL INVESTIGATION

(i) A new elastic stress strain model for dry granular material behaviour has been proposed, checked and found satisfactory for the range of stress paths which can currently be applied using triaxial and hollow cylinder testing facilities.

(ii) A new plastic stress strain model for dry granular material behaviour has been proposed. It has been much less rigorously checked than the elastic model but appears fairly satisfactory.

(iii) A short triaxial test routine has been developed enabling the parameters governing elastic and plastic behaviour to be found.

(iv) It has been shown that the elastic stiffness of a dry granular material is almost independent of the state of compaction.

(v) It has been shown that susceptibility to plastic strain in a dry granular material is greatly dependent on the state of compaction.

(vi) It has been shown that a uniform material has greater elastic stiffness than a broadly graded material.

(vii) It has been shown that a broadly graded material has greater shear strength than a uniform material.

(viii) It has been shown that a material containing large particles has greater elastic stiffness and shear strength, than one with smaller particles.

(ix) A number of different materials have been tested and ranked for both elastic and plastic properties.

(x) It has been shown that elastic stiffness of a dry granular material is largely dependent on the microtexture at particle contacts which determines inter-particle friction.

(xi) It has been shown that shear strength and resistance to plastic strain are largely dependent on macrotexture, that is visible roughness, and angularity.

(xii) The effective stress principle has been shown to be applicable for partially saturated granular materials.

(xiii) Negative pore pressures due to suction have been deduced in aggregates used in road construction.

11.2.1 Other Materials

Although a range of materials has been tested in this project there remains a very large number of possible aggregates to investigate. They include a variety of igneous rocks, other limestone sources together with softer sandstones, many more natural sands and gravels, and such materials as colliery waste, furnace ash, crushed brick etc. Since a standard test routine has been devised from which all the relevant behavioural parameters may be deduced, such an investigation would not necessarily be very time consuming.

11.2.2 Correlation with Stone Properties

It has been stated that the micro- and macrotexture of individual stones indicates the likely elastic and plastic properties of the aggregate as a whole. This, it is thought, is worthy of further research since it may enable a very quick assessment of a particular mineral in situations where sophisticated testing is not possible. In particular, the pendulum test, presently used for skid resistance assessment, may be of use to quantify microtexture. Alternatively, it may be feasible to design a smaller, portable friction tester, possibly based on discovering a slope at which sliding can take place. The other assessment technique necessary is for macrotexture and this demands an investigation into the various methods by which angularity and roughness can be quantified.

11.2.3 Permeability

A very important area of research, which this thesis has only touched on, is the prediction of aggregate permeability from a knowledge of the particle size distribution and, possibly, the shape of stone involved. At present there is no completely trustworthy system but a project is currently in progress at Nottingham which may yield useful answers. The necessity for such a predictive tool is evident from the number of highway problems which can be traced to a saturated low permeability granular layer.

11.3 COMPUTER ANALYSIS

A new pavement analysis computer program, GRANMAT, using an iterative discreet point approach has been written for use on a microcomputer. It uses the elastic and plastic stress strain equations developed during this project for characterising granular material and is particularly applicable to unpaved or thinly paved roads.

The problems associated with GRANMAT have been fully revealed in chapter 7, where it is seen that there are difficulties with convergence and some inherent inaccuracy. It is also restricted to a three layer situation. The following points suggest ways in which it may be possible to improve it.

(a) Increase the flexibility to enable multiple layers of granular material to be analysed.

(b) Extend the grid of discreet points to cover the surfacing layer, enabling a correct three dimensional linear elastic analysis to be performed rather than considering it as a plate in bending.

(c) When considering the horizontal or vertical differential of a variable, a parabolic curve fit should be used rather than the straight line assumption presently made.

(d) It may be possible to improve the iterative procedure and achieve a better convergence.

A study should be made of the differences between the strains predicted by GRANMAT and a linear elastic program such as BISTRO. In this way, the circumstances under which linear elastic assumptions are satisfactory could be determined. It would also be possible to develop a way of selecting a linear elastic stiffness for a granular material appropriate to a particular road structure.

For rapid analysis an extensive parametric study using GRANMAT may allow the development of equations using a multiple regression technique for maximum subgrade strain and asphalt tensile strain, even for surface deflection profile. Such equations would be useful in back-analysing stiffnesses from a

Falling Weight Deflectometer deflection bowl, as well as in rapid design using a programmable calculator.

11.4 SITE WORK

(i) The density achieved by compaction of a granular material has been shown to be dependent on moisture content and subgrade support stiffness, as well as other factors.

(ii) The Falling Weight Deflectometer has been shown to be effective in testing directly on granular material. From it individual layer stiffnesses can be back-calculated.

(iii) The Clegg Impact Hammer, it is suggested, responds mainly to the elastic stiffness of the top few centimetres of material but gives a large scatter of results.

(iv) The Dynamic Cone Penetrometer, it is suggested, responds to the shear strength of the material it is passing through and, therefore, to density.

(v) The Plate Bearing Test, it is suggested, is mainly a plastic strain test of the granular material, also responsive to density, but is affected by the stiffness of underlying material.

(vi) The BOMAG Terrameter has been used and found to indicate

the point at which further compaction is harmful rather than beneficial.

11.4.1 Further Data

Some of the above points are made with caution because of the comparatively small amount of data that has so far been collected. In particular the dependencies suggested for the Clegg hammer and dynamic cone penetrometer require a great deal more data from a variety of sites before they can be stated with confidence. Particular attention, it is felt, is due to effects of particle size beyond its influence on strength and stiffness. Experience with the BOMAG Terrameter should also be sought and the results of previous research by BOMAG studied and collated.

11.4.2 Apparatus Development

It has been stated that the dynamic cone penetrometer presently in use at Nottingham is an awkward and unreliable device, subject to frequent breakage. A version should therefore be designed and tested using no threaded connections, a frame to prevent toppling and a mechanical lifting device, probably a continuously rotating chain with a catch mechanism.

One of the major problems with the Clegg hammer, leading to severe scatter of results, is the small size of the plunger in relation to individual stones. The feasibility of a larger contact area, say 100mm diameter, should therefore be explored.

In this connection the Dynoplaque, recently developed at the Ponts et Chaussées Laboratories in France should be considered.

The possibility of using a simplified version of the Terrameter, perhaps a single accelerometer with associated electronics should be investigated for use on small vibrating rollers.

11.5 DESIGN

The results of several GRANMAT runs have been considered in conjunction with all the points associated with materials and site work above and design recommendations made. In particular, choice of material and grading has been examined for different pavement structures.

REFERENCES

ALARÇON, A., CHAMEAU, J.L. and LEONARDS, G.A. (1986), "A new apparatus for investigating the stress strain characteristics of sands", Geotechnical Testing Journal, GTJODJ, Vol 9, No 4, pp 204-212.

ARTHUR, J.R.F., CHUA, K.S. and DUNSTAN, T. (1977), "Induced anisotropy in a sand", Geotechnique 27, no 1, pp 13-30.

BARKSDALE, R.D. (1972), "Repeated load test evaluation of base course materials", Georgia Highway Department Research Project 7002, Georgia Institute of Technology, Atlanta, Georgia.

BARKSDALE, R.D., ROBNETT, Q., LAI, J. and ZEEVAERT - WOLFF, A. (1982), "Experimental and theoretical behaviour of geotextile reinforced aggregate soil systems", Proc. 2nd Int. Conf. Geotextiles, Las Vegas, Vol 2, pp 375 - 380.

BICZYSKO, S.J. (1985), "Permeable sub-bases in highway pavement construction", Proc. 2nd Symp. Unbound Aggregates in Roads, Nottingham, pp 81 - 92.

BOWLING, A.J. (1980), "Investigations into the deformability of rockfill", Proc. 3rd Australia - New Zealand Geomechanical Conference.

BOYCE, J.R. (1976), "The behaviour of a granular material under repeated loading" PhD. Thesis, University of Nottingham.

BRETONNIÈRE, S. (1963), "Les deflectometres a boulet pour l'étude des deflections des chaussées sous charges dynamiques", Bulletin de Liaison, no 2.

BRODRICK, B.V. (1977), "The development and performance of a wheel loading facility and in-situ instrumentation for pavement experiments", M.Phil. Thesis, University of Nottingham.

BROWN, S.F. (1974), "Repeated load testing of a granular material", Journal of the Geotechnical Engineering Division, ASCE, Vol 100, No GT7, pp 825 - 841.

BROWN, S.F. and ANSELL, P. (1980), "The influence of repeated shear reversal on the compaction of granular material", Proc. Int. Conf. Compaction, Paris, Vol 1, pp 25-27.

BROWN, S.F. and BRODRICK, B.V. (1977), "Stress and strain measurements in flexible pavements", Proc. Conf. Measurements in Civil Engineering, BSSM, ICE Newcastle.

BROWN, S.F., BRUNTON, J.M. and STOCK, A.F. (1985), "The analytical design of bituminous pavements", Proc. ICE, Part 2, Vol 79, pp 1 - 31.

BROWN, S.F. and PAPPIN, J.W. (1982), "Use of a pavement test facility for the validation of analytical design methods", Proc. 5th Int. Conf. The Structural Design of Asphalt Pavements, Ann Arbor, Michigan, Vol 1, pp 209 - 220.

BROWN, S.F. and PELL, P.S. (1967), "An experimental investigation of the stresses, strains and deflections in a layered pavement structure subjected to dynamic loads", Proc. 2nd Int. Conf. The Structural Design of Asphalt Pavements, Ann Arbor, Michigan, pp 487 - 504.

CLEGG, B. (1976), "An impact testing device for in-situ base course evaluation", Proc. 8th Conf. Australian Road Research Board, Perth, Session 8, pp 1 - 6.

DAWSON, A.R. (1985), "Water movement in road pavements", Proc. 2nd Symp. Unbound Aggregates in Roads, Nottingham.

DAY, J.B.A. (1981), "Proof testing of unbound layers", Proc. 1st Symp. Unbound Aggregates in Roads, Nottingham, pp 15 - 20.

DEPARTMENT OF TRANSPORT, (1986), "Specification for Highway Works", HMSO.

DODDIHAL, S.R. and PANDEY, B.B. (1984), "Stresses in full depth granular pavements", Transport and Road Research Laboratory, TRR 954, pp 94 - 100.

DUNCAN, J.M. and CHANG, C.Y. (1970), "Analysis of soil movement around a deep excavation", Journal of Soil Mechanics and Foundation Division, ASCE, Vol 96, No SM5, pp 1655 - 1681.

EARLAND, M.G. and PIKE, D.C. (1986), "Stability of gravel sub-bases", Transport and Road Research Laboratory, RR 64.

FUJII, H. WATANABE, T. and SAWANDA, T. (1980), "The stresses in-situ while compacting with different types of compaction equipment", Proc. Int. Conf. Compaction, Paris, Vol 1, pp 41 - 46.

GRACE, H. (1981), "The sub-surface drainage of road pavements", Proc. 1st Symp. Unbound Aggregates in Roads, Nottingham, pp 71 - 78.

HAZEN, A. (1892), "Some physical properties of sands and gravels with special reference to their use in filtration", 24th Annual Report, Massachusetts State Board of Health.

HICKS, R.G. (1970), "Factors influencing the resilient properties of granular materials", PhD. Dissertation, University of California, Berkeley.

HICKS, R.G. and MONISMITH, C.L. (1971), "Factors influencing the resilient response of granular materials", Highway Research

Record No. 345, pp 15 - 31.

HIGHT, D.W., GENS, A. and SYMES, M.J. (1983), "The development of a new hollow cylinder apparatus for investigating the effects of principal stress rotation in soils", Geotechnique 33.

JUANG, C.H. and HOLTZ, R.D. (1986), "A probabalistic permeability model and the pore size density function", Int. Journal Numerical and Analytical Methods in Geotechnics, Vol 10, pp 543-553.

KENNEDY, C.K. (1981), "The influence of compaction and grading on the structural behaviour of granular material", Proc. 1st Symp. Unbound Aggregates in Roads, Nottingham, pp 9-14.

KIRSCHNER, R. (1986)a, "Compaction test on rock fill using the Terrameter BTM", BOMAG Job Report, No. 8607/JR - 001/TP.

KIRSCHNER, R. (1986)b, "Dynamic compaction control in earthworks", BOMAG Product Information, No 8607/PI - 0016/TP.

KLEJN, E.G. and SAVAGE, P.F. (1982), "The application of the pavement DCP to determine the bearing properties and performance of road pavements", Proc. Int. Symp. Bearing Capacity of Roads and Airfields, Trondheim, Norway, Vol 1, pp 238 - 246.

LEFLAIVE, E. and SCHAEFFNER, M. (1980), "The importance of layer thickness in compaction of embankments", Proc. Int. Conf. Compaction, Paris, Vol 1, pp 267 - 270.

LENTZ, R.W. (1979), "Permanent deformation of cohesionless subgrade material under cyclic loading", PhD. Dissertation, Michigan State University, East Lansing.

LOACH, S.C. (1987), "Repeated loading of fine grained soils for pavement design", PhD. Thesis, University of Nottingham.

LUONG, M.P. (1985), "Characteristic threshold and infra-red vibrothermography of sand", Geotechnical Testing Journal, GTJODJ, Vol 9, No 2, pp 80 - 86.

MAMLOUK, M.S. and DAVIES, T.G. (1984), "Elastodynamic analysis of pavement deflections", Transport Engineering Journal, ASCE, Vol 110, No 6, pp 536 - 550.

MARACHI, N.D., CHAN, C.K. and SEED, H.B. (1972), "Evaluation of properties of rockfill materials", Journal of Soil Mechanics and Foundations Division, ASCE, Vol 98, No SM1, pp 95 - 114.

MAYHEW, H.C. (1983), "Resilient properties of unbound roadbase under repeated triaxial loading", Transport and Road Research Laboratory, LR 1088.

McCULLOCH, L.M. (1981), "A field and laboratory study of road pavement sub-bases", MSc. Thesis, Queen's University, Belfast.

McINNES, D.B. (1984), "Total suction measurement of crushed rock basecourse material", Australian Road Research, No 14 (3), Tech. Note No 2, pp 153 - 156.

McVAY, M. and TAESIRI, Y. (1985), "Cyclic behaviour of pavement base materials", Journal of the Geotechnical Engineering Division, ASCE, Vol 111, No 1.

MOBIL OIL CO. (1985), "Asphalt pavement design manual for the UK".

O'REILLY, M.P. (1985), "Mechanical properties of granular materials for use in thermal energy stores", PhD. Thesis, University of Nottingham.

O'REILLY, M.P., BROWN, S.F. and THOM, N.H. (1987), "The University of Nottingham hollow cylinder apparatus", Report to SERC.

OVERY, R.F. (1982), "The behaviour of anisotropically consolidated silty clay under cyclic loading", PhD. Thesis, University of Nottingham.

PAPPIN, J.W. (1979), "Characteristics of a granular material for pavement analysis", PhD. Thesis, University of Nottingham.

PEUTZ, M.G.F., VAN KEMPEN, H.P.M. and JONES, A. (1968), "Layered systems under normal surface loads", Highway Research Record 228, pp 34 - 35.

PIKE, D.C. (1973), "Shear box tests on graded aggregates", Transport and Road Research Laboratory, LR 584.

POWELL, W.D., POTTER, J.F., MAYHEW, H.C. and NUNN, M.E. (1984), "The structural design of bituminous roads", Transport and Road Research Laboratory, LR 1132.

READES, D.W. and GREEN, G.E. (1976), "Independent stress control and triaxial extension tests on sand", Geotechnique 36, No 4, pp 551 - 576.

RONER, G.J. (1985), "Some effects of shape, gradation and size on the performance of railroad ballast", MSc. Dissertation, University of Massachusetts, Amherst.

ROSCOE, K.J. (1953), "An apparatus for the application of simple shear to soil samples", Proc. 3rd Int. Conf. Soil Mechanics, Zurich, Vol 1.

ROY, M. (1981), "Drainage of a road pavement", Proc. 1st Symp. Unbound Aggregates in Roads, Nottingham, pp 79 - 90.

SCHOFIELD, A.N. and WROTH, C.P. (1968), "Critical state soil mechanics", McGraw Hill Publishing Co., London.

SELIG, E.T., LIN, H., DWYER, L.J., DUANN, S-W. and TZENG, H. (1986), "Layered system performance evaluation", Phase 2 Final Report, No DOT/OST/p-34/86-047, University of Massachusetts, Amherst.

SHARP, R.W. (1983), "Shakedown analysis and design of pavements", PhD. Thesis, University of Sydney, Australia.

SHAW, P. (1980), "Stress-strain relationships for granular materials under repeated loading", PhD. Thesis, University of Nottingham.

SKEMPTON, A.W. (1954), "The pore pressure coefficients A and B", Geotechnique 4, pp 143 - 147.

SØRENSON, A. and HAYVEN, M. (1982), "The Dynatest 8000 falling weight deflectometer test system", Proc. Int. Symp. Bearing Capacity of Roads and Airfields, Trondheim, Norway, Vol 1, pp 464-470.

SOUSA, J.B. and MONISMITH, C.L. (1987), "Dynamic response of paving materials", Paper presented to TRB Annual Symposium, Washington, DC.

SWEERE, G.T.H., PENNING, A. and VOS, E. (1987), "Development of a structural design procedure for asphalt pavements with crushed rubble base courses", Paper presented to 6th Int. Conf. Structural Design of Asphalt Pavements, Ann Arbor, Michigan.

SYMES, M.J.P.R., GENS, A. and HIGHT, D.W. (1984), "Undrained anisotropy and principal stress rotation in saturated sand", Geotechnique 34, No 1, pp 11-27.

TAM, W.S. (1987), "Pavement evaluation and overlay design", PhD. Thesis, University of Nottingham.

TERZAGHI, K. (1936), "The shearing resistance of saturated soils", Proc. 1st Int. Conf. Soil Mechanics, Cambridge, Massachusetts, Vol 1, pp 54 - 56.

THOM, N.H. and BROWN, S.F. (1985), "Design of road foundations", Report NHT/1 to SERC and ICI Fibres, University of Nottingham.

UZAN, J. (1985), "Granular material characterization", Transportation Research Record 1022, pp 52 - 58.

VALEUX, J.C. and MOREL, G. (1980), "Influence of bearing capacity of underlying material on the compaction of pavement layers", Int. Conf. Compaction, Paris, Vol 2, pp 475 - 480.

WONG, R.K.S. and ARTHUR, J.R.F. (1985), "Induced and inherent anisotropy in sand", Geotechnique 35, No 4, pp 471 - 481.

MASTERS OF PLATES

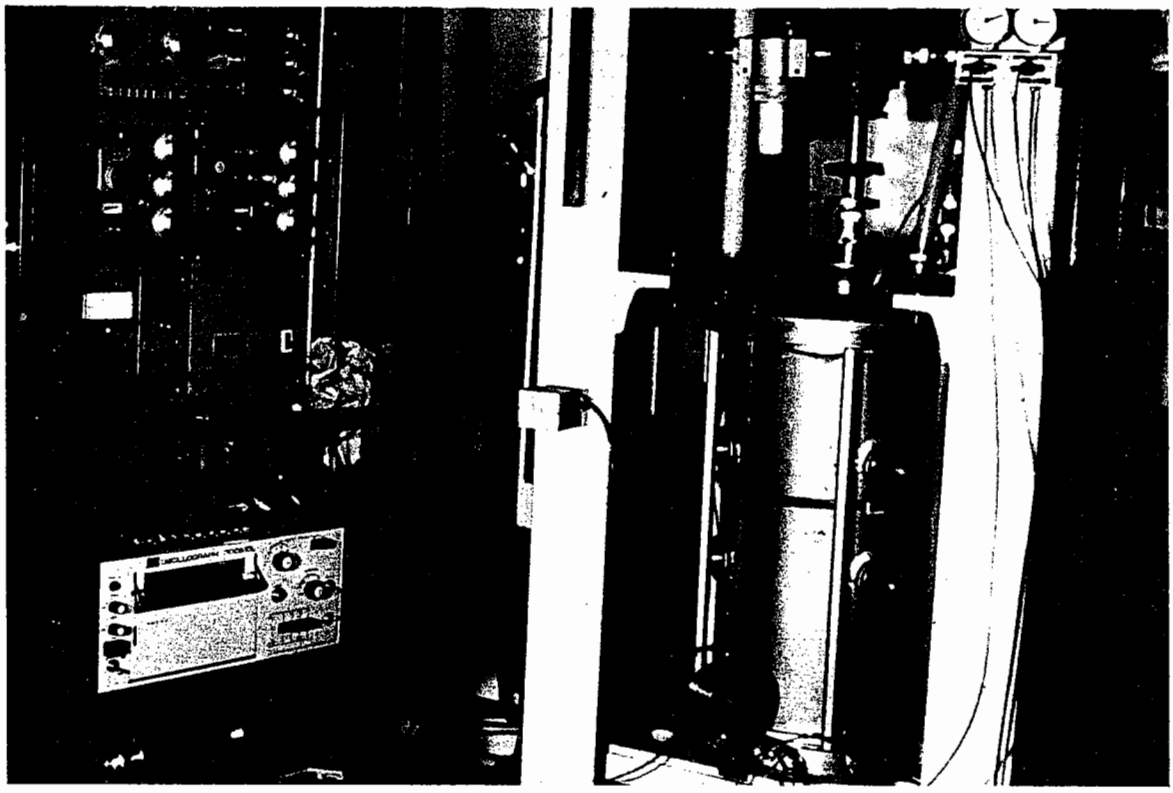

PLATE 1 150mm Triaxial Facility - General View

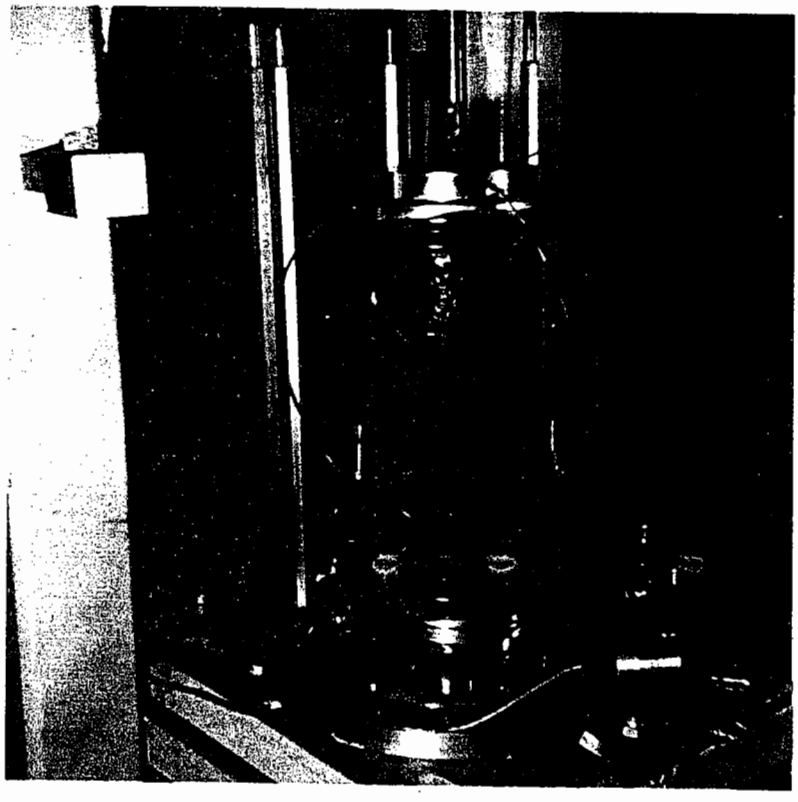

PLATE 2

150mm Triaxial Facility - Specimen and Instrumentation

PLATE 3

75mm Triaxial
Facility

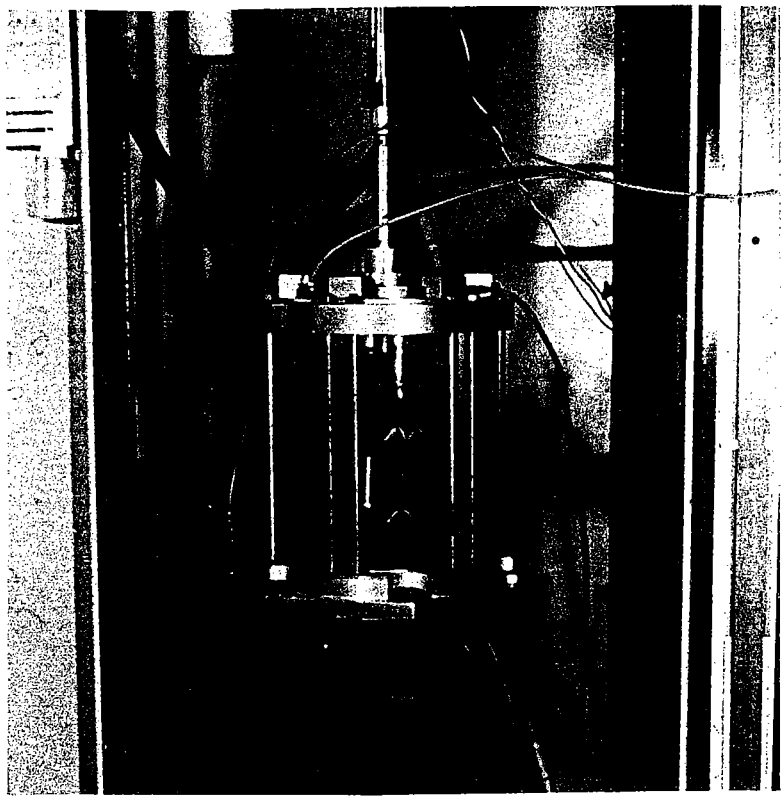

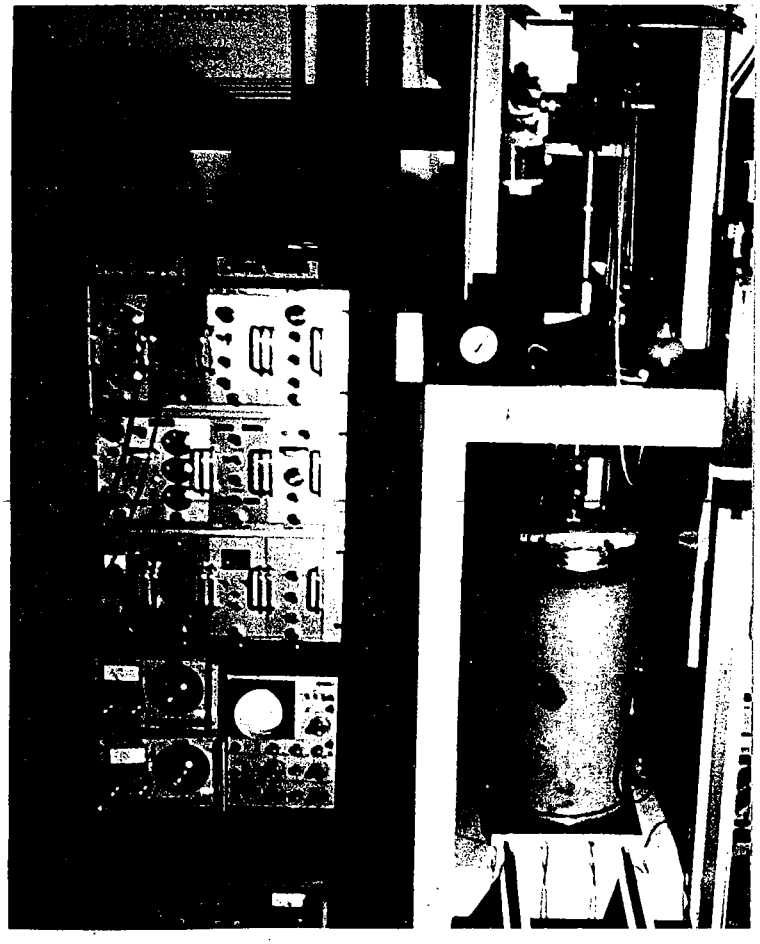

PLATE 4

Hollow Cylinder
Apparatus -
General View

PLATE 5

Hollow Cylinder Apparatus - Instrumentation Detail

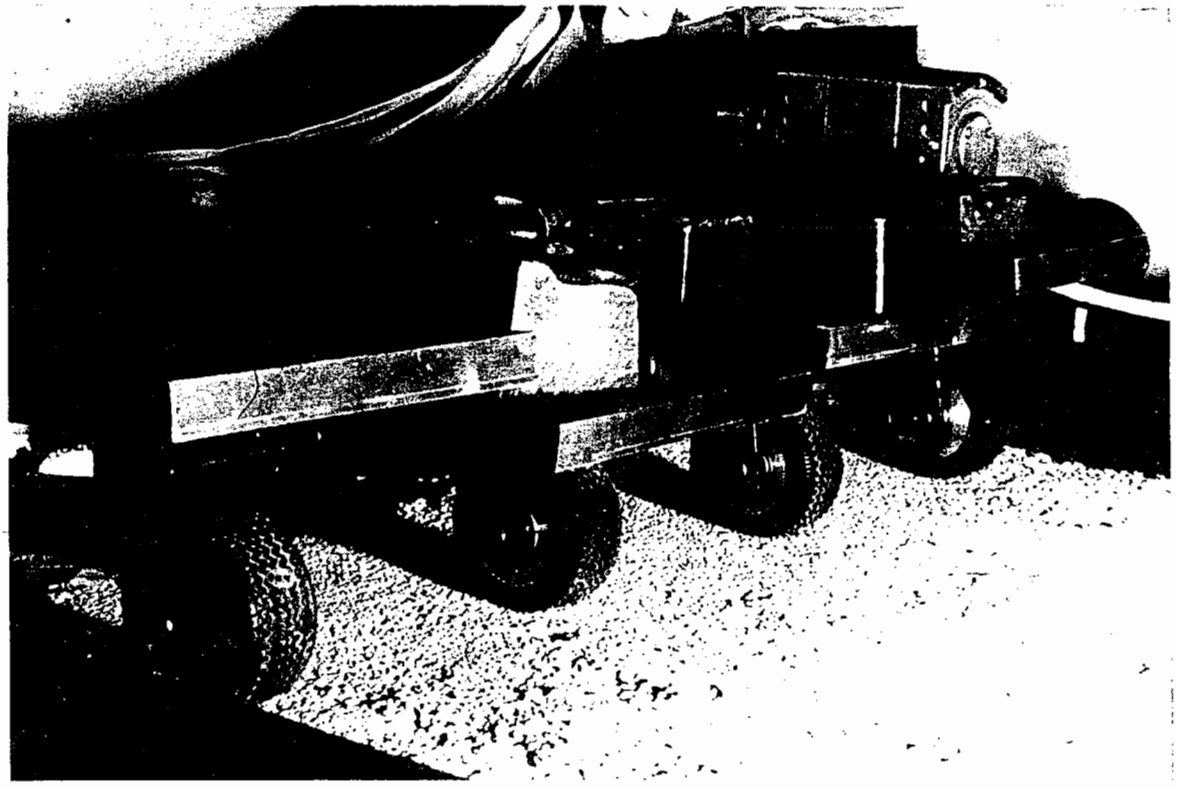

PLATE 6 Miniature Pavement Tester

PLATE 7

Plate Bearing Test

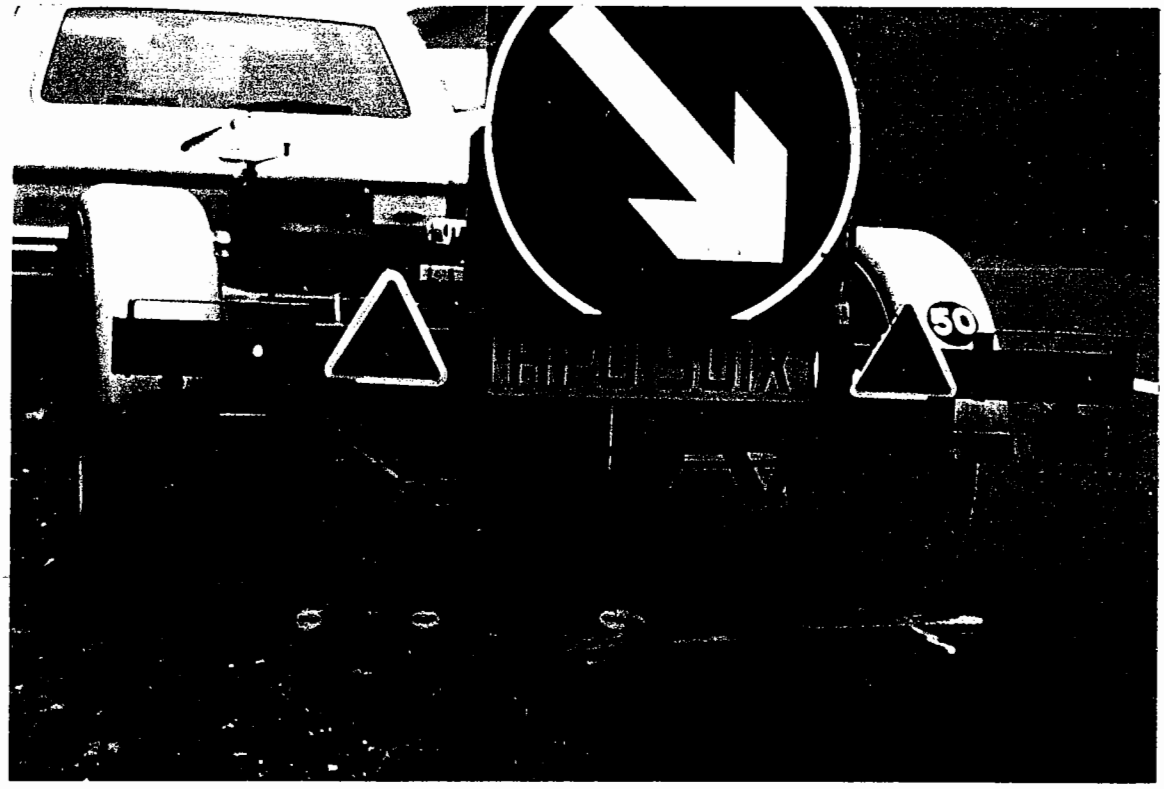

PLATE 8 Falling Weight Deflectometer

PLATE 9

Clegg Impact Hammer

PLATE 10

Dynamic Cone
Penetrometer

APPENDIX A

ELASTIC STRESS STRAIN DATA FROM THE HOLLOW CYLINDER APPARATUS

TESTS ON GRANITIC SAND

	Stress Path			Strains				
No.	Confining Stress	Axial Deviator Stress	Torsional Shear Stress	Axial Strain	Circum-ferential Strain	Radial Strain	45° Strain	Torsional Shear Strain
1	75	0-30	0	165	-58	-54	54	1
2	75	0-30	10	167	-54	-48	43	-27
3	75	0-30	20	163	-46	-69	41	-35
4	75	0-30	30	169	-47	-48	26	-70
5	75	30-60	30	134	-47	-35	25	-37
6	75	30-60	20	129	-40	-42	36	-17
7	75	30-60	10	135	-44	-46	38	-15
8	75	30-60	0	135	-47	-35	49	10
9	75	-40--10	0	320	-89	-73	121	11
10	75	-40--10	10	298	-80	-52	72	-74
11	75	90-120	0	101	-48	-27	23	-7
12	75	-20-0	0	144	-46	-42	51	4
13	75	-20-0	10	152	-45	-31	44	-19
14	75	-20-0	20	160	-43	-46	35	-47
15	75	0-60	30	384	-134	-115	65	-120
16	75	0-60	20	393	-149	-121	87	-70
17	75	0-60	10	381	-144	-100	104	-29
18	75	0-60	0	369	-142	-133	130	33
19	75	-20-40	0	495	-191	-154	180	56
20	75	-20-40	10	471	-164	-144	128	-51
21	75	-20-40	20	498	-167	-144	110	-111
22	75	-40-20	10	778	-242	-204	222	-92
23	75	-40-20	0	762	-244	-202	224	-70
24	75	30-90	0	303	-131	*	93	14
25	75	30-90	10	289	-123	*	82	-2
26	75	30-90	20	281	-119	*	63	-36
27	75	60-120	0	240	-114	*	77	28
28	75	0-120	0	765	-367	-286	244	90
29	75	-20-100	0	995	-424	-354	329	87
30	75	-20-100	10	898	-366	-313	255	-22
31	75	-20-100	20	991	-399	-323	200	-192
32	75	-40-80	10	1433	-529	-450	401	-102
33	75	-40-80	0	1363	-516	-417	480	113
34	75	-40-120	0	1754	-734	-609	617	214
35	75	0	0-10	0	0	0	79	158
36	75	-20	0-10	-1	0	0	84	169
37	75	-40	0-10	-9	0	0	110	229
38	75	30	0-10	5	-1	0	68	132
39	75	60	0-10	7	-1	0	59	112
40	75	90	0-10	4	0	0	50	96
41	75	90	10-20	2	-2	0	48	96
42	75	60	10-20	1	-6	0	51	107
43	75	30	10-20	0	-4	0	61	126

Notes:
1. All stresses are expressed in kiloPascals
2. All strains are expressed in microstrain
3. Torsional shear describes shear applied to horizontal and vertical planes in the wall of the specimen by application of a torque
4. The 45° strain is at 45° to axial and circumferential directions
5. Torsional shear strain is derived from other strains (= 2 x 45° less axial less circumferential)

	Stress Path			Strains				
No.	Confining Stress	Axial Deviator Stress	Torsional Shear Stress	Axial Strain	Circum-ferential Strain	Radial Strain	45° Strain	Torsional Shear Strain
44	75	0	10-20	0	-7	0	72	151
45	75	-20	10-20	-2	-11	0	91	195
46	75	0	20-30	-2	-18	0	77	174
47	75	30	20-30	0	-14	0	61	136
48	75	60	20-30	0	-6	0	57	120
49	75	60	10-30	-1	-17	0	135	288
50	75	30	10-30	-3	-22	0	155	335
51	75	0	10-30	-13	-30	0	195	433
52	75	0	0-20	-10	-8	0	206	430
53	75	-20	0-20	-21	-13	0	225	484
54	75	30	0-20	1	-7	0	162	330
55	75	60	0-20	4	-5	0	139	279
56	75	90	0-20	4	-3	0	128	255
57	75	90	-10-10	0	3	0	136	269
58	75	60	-10-10	2	4	0	147	288
59	75	30	-10-10	12	8	0	158	296
60	75	0	-10-10	2	7	0	183	357
61	75	-30	-10-10	-1	7	0	245	484
62	75	0	0-30	-9	-36	0	332	709
63	75	30	0-30	-1	-26	0	260	547
64	75	60	0-30	0	-22	0	229	480
65	75	60	-10-20	3	0	0	229	455
66	75	90	-10-20	1	1	0	214	426
67	75	30	-10-20	10	-2	0	271	534
68	75	0	-10-20	0	0	0	333	666
69	75	-20	-10-20	15	-8	0	379	751
70	75	-20	-20-20	28	14	0	614	1186
71	75	0	-20-20	27	14	0	504	967
72	75	30	-20-20	33	12	0	406	767
73	75	60	-20-20	20	7	0	359	691
74	75	90	-20-20	19	11	0	325	620
75	75	60	-10-30	3	-15	0	346	704
76	75	30	-10-30	4	-22	0	400	818
77	75	0	-10-30	-7	-29	0	479	994
78	75	0	-20-30	16	-18	0	673	1348
79	75	30	-20-30	21	-12	0	562	1115
80	75	60	-20-30	17	-6	0	496	981
81	75	60	-30-30	36	22	0	665	1272
82	75	30	-30-30	43	22	0	789	1513
83	75	0	-30-30	55	34	0	1036	1983
84	75	0-30	10-0	181	-56	-26	-11	-147
85	75	0-30	0-10	186	-67	-56	149	179
86	75	30-60	0-10	133	-51	-56	105	128
87	75	30-60	10-0	126	-47	-56	-16	-111
88	75	-40--10	10-0	364	-91	-65	0	-273
89	75	-40--10	0-10	381	-102	-83	266	253
90	75	-20-0	0-10	151	-51	-38	152	204
91	75	-20-0	10-0	151	-40	-44	-33	-177
92	75	0-60	10-0	318	-128	-113	25	-140
93	75	0-60	0-10	329	-122	-100	211	215
94	75	30-90	10-0	250	-109	-92	16	-109
95	75	30-90	0-10	265	-108	-108	158	159
96	75	-20-40	10-0	396	-148	-136	43	-162
97	75	-20-40	0-10	450	-159	-133	272	253

	Stress Path			Strains				
No.	Confining Stress	Axial Deviator Stress	Torsional Shear Stress	Axial Strain	Circum-ferential Strain	Radial Strain	45° Strain	Torsional Shear Strain
98	75	-40-20	10-0	582	-181	-156	63	-275
99	75	-40-20	0-10	639	-213	-179	372	318
100	75	-20-100	0-10	810	-331	-296	398	317
101	75	-20-100	10-0	779	-336	-286	150	-143
102	75	-40-80	10-0	1174	-438	-367	225	-286
103	75	-40-80	0-10	1166	-449	-396	523	329
104	75	-20-100	10-20	770	-336	-275	338	242
105	75	-20-100	20-10	763	-302	-281	104	-253
106	75	30-90	20-10	244	-99	-75	5	-135
107	75	30-90	10-20	236	-106	-79	142	154
108	75	0-60	20-10	328	-110	-117	13	-192
109	75	0-60	10-20	327	-137	-111	191	192
110	75	-20-40	10-20	419	-154	-138	239	213
111	75	-20-40	20-10	438	-130	-131	27	-254
112	75	0-30	20-10	177	-52	-74	-21	-167
113	75	0-30	10-20	176	-71	-67	124	143
114	75	30-60	10-20	127	-57	-46	99	128
115	75	30-60	20-10	122	-41	-40	-25	-131
116	75	-20-0	20-10	161	-32	-25	-43	-215
117	75	-20-0	10-20	152	-54	-42	141	184
118	75	0-30	20-30	166	-68	-46	116	134
119	75	0-30	30-20	176	-37	-48	-33	-205
120	75	30-60	30-20	136	-35	-35	-23	-147
121	75	30-60	20-30	124	-58	-42	93	120
122	75	0-60	20-30	323	-137	-106	159	132
123	75	0-60	30-20	333	-94	-111	-1	-241
124	75	0-30	-10-10	179	-52	-58	260	393
125	75	30-60	-10-10	145	-44	-65	212	323
126	75	0-30	10--10	162	-62	-58	-110	-320
127	75	-40--10	-10-10	418	-99	-85	467	615
128	75	-20-0	-10-10	198	-44	-44	300	446
129	75	-40-20	-10-10	790	-233	-219	604	651
130	75	-20-40	-10-10	517	-175	-154	444	546
131	75	0-60	-10-10	379	-139	-129	341	442
132	75	30-90	-10-10	294	-121	-102	269	365
133	75	-20-100	-10-10	914	-364	-379	587	624
134	75	-40-80	-10-10	1346	-478	-442	864	860
135	75	-20-0	0-20	149	-47	-40	252	402
136	75	-20-0	20-0	167	-31	-31	-151	-438
137	75	0-30	20-0	179	-45	-46	-109	-352
138	75	0-30	0-20	182	-68	-58	239	364
139	75	30-60	0-20	137	-58	-48	185	291
140	75	30-60	20-0	124	-34	-33	-97	-284
141	75	0-60	20-0	345	-116	-115	-63	-355
142	75	0-60	0-20	342	-132	-138	298	386
143	75	-20-40	0-20	456	-165	-140	365	439
144	75	-20-40	20-0	462	-133	-133	-72	-473
145	75	-20-100	0-20	831	-348	-294	500	517
146	75	-20-100	20-0	840	-320	-294	4	-512
147	75	0-60	10-30	314	-148	-106	270	374
148	75	0-60	30-10	361	-95	-108	-89	-444
149	75	0-30	30-10	196	-28	-69	-127	-422
150	75	0-30	10-30	160	-79	-50	222	363
151	75	30-60	10-30	131	-72	-48	183	307

	Stress Path			Strains				
No.	Confining Stress	Axial Deviator Stress	Torsional Shear Stress	Axial Strain	Circum-ferential Strain	Radial Strain	45° Strain	Torsional Shear Strain
152	75	30-60	30-10	132	-24	-40	-107	-322
153	75	0-30	30-0	200	-27	-40	-229	-631
154	75	0-30	0-30	183	-95	-46	336	584
155	75	30-60	0-30	138	-76	-71	272	482
156	75	30-60	30-0	135	-22	-50	-194	-501
157	75	0-60	0-30	341	-158	-113	375	567
158	75	0-60	30-0	375	-94	-113	-188	-657
159	75	-20-0	20--10	178	-41	-46	-283	-703
160	75	-20-0	-10-20	160	-59	-31	401	701
161	75	0-60	20--10	323	-121	-92	-160	-522
162	75	0-60	-10-20	341	-134	-106	397	587
163	75	0-30	-10-20	189	-73	-52	350	584
164	75	0-30	20--10	172	-55	-44	-222	-561
165	75	30-60	20--10	131	-53	-46	-188	-454
166	75	30-60	-10-20	140	-54	-35	287	488
167	75	30-90	-10-20	255	-120	-117	325	515
168	75	30-90	20--10	253	-109	-117	-147	-438
169	75	-20-40	-10-20	434	-157	-152	485	693
170	75	-20-40	20--10	429	-144	-144	-190	-665
171	75	-20-100	20--10	767	-317	-311	-73	-596
172	75	-20-100	-10-20	740	-332	-271	547	686
173	75	-20-100	20--20	774	-333	-288	-215	-871
174	75	-20-40	20--20	426	-172	-152	-326	-906
175	75	0-60	20--20	345	-148	-119	-294	-785
176	75	30-90	20--20	256	-139	-102	-259	-635
177	75	-20-0	20--20	152	-67	-40	-487	-1059
178	75	0-30	20--20	173	-77	-58	-366	-828
179	75	30-60	20--20	126	-70	-34	-312	-680
180	75	0-30	30--10	200	-32	-67	-371	-910
181	75	0-30	-10-30	192	-92	-60	477	854
182	75	30-60	-10-30	146	-74	-54	397	722
183	75	30-60	30--10	131	-35	-38	-306	-708
184	75	0-60	30--10	368	-102	-111	-310	-886
185	75	0-60	-10-30	349	-147	-125	528	854
186	75	0-60	-20-30	402	-150	-138	716	1180
187	75	0-60	30--20	376	-122	-117	-429	-1112
188	75	30-60	30--20	135	-46	-35	-431	-951
189	75	30-60	-20-30	183	-67	-60	547	978
190	75	0-30	-20-30	230	-79	-85	661	1171
191	75	0-30	30--20	199	-56	-44	-499	-1141
192	75	0-30	-30-30	325	-52	-96	969	1665
193	75	30-60	-30-30	213	-46	-59	738	1309
194	75	0-60	-30-30	484	-133	-156	1002	1653
195	50	0-30	0	221	-83	-48	78	18
196	50	0-30	10	215	-69	-60	66	-14
197	50	0-30	20	232	-77	-67	55	-45
198	50	30-60	20	145	-58	-65	30	-27
199	50	30-60	10	156	-71	-54	38	-9
200	50	30-60	0	140	-60	-46	44	8
201	50	-20-0	0	235	-62	-58	83	-7
202	50	-20-0	10	227	-71	-50	59	-38
203	50	-20-40	10	672	-241	-213	179	-73
204	50	-20-40	0	657	-238	-221	225	31
205	50	0-60	0	421	-183	-169	149	60

	Stress Path			Strains				
No.	Confining Stress	Axial Deviator Stress	Torsional Shear Stress	Axial Strain	Circum-ferential Strain	Radial Strain	45° Strain	Torsional Shear Strain
206	50	0–60	10	426	-174	-152	97	-58
207	50	0–60	20	452	-171	-152	59	-163
208	50	-20	0–10	-7	-4	0	154	319
209	50	0	0–10	0	-1	0	120	241
210	50	30	0–10	2	-3	0	94	189
211	50	60	0–10	2	-1	0	76	151
212	50	60	10–20	0	-8	0	76	160
213	50	30	10–20	-1	-17	0	95	208
214	50	0	10–20	-8	-22	0	122	274
215	50	-20	-10–10	6	9	0	441	867
216	50	0	-10–10	11	9	0	322	624
217	50	30	-10–10	13	7	0	240	460
218	50	60	-10–10	10	5	0	192	369
219	50	60	0–20	1	14	0	181	375
220	50	30	0–20	0	-23	0	216	455
221	50	0	0–20	-18	-38	0	287	630
222	50	0	-10–20	-3	-33	0	558	1152
223	50	30	-10–20	6	-16	0	389	788
224	50	60	-5–25	-8	-32	0	293	626
225	50	60	-15–25	2	-56	0	435	924
226	50	30	-15–25	-10	-80	0	531	1152
227	50	0	-15–25	-52	-155	0	722	1651
228	50	0	-20–20	46	21	0	892	1717
229	50	30	-20–20	37	14	0	634	1217
230	50	60	-20–20	26	13	0	496	953
231	50	-20–0	0–10	205	-67	-77	213	288
232	50	-20–0	10–0	229	-58	-77	-73	-317
233	50	0–30	10–0	212	-77	-54	-47	-229
234	50	0–30	0–10	209	-81	-69	184	240
235	50	30–60	0–10	138	-61	-79	137	197
236	50	30–60	10–0	140	-58	-63	-45	-172
237	50	-20–40	0–10	590	-224	-215	337	308
238	50	-20–40	10–0	608	-217	-215	7	-377
239	50	0–60	10–0	411	-173	-158	-12	-262
240	50	0–60	0–10	396	-168	-142	247	266
241	50	0–60	10–20	395	-184	-152	211	211
242	50	0–60	20–10	435	-143	-150	-48	-388
243	50	30–60	20–10	141	-43	-53	-54	-206
244	50	30–60	10–20	133	-70	-63	121	179
245	50	0–30	10–20	191	-87	-65	156	208
246	50	0–30	20–10	227	-54	-83	-80	-333
247	50	0–30	10–-10	224	-94	-75	-195	-520
248	50	30–60	10–-10	147	-73	-51	-154	-382
249	50	-20–0	10–-10	255	-88	-67	-265	-697
250	50	-20–40	10–-10	693	-268	-240	-114	-658
251	50	0–60	10–-10	436	-199	-173	-123	-483
252	50	0–60	20–0	460	-152	-167	-173	-654
253	50	0–60	0–20	408	-197	-167	358	505
254	50	30–60	0–20	139	-81	-37	234	410
255	50	30–60	20–0	150	-48	-43	-161	-424
256	50	0–30	20–0	260	-49	-67	-209	-629
257	50	0–30	0–20	214	-106	-79	305	502
258	50	0–30	-10–20	258	-114	-90	525	906
259	50	0–30	20–-10	249	-65	-90	-377	-938

	Stress Path			Strains				
No.	Confining Stress	Axial Deviator Stress	Torsional Shear Stress	Axial Strain	Circum-ferential Strain	Radial Strain	45° Strain	Torsional Shear Strain
260	50	30–60	20--10	162	-61	-56	-300	-701
261	50	30–60	-10–20	172	-83	-65	397	705
262	50	0–60	-10–20	454	-209	-167	569	893
263	50	0–60	20--10	464	-170	-175	-296	-886
264	50	0–60	20--20	462	-212	-175	-495	-1240
265	50	30–60	20--20	161	-100	-84	-487	-1035
266	50	0–30	20--20	272	-121	-104	-610	-1371
267	25	0–30	0	385	-161	-133	40	-144
268	25	0–30	10	363	-163	-136	58	-84
269	25	0–30	10–0	480	-165	-195	-161	-637
270	25	0–30	0–10	411	-202	-171	309	409
271	25	30	0–10	13	-16	0	168	339
272	25	0	0–10	12	-35	0	272	567
273	25	0	-10–10	28	35	0	832	1601
274	25	30	-10–10	27	17	0	441	838
275	25	0–30	-10–10	560	-196	-225	873	1382
276	25–50	0	0	137	110	(500)	122	-3
277	25–75	0	0	214	221	(875)	187	-61
278	50	0–160	0	1260	-845	-600	300	185

APPENDIX B

CONSTANTS DESCRIBING ELASTIC AND PLASTIC BEHAVIOUR

General form of Elastic Strain Equations

$$\varepsilon_s = A \left[\delta \ln \frac{s + t}{s - t} \right]^B \cdot (\delta t + \tfrac{1}{3} \delta s)^C$$

$$\varepsilon_v = D \left[\delta \ln p \right]^E \cdot (\delta p)^F - G \sum_{6}^{1} (\delta((\ln \frac{s + t}{s - t})^2)^H)$$

General form of Plastic Strain Equations

$$\varepsilon_{sp} = -\frac{1}{L} \ln \left[\frac{\sigma_f - \sigma_{max}}{\sigma_f} \right] - \frac{1}{M_1} (\delta t + \tfrac{1}{3} \delta s) \ln (N)$$

$$\varepsilon_{vp} = \frac{1}{M_2} (\Sigma \delta \sigma + 2 \Sigma \delta t) \ln (N) - \tfrac{1}{2} \varepsilon_{sp}$$

Symbols

σ	= normal stress
t	= shear stress
s	= mean in-plane stress
p	= mean normal stress
ε	= strain
N	= number of load applications
δ	= 'change in'

Subscripts

s	= shear
v	= volumetric
p	= plastic
f	= failure
max	= maximum

Constants A,B,C,D,E,F,G,H,L,M_1 ,M_2

PART 1. Dolomitic Limestone - Grading and Compaction Variation

Grading Parameter	Level of Compaction	Constants A	B	C	D	E	F	G	H	L	M_1	M_2
n = 5	zero	67	.82	.49	50	.46	.62	95	1.00	47	4.7	120
	light	50	.88	.56	255	.78	.23	220	1.08	40	5.3	102
	heavy	61	.89	.47	58	.44	.55	200	1.00	221	3.9	444
n = 2	zero	34	.97	.66	148	.69	.35	145	.90	58	3.6	81
	light	39	.85	.52	102	.52	.44	300	1.00	80	2.5	184
	heavy	81	.82	.43	70	.59	.50	114	.73	107	4.9	553
n = 1	zero	63	1.06	.53	150	.67	.36	415	.81	71	3.6	162
	light	153	1.00	.35	150	.66	.37	121	.60	70	2.4	163
	heavy	126	.79	.34	103	.67	.41	106	.85	88	3.7	210
n = .7	zero	158	1.06	.37	162	.78	.35	217	.86	62	2.3	157
	light	94	.87	.42	107	.69	.44	137	.75	80	2.2	210
	heavy	139	.92	.33	100	.64	.45	188	.83	110	4.0	376
n = .5	zero	186	1.05	.36	143	.70	.41	325	.91	54	2.5	92
	light	192	.94	.28	89	.65	.46	114	.82	66	2.2	163
	heavy	59	1.05	.57	117	.64	.41	187	.78	110	2.2	461
n = .35	zero	280	1.19	.27	84	.67	.48	206	1.32	120	1.0	48
	light	148	1.10	.40	132	.76	.38	225	1.33	58	2.3	80
	heavy	170	1.09	.31	221	.87	.27	270	1.36	126	2.7	671
n = .25	zero	245	1.45	.38	83	.73	.47	334	1.34	72	2.8	90
	light	528	1.31	.15	58	.65	.52	320	1.14	49	1.8	205
	heavy	385	1.42	.23	205	.72	.30	412	1.58	*	*	*

Notes:
1. Grading Parameter 'n' relates to the equation in fig 5.6
2. Constants A,D and G are expressed in microstrain
3. Constants B, C, E, F, H and L are dimensionless
4. Constants M_1 and M_2 are expressed in MegaPascals
5. * indicates no data available

PART 2. Other Materials

Material (Source)	Constants										
	A	B	C	D	E	F	G	H	L	M_1	M_2
Carboniferous Limestone (Dene, Derbyshire)	75	.90	.33	104	.85	.29	117	1.00	80	8.9	*
Carboniferous Limestone (ex A610 Kimberley, Nottinghamshire)	75	1.59	.33	25	.76	.51	170	1.04	107	16.8	4650
Carboniferous Limestone (Chipping Sodbury, Gloucestershire)	82	1.37	.25	80	1.00	.31	84	1.00	*	*	*
Carboniferous Limestone (ex Wakefield Haul Road, Yorkshire)	107	1.06	.32	360	1.18	0	140	1.32	107	14.4	2060
Dolomitic Limestone (Whitwell, Nottinghamshire)	80	1.05	.36	160	.97	.16	132	1.22	134	10.5	2490
Oolitic Limestone (ex A52 Friskney, Lincolnshire)	28	.80	.60	40	.73	.47	116	1.31	540	6.5	2400
Oolitic Limestone (ex A52 Bicker, Lincolnshire)	113	.96	.31	61	.90	.38	105	1.16	800	2.9	800
Granite (Mountsorrel, Leicestershire)	65	.72	.45	62	.62	.48	118	1.19	107	5.1	483
Crushed Concrete (Norfolk)	66	.78	.42	87	.65	.40	108	1.10	124	12.4	1030
Crushed Concrete (The Netherlands)	75	1.00	.35	132	1.00	.25	135	1.28	*	*	*
Steel Slag (Scunthorpe, Humberside)	43	.83	.45	54	.72	.40	98	1.13	70	7.1	1060
Sandstone (Norfolk)	43	.93	.56	68	.73	.43	107	1.12	200	12.4	3800
Sand & Gravel (Attenborough, Nottinghamshire)	75	.95	.46	88	.72	.38	164	1.28	161	3.0	238
Sand & Gravel (South Wales)	114	.96	.27	70	.81	.36	230	1.00	160	4.6	2200
Sand & Gravel (Wymondham, Norfolk)	280	1.07	.30	125	.86	.34	232	1.89	107	*	*

PART 2. (continued)

Material (Source)	Constants										
	A	B	C	D	E	F	G	H	L	M_1	M_2
Sand & Gravel (ex A52 Friskney, Lincolnshire)	1420	1.79	0	112	1.02	.40	1060	1.79	95	1.7	177
Sand (Mid-Ross, Scotland)	300	1.10	.26	177	.78	.33	270	.58	160	8.3	*
Granitic Sand (Bardon Hill, Leicestershire)	194	1.00	.42	260	.82	.25	61	1.00@	46	6.4	250

Notes:
1. Constants A, D and G are expressed in microstrain
2. Constants B, C, E, F, H and L are dimensionless
3. Constants M_1 and M_2 are expressed in MegaPascals
4. * indicates no data available
5. @ indicates a stress path length dependecy for dilatent volumetric strain with power .42

APPENDIX C

COMPUTER PROGRAM 'GRANMAT'

WRITTEN IN TURBO-BASIC

Variables Used in Granmat

A$	Moisture Indicator
B1 (R,Z)	Vertical Stress in Granular Base (kPa)
B2 (R,Z)	Radial Stress in Granular Base (kPa)
B3 (R,Z)	Tangential Stress in Granular Base (kPa)
B4 (R,Z)	Shear Stress in Granular Base (kPa)
B5 (R,Z)	Vertical Displacement in Granular Base. (microns)/Temporary Variable
B6 (R,Z)	Radial Displacement in Granular Base (microns)/ Temporary Variable
B7 (R,Z)	Mean In-Plane Stress (kPa)/Temporary Variable
B$	Batch Routine Indicator
C1	Compression Coefficient - Granular Base
C2	Dilation Coefficient - Granular Base
C3	Shear Coefficient - Granular Base
C4	Compression Stress Path Length Index - Granular Base
C5	Dilation Stress Path Length Index - Granular Base
C6	Shear Stress Path Length Index - Granular Base
C7	Principal Stress Ratio at Failure - Granular Base
C8	Interlock Stress - Granular Base (kPa)
C9	Strain at 80% Failure Stress (%)
CP	Load Contact Pressure - variable (kPa)
CQ	Load Contact Pressure - peak (kPa)
CS	Plastic Shear Coefficient - Granular Base (MPa)
CV	Plastic Volumetric Coefficient - Granular Base (MPa)
D1	Thickness of Asphalt (mm)
D2	Thickness of Granular Base (mm)
D3	Thickness of Subgrade (m)
DP	Single Particle Depth (mm)
DR (R,Z)	Radial Strain (microstrain)/Transverse Plastic Strain (microstrain)
DS	Degree of Saturation (%)
DZ (R,Z)	Vertical Strain (microstrain)
D$	Date/Title
E1	Elastic Stiffness of Asphalt (GPa)
E3	Elastic Stiffness of Subgrade (MPa)
F(R)	Shear Force in Asphalt
F1	Compression Power - Granular Base
F2	Dilation Power - Granular Base
F3	Shear Power - Granular Base
F$	Output Type Indicator
G3	Shear Modulus of Subgrade (MPa)
G$	Screen/Printer Indicator
I1(2)	Initial Sum of 3 Orthogonal Stresses (kPa)
I2(2)	Initial Shear Stress Ratio Parameter, Squared
J	Counter
J1	Temporary Variable
J2	Temporary Variable
J3	Temporary Variable
J4	Temporary Variable
J5	Temporary Variable
J6	Temporary Variable
J7	Temporary Variable

J8	Temporary Variable
K0	Initial Horizontal/Vertical Stress Ratio - Granular Base
K1	Subgrade Stiffness Parameter
K2	Subgrade Stiffness Parameter
K3	Bulk Modulus of Subgrade (MPa)
KB	Permeability of Granular Base (m/sec)
M(R)	Bending Moment of Asphalt
M1	Density of Asphalt (kg/m^3)
M2	Density of Granular Base (kg/m^3)
M3	Density of Subgrade (kg/m^3)
N	Iteration Number
N(R)	Slope at Surface
N1	Convergence Indicator
N2	Convergence Indicator
NP	Temporary Variable
NQ	Logarithm of Number of Passes to Failure
Q (R,Z)	Change in Pore Volume
Q1	Temporary Variable
Q2	Temporary Variable
Q3	Temporary Variable
Q4	Temporary Variable
Q5	Temporary Variable
Q6	Temporary Variable
Q7	Temporary Variable
Q8	Temporary Variable
q9	Temporary Variable
R	Radial Indicator
R2	Number of Radial Divisions - Granular Base
R3	Number of Radial Divisions - Subgrade
RL	Radius of Load (mm)
S1 (R,Z)	Vertical Stress in Subgrade (kPa)
S2 (R,Z)	Radial Stress in Subgrade (kPa)
S3 (R,Z)	Tangential Stress in Subgrade (kPa)
S4 (R,Z)	Shear Stress in Subgrade (kPa)
S5 (R,Z)	Vertical Displacement in Subgrade (microns)
S6 (R,Z)	Radial Displacement in Subgrade (microns)
SPL	Stress Path Length
SU	Suction in Granular Base (kPa)
S$	Subgrade Type Indicator
T	Pulse Duration Indicator
T$	Correctness Indicator
U (R,Z)	Temporary Variable
V	Counter/Temporary Variable
V (R,Z)	Temporary Variable
W (R,Z)	Temporary Variable
W1	Stress due to Self Weight of Asphalt (kPa)
W2	Stress due to Self Weight of Granular Base (kPa/mm)
W3	Stress due to Self Weight of Subgrade (kPa/mm)
X	Basic Grid Dimension (mm)
X(R)	Radial Distance (mm)
Y(Z)	Vertical Distance in Subgrade (mm)
Z	Vertical Indicator
Z2	Number of Vertical Divisions in Granular Base
Z3	Number of Vertical Divisions in Subgrade

```
REM   GRANMAT
REM    INPUT AND CONTROL
REM      SCREEN INPUT
10:
    CLS
    COLOR 31,4
    PRINT"HELLO, WELCOME TO GRANMAT"
    COLOR 10,0
    PRINT""
    INPUT"DATE/TITLE ";D$
    INPUT"THICKNESS(mm):SURFACING ";D1
    INPUT"               BASE      ";D2
    INPUT"         (m): SUBGRADE  ";D3
    INPUT"BASIC GRID DIMENSION(mm)";X
    X=D2/INT(D2/X+.8)
    IF D1=0 THEN INPUT"SINGLE PARTICLE DEPTH(mm) ";DP
    IF D1≠0 THEN INPUT"SURFACING STIFFNESS(GPa)  ";E1
    COLOR 11,0
    CLS
    PRINT"GRANULAR BASE PARAMETERS"
    INPUT"  COMPRESSION COEFFICIENT  ";C1
    INPUT"   POWER                   ";F1
    INPUT"   STRESS PATH LENGTH INDEX";C4
    INPUT"  DILATION COEFFICIENT     ";C2
    INPUT"   POWER                   ";F2
    INPUT"   STRESS PATH LENGTH INDEX";C5
    INPUT"  SHEAR COEFFICIENT        ";C3
    INPUT"   POWER                   ";F3
    INPUT"   STRESS PATH LENGTH INDEX";C6
    INPUT"  FAILURE RATIO(S1/S3)     ";C7
    INPUT"  INTERLOCK(KPa)           ";C8
    INPUT"  SHEAR AT 80% FAILURE(%)  ";C9
    C9=160.944/C9
    INPUT"  PLASTIC SHEAR COEF.(MPa) ";CS
    INPUT"  PLASTIC VOL. COEF.(MPa)  ";CV
    COLOR 12,0
    CLS
    PRINT"SUBGRADE PARAMETERS"
    INPUT"  LINEAR,K-THETA,LOACH ";S$
    IF S$="LINEAR" THEN INPUT"  MODULUS ";E3
    IF S$="K-THETA" THEN INPUT"  K1 ";K1
    IF S$="K-THETA" THEN INPUT"  K2 ";K2
    IF S$="LOACH" THEN INPUT"  A ";K1
    IF S$="LOACH" THEN INPUT"  B ";K2
    COLOR 14,0
    CLS
    IF D1=0 THEN INPUT"DENSITY(kg/cum):BASE      ";M2
    IF D1=0 THEN GOTO 67
    INPUT"DENSITY(kg/cum):SURFACING ";M1
    INPUT"                 BASE      ";M2
67:
    INPUT"                 SUBGRADE  ";M3
    INPUT"INITIAL STRESS RATIO ";K0
    INPUT"LOAD: PRESSURE(KPa) ";CP
    INPUT"      RADIUS(mm)    ";RL
    INPUT"VERY WET(Y/N) ";A$
    IF A$="N" THEN INPUT"BASE SUCTION(KPa) ";SU
    IF A$="N" THEN GOTO 84
    INPUT"BASE PERMEABILITY(m/sec) ";KB
    INPUT"DEGREE OF SATURATION(%)  ";DS
```

```
    INPUT"LOAD PULSE DURATION(sec) ";DU
84:
    COLOR 10,0
    CLS
    G$="P"
    GOTO 7010
88:
    INPUT"ALL OK(Y/N)";T$
    IF T$="N" THEN GOTO 10
    INPUT"FULL OR REDUCED OUTPUT(F/R)";F$
    IF F$="R" THEN INPUT"TO SCREEN OR PRINTER(S/P)";G$
    INPUT"BATCH ROUTINE IN USE(Y/N)";B$
    A=0
REM  GRID DIMENSIONS
    Z2=D2/X
    Q1=0:Q2=X:Q3=0
115:
    Q1=Q1+Q2
    Q3=Q3+1:Q2=Q2*2
    IF D3*1000≥Q1 THEN GOTO 115
    Z3=Q3
    Q1=0:Q2=X:Q3=0
140:
    Q1=Q1+Q2
    Q3=Q3+1
    IF Q1≥RL+D1+D2 OR Q1≥4*RL THEN Q2=Q2*2
    IF Q1≠3000 THEN GOTO 140
    R2=Q3
    Q1=0:Q2=1
165:
    IF Q1≥D3*.6-3 THEN GOTO 166
    Q1=Q1+Q2:Q3=Q3+1:Q2=Q2*2:GOTO 165
166:
    R3=Q3
REM    DIMENSIONING
    Q1=Z2
    IF Z3≥Z2 THEN Q1=Z3
    DIM B1(R2,Z2),B2(R2,Z2),B3(R2,Z2),B4(R2,Z2),B5(R2,Z2),B6(R2,Z2)
    DIM B7(R2,Z2),S1(R3,Z3),S2(R3,Z3),S3(R3,Z3),S4(R3,Z3),S5(R3,Z3)
    DIM S6(R3,Z3),W(R3,Q1),V(R3,Q1),M(R2),N(R2),F(R2),I1(Z2),I2(Z2)
    DIM X(R3),Y(Z3),DR(R3,Q1),DZ(R3,Q1),Q(R2,Z2),U(R2,Z2)
REM    X,Y CO-ORDINATES
300:
    Q1=0:Q2=X:R=0
  DO WHILE R≠R2
    X(R)=Q1:Q1=Q1+Q2:R=R+1
    IF Q1≥RL+D1+D2 OR Q1≥RL*4 THEN Q2=Q2*2
  LOOP
    X(R2)=3000:Q2=1:R=R+1
  DO WHILE R≠R3
    X(R)=X(R-1)+1000*Q2:Q2=Q2*2:R=R+1
  LOOP
    IF R3≥R2 THEN X(R3)=3000+(D3*.6-3)*1000
    Q1=0:Q2=X:Z=0
  DO WHILE Z≠Z3
    Y(Z)=Q1:Q1=Q1+Q2:Z=Z+1:Q2=Q2*2
  LOOP
    Y(Z3)=D3*1000
REM    INITIAL VALUES
    W1=M1*D1/101937:W2=M2/101937:W3=M3/101937
```

```
    IF D1=0 THEN W1=DP*W2
    IF S$="LINEAR" THEN G3=E3/1.4
110:
    N=0
  FOR Z=0 TO Z2:FOR R=0 TO R2
    B1(R,Z)=W1+W2*X*Z+SU:B2(R,Z)=(W1+W2*X*Z)*K0+SU:B3(R,Z)=B2(R,Z)
    B4(R,Z)=0:B5(R,Z)=0:B6(R,Z)=0:U(R,Z)=0:Q(R,Z)=0
  NEXT R
    R=0
    I1(Z)=B1(R,Z)+2*B2(R,Z)
    I2(Z)=LOG(B1(R,Z)/B2(R,Z)):I2(Z)=I2(Z)*I2(Z)
  NEXT Z
  FOR Z=0 TO Z3:FOR R=0 TO R3
    S1(R,Z)=W1+W2*D2+W3*Y(Z):S2(R,Z)=S1(R,Z):S3(R,Z)=S1(R,Z)
    S4(R,Z)=0:S5(R,Z)=0:S6(R,Z)=0
  NEXT R,Z
    N2=1:V=0
    IF A$="N" THEN GOTO 530
    CQ=CP:CP=CP*.02
    GOTO 530
REM    CONTROL
510:
    N=N+1
    PRINT"     ITERATION"N":";N1
    IF N2≠1 THEN GOTO 540
    IF N1≠(R2*Z2/100)^.75*CP*RL*RL/4500 AND A$="N" THEN GOTO 540
    IF N≠49 THEN GOTO 540
530:
    N1=0:IF D1=0 THEN GOTO 1410
    GOTO 1010
540:
    IF N1≠(R2*Z2/100)^.75*CP*RL*RL/(4500/((N/50)^4)) THEN GOTO 530
    N2=N2-.1
    IF N2≠.05 THEN GOTO 6010
    GOTO 530
REM  SURFACING LAYER ANALYSIS
REM    SLOPE DISTRIBUTION
1010:
    FOR R=1 TO R2-1
    N(R)=(B5(R-1,0)-B5(R+1,0))/(X(R+1)-X(R-1))
    IF V=0 THEN GOTO 1035
    IF N(R)≠N(R-1) THEN N(R)=N(R-1)
    GOTO 1040
1035:
    IF N(R)≠N(R-1) THEN V=1
1040:
    NEXT R:V=0
REM    MOMENT DISTRIBUTION
    M(0)=-N(1)*E1*D1*D1*D1/(12*X)
    M(R2)=N(R2-1)*E1*D1*D1*D1/(12*(X(R2)-X(R2-1)))
    FOR R=1 TO R2:IF R=R2 THEN GOTO 1130
    M(R)=(N(R-1)-N(R+1))*E1*D1*D1*D1/(12*(X(R+1)-X(R-1)))
1130:
    IF V=0 THEN GOTO 1145
    IF M(R)≠M(R-1) THEN M(R)=M(R-1)
    GOTO 1150
1145:
    IF M(R)≠M(R-1) AND X(R)≠RL THEN V=1
1150:
    NEXT R:V=0
```

```
REM    SHEAR FORCE DISTRIBUTION
    F(0)=0
    F(R2)=(M(R2)-M(R2-1))*3000/(3000-X(R2-1))+M(R2)
    FOR R=1 TO R2
    IF R=R2 THEN GOTO 1235
    F(R)=(M(R+1)-M(R-1))*X(R)/(X(R+1)-X(R-1))+M(R)
1235:
    F(R)=F(R)+N(R)*E1*D1*D1*D1/(12*X(R))
    IF V=0 THEN GOTO 1250
    IF F(R)¾F(R-1) THEN F(R)=F(R-1):GOTO 1255
1250:
    IF F(R)¼F(R-1) AND X(R)¾RL THEN V=1
1255:
    IF F(R)¼0 THEN F(R)=0
    NEXT R:V=0
    FOR R=0 TO R2-1
    IF X(R)¼RL THEN F(R)=F(R)+(RL*RL-X(R)*X(R))*CP/2000
    NEXT R
REM    SUPPORT STRESS DISTRIBUTION
    W(0,0)=(F(0)-F(1))*2000/(X*X)+W1
    W(R2,0)=(F(R2-1)-F(R2))*2000/(9000000-X(R2-1)*X(R2-1))+W1
    FOR R=R2 TO 0 STEP-1
    IF R=R2 THEN GOTO 1345
    IF R=0 THEN 1340
    W(R,0)=(F(R-1)-F(R+1))*2000/(X(R+1)*X(R+1)-X(R-1)*X(R-1))+W1
1340:
    IF W(R,0)¼W(R+1,0) THEN W(R,0)=W(R+1,0)
1345:
    IF W(R,0)¼1 THEN W(R,0)=1
    NEXT R
    FOR R=0 TO R2
    W(R,0)=W(R,0)*.5+(B1(R,0)-SU)*.5+SU
    NEXT R
    GOTO 2010
REM    UNSURFACED CONDITION
1410:
    FOR R=0 TO R2
    IF X(R)¼RL THEN W(R,0)=CP+W2*DP+SU
    IF X(R)¾RL THEN GOTO 1430
    W(R,0)=W2*DP+SU
1430:
    NEXT R
REM  BASE ANALYSIS
REM    BASE VERTICAL STRESS
2010:
    FOR Z=0 TO Z2:FOR R=R2 TO 0 STEP-1
    IF R=0 THEN V(0,Z)=B4(1,Z)*2/X
    IF R=R2 THEN V(R,Z)=-B4(R-1,Z)/(3000-X(R-1))
    IF R=0 OR R=R2 THEN GOTO 2020
    V(R,Z)=(B4(R+1,Z)-B4(R-1,Z))/(X(R+1)-X(R-1))+B4(R,Z)/X(R)
2020:
    IF Z=0 THEN GOTO 2062
    W(R,Z)=W(R,Z-1)+X*W2+(V(R,Z-1)+V(R,Z))*.5*X
    IF R=R2 THEN GOTO 2062
    IF W(R,Z)¼W(R+1,Z) THEN W(R,Z)=W(R+1,Z)
REM      CONSTRAINING AND BALANCING
2062:
    N1=N1+ABS(W(R,Z)-B1(R,Z))
    NEXT R
    Q1=0
```

```
    FOR R=1 TO R2
    Q2=.5*(W(R,Z)+W(R-1,Z))-W1-SU-W2*X*Z
    Q1=Q1+Q2*(X(R)*X(R)-X(R-1)*X(R-1))
    NEXT R
    FOR R=0 TO R2
    W(R,Z)=(W(R,Z)-W1-SU-W2*X*Z)*CP*RL*RL/Q1+W1+SU+W2*X*Z
    W(R,Z)=W(R,Z)-U(R,Z)
    B1(R,Z)=W(R,Z)*.2*N2+B1(R,Z)*(1-.2*N2)
    IF B1(R,Z)<(B2(R,Z)-C8)/C7 THEN B1(R,Z)=(B2(R,Z)-C8)/C7+1
    IF B1(R,Z)<(B3(R,Z)-C8)/C7 THEN B1(R,Z)=(B3(R,Z)-C8)/C7+1
    IF B1(R,Z)<.5 THEN B1(R,Z)=.5
    NEXT R,Z
REM    BASE RADIAL STRESS
    FOR Z=0 TO Z2:FOR R=0 TO R2
    IF R=0 THEN DR(0,Z)=B6(1,Z)*1000/X
    IF R=R2 THEN DR(R,Z)=-B6(R-1,Z)*1000/(3000-X(R-1))
    IF R=0 OR R=R2 THEN GOTO 2120
    DR(R,Z)=(B6(R+1,Z)-B6(R-1,Z))*1000/(X(R+1)-X(R-1))
2120:
    IF Z=0 THEN DZ(R,Z)=(B5(R,1)-B5(R,0))*1000/X
    IF Z=Z2 THEN DZ(R,Z)=(B5(R,Z)-B5(R,Z-1))*1000/X
    IF Z=0 OR Z=Z2 THEN GOTO 2128
    DZ(R,Z)=(B5(R,Z+1)-B5(R,Z-1))*500/X
2128:
    W(R,Z)=(1+(K0-1)*(W1+W2*X*Z)/(W1+W2*X*Z+SU))*B1(R,Z)
    SPL=.5*ABS(B1(R,Z)-B2(R,Z)+(K0-1)*(W1+W2*X*Z))
    SPL=SPL+.16667*ABS(B1(R,Z)+B2(R,Z)-(1+K0)*(W1+W2*X*Z))
    IF SPL<1 THEN SPL=1
    Q8=(ABS(DR(R,Z)-DZ(R,Z))*.5/(C3*SPL^C6))^(1/F3)
    IF Q8>10 THEN Q8=10
    IF DR(R,Z)<DZ(R,Z) THEN Q8=-Q8
    W(R,Z)=W(R,Z)/EXP(Q8)
REM      CONSTRAINING
    IF W(R,Z)>2*CP+SU THEN W(R,Z)=2*CP+SU
    IF W(R,Z)<1 THEN W(R,Z)=1
    IF R<3 THEN GOTO 2174
    IF V=0 THEN GOTO 2172
    IF W(R,Z)>W(R-1,Z) THEN W(R,Z)=W(R-1,Z)
    IF W(R,Z)<B2(R2,Z) THEN W(R,Z)=B2(R2,Z)
    GOTO 2174
2172:
    IF X(R-2)>RL AND W(R,Z)<W(R-1,Z) THEN V=1
2174:
    N1=N1+ABS(W(R,Z)-B2(R,Z))
    B2(R,Z)=B2(R,Z)*(1-.2*N2)+W(R,Z)*.2*N2
    IF B2(R,Z)<(B1(R,Z)-C8)/C7 THEN B2(R,Z)=(B1(R,Z)-C8)/C7+1
    NEXT R:V=0:NEXT Z
REM    BASE TANGENTIAL STRESS
    FOR Z=0 TO Z2:FOR R=0 TO R2
    IF R=R2 THEN V(R,Z)=(B2(R,Z)+U(R,Z)-B2(R-1,Z)-U(R-1,Z))/(3000-X(R-1))
    IF R=0 THEN V(R,Z)=(B2(1,Z)+U(1,Z))/X
    IF R=0 OR R=R2 THEN GOTO 2220
    V(R,Z)=(B2(R+1,Z)+U(R+1,Z)-B2(R-1,Z)-U(R-1,Z))/(X(R+1)-X(R-1))
2220:
    IF Z=0 THEN V(R,0)=V(R,0)+(B4(R,0)-B4(R,1))/X
    IF Z=Z2 THEN V(R,Z2)=V(R,Z2)+(B4(R,Z2-1)-B4(R,Z2))/X
    IF Z=0 OR Z=Z2 THEN GOTO 2228
    V(R,Z)=V(R,Z)-(B4(R,Z+1)-B4(R,Z-1))*.5/X
2228:
    W(R,Z)=X(R)*V(R,Z)+B2(R,Z)
```

```
REM      CONSTRAINING AND AVERAGING
    IF W(R,Z)≠1 THEN W(R,Z)=1
    NEXT R
    FOR R=0 TO R2
    IF R=0 OR R=R2 THEN GOTO 2270
    IF X(R)≠RL*2+Z*X AND W(R,Z)≠2*W(R2,Z) THEN W(R,Z)=W(R2,Z)*2
    W(R,Z)=(W(R-1,Z)+W(R,Z)*3+W(R+1,Z))/5
    IF Z=0 OR Z=Z2 THEN GOTO 2270
    W(R,Z)=(W(R,Z-1)+W(R,Z)*3+W(R,Z+1))/5
2270:
    B3(R,Z)=B3(R,Z)*.9+W(R,Z)*.1
    IF B3(R,Z)≠(B2(R,Z)-C8)/C7 THEN B3(R,Z)=(B2(R,Z)-C8)/C7+1
    IF B3(R,Z)≠(B1(R,Z)-C8)/C7 THEN B3(R,Z)=(B1(R,Z)-C8)/C7+1
    IF B3(R,Z)≠B1(R,Z)*C7+C8 THEN B3(R,Z)=B1(R,Z)*C7+C8-1
    NEXT R,Z
REM    BASE SHEAR STRESS
    FOR R=1 TO R2-1
    V(R,0)=(B6(R,1)-B6(R,0))/X
    V(R,Z2)=(B6(R,Z2)-B6(R,Z2-1))/X
    FOR Z=1 TO Z2-1
    V(R,Z)=(B6(R,Z+1)-B6(R,Z-1))*.5/X
    NEXT Z
    FOR Z=0 TO Z2
    V(R,Z)=V(R,Z)+(B5(R+1,Z)-B5(R-1,Z))/(X(R+1)-X(R-1))
    SPL=B4(R,Z)+.16667*ABS(B1(R,Z)+B2(R,Z)-(1+K0)*(W1+W2*X*Z))
    IF SPL≠1 THEN SPL=1
    Q8=(ABS(V(R,Z))*500/(C3*SPL^C6))^(1/F3)
    IF Q8≠10 THEN Q8=10
    IF V(R,Z)≠0 THEN Q8=-Q8
    V(R,Z)=EXP(Q8)
    B7(R,Z)=(B1(R,Z)+B2(R,Z))*.5
    W(R,Z)=B7(R,Z)*(V(R,Z)-1)/(V(R,Z)+1)
    IF W(R,Z)≠0 THEN W(R,Z)=0
    N1=N1+ABS(W(R,Z)-B4(R,Z))
    B4(R,Z)=B4(R,Z)*(1-.2*N2)+W(R,Z)*.2*N2
    NEXT Z,R
    FOR Z=0 TO Z2
    B7(0,Z)=(B1(0,Z)+B2(0,Z))*.5
    B7(R2,Z)=(B1(R2,Z)+B2(R2,Z))*.5
    NEXT Z
    GOTO 3010
REM    BASE VERTICAL DISPLACEMENT
2410:
    FOR Z=Z2 TO 0 STEP-1:FOR R=R2 TO 0 STEP-1
    Q1=LOG(B1(R,Z)/B2(R,Z)):Q1=Q1*Q1
    Q2=LOG(B2(R,Z)/B3(R,Z)):Q2=Q2*Q2
    Q3=LOG(B3(R,Z)/B1(R,Z)):Q3=Q3*Q3
    IF ABS(B4(R,Z))+1≠B7(R,Z) THEN GOTO 2420
    Q4=10:GOTO 2425
2420:
    Q4=LOG((B7(R,Z)+B4(R,Z))/(B7(R,Z)-B4(R,Z))):Q4=Q4*Q4
2425:
    SPL=.5*ABS(B1(R,Z)-B2(R,Z)+(K0-1)*(W1+W2*Z*X))
    SPL=SPL+.16667*ABS(B1(R,Z)+B2(R,Z)-(1+K0)*(W1+W2*X*Z))
    IF SPL≠1 THEN SPL=1
    V(R,Z)=(ABS(Q1-I2(Z)))^F2*C2*SPL^C5
    IF Q1≠I2(Z) THEN V(R,Z)=-V(R,Z)
    SPL=.5*ABS(B2(R,Z)-B3(R,Z))
    SPL=SPL+.16667*ABS(B2(R,Z)+B3(R,Z)-2*K0*(W1+W2*X*Z))
    IF SPL≠1 THEN SPL=1
```

```
    V(R,Z)=Q2^F2*C2*SPL^C5+V(R,Z)
    SPL=.5*ABS(B1(R,Z)-B3(R,Z)+(KO-1)*(W1+W2*X*Z))
    SPL=SPL+.16667*ABS(B1(R,Z)+B3(R,Z)-(1+KO)*(W1+W2*X*Z))
    IF SPL#1 THEN SPL=1
    Q8=(ABS(Q3-I2(Z)))^F2*C2*SPL^C5
    IF Q3#I2(Z) THEN Q8=-Q8
    V(R,Z)=Q8+V(R,Z)
    SPL=B4(R,Z)+.16667*ABS(B1(R,Z)+B2(R,Z)-(1+KO)*(W1+W2*X*Z))
    IF SPL#1 THEN SPL=1
    V(R,Z)=Q4^F2*C2*SPL^C5+V(R,Z)
    Q1=B1(R,Z)+B2(R,Z)+B3(R,Z):SPL=ABS(Q1-I1(Z))
    IF SPL#1 THEN SPL=1
    Q8=(ABS(LOG(Q1/I1(Z))))^F1*C1*SPL^C4
    IF Q1#I1(Z) THEN Q8=-Q8
    V(R,Z)=V(R,Z)-Q8
    IF Q9=1001 THEN 2496
    SPL=ABS(B1(R,Z)-B2(R,Z)+(KO-1)*(W1+W2*X*Z))*.5
    SPL=SPL+.16667*ABS(B1(R,Z)+B2(R,Z)-((1+KO)*W1+W2*X*Z))
    IF SPL#1 THEN SPL=1
    Q8=LOG((KO-(KO-1)*SU/(W1+W2*X*Z+SU))*B1(R,Z)/B2(R,Z))
    Q1=4*C3*(ABS(Q8))^F3*SPL^C6
    IF Q8#0 THEN Q1=-Q1
    SPL=.5*ABS(B2(R,Z)-B3(R,Z))
    SPL=SPL+.16667*ABS(B2(R,Z)+B3(R,Z)-2*KO*(W1+W2*X*Z))
    IF SPL#1 THEN SPL=1
    Q2=2*C3*(ABS(LOG(B2(R,Z)/B3(R,Z))))^F3*SPL^C6
    IF B2(R,Z)#B3(R,Z) THEN Q2=-Q2
    DZ(R,Z)=(V(R,Z)-Q1-Q2)/3
    IF DZ(R,Z)#0 THEN DZ(R,Z)=0
    IF Z=Z2 THEN W(R,Z)=S5(R,0)
    IF Z=Z2 THEN GOTO 2488
    W(R,Z)=W(R,Z+1)-(DZ(R,Z)+DZ(R,Z+1))*X/2000
    IF R=R2 THEN GOTO 2488
    IF W(R,Z)#W(R+1,Z) THEN W(R,Z)=W(R+1,Z)
    IF R=0 THEN W(R,Z)=W(R+1,Z)
2488:
    N1=N1+ABS(W(R,Z)-B5(R,Z))
    B5(R,Z)=W(R,Z)
2496:
    NEXT R,Z
    IF Q9=1001 THEN GOTO 4054
REM    BASE RADIAL DISPLACEMENT
    FOR Z=0 TO Z2:FOR R=1 TO R2-1
    IF Z=0 AND D1#0 THEN W(R,Z)=N(R)*.5*D1
    IF Z=0 AND D1=0 AND X(R)#RL THEN W(R,Z)=0
    IF Z=0 AND D1#0 THEN GOTO 2580
    IF Z=0 AND D1=0 AND X(R)#RL THEN GOTO 2580
    SPL=ABS(B1(R,Z)-B2(R,Z)+(KO-1)*(W1+W2*X*Z))*.5
    SPL=SPL+.16667*ABS(B1(R,Z)+B2(R,Z)-(1+KO)*(W1+W2*X*Z))
    IF SPL#1 THEN SPL=1
    Q8=LOG((KO-(KO-1)*SU/(W1+W2*X*Z+SU))*B1(R,Z)/B2(R,Z))
    Q1=2*C3*(ABS(Q8))^F3*SPL^C6
    IF Q8#0 THEN Q1=-Q1
    SPL=.5*ABS(B2(R,Z)-B3(R,Z))
    SPL=SPL+.16667*ABS(B2(R,Z)+B3(R,Z)-2*KO*(W1+W2*X*Z))
    IF SPL#1 THEN SPL=1
    Q8=LOG(B2(R,Z)/B3(R,Z))
    Q2=4*C3*(ABS(Q8))^F3*SPL^C6
    IF Q8#0 THEN Q2=-Q2
    W(R,Z)=(V(R,Z)+Q1+Q2)*X(R)/3000
```

```
    IF W(R,Z)≠0 THEN W(R,Z)=0
    IF X(R)≠RL THEN GOTO 2580
    IF V=0 THEN GOTO 2575
    IF W(R,Z)≠W(R-1,Z) THEN W(R,Z)=W(R-1,Z)
    GOTO 2580
2575:
    IF W(R,Z)≠W(R-1,Z) THEN V=1
    IF D1=0 AND X(R-1)≠RL+X*Z THEN V=1
2580:
    N1=N1+ABS(B6(R,Z)-W(R,Z))
    B6(R,Z)=B6(R,Z)*(1-.1*N2)+W(R,Z)*.1*N2
    NEXT R:V=0:NEXT Z
    IF A$="Y" THEN GOTO 4010
    GOTO 510
REM  SUBGRADE ANALYSIS
REM    SUBGRADE VERTICAL STRESS
3010:
    FOR Z=0 TO Z3:FOR R=R3 TO 0 STEP-1
    IF R=0 THEN V(0,Z)=S4(1,Z)*2/X
    IF R=R3 THEN V(R,Z)=-S4(R-1,Z)/(X(R3)-X(R-1))
    IF R=0 OR R=R3 THEN GOTO 3020
    V(R,Z)=(S4(R+1,Z)-S4(R-1,Z))/(X(R+1)-X(R-1))+S4(R,Z)/X(R)
3020:
    IF Z≠0 THEN GOTO 3030
    IF R≠R2 THEN S1(R,Z)=W1+W2*D2
    IF R≠R2 THEN W(R,Z)=S1(R,Z)
    IF R≠R2 THEN GOTO 3036
    S1(R,Z)=B1(R,Z2)+U(R,Z2)-SU:W(R,Z)=S1(R,Z):GOTO 3036
3030:
    W(R,Z)=W(R,Z-1)+((V(R,Z-1)+V(R,Z))*.5+W3)*(Y(Z)-Y(Z-1))
    IF R=R3 THEN GOTO 3036
    IF W(R,Z)≠W(R+1,Z) THEN W(R,Z)=W(R+1,Z)
3036:
    NEXT R
REM      CONSTRAINING AND BALANCING
    IF Z=0 THEN GOTO 3082
    Q1=0
    FOR R=1 TO R3
    Q2=.5*(W(R,Z)+W(R-1,Z))-W1-W2*D2-W3*Y(Z)
    Q1=Q1+(X(R)*X(R)-X(R-1)*X(R-1))*Q2
    NEXT R
    Q3=CP*RL*RL/Q1
    FOR R=0 TO R3
    W(R,Z)=W(R,Z)*Q3-(W1+W2*D2+W3*Y(Z))*(Q3-1)
    S1(R,Z)=W(R,Z)*.5*N2+S1(R,Z)*(1-.5*N2)
    NEXT R
3082:
    NEXT Z
REM    SUBGRADE RADIAL STRESS
    FOR Z=0 TO Z3:FOR R=0 TO R3
    IF Z=Z3 THEN DZ(R,Z)=-S5(R,Z-1)/(Y(Z)-Y(Z-1))
    IF Z=0 THEN DZ(R,Z)=(S5(R,1)-S5(R,0))/X
    IF Z=Z3 OR Z=0 THEN GOTO 3120
    DZ(R,Z)=(S5(R,Z+1)-S5(R,Z-1))/(Y(Z+1)-Y(Z-1))
3120:
    IF R=0 THEN DR(R,Z)=S6(1,Z)/X
    IF R=R3 THEN DR(R,Z)=-S6(R-1,Z)/(X(R3)-X(R-1))
    IF R=0 OR R=R3 THEN GOTO 3128
    DR(R,Z)=(S6(R+1,Z)-S6(R-1,Z))/(X(R+1)-X(R-1))
3128:
```

```
    IF S$="K-THETA" THEN G3=K1*(S1(R,Z)+S2(R,Z)+S3(R,Z))^K2/1.4
    IF S$="LINEAR" OR S$="K-THETA" THEN GOTO 3146
    Q1=(S1(R,Z)+S2(R,Z))*.5:Q2=(S1(R,Z)-S2(R,Z))*.5
    Q2=(Q2*Q2+S4(R,Z)*S4(R,Z))^.5
    Q1=Q1+Q2:Q2=Q1-2*Q2
    Q1=(Q1-Q2)*(Q1-Q2)+(Q2-S3(R,Z))*(Q2-S3(R,Z))+(S3(R,Z)-Q1)*(S3(R,Z)-Q1)
    Q1=(Q1*.5)^.5
    IF Q1=0 THEN Q1=1
    G3=((W1+W2*D2+W3*Y(Z))/Q1)^K2*Q1/(3*K1)
3146:
    W(R,Z)=S1(R,Z)-(DR(R,Z)-DZ(R,Z))*G3*2
REM      CONSTRAINING
    IF R=0 THEN GOTO 3176
    IF V¼2 THEN GOTO 3168
    IF W(R,Z)¾W(R-1,Z) THEN W(R,Z)=W(R-1,Z)
    GOTO 3176
3168:
    IF V=0 THEN GOTO 3174
    IF W(R,Z)¼W(R-1,Z) AND X(R)¾RL+100 THEN V=2
    GOTO 3176
3174:
    IF W(R,Z)¾W(R-1,Z) AND X(R)¾RL*2 THEN V=1
3176:
    S2(R,Z)=S2(R,Z)*(1-.2*N2)+W(R,Z)*.2*N2
    NEXT R:V=0:NEXT Z
REM    SUBGRADE TANGENTIAL STRESS
    FOR Z=0 TO Z3:FOR R=0 TO R3
    IF R=0 THEN W(R,Z)=S2(R,Z)
    IF R=0 THEN GOTO 3232
    IF R=R3 THEN V(R,Z)=(S2(R,Z)-S2(R-1,Z))/(X(R3)-X(R-1))
    IF R=R3 THEN GOTO 3230
    V(R,Z)=(S2(R+1,Z)-S2(R-1,Z))/(X(R+1)-X(R-1))
    IF Z=0 THEN V(R,Z)=V(R,Z)-(S4(R,Z+1)-S4(R,Z))/X
    IF Z=Z3 THEN V(R,Z)=V(R,Z)-(S4(R,Z)-S4(R,Z-1))/(Y(Z)-Y(Z-1))
    IF Z=0 OR Z=Z3 THEN GOTO 3230
    V(R,Z)=V(R,Z)-(S4(R,Z+1)-S4(R,Z-1))/(Y(Z+1)-Y(Z-1))
3230:
    W(R,Z)=S2(R,Z)+V(R,Z)*X(R)
3232:
    NEXT R
REM      CONSTRAINING AND AVERAGING
    FOR R=0 TO R3
    IF X(R)¾RL*2 AND W(R,Z)¾W(R3,Z)*2 THEN W(R,Z)=W(R3,Z)*2
    S3(R,Z)=S3(R,Z)*.9+W(R,Z)*.1
    IF R=0 OR R=R3 THEN GOTO 3268
    S3(R,Z)=(S3(R-1,Z)+S3(R,Z)*3+S3(R+1,Z))/5
3268:
    NEXT R,Z
REM    SUBGRADE SHEAR STRESS
    FOR Z=0 TO Z3:FOR R=1 TO R3-1
    IF Z=0 AND R¼R2 THEN S4(R,Z)=B4(R,Z2)
    IF Z=0 THEN GOTO 3355
    IF Z=Z3 THEN V(R,Z)=-S6(R,Z-1)/(Y(Z)-Y(Z-1))
    IF Z=Z3 THEN GOTO 3336
    V(R,Z)=(S6(R,Z+1)-S6(R,Z-1))/(Y(Z+1)-Y(Z-1))
3336:
    V(R,Z)=V(R,Z)+(S5(R+1,Z)-S5(R-1,Z))/(X(R+1)-X(R-1))
    IF S$="K-THETA" THEN G3=K1*(S1(R,Z)+S2(R,Z)+S3(R,Z))^K2/1.4
    IF S$="LINEAR" OR S$="K-THETA" THEN GOTO 3348
    Q1=(S1(R,Z)+S2(R,Z))*.5:Q2=(S1(R,Z)-S2(R,Z))*.5
```

```
    Q2=(Q2*Q2+S4(R,Z)*S4(R,Z))^.5
    Q1=Q1+Q2:Q2=Q1-2*Q2
    Q1=(Q1-Q2)*(Q1-Q2)+(Q2-S3(R,Z))*(Q2-S3(R,Z))+(S3(R,Z)-Q1)*(S3(R,Z)-Q1)
    Q1=(Q1*.5)^.5
    IF Q1=0 THEN Q1=1
    G3=((W1+W2*D2+W3*Y(Z))/Q1)^K2*Q1/(3*K1)
3348:
    W(R,Z)=V(R,Z)*G3
    IF W(R,Z)¾W(R,Z-1)*.5 THEN W(R,Z)=W(R,Z-1)*.5
    S4(R,Z)=W(R,Z)*.2*N2+S4(R,Z)*(1-.2*N2)
3355:
    NEXT R,Z
REM    SUBGRADE VERTICAL DISPLACEMENT
    FOR Z=Z3-1 TO 0 STEP-1:FOR R=R3 TO 0 STEP-1
    IF S$="K-THETA" THEN G3=K1*(S1(R,Z)+S2(R,Z)+S3(R,Z))^K2/1.4
    IF S$="LINEAR" OR S$="K-THETA" THEN GOTO 3420
    Q1=(S1(R,Z)+S2(R,Z))*.5:Q2=(S1(R,Z)-S2(R,Z))*.5
    Q2=(Q2*Q2+S4(R,Z)*S4(R,Z))^.5
    Q1=Q1+Q2:Q2=Q1-2*Q2
    Q1=(Q1-Q2)*(Q1-Q2)+(Q2-S3(R,Z))*(Q2-S3(R,Z))+(S3(R,Z)-Q1)*(S3(R,Z)-Q1)
    Q1=(Q1*.5)^.5
    IF Q1=0 THEN Q1=1
    G3=((W1+W2*D2+W3*Y(Z))/Q1)^K2*Q1/(3*K1)
3420:
    K3=G3*7/3
    DZ(R,Z)=(S2(R,Z)+S3(R,Z)-(W1+W2*D2+W3*Y(Z))*2)*(.5/G3-1/K3)
    DZ(R,Z)=(DZ(R,Z)-(S1(R,Z)-W1-W2*D2-W3*Y(Z))*(1/G3+1/K3))/3
    IF Z=Z3-1 THEN W(R,Z)=-DZ(R,Z)*(Y(Z3)-Y(Z))
    IF Z¼Z3-1 THEN W(R,Z)=W(R,Z+1)-(DZ(R,Z)+DZ(R,Z+1))*.5*(Y(Z+1)-Y(Z))
    IF R=R3 THEN GOTO 3445
    IF W(R,Z)¼W(R+1,Z) THEN W(R,Z)=W(R+1,Z)
    IF R=0 THEN W(R,Z)=W(R+1,Z)
3445:
    S5(R,Z)=W(R,Z)*.2*N2+S5(R,Z)*(1-.2*N2)
    NEXT R,Z
REM    SUBGRADE RADIAL DISPLACEMENT
    FOR Z=0 TO Z3-1:FOR R=1 TO R3
    IF S$="K-THETA" THEN G3=K1*(S1(R,Z)+S2(R,Z)+S3(R,Z))^K2/1.4
    IF S$="LINEAR" OR S$="K-THETA" THEN GOTO 3520
    Q1=(S1(R,Z)+S2(R,Z))*.5:Q2=(S1(R,Z)-S2(R,Z))*.5
    Q2=(Q2*Q2+S4(R,Z)*S4(R,Z))^.5
    Q1=Q1+Q2:Q2=Q1-2*Q2
    Q1=(Q1-Q2)*(Q1-Q2)+(Q2-S3(R,Z))*(Q2-S3(R,Z))+(S3(R,Z)-Q1)*(S3(R,Z)-Q1)
    Q1=(Q1*.5)^.5
    IF Q1=0 THEN Q1=1
    G3=((W1+W2*D2+W3*Y(Z))/Q1)^K2*Q1/(3*K1)
3520:
    W(R,Z)=((S1(R,Z)-S3(R,Z))*.5/G3+DZ(R,Z))*X(R)
    IF W(R,Z)¼0 THEN W(R,Z)=0
    S6(R,Z)=S6(R,Z)*.95+W(R,Z)*.05
    S6(R,Z)=S6(R,Z)-S6(R3,Z)*X(R)/X(R3)
    NEXT R
    FOR R=1 TO R3-1
    S6(R,Z)=(S6(R-1,Z)+S6(R,Z)*3+S6(R+1,Z))/5
    NEXT R,Z
    GOTO 2410
  $SEGMENT
REM  PORE WATER EFFECTS
REM    PORE PRESSURE CALCULATION
4010:
```

```
    FOR Z=0 TO Z2:FOR R=0 TO R2
    IF Z=0 THEN DZ(R,Z)=(B5(R,1)-B5(R,0))/X
    IF Z=Z2 THEN DZ(R,Z)=(B5(R,Z)-B5(R,Z-1))/X
    IF Z=0 OR Z=Z2 THEN GOTO 4020
    DZ(R,Z)=(B5(R,Z+1)-B5(R,Z-1))*.5/X
4020:
    IF R=0 THEN DZ(R,Z)=DZ(R,Z)+2*B6(1,Z)/X
    IF R=R2 THEN DZ(R,Z)=DZ(R,Z)-B6(R2-1,Z)/(X(R2)-X(R2-1))
    IF R=0 OR R=R2 THEN GOTO 4028
    DZ(R,Z)=DZ(R,Z)+B6(R,Z)/X(R)+(B6(R+1,Z)-B6(R-1,Z))/(X(R+1)-X(R-1))
4028:
    DZ(R,Z)=DZ(R,Z)-Q(R,Z)
    DR(R,Z)=V(R,Z)
    W(R,Z)=B1(R,Z)
    IF B2(R,Z)<W(R,Z) THEN W(R,Z)=B2(R,Z)
    IF B3(R,Z)<W(R,Z) THEN W(R,Z)=B3(R,Z)
    IF B7(R,Z)+B4(R,Z)<W(R,Z) THEN W(R,Z)=B7(R,Z)+B4(R,Z)
    IF B7(R,Z)-B4(R,Z)<W(R,Z) THEN W(R,Z)=B7(R,Z)-B4(R,Z)
    W(R,Z)=W(R,Z)/3
    IF DZ(R,Z)>0 THEN W(R,Z)=-W(R,Z)
    B1(R,Z)=B1(R,Z)-W(R,Z):B2(R,Z)=B2(R,Z)-W(R,Z):B3(R,Z)=B3(R,Z)-W(R,Z)
    B7(R,Z)=B7(R,Z)-W(R,Z)
    NEXT R,Z
    Q9=1001:GOTO 2410
4054:
    Q9=0
    FOR Z=0 TO Z2:FOR R=0 TO R2
    B1(R,Z)=B1(R,Z)+W(R,Z):B2(R,Z)=B2(R,Z)+W(R,Z):B3(R,Z)=B3(R,Z)+W(R,Z)
    Q2=W(R,Z)*10000*(100-DS)/(U(R,Z)+100+W(R,Z))
    W(R,Z)=W(R,Z)*DZ(R,Z)*1000/(DR(R,Z)-V(R,Z)-Q2)
    U(R,Z)=U(R,Z)+W(R,Z)*.1*N2
    IF Z=0 AND D1=0 THEN U(R,Z)=0
    NEXT R,Z
    IF N<49 THEN GOTO 510
REM    PORE WATER FLOW
    Q1=KB*10000*DU
    FOR Z=0 TO Z2:FOR R=1 TO R2
    W(R,Z)=(U(R-1,Z)-U(R,Z))*Q1*(X(R-1)+X(R))*X/(X(R)-X(R-1))
    IF Z=0 OR Z=Z2 THEN W(R,Z)=W(R,Z)*.5
    NEXT R,Z
    FOR Z=1 TO Z2
    V(0,Z)=(U(0,Z-1)-U(0,Z))*Q1*X*.25
    V(R2,Z)=(U(R2,Z-1)-U(R2,Z))*Q1*(X(R2)*X(R2)-(X(R2)+X(R2-1))^2*.25)/X
    FOR R=1 TO R2-1
    V(R,Z)=(U(R,Z-1)-U(R,Z))*Q1*((X(R+1)+X(R))^2-(X(R)+X(R-1))^2)*.25/X
    NEXT R,Z
    Q2=(-W(1,0)-V(0,1))/(X*X*X*.125)
    Q(0,0)=Q(0,0)+Q2*200
    FOR R=1 TO R2-1
    Q2=(W(R,0)-W(R+1,0)-V(R,1))/(((X(R+1)+X(R))^2-(X(R)+X(R-1))^2)*X*.125)
    Q(R,0)=Q(R,0)+Q2*200
    NEXT R
    Q2=(W(R2,0)-V(R2,1))/((X(R2)*X(R2)-(X(R2)+X(R2-1))^2*.25)*X*.5)
    Q(R2,0)=Q(R2,0)+Q2*200
    FOR Z=1 TO Z2-1
    Q2=(-W(1,Z)+V(0,Z)-V(0,Z+1))/(X*X*X*.25):Q(0,Z)=Q(0,Z)+Q2*200
    FOR R=1 TO R2-1
    Q2=W(R,Z)-W(R+1,Z)+V(R,Z)-V(R,Z+1)
    Q2=Q2/(((X(R+1)+X(R))^2-(X(R)+X(R-1))^2)*X*.25)
    Q(R,Z)=Q(R,Z)+Q2*200
```

```
    NEXT R
    Q2=(W(R2,Z)+V(R2,Z)-V(R2,Z+1))/((X(R2)*X(R2)-(X(R2)+X(R2-1))^2*.25)*X)
    Q(R2,Z)=Q(R2,Z)+Q2*200
    NEXT Z
    Q2=(-W(1,Z2)+V(0,Z2))/(X*X*X*.125):Q(0,Z2)=Q(0,Z2)+Q2*200
    FOR R=1 TO R2-1
    Q2=W(R,Z2)-W(R+1,Z2)+V(R,Z2)
    Q2=Q2/(((X(R+1)+X(R))^2-(X(R)+X(R-1))^2)*X*.125)
    Q(R,Z2)=Q(R,Z2)+Q2*200
    NEXT R
    Q2=(W(R2,Z2)+V(R2,Z2))/((X(R2)*X(R2)-(X(R2)+X(R2-1))^2*.25)*X*.5)
    Q(R2,Z2)=Q(R2,Z2)+Q2*200
    IF CP¼CQ THEN CP=CP+CQ*.02
    GOTO 510
REM  BASE PLASTIC DEFORMATION
REM    STRESS PATH DETERMINATION
5010:
    NQ=LOG(100000000)
    FOR R=0 TO R2:FOR Z=0 TO Z2
    U(R,Z)=0:W(R,Z)=0
    FOR V=R2 TO R STEP-1
    IF V=0 THEN Q3=B3(V,Z)
    IF V=0 THEN GOTO 5045
    Q1=(X(V)*X(V)-X(R)*X(R))^.5
    Q3=B3(V,Z)*Q1/X(V)+B2(V,Z)*X(R)/X(V)
5045:
    Q2=B1(V,Z)-Q3:Q4=.5*(B1(V,Z)+Q3)
    IF V¼R2 THEN GOTO 5050
    Q5=Q2:Q6=Q2:Q7=Q4:Q8=Q4:J1=B1(V,Z):J2=J1:J3=B2(R,Z):J4=J3
    J5=B3(V,Z):J6=J5:J7=B4(V,Z):J8=J7
5050:
    IF Q2¾Q5 THEN Q5=Q2
    IF Q4¾Q7 THEN Q7=Q4
    IF Q2¼Q6 THEN Q6=Q2
    IF Q4¼Q8 THEN Q8=Q4
    IF R=0 AND V¾0 THEN GOTO 5070
    Q4=(B1(V,Z)-Q3)/(Q3*(C7-1)+C8)
    IF Q4¾W(R,Z) THEN W(R,Z)=Q4
5070:
    Q4=(Q3-B1(V,Z))/(B1(V,Z)*(C7-1)+C8)
    IF Q4¾U(R,Z) THEN U(R,Z)=Q4
    IF B1(V,Z)¾J1 THEN J1=B1(V,Z)
    IF B1(V,Z)¼J2 THEN J2=B1(V,Z)
    IF B2(V,Z)¾J3 THEN J3=B2(V,Z)
    IF B2(V,Z)¼J4 THEN J4=B2(V,Z)
    IF B3(V,Z)¾J5 THEN J5=B3(V,Z)
    IF B3(V,Z)¼J6 THEN J6=B3(V,Z)
    IF B4(V,Z)¾J7 THEN J7=B4(V,Z)
    IF B4(V,Z)¼J8 THEN J8=B4(V,Z)
    NEXT V
REM    STRAIN CALCULATION
    B5(R,Z)=.5*(Q5-Q6)+.33333*(Q7-Q8)
    V(R,Z)=J1-J2+J3-J4+J5-J6+(J7-J8)*2
    IF B5(R,Z)=0 THEN GOTO 5135
    NP=(1-W(R,Z))*CS*1000/B5(R,Z)
    IF NP¼NQ THEN NQ=NP
    NP=(1-U(R,Z))*CS*1000/B5(R,Z)
    IF NP¼NQ THEN NQ=NP
5135:
    NEXT Z,R
```

```
    J=1
5145:
    IF J≠EXP(NQ) THEN GOTO 6910
    FOR R=0 TO R2:FOR Z=0 TO Z2
    B6(R,Z)=LOG(1-W(R,Z)-B5(R,Z)*.001*LOG(J)/CS)
    B6(R,Z)=-(B6(R,Z)-LOG(1-U(R,Z)-B5(R,Z)*.001*LOG(J)/CS))/C9
    B7(R,Z)=.001*V(R,Z)*LOG(J)/CV-.5*ABS(B6(R,Z))
    B6(R,Z)=.5*(B6(R,Z)+B7(R,Z))
    B7(R,Z)=B6(R,Z)-B7(R,Z)
    NEXT Z,R
REM     DEFORMATION CALCULATION
    FOR Z=Z2 TO 0 STEP-1:FOR R=0 TO R2
    IF R=0 THEN DR(R,Z)=0
    IF R≠0 THEN DR(R,Z)=DR(R-1,Z)+(B7(R,Z)+B7(R-1,Z))*(X(R)-X(R-1))*500
    NEXT R
    FOR R=0 TO R2
    IF Z=Z2 THEN DZ(R,Z)=0
    IF Z≠Z2 THEN DZ(R,Z)=DZ(R,Z+1)+(B6(R,Z)+B6(R,Z+1))*X*500
    NEXT R,Z
    GOTO 6800
REM  OUTPUT ROUTINE
REM    OUTPUT OF PAVEMENT DETAILS TO SCREEN
7010:
    PRINT"GRANMAT          ";D$
    PRINT D1"mm SURFACING -";E1"GPa -";M1"kg/cum"
    PRINT D2"mm BASE -";M2"kg/cum"
    PRINT "       PARAMETERS: COMP -";C1;F1;C4
    PRINT "                     DIL -";C2;F2;C5
    PRINT "                   SHEAR -";C3;F3;C6
    PRINT "                 PLASTIC -";C7;C8;C9;CS;CV
    PRINT "       K0 =";K0
    IF A$="Y" THEN GOTO 7024
    PRINT "       SUCTION =";SU"KPa":GOTO 7026
7024:
    PRINT "       PERMEABILITY =";KB"m/sec"
    PRINT "       SATURATION =";DS"%"
7026:
    IF D1=0 THEN PRINT "       SINGLE PARTICLE DEPTH =";DP"mm"
    IF S$="LINEAR" THEN PRINT D3"m SUBGRADE -";E3"MPa -";M3"kg/cum"
    IF S$="K-THETA" THEN PRINT D3"m SUBGRADE - K1 =";K1" K2 =";K2;M3"kg/cum"
    IF S$="LOACH" THEN PRINT D3"m SUBGRADE - A =";K1" B =";K2;M3"kg/cum"
    PRINT " LOAD =";CP"KPa over";RL"mm RADIUS"
    IF A$="Y" THEN PRINT "       DURATION =";T"secs"
    PRINT " BASIC GRID DIMENSION =";X"mm"
    IF G$="S" THEN GOTO 8100
    GOTO 88
REM    OUTPUT OF PAVEMENT DETAILS
6010:
    IF G$="S" THEN GOTO 7010
    IF A≠0 AND F$="R" THEN GOTO 8000
    LPRINT""
    LPRINT"       GRANMAT     ";D$
    LPRINT D1"mm SURFACING -";E1"GPa -";M1"kg/cum"
    LPRINT D2"mm BASE -";M2"kg/cum"
    LPRINT "       PARAMETERS: COMP -";C1;F1;C4
    LPRINT "                     DIL -";C2;F2;C5
    LPRINT "                   SHEAR -";C3;F3;C6
    LPRINT "                 PLASTIC -";C7;C8;C9;CS;CV
    LPRINT "       K0 =";K0
    IF A$="Y" THEN GOTO 6024
```

```
    LPRINT "      SUCTION =";SU"KPa":GOTO 6026
6024:
    LPRINT "      PERMEABILITY =";KB"m/sec"
    LPRINT "      SATURATION =";DS"%"
6026:
    IF D1=0 THEN LPRINT "      SINGLE PARTICLE DEPTH =";DP"mm"
    IF S$="LINEAR" THEN LPRINT D3"m SUBGRADE -";E3"MPa -";M3"kg/cum"
    IF S$="K-THETA" THEN LPRINT D3"m SUBGRADE - K1 =";K1" K2 =";K2;M3"kg/cum"
    IF S$="LOACH" THEN LPRINT D3"m SUBGRADE - A =";K1" B =";K2;M3"kg/cum"
    LPRINT " LOAD =";CP"KPa over";RL"mm RADIUS"
    IF A$="Y" THEN LPRINT "      DURATION =";T"secs"
    LPRINT " BASIC GRID DIMENSION =";X"mm"
    IF F$="R" THEN GOTO 8000
REM    OUTPUT OF GRID DIMENSIONS
    LPRINT""
    LPRINT"grid dimensions"
    FOR R=0 TO R3:LPRINT X(R)*.001;:NEXT R:LPRINT""
    FOR Z=1 TO Z2:LPRINT X*Z*.001
    NEXT Z
    LPRINT"-------------------------------------------------------------------"
    FOR Z=0 TO Z3:LPRINT (Y(Z)+D2)*.001
    NEXT Z
REM    OUTPUT OF VERTICAL STRESS
    LPRINT""
    LPRINT"vertical stress"
    FOR Z=0 TO Z2
    FOR R=0 TO R2:LPRINT USING "££££";INT(B1(R,Z));:NEXT R:LPRINT"":NEXT Z
    LPRINT"-------------------------------------------------------------------"
    FOR Z=0 TO Z3
    FOR R=0 TO R3:LPRINT INT(S1(R,Z));:NEXT R:LPRINT"":NEXT Z
REM    OUTPUT OF RADIAL STRESS
    LPRINT""
    LPRINT"radial stress"
    FOR Z=0 TO Z2
    FOR R=0 TO R2:LPRINT INT(B2(R,Z));:NEXT R:LPRINT"":NEXT Z
    LPRINT"-------------------------------------------------------------------"
    FOR Z=0 TO Z3
    FOR R=0 TO R3:LPRINT INT(S2(R,Z));:NEXT R:LPRINT"":NEXT Z
REM    OUTPUT OF TANGENTIAL STRESS
    LPRINT""
    LPRINT"tangential stress"
    FOR Z=0 TO Z2
    FOR R=0 TO R2:LPRINT INT(B3(R,Z));:NEXT R:LPRINT"":NEXT Z
    LPRINT"-------------------------------------------------------------------"
    FOR Z=0 TO Z3
    FOR R=0 TO R3:LPRINT INT(S3(R,Z));:NEXT R:LPRINT"":NEXT Z
REM    OUTPUT OF SHEAR STRESS            LPRINT""
    LPRINT""
    LPRINT"shear stress"
    FOR Z=0 TO Z2
    FOR R=0 TO R2:LPRINT INT(B4(R,Z));:NEXT R:LPRINT"":NEXT Z
    LPRINT"-------------------------------------------------------------------"
    FOR Z=0 TO Z3
    FOR R=0 TO R3:LPRINT INT(S4(R,Z));:NEXT R:LPRINT"":NEXT Z
REM    OUTPUT OF VERTICAL DISPLACEMENT
    LPRINT""
    LPRINT"vertical displacement"
    FOR Z=0 TO Z2
    FOR R=0 TO R2:LPRINT INT(B5(R,Z));:NEXT R:LPRINT"":NEXT Z
    LPRINT"-------------------------------------------------------------------"
```

```
    FOR Z=0 TO Z3
    FOR R=0 TO R3:LPRINT INT(S5(R,Z));:NEXT R:LPRINT"":NEXT Z
REM    OUTPUT OF RADIAL DISPLACEMENT
    LPRINT""
    LPRINT"radial displacement"
    FOR Z=0 TO Z2
    FOR R=0 TO R2:LPRINT INT(B6(R,Z));:NEXT R:LPRINT"":NEXT Z
    LPRINT"-----------------------------------------------------------------"
    FOR Z=0 TO Z3
    FOR R=0 TO R3:LPRINT INT(S6(R,Z));:NEXT R:LPRINT"":NEXT Z
REM    OUTPUT OF PORE PRESSURE
    LPRINT""
    LPRINT"pore pressure"
    FOR Z=0 TO Z2
    FOR R=0 TO R2:LPRINT INT(U(R,Z));:NEXT R:LPRINT"":NEXT Z
    GOTO 5010
REM    OUTPUT OF PLASTIC VERTICAL DISPLACEMENT
6800:
    IF G$="S" THEN GOTO 8300
    IF F$="R" THEN GOTO 8200
    LPRINT""
    IF J=1 THEN LPRINT"plastic vertical displacement -";J"pass"
    IF J<>1 THEN LPRINT"plastic vertical displacement -";J"passes"
    FOR Z=0 TO Z2
    FOR R=0 TO R2:LPRINT INT(DZ(R,Z));:NEXT R:LPRINT"":NEXT Z
REM    OUTPUT OF PLASTIC TRANSVERSE DISPLACEMENT
    LPRINT""
    IF J=1 THEN LPRINT"plastic transverse displacement -";J"pass"
    IF J<>1 THEN LPRINT"plastic transverse displacement -";J"passes"
    FOR Z=0 TO Z2
    FOR R=0 TO R2:LPRINT INT(DR(R,Z));:NEXT R:LPRINT"":NEXT Z
6900:
    J=J*10
    GOTO 5145
6910:
    IF G$="S" THEN PRINT""
    IF G$="P" THEN LPRINT""
    IF G$="S" THEN PRINT EXP(NQ)"passes to failure"
    IF G$="P" THEN LPRINT EXP(NQ)"passes to failure"
    IF B$="Y" THEN GOTO 9000
    GOTO 10000
REM    REDUCED OUTPUT
8000:
    IF B$="Y" THEN LPRINT"A =";A
    IF D1<>0 THEN LPRINT"Asphalt Tensile Strain =";INT(B6(1,0)*1000/X)"microstr
    LPRINT"Maximum Subgrade Strain =";INT((S5(0,0)-S5(0,1))*1000/X)"microstrai
    LPRINT"Maximum Subgrade Stress =";INT(S1(0,0))"KPa (originally";INT(W1+W2*
    LPRINT"Deflection Bowl:"
    FOR R=0 TO R2:LPRINT X(R)*.001;:NEXT R:LPRINT""
    FOR R=0 TO R2:LPRINT INT(B5(R,0));:NEXT R:LPRINT""
    GOTO 5010
8100:
    IF D1<>0 THEN PRINT"Asphalt Tensile Strain =";INT(B6(1,0)*1000/X)"microstra
    PRINT"Maximum Subgrade Strain =";INT((S5(0,0)-S5(0,1))*1000/X)"microstrain
    PRINT"Maximum Subgrade Stress =";INT(S1(0,0))"KPa (originally";INT(W1+W2*D
    PRINT"Deflection Bowl:"
    FOR R=0 TO R2:PRINT X(R)*.001;:NEXT R:PRINT""
    FOR R=0 TO R2:PRINT INT(B5(R,0));:NEXT R:PRINT""
    GOTO 5010
8200:
```

```
    IF J=1 THEN LPRINT"rut depth:";INT(DZ(0,0));
    IF J<>1 THEN LPRINT",";INT(DZ(0,0));
    GOTO 6900
8300:
    IF J=1 THEN PRINT"rut depth:";INT(DZ(0,0));
    IF J<>1 THEN PRINT",";INT(DZ(0,0));
    GOTO 6900
9000:  batch  routine
10000:
    COLOR 11,0
    PRINT"PROGRAM TERMINATED - AVAILABLE FOR OTHER USERS"
    PRINT"PRESS Esc FOLLOWED BY Alt X TO EXIT TURBOBASIC SYSTEM"
    END
```

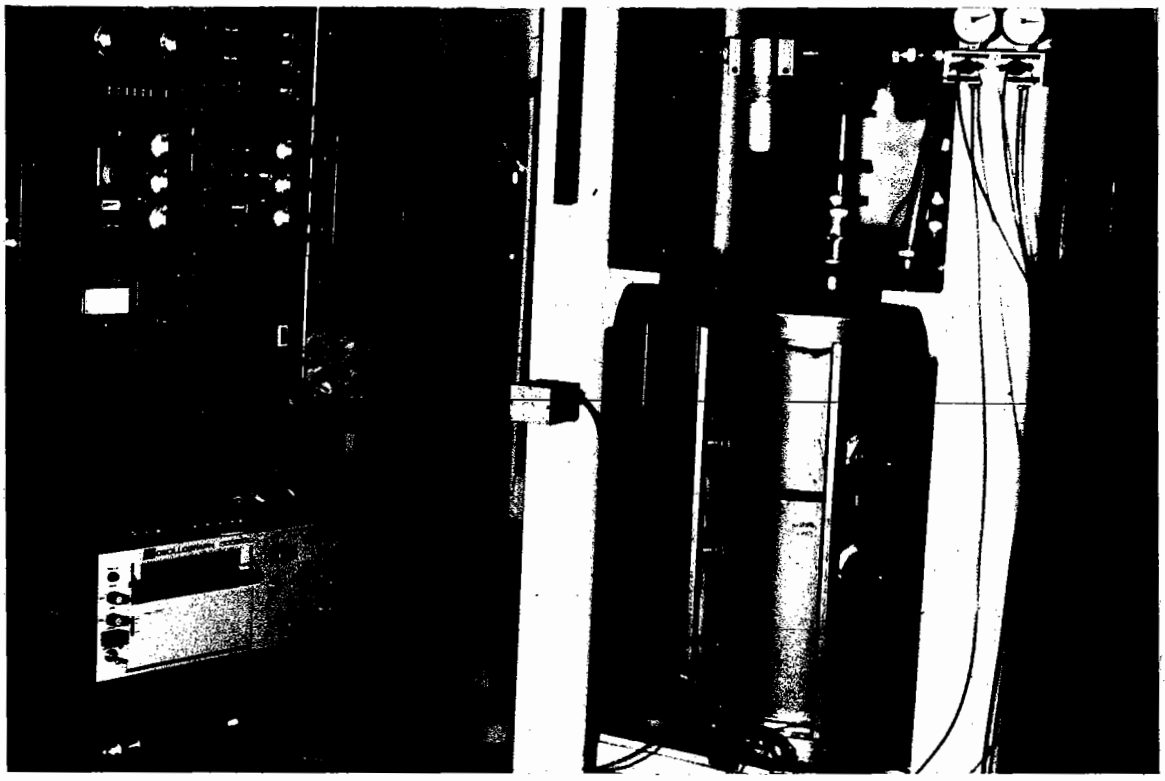

PLATE 1 150mm Triaxial Facility - General View

PLATE 2

150mm Triaxial Facility - Specimen and Instrumentation

PLATE 3

75mm Triaxial
Facility

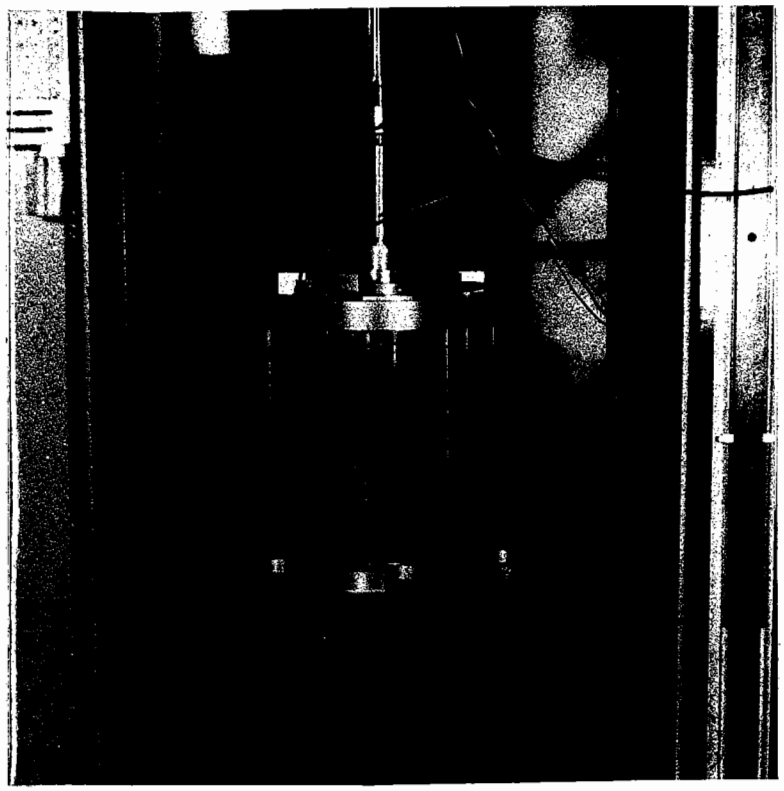

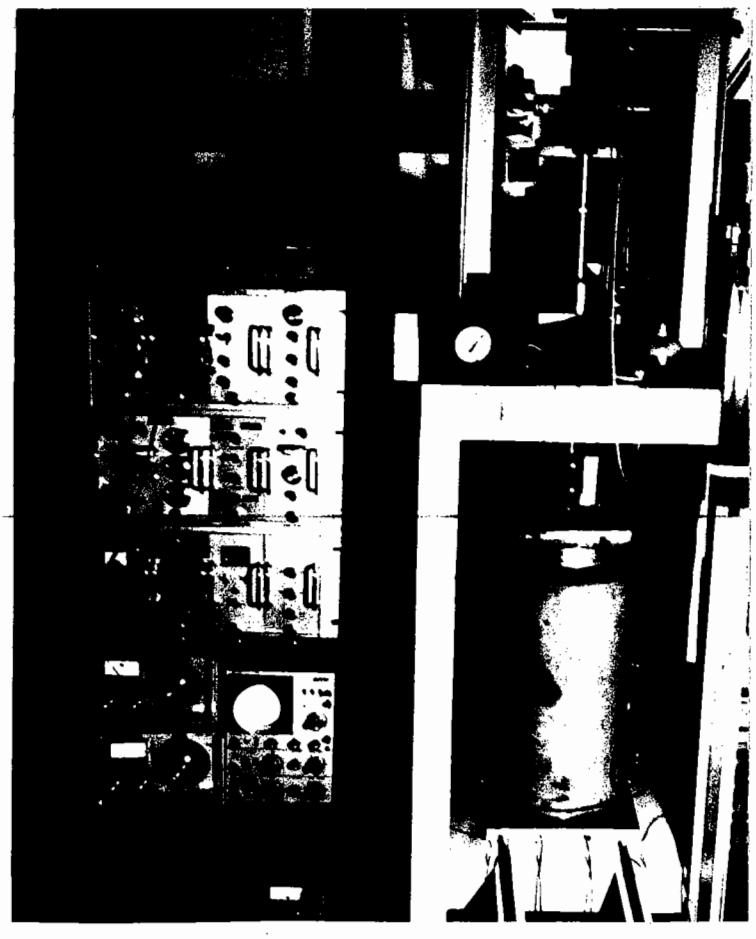

PLATE 4

Hollow Cylinder
Apparatus -
General View

PLATE 5

Hollow Cylinder Apparatus - Instrumentation Detail

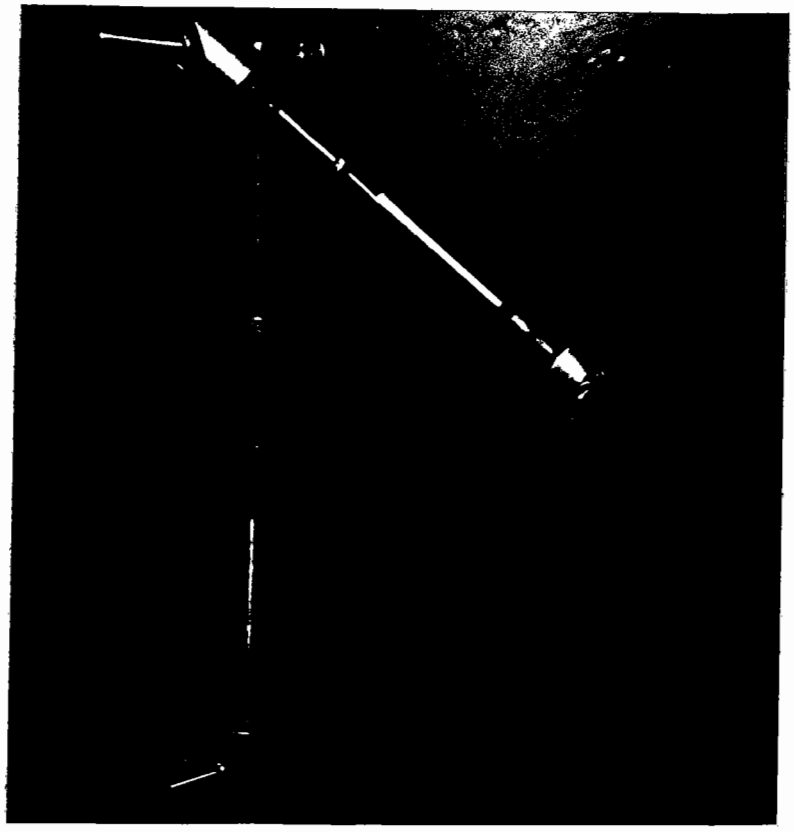

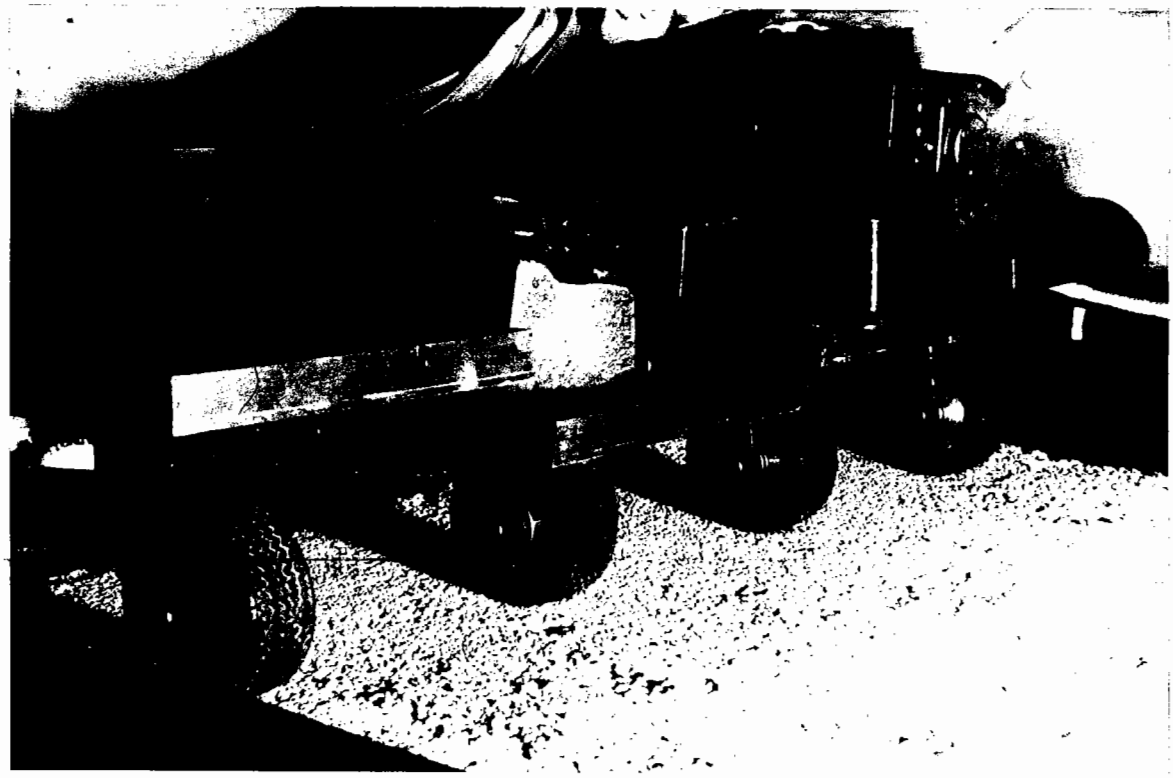

PLATE 6 Miniature Pavement Tester

PLATE 7

Plate Bearing Test

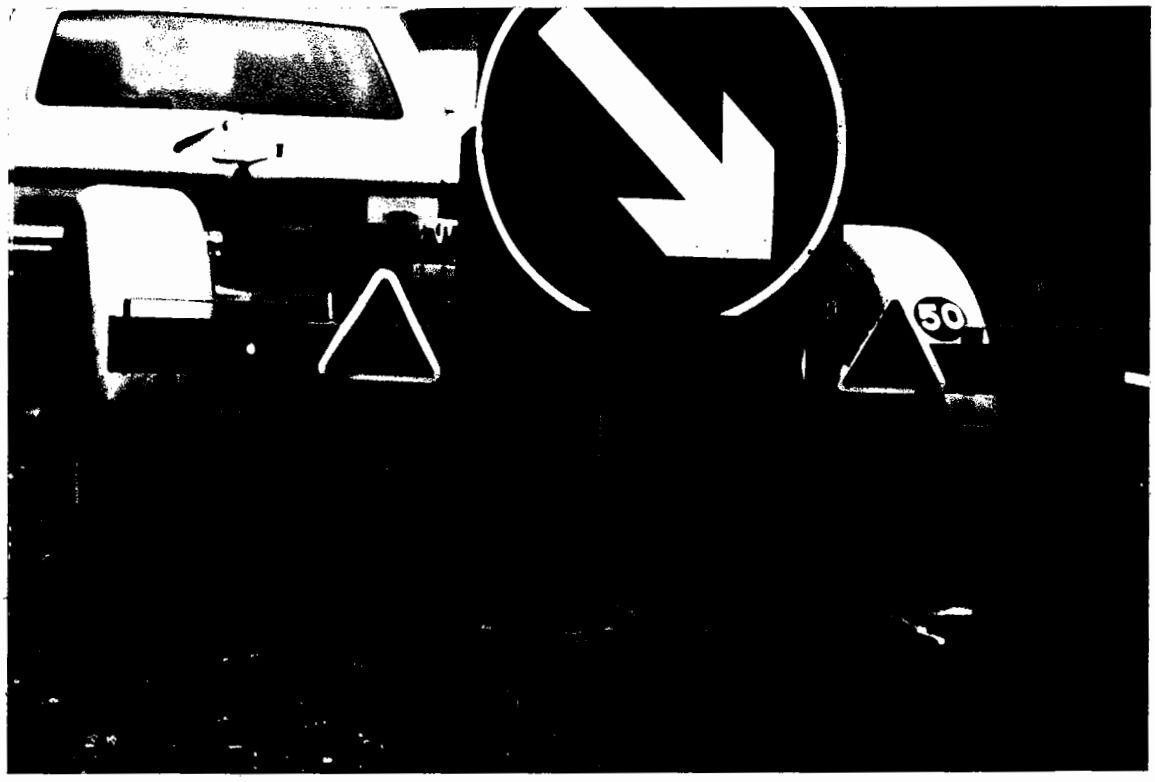

PLATE 8 Falling Weight Deflectometer

PLATE 9

Clegg Impact Hammer

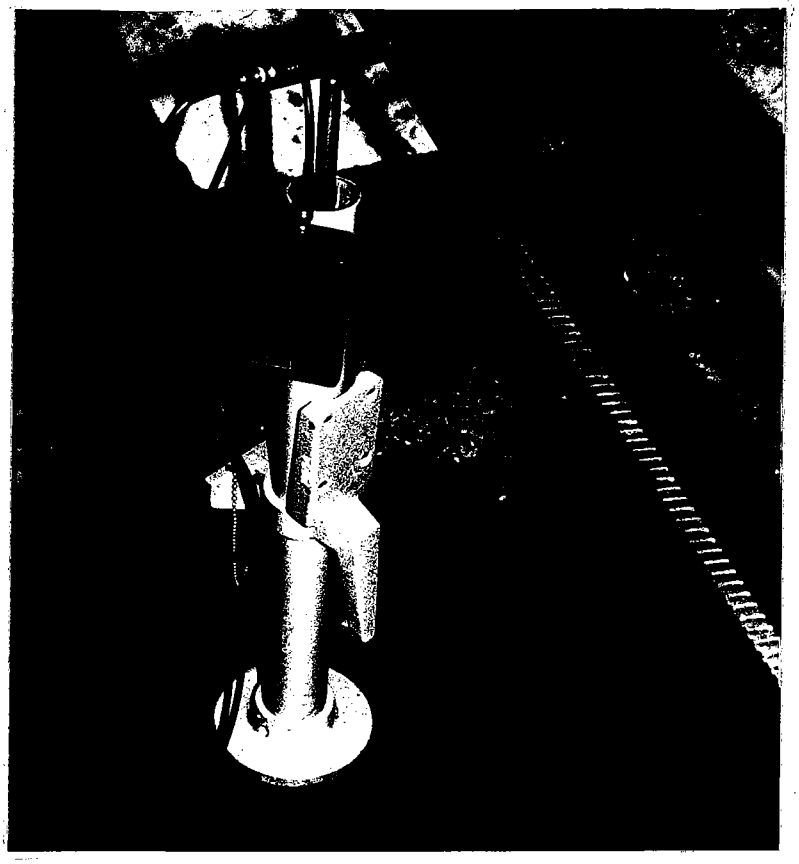

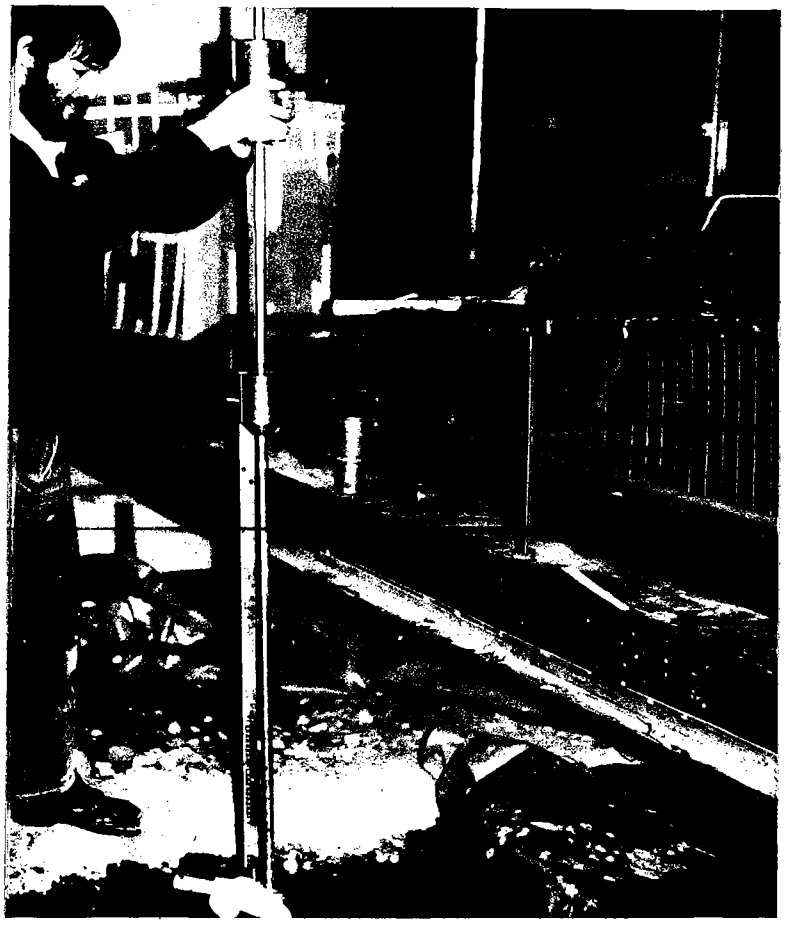

PLATE 10

Dynamic Cone
Penetrometer